Overcoming suppressive myeloid cells for neuroblastoma therapeutics

Jennifer Vanessa Frosch

UCL

A thesis submitted to University College London (UCL) for the degree of

DOCTOR OF PHILOSOPHY

I, Jennifer Vanessa Frosch confirm that the work presented in this thesis is my own. Where information has been derived from other sources, I confirm that this has been indicated in the thesis.

_____

Jennifer Vanessa Frosch

ABSTRACT

Neuroblastoma is a paediatric solid tumour with poor survival rates among patients within the high-risk group, despite advances in therapy. Although chimeric antigen receptor (CAR) T cells have proven to be an effective cell-based treatment in blood cancers, the immunosuppressive environment that is formed by the tumour and infiltrating alternatively activated immune cells heavily affects the efficacy of such immunotherapies when translated. Myeloid derived suppressor cells (MDSC) are a key group among tumour-induced immune cells and have been shown to correlate with cancer stage, disease progression, and resistance to standard therapies. Therefore, the aim of this work was to provide a neuroblastoma-based model to study interactions between CAR T cells and suppressive myeloid cells, and to investigate ways to overcome the suppressive effects. We have shown that an *in vitro* polarisation assay, using neuroblastoma-conditioned media, drives healthy monocytes towards MDSC-like phenotypes. Furthermore, these neuroblastoma-conditioned monocytes (NbM) significantly inhibited proliferation and activation (IFN-γ release) in co-cultures with primary and CAR-modified T cells. In a drug retargeting context, Sunitinib malate, a tyrosine kinase inhibitor, could partially recover T cell functions through inhibition of NbM. Moreover, a preliminary chemical library screen showed that the assay can achieve high throughput results suitable to investigate drug effects on suppressive monocytes. As an alternative approach to overcome myeloid cells in a solid tumour context, we designed an inducible anti-CD33 CAR under the control of a neuroblastoma driven synthetic Notch receptor, to enable the localised targeting of myeloid population only in the presence of tumour markers. However, we show that, in contrast to the prototypic CD19 induction, substitution with neuroblastoma-specific binding domains results in tonic signalling and failure of responder induction by tumour cells despite successful induction by cross

linking. Taken together, we have successfully developed a neuroblastoma-based model to screen for strategies to overcome myeloid cell-mediated T cell suppression in the tumour microenvironment and have provided the basis for both drug retargeting and cell engineering-based approaches.

IMPACT STATEMENT

Recent successes in clinical trials have shown that CAR T cell immunotherapy works well in patients with blood cancer, but there are problems with translating the treatment to solid cancers. A major reason for the reduced efficacy is the tumour microenvironment – a combination of recruited cells, molecules and blood vessels surrounding the tumour – which hinders the function of the immune system's effectors. We have established an *in vitro* model mimicking MDSC, which are a prominent cell type of the cancer microenvironment and correlate with cancer progression and therapy outcomes. This thesis provides a neuroblastoma-based assay to study interactions of CAR T cells with suppressive myeloid cells at the tumour site, which can be used to gain new insights in mechanisms of myeloid-derived suppression as well as to screen for ways to overcome this effect. We have demonstrated an application of the model in form of a novel high-throughput assay which enables the fast screening for MDSC-inhibitory drugs. Lastly, investigating synthetic Notch receptors, we showed an alternative approach to eliminate myeloid cells in tumour proximity. Taken together, these findings will contribute to better understand T cell suppression in the tumour microenvironment and lay the basis for studying ways to overcome it. Ultimately, this will help to improve the design of cell-based immunotherapy approaches for solid cancers, such as neuroblastoma.

Acknowledgements

I owe my deepest gratitude to a number of people, who offered their support and friendship over the years leading up to this PhD thesis.

First and foremost, I want to thank John Anderson and Karin Straathof for supervising this project and their guidance throughout. John, you have not only shaped me as a scientist but also showed me how to face hardships and experimental failures with positivity and resilience. I will aspire to keep the 'Anderson attitude' throughout my career and will remember to always see the bright side.

Secondly, I feel blessed with all the lovely friends I got to meet in the DBC Cancer section, and I want to thank all of them for the continuous encouragement and support. I want to particularly say thanks to the students that started their PhD alongside me – Dilu, Katie, Emma – our PhD venting therapy sessions will be missed, and I was extremely proud seeing this strong team of women in STEM stick together. I equally appreciated all the other (ex) lab members of the Anderson/Straathof/Fisher teams and hope that the social character will be preserved and that their collective knowledge and passion for science will continue to aspire young researchers in academia. Special thanks also go out to Ayad Eddaoudi, for his flow cytometry magic and for the lovely chats in between.

I wouldn’t have made it through ten years of education without the incredible support system in my personal life. I want to express my deepest gratitude to my amazing friends, in particular Ines, Christian and Ioanna, who always were there for me with open ears and words of wisdom. Moreover, I want to thank my person: Tom. I went to London to get a PhD and didn’t expect to find my best friend and soul mate along the way, and I am so eternally grateful that you stuck with me throughout this bumpy ride.

Weiterhin möchte ich meiner Familie danken, besonders meinem Opa, der mich immer ermutigt hat, das Beste aus meinem Leben zu machen. Lieber Opa, du hast so viel für unsere Familie erreicht und ich hoffe ich kann dich mit meiner Doktorarbeit stolz machen und dir damit für die jahrelange Unterstützung danken.

Mama und Papa, der letzte Abschnitt ist euch gewidmet. Ohne euch wäre ich nicht hier und ich kann nicht genug sagen, wie dankbar ich für eure Liebe, Unterstützung, und Aufmunterung bin. Ihr habt mir beigebracht das Leben mit Humor und Positivität zu meistern. Wenn ich einmal nur halb so ein toller Mensch wie jeder von euch werde, bin ich zufrieden, ob Doktortitel oder nicht.

TABLE OF CONTENTS

LIST OF FIGURES

LIST OF TABLES

LIST OF EQUATIONS

ABBREVIATIONS

ACT	Adoptive cell therapy
ADCC	Antibody-dependent cell-mediated cytotoxicity
ALK	Anaplastic lymphoma kinase
AP-1	Activator protein 1
APC	Antigen-presenting cells
Arg	Arginase
ATRA	All-trans retinoic acid
BD	Binding domain
BFP	Blue fluorescent protein
BiTE	bispecific T cell engager
Ca2+	Calcium ions
CAF	Cancer-associated fibroblast
CAR	Chimeric antigen receptor
CBA	Cytokine bead array
CD	Cluster of differentiation
CPI	Checkpoint inhibitors
CTL	Cytotoxic T lymphocyte
CTLA-4	Cytotoxic T-lymphocyte antigen 4
DAG	Diacylglycerol
DAMP	Damage-associated molecular pattern
DC	Dendritic cell
DCF	2', 7'-dichlorofluorescein
DCFDA	2',7'-dichlorofluorescin diacetate
DN	Double negative
DP	Double-positive
ECM	Extracellular matrix
EFS	Event-free survival
ELISA	Enzyme-linked immunosorbent assay
eMDSC	Early-stage MDSC
ER	Endoplasmic reticulum
FCS	Fetal calf serum
FSC	Forward scatter
Gem	Gemcitabine hydrochloride

GFP	Green fluorescent protein
HBV	Hepatitis B virus
HPV	Human papillomavirus
iCAR	Inhibitory CAR
IDO	Indoleamine-2,3-dioxygenase
IFN-	Interferon
IL	Interleukin
iNOS	Nitric oxide synthase
INRG	International Neuroblastoma Risk Group
INRGSS	INRG staging system
INSS	International Neuroblastoma Staging System
IP3	Inositol triphosphate
IS	Immunological synapse
ITAM	Immune-receptor tyrosine-based activation motif
iTreg	Induced regulatory T cell
LAT	Linker of activated T cells
LB	Luria Bertani
LTR	Long terminal repeat
M-MDSC	Monocytic MDSC
mAb	Monoclonal antibody
MAPK	Mitogen activated protein kinase
MDSC	Myeloid derived suppressor cells
MFI	Mean fluorescent intensity
MHC	Major histocompatibility complex
MOI	Multiplicity of infection
Nb	Neuroblastoma
NbM	Neuroblastoma-conditioned monocytes
NFAT	Nuclear factor of activated T cells
NFkB	Nuclear factor kappa-light-chain-enhancer of activated B cells
NK cells	Natural killer cells
NO	Nitric oxide
nTreg	Natural regulatory T cell
OD	Optical density
PBMC	Peripheral blood mononuclear cell

PBS	Phosphate buffered saline
PCR	Polymerase chain reaction
PD-1	Programmed death-1
PD-L1	Anti-programmed death-ligand 1
PGE2	Prostaglandin E2
PGK	Phosphoglycerate kinase 1
PIP-2	Phosphatidylinositol 4,5 biphosphate
PKC-q	Protein kinase C-theta
PLC-g 1	Phospholipase C-gamma 1
PMN-MDSC	Polymorphonuclear MDSC
RNS	Reactive nitrogen species
ROS	Reactive oxygen species
scFv	Single chain variable fragment
SLP-76	SH2-domain-containing leukocyte protein of 76 kDa
SMAC	Supramolecular activation cluster
SP	Single positive
SSC	Side scatter
Sun	Sunitinib malate
synNotch	Synthetic Notch
TAM	Tumour-associated macrophage
TBHP	Tert-butyl hydrogen peroxide
TCR	T cell receptor
Tfh	Follicular T helper cell
Th	T helper cell
TIL	Tumour-infiltrating lymphocyte
TK	Tyrosine kinase
TMB	Tumour mutation burden
TME	Tumour microenvironment
TNF	Tumour necrosis factor
TRE	Tet responsive element
Treg	Regulatory T cell
UAS	Upstream activation sequence
VC	Vehicle control
VEGF	Vascular endothelial growth factor
WT	Wild type

ZAP-70	Zeta-chain-associated protein

1. INTRODUCTION

1.1.Neuroblastoma

1.1.1. Epidemiology and genetics

Epidemiology

With just under 100 newly diagnosed children each year in the UK, neuroblastoma is the most common extracranial solid tumour of early childhood. It accounts for approximately 10% of paediatric tumours and up to 15% of cancer-related deaths in children (Whittle et al., 2017). The disease mainly is diagnosed in children of young age and shows decreasing cases over the first 10 years, with the median age of patients at diagnosis being 19 months. In adolescents and young adults it occurs only rarely but tends to be more aggressive (Mossé et al., 2014). Furthermore, neuroblastoma incidence in boys is slightly higher than in girls and tends to be more aggressive with lower survival rates in African American and Native American patients (Henderson et al., 2011).

Neuroblastoma arises during fetal or early post-natal life from sympathoadrenal precursor cells derived from the neural crest. During normal development the multipotent neural crest cell precursors migrate from the neural tube to various locations of the body and differentiate appropriately into diverse cell lineages, such as melanocytes, craniofacial cartilage and bone, smooth muscle, as well as peripheral and enteric neurons and glia. Cells migrating to the dorsal aorta first differentiate into sympathoadrenal progenitor cells, and eventually give rise to the peripheral nervous system (Matthay et al., 2016). However, defects in neural crest cell migration, maturation, or differentiation – which affect these crucial processes during fetal development – can lead to the formation of neuroblastoma.

Notably, neuroblastoma presents with clinical and biological heterogeneity between patients. Cases range from low-risk disease, where tumours can regress spontaneously without the need for treatment, to high-risk patients with widespread metastatic burden and poor outcomes despite aggressive multimodal therapeutic approaches. The underlying aetiology remains mostly unclear, with environmental factors being suggested but not yet proven to be directly linked (Whittle et al., 2017). Hereditary occurrence only accounts for approximately 1–2% of all cases and has been identified to be characterised with an autosomal dominant inheritance with incomplete penetrance (Shojaei-Brosseau et al., 2004). The majority of neuroblastoma diagnoses appear to be isolated cases in families.

Genetics

Generally, neuroblastoma tumours are characterised by their irregular DNA content, with 55% of primary neuroblastomas being triploid or 'near-triploid' and the reminding cases being either 'near-diploid' or 'near-tetraploid' (Kaneko et al., 1987). Near-triploid tumours are linked to a more favourable outcome with good survival rates, compared to those with near-diploid or near-tetraploid DNA content (Look et al., 1984).

Among the known molecular abnormalities, *MYCN* amplification has been used as a powerful prognostic indicator, being present in approximately one quarter of all primary neuroblastoma cases, and in 40% of tumours among patients with advanced disease (Brodeur et al., 1984). The proto-oncogene *MYCN* is located on the distal short arm of chromosome 2 (2p24) and encodes the transcriptional factor N-Myc, which under healthy conditions is only expressed in nervous and mesenchymal tissues during normal brain development. Sharing redundancy with other Myc family members, N-Myc regulates genes involved in a plethora of cellular functions spanning cell growth, proliferation,

apoptosis, and differentiation (Nakagawara et al., 2018). High levels of N-Myc expression due to amplification of the *MYCN* locus play a crucial oncogenic role in the development of neuroblastoma and have been shown to positively correlate with advanced disease stage, unfavourable biology, and poor outcome of disease (Brodeur et al., 1984).

Moreover, common occurrence of allelic deletions on chromosomes 1p and 11q suggest the existence of tumour suppressor genes which are lost in neuroblastoma. Deletions in the short arm of chromosome 1 (1p) correlate with both *MYCN* amplification and other high-risk features and appear in 30% of all neuroblastomas and in 70% of advanced-stage cases (Fong et al., 1989; Gilbert et al., 1984). Loss of part of the long arm of chromosome 11 (11q) can be found in about 40% of patients and is inversely correlated with *MYCN* amplification, albeit being associated with high-risk disease (Attiyeh et al., 2005).

Lastly, anaplastic lymphoma kinase (ALK) has been identified as a major oncogene involved with hereditary neuroblastoma (Mossé et al., 2008), albeit inherited disease remains rare. Germline mutations of the tyrosine kinase domain of the *ALK* oncogene, which is located on the short arm of chromosome 2 (2p23), lead to a constitutive activation of the receptor outside its normal purpose during embryonic and neonatal brain development (Nakagawara et al., 2018). The constitutively activated ALK acts as an oncogene by affecting several downstream signalling pathways, such as the RAS/MAPK pathway and the PI3K pathway, and thus inducing cell transformation (Carpenter and Mossé, 2012). Moreover, somatically acquired mutations of *ALK* have been observed in approximately 10% of primary tumours (Matthay et al., 2016). Being not only in proximal location (2p23 and 2p24, respectively) but also a direct transcriptional target of N-Myc, *ALK* is often co-amplified with *MYCN* (Hasan et al., 2013).

1.1.2. Classification

Similar to other cancer diseases, neuroblastoma is diagnosed through a combination of radiographic imaging, laboratory tests, and tumour or bone marrow biopsy. To ensure appropriate treatment, the patient then needs to be stratified to a risk group based on the presence or absence of certain clinical and molecular risk factors.

First established in 1986 and later revised in 1993, the International Neuroblastoma Staging System (INSS) provides a surgicopathologic system for neuroblastoma staging according to the extent of surgical excision of tumour at diagnosis and the prevalence of metastases (Brodeur et al., 1993). Based on these factors, neuroblastoma disease can be classified into stages 1, 2A/2B, 3, 4, or 4S, where early stage (1 and 2) tumours correlate with better prognosis than advanced staged ones (3 and 4).

After years of varying approaches to classifying patient risk before treatment, the International Neuroblastoma Risk Group (INRG) proposed a system to assimilate pre-treatment risk stratification between clinical trials, therefore making them more comparable (Cohn et al., 2009). To determine a universal system, investigators looked at prognostic factors spanning both clinical (tumour stage, age) and tumour biological features (histology, DNA ploidy, *MYCN* amplification, chromosomal aberrations, molecular markers) using data from over 8000 neuroblastoma patients (Cohn et al., 2009; Monclair et al., 2009). The resulted INRG classification assigns patients to one of four risk groups – very low risk, low risk, intermediate risk, and high risk – based on seven clinically relevant and statistically significant factors. These include tumour stage, patient age, tumour histology and differentiation, *MYCN* amplification, chromosome 11q aberration, and DNA ploidy (Cohn et al., 2009). Tumour stage can be assessed as low-

risk or high-risk according to the INRG staging system (INRGSS), which is based on preoperative radiological features and image-defined risk factors (Monclair et al., 2009).

The 5-year event-free survival (EFS) has been stated by the INRG as >85%, >75–≤85%, ≥50–≤75%, or <50% for ultra-low-risk, low-risk, intermediate-risk, and high-risk groups, respectively (Nakagawara et al., 2018).

1.1.3. Treatment strategies

Treatment options for neuroblastoma patients range from surgery, chemo- and radiotherapy to multimodal approaches, including myeloablative chemotherapy and autologous stem cell transplantation.

Since risk and aggression of disease is so heterogeneous between the groups, treatment is based on the individual patient's risk classification. For low-risk patients treatments aim to keep therapy-associated toxicity to a minimum while sustaining efficacy, while those with high-risk disease will receive intensive multimodal therapy to attempt preventing relapse. While this strategy has proven efficient for low- and intermediate-risk cases, where a long-lasting cure is seen in over 90% of patients, it only achieves tumour regression in less than 50% of neuroblastoma patients with high-risk disease (Park et al., 2013) (see **Figure 1-1**).

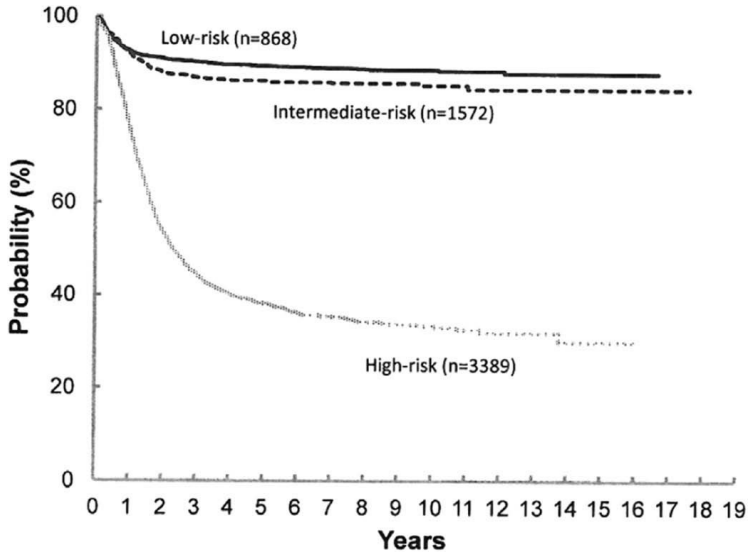

Figure 1-1 Event free survival of neuroblastoma patients with low-, intermediate- and high-risk disease. Event free Kaplan-Mierer survival curves for each risk group calculated from the time of diagnosis (in years). Patients included are from the ANBL00B1 study and Children's Cancer Group, Paediatric Oncology Group studies between 1990 and 2010. Data courtesy of W. London, Children's Oncology Group statistical office. Taken from (Park et al., 2013).

Low- and intermediate-risk disease

Slightly more than half of newly diagnosed patients present with non-high-risk neuroblastoma. The heterogeneous group ranges from very-low-risk to intermediate-risk cases but generally is associated with good outcome (Whittle et al., 2017).

Among patients under 18 months of age, neuroblastoma often regresses spontaneously without treatment, so that it is suggested that half of the cases arising in the first year of life aren't detected in the first place (Nakagawara et al., 2018). Therefore, in low-risk patients the first approach is often observation alone, with surgical resection if applicable. Study P9641 by the Children's Oncology Group demonstrated excellent survival rates in the participating 915 non-high-risk patients, when treated with surgery alone (5-year OS rate of 99% for INSS stage 1 and 4S tumours, and 96% for asymptomatic stage 2A or 2B tumours) (Strother et al., 2012).

In intermediate-risk disease surgical resection is often complemented with moderate doses of multiagent chemotherapy, when residual tumour is found or when complete tumour section presents difficult. Generally, therapy approaches of non-high-risk neuroblastoma have been focussing on reduction of therapy intensity for the sake of minimising side effects from chemotherapy exposure and the risks of surgery. Nevertheless, outcomes continue to remain excellent within this group.

High-risk-disease

The remaining half of newly diagnosed patients are categorised into the high-risk group. Despite constant improvements in treatment strategies, including multimodal approaches, patients in this group continue to have poor chances of cure, with 40-50% long-term survival (Whittle et al., 2017).

The standard treatment regimen consists of four steps: induction chemotherapy, local control with surgery and radiotherapy, consolidation using myeloablative chemotherapy and autologous stem cell rescue, and maintenance therapy. The maintenance phase describes the time after completing the multimodal therapy course, where patients are monitored for evidence of residual disease and relapse. Survival rates show that complete clinical remission can be achieved with this strategy, however patients responding poorly or experiencing relapse remain common. Patients' 5-year survival rates have been reported to drop to 20% after the first relapse of disease (London et al., 2011).

Chemotherapy and molecularly targeted radiotherapy have demonstrated efficiency in the treatment of patients with relapsed neuroblastoma, however subsequent relapses and disease progression often limit the further treatment options of these children (Whittle et al., 2017). Novel treatments are needed, such as improved immunotherapy-based approaches.

1.2. T cell immunology

1.2.1. Role of T cells in immune response

Innate and adaptive immunity

The human immune response presents as an interplay of two complex defence strategies: the innate and adaptive immune system. Whilst innate immunity acts as an initial barrier to external threats detected in the host organism, adaptive immunity is a memory-based long-term system that can further specify threats, also among host cells (Yatim and Lakkis, 2015). Most importantly, the immune system can distinguish between pathogens (non-self) and host tissue (self), sensing either pathogen associated molecular patterns on target surfaces (innate immunity) (Ozinsky et al., 2000), or via highly specific antigen receptors mediating humoral and cellular immune responses (adaptive immunity).

Lymphocytic cells, which are relatively uniform in appearance but have varied functions, can be found in both innate and adaptive defences. The three main cell types of lymphocytic origin are natural killer (NK), B and T cells. NK cells do not convey long-term immunologic memory and contribute significantly to the innate response, alongside other effectors, such as dendritic cells (DC), macrophages, mast cells, and γδT cells. B and T cells, in contrast, provide an enormous repertoire of antigen-specific responses which can be restored upon re-encounter of pathogens, and are the effector cells of the adaptive immune system (LaRosa and Orange, 2008). Considering the aim of this thesis work being the improvement of CAR T cell immunotherapy of high-risk neuroblastoma, the following sections will focus only on T cell biology.

T cell development

T cells arise from committed haematopoietic progenitors originating in the bone marrow. Those precursors migrating to the thymus receive appropriate signals via the Notch receptor and commit to the T cell lineage (La Motte-Mohs et al., 2005). A subsequent arrangement of random variable (V), diversity (D), and joining (J) somatic gene segments during generation of the TCR provides the broad specificity of the T cell receptor repertoire (Little et al., 2015). **Figure 1-2** gives an overview of T cell maturation processes inside the thymus. These early T cell precursors do not express the CD4 or CD8 co-receptors, hence are designated as double-negative (DN) thymocytes. For the expression of functional receptors, the gene segments for the α, β, γ, and δ chains have to undergo recombination and pair to form either an αβTCR or γδTCR. This rearrangement begins at the δ and γ loci, which in the case of successful γδTCR expression results in a commitment to the γδT cell lineage. If formation of a functional γδTCR fails, recombination of the β loci results in βTCR expression, which then forms a pre-TCR through pairing with a non-rearranged α chain (pre-Tα) (von Boehmer and Fehling, 1997). Only when the pre-TCR is successfully assembled and signals are both CD4 and CD8 expressed, leading to a double-positive (DP) population. The formation of the definite αβTCR is completed after a final recombination of α loci, which then replace the surrogate α receptor in the pre-TCR. During a subsequent positive and negative selection, functional T cells are selected for survival. To ensure correct antigen binding, the DP cells interact with peptide-loaded MHC molecules on thymic cortical epithelial cells, where they are positively selected for those whose TCRs show sufficient affinity (see **Figure 1-2**, 1). TCR-stimulated DP cells lose either the CD4 or CD8 co-receptor, depending on which MHC type was bound, and continue to a second selection process in the thymic medulla. Here, reactivity to self-antigens is thoroughly tested via interaction

with medullary epithelial and bone marrow-derived antigen-presenting cells (APC) ensuring the formation of a central tolerance. Those reacting too strongly to the presented self-signals are negatively selected by apoptosis, whereas those which do not bind self-MHC survive (see **Figure 1-2**, 2) (LaRosa and Orange, 2008; von Boehmer et al., 1989). This step concludes T cell development, and T cells can migrate out of the thymus to the peripheral lymphoid organs.

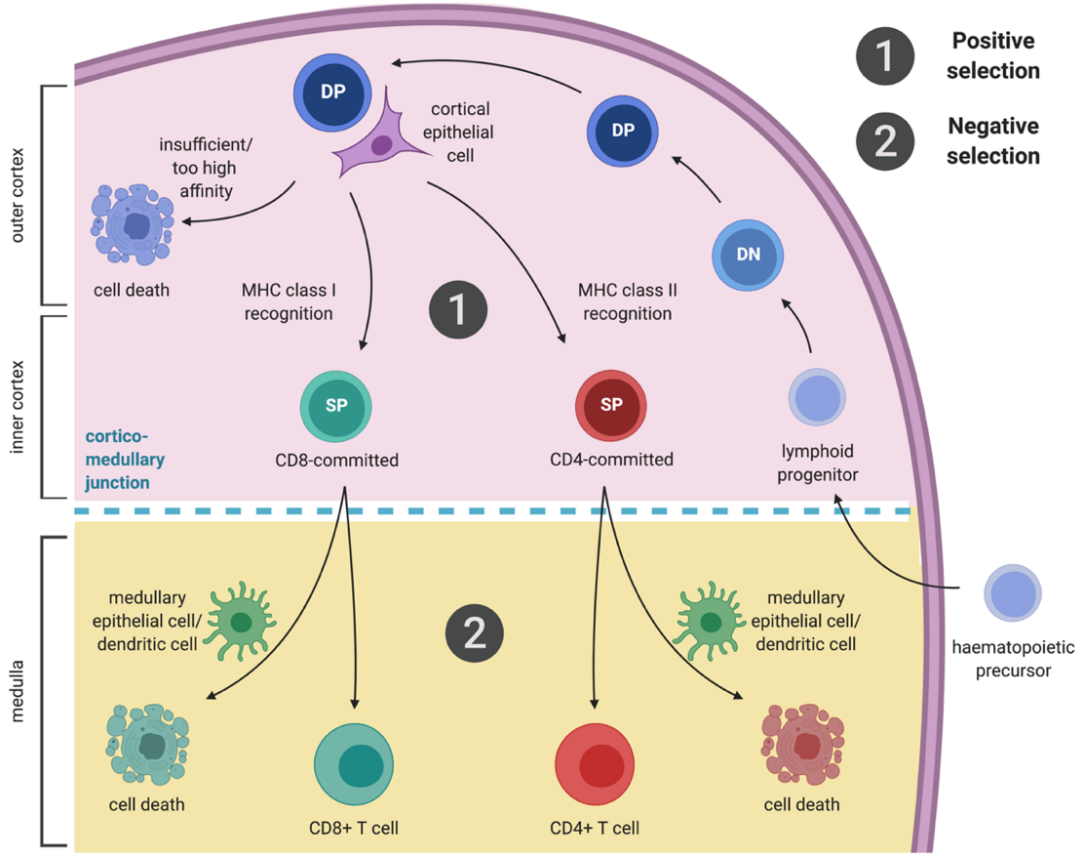

Figure 1-2 Positive and negative selection of CD4+ and CD8+ T cells in the thymus. Haematopoietic precursor cells from the bone marrow migrate to the thymus where they commit to the T cell lineage. First T cell precursors express both CD4 and CD8 on their surface (double positive, DP). In a first positive selection process in the thymic cortex DP cells encounter antigen presenting cortical epithelial cells. Only cells binding antigen presented on MHC I or MHC II molecules will be stimulated and continue differentiation towards either expressing CD8 or CD4 (single positive, SP). DP cells unable to detect antigen will die off from insufficient stimulation. SP cells progress to the medulla where they are presented with self-antigen via medullary epithelial cells and APC migrated from the bone marrow. Self-antigen binding SP cells will be negatively selected and undergo apoptosis, while those that do not bind self-MHC survive and are free to migrate into circulation. Adapted from (Germain, 2002).

T cell subsets and their functions

There are two main effector T cell populations, CD4+ and CD8+ T cells, which both are essential for the cell-mediated clearance of intracellular pathogens and tumours. Whilst those expressing the CD8 co-receptor exercise functions to directly kill target cells, CD4 co-receptor expressing T cells can be divided into several subpopulations, some of which carry immunogenic and others -regulatory functions.

CD8+ effector T cells can only bind antigens presented via MHC class I molecules. Upon activation, this subpopulation will rapidly expand and differentiate into cytotoxic T lymphocytes (CTLs). The highly efficient killing mediated by these cells can occur through activation of two separate apoptotic pathways. Firstly, signalling through the TCR initiates a calcium-dependent mechanism, leading to changes in the microtubule organisation centre and polarisation of both the Golgi complex and cytosolic lytic granules towards the target. This induces targeted release of the secretory granules into the immunologic synapse, freeing the contained lytic factors perforin and granzymes. Whilst perforin effects the formation of pores in the plasma membranes of targets, granzymes can enter cells through them and trigger the mitochondrial apoptotic pathway (Jenkins and Griffiths, 2010). Additionally, CD8+ effectors produce both IFN-γ and TNFα to further support the immune response. Secondly, activated CTLs express FasL on their surface, a member of the tumour necrosis factor family. When FasL binds to its ligand Fas, a glycoprotein widely expressed on lymphoid and non-lymphoid tissues, the receptor trimerizes and triggers caspase 8 activation, ultimately leading to cell apoptosis (Berke, 1995).

Unlike CD8+ T cells, CD4+ T cells can only bind MHC class II molecules and undergo differentiation once activated, resulting in various subsets distinguished by effector

functions and cytokine footprint. The differentiation repertoire of CD4+ T cells originally was thought to be limited to two subsets: type 1 T helper (Th1) or type 2 helper (Th2) cells (Mosmann et al., 1986). However, many additional CD4+ effectors have been identified since, including Th9, Th17, regulatory T cells (Tregs), and follicular T helper cells (Tfh) (Wan and Flavell, 2009).

The role of Th1 cells is building a bridge between the innate system and T cell responses through pro-inflammatory cytokines IFN-γ, TNFα, and TNFβ. Therefore, Th1 cells are involved both in fighting intracellular pathogens as well as tumour cells. The master regulator driving the Th1 program is T-bet (Wan and Flavell, 2009).

The function of Th2 cells is mostly mediated via release of IL-4, IL-5, IL-9, IL-10, and IL-13, thus promoting B cell antibody responses and eosinophil recruitment when battling foreign organisms and parasites. The master transcription factor regulator connected to Th2 cells is GATA-3 (Mosmann et al., 1986; Zhang et al., 1997).

Similarly, Tfh promote B cell antibody generation and memory formation through expression of the B cell-promoting cytokines IL-10 and IL-21 (Wan and Flavell, 2009).

Named after their ability to produce IL-17, Th17 cells function by inducing the recruitment and proliferation of neutrophils during bacterial and fungal infections. They additionally can produce IL-21 and IL-22 and are driven by the transcription factor Rorγt (LaRosa and Orange, 2008; Wan and Flavell, 2009).

Lastly, Tregs are the only T helper cell subset specialised for immunoregulatory functions and play a fundamental role in the maintenance of self-tolerance and immune homeostasis. They generally are characterised by the signature transcription factor Foxp3 but can be further divided into natural Tregs (nTregs) found in the thymus and

peripherally induced Tregs (iTregs). Both subsets share functional activity, however they differ in TCR repertoires, expanding TCR diversity. Tregs exert their immunosuppressive effects through the release of cytokines IL-10 and TGF-β, suppression of TCR signalling and IL-2 consumption, and induction of effector cell death by perforin and granzymes (Schmidt et al., 2012).

1.2.2. The T cell-mediated response

TCR signalling

When a T cell encounters antigens presented via APC, the TCR undergoes changes leading to a cascade of cellular pathways. For this, a fully functional TCR-CD3 complex has to be expressed on the cell surface of the effector T cell. This complex is composed of one αβTCR heterodimer and the CD3 signalling complex, comprising one CD3γε, one CD33δε, and one CD3ζζ dimer (see **Figure 1-3**). Among the CD3 subunits, the CD3ζ chains play an essential role as they harbour immune-receptor tyrosine-based activation motifs (ITAMs) in their cytoplasmic regions, which function as docking sites for the intracellular TCR signalling pathways following TCR engagement. **Figure 1-3** gives an overview of the events which happen intracellularly after target recognition. The first step of TCR signal transduction is the phosphorylation of ITAM tyrosine residues on the CD3ζ chain by the lymphocyte specific protein Lck. The Lck tyrosine kinase associates with the cytoplasmic regions of CD4 and CD8 co-receptors which cluster to the TCR when encountering MHC molecules (Barber et al., 1989). The phosphorylated ITAMs function as a docking site for the tyrosine kinase ZAP-70 (ζ-chain-associated protein), which in turn is phosphorylated by Lck as well, leading to its activation (Chan et al., 1992). Subsequently, ZAP-70 phosphorylates both the transmembrane scaffold protein

LAT (linker of activated T cells) and the adaptor protein SLP-76 (SH2-domain-containing leukocyte protein of 76 kDa). The phosphorylated proteins both then bind the adaptor protein Gads, forming the proximal signalling complex, which in succession leads to the activation of phospholipase C-γ 1 (PLC-γ 1) (Beach et al., 2007; Liu et al., 1999). This enzyme metabolises phosphatidylinositol 4,5 biphosphate (PIP-2) into the products inositol triphosphate (IP3) and diacylglycerol (DAG) The two second messenger proteins mediate T cell activation by three separate downstream mechanisms.

Firstly, DAG activates the guanine-nucleotide exchange factor RasGRP, which in turn activates Ras and the downstream mitogen activated protein kinase (MAPK) cascade. Signalling through this pathway ultimately leads to the activation of the transcription factor activator protein 1 (AP-1) (Roose et al., 2005). Secondly, DAG signalling activates protein kinase C-theta (PKC-θ), which leads to the activation of scaffold protein CARMA and the release of the nuclear factor kappa-light-chain-enhancer of activated B cells (NFκB) transcription factor (Smith-Garvin et al., 2009). Both AP-1 and NFκB translocate to the nucleus where they induce transcription of their respective target genes. AP-1 pairs with cofactor nuclear factor of activated T cells (NFAT) to provide co-stimulation and inhibit exhaustion, whilst NFκB drives inflammatory pathways.

Lastly, diffusive IP3 induces the release of calcium ions (Ca2+) from the endoplasmic reticulum (ER) into the cytosol through ligand gated Ca2+ channels and a subsequent uptake of calcium from the extracellular microenvironment. The rapid increase in cytosolic Ca2+ activates the calcium dependent regulatory protein calmodulin, which in turn activates the protein phosphatase calcineurin. This enables the release of the transcription factor NFAT through dephosphorylation and its translocation to the nucleus,

where it switches on genes crucial for T cell activation together with AP-1 (Hogan et al., 2003).

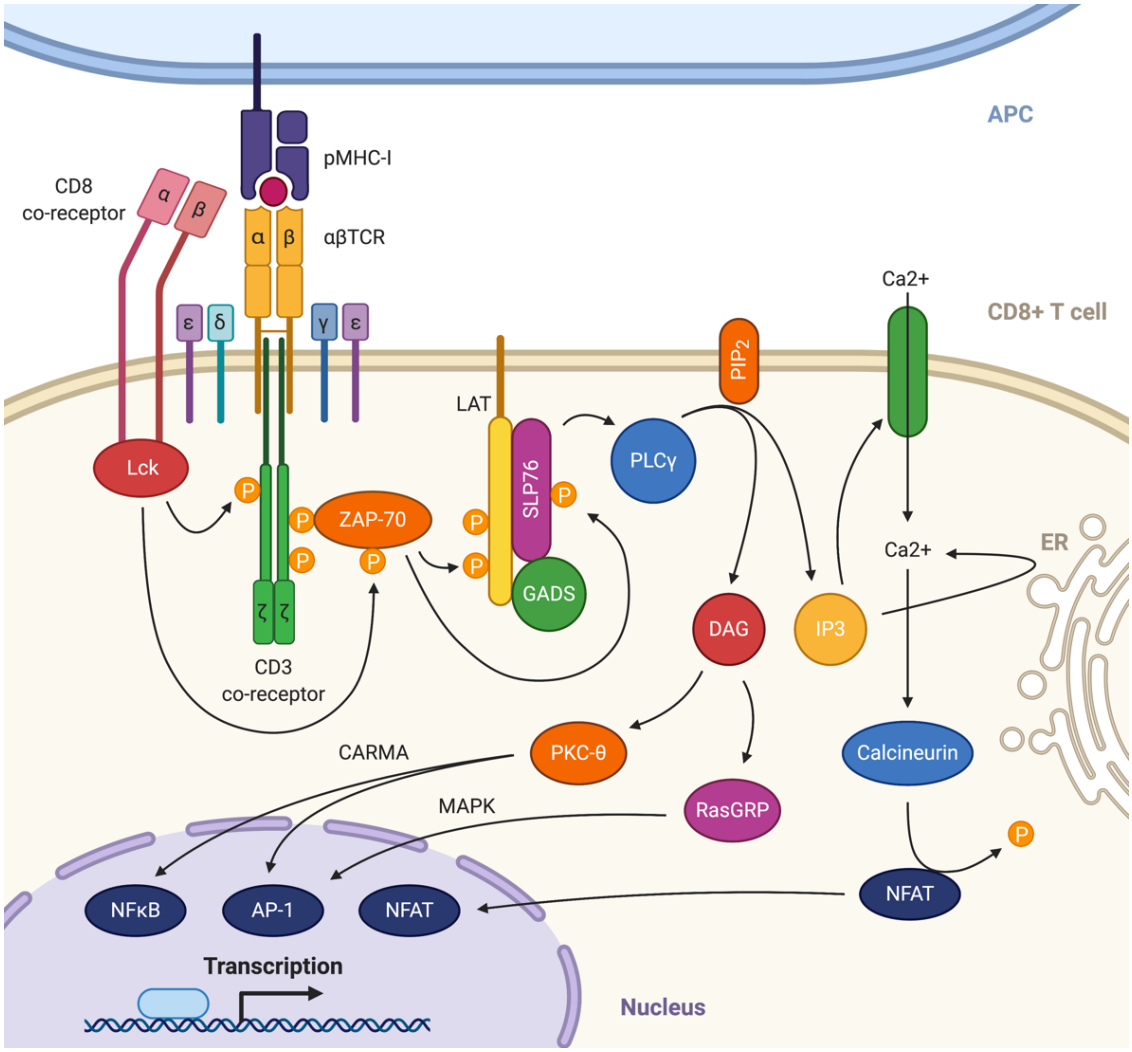

Figure 1-3 T cell receptor structure and signalling upon antigen binding. The figure displays TCR signalling in a CD8+ T cell binding antigen presented via MHC class I. When the TCR complex binds, Lck phosphorylates ITAMs on the CD3ζ chains, leading to recruitment and phosphorylation of ZAP-70. ZAP-70 then phosphorylates LAT and SLP76, which form a complex with GADS and activate PLCγ. This enables the cleavage of PIP2 into DAG and IP3, which subsequently lead to the release of transcription factors NFκB, AP-1 and NFAT into the nucleus, where they induce transcription of genes associated with cell proliferation and differentiation. Adapted from (Schwartzberg et al., 2005).

T cell activation

The previously described pathways activated by the TCR may be essential for the cellular program of T cells, however two secondary signals are needed for a complete primary activation of naïve T cells and the development of effector functions. Besides TCR signalling (signal 1), T cells need to receive co-stimulatory inputs via surface molecules expressed on APC (signal 2) and inflammatory cytokines (signal 3) secreted into the microenvironment. This initial process where a T cell is activated by the three necessary signals is described as T cell priming. Importantly, if a T cell encounters antigen presented on APC without co-stimulation through signal 2 or 3, it will result in cell anergy: a non-responsive cellular state where cells are unable to expand and acquire further effector functions. This anergic state is an important safety switch for auto-reactive T cells engaging with self-antigen (LaRosa and Orange, 2008).

The major co-stimulatory molecules providing signal 2 on T cells are CD28, which can bind CD80 and CD86 on activated APC, as well as members of the TNF receptor superfamily (41BB, CD27, OX40). Binding of the ligands induces co-stimulatory intracellular signals associated with T cell proliferation, cytokine production, and cell survival (Chen and Flies, 2013; Smith-Garvin et al., 2009). For ideal development of effector functions, T cells furthermore depend on cytokine-mediated signals. APCs, for one, support CD4+ and CD8+ T cell responses with the release of IL-1 and IL-12. Moreover, Th1 cells and other populations drive CD8+ T cell proliferation through type I IFN and IL-2. (Curtsinger and Mescher, 2010).

Once this process of priming is completed, T cells rapidly increase metabolism and proliferation, and undergo differentiation into the different T cell subtypes. Subsequent T

cell metabolism is mainly dependent on specific cytokine stimulation, including IL-2, IL-15, and IL-7 (LaRosa and Orange, 2008).

T cell regulation

To avoid overexaggerated T cell mediated responses and ensure immune homeostasis, T cell regulating pathways are crucial. Additional to the formation of central tolerance in the thymus, a peripheral tolerance of circulating T cells is ensured through Treg-mediated regulation and anergy when TCRs bind antigen without co-stimulatory signals. Besides the necessity for all three signals during T cell priming, a combination of TCR-generated signals and co-inhibitory CD28-related molecules ensure T cell regulation after activation. Examples for these regulatory co-receptors are the co-inhibitory receptor cytotoxic T-lymphocyte antigen 4 (CTLA-4) and programmed death-1 (PD-1), which limit proliferation of activated T cells to help maintain steady state (Chen, 2004). CTLA-4 shares its ligands CD80 and CD86 with the co-stimulatory receptor CD28 and thus competes for its binding. Both receptors are expressed within 24 to 48 hours after stimulation on activated T cells (Smith-Garvin et al., 2009). Furthermore, in cases of chronic inflammation an altered differentiation state, termed T cell exhaustion, can be observed. This describes the progressive loss of effector functions, induction of inhibitory receptors, faulty metabolism, and the inability to transition to quiescence in T cells, when faced with chronic antigen stimulation (Wherry and Kurachi, 2015). Although limited in their function, these cells can still halt pathogen replication, leading to a host-pathogen stalemate in case of persisting infections.

1.3. Tumour immunology

1.3.1. The role of the immune system in cancer

We now know that the immune system plays a crucial role in recognizing and destroying transformed cells as well as in the development of tumour escape mechanisms. However, this concept has changed a lot over the last century and has only most recently been revised by Schreiber and colleagues in 2011 (Schreiber et al., 2011). Hence, the following chapter is to give an overview about the formation of the immunosurveillance hypothesis and the revised concept of cancer immunoediting.

Immune surveillance

The first person to suggest the involvement of immunity in the clearance of tumours was Paul Ehrlich in the early 1900s. He predicted that without the protection delivered by the immune system, cancer would be a common occurrence in long-lived organisms (Ehrlich, 1908). This theory was only further validated 50 years later though, once more knowledge on the immune system and tumour antigens were established (Dunn et al., 2002). The demonstration of tumour-associated antigens capable of detection by the adaptive immune system was a critical argument favouring the involvement of an immune response in cancer. During the next two decades Sir Macfarlane Burnet and Lewis Thomas formed the "cancer immunosurveillance" hypothesis, which suggested that adaptive immunity was constantly preventing cancer formation in immunocompetent hosts and therefore eliminated the tumours before any clinical symptoms (Burnet, 1970, 1957; Thomas and Lawrence, 1959). It was assumed that lymphocytes were acting as key players in this process.

With the promise of proving the hypothesis, experiments followed trying to demonstrate increased incidences of cancer in hosts with impaired immunity. However, subsequent

studies performed by Stutman and colleagues showed no evidence for a difference in cancer susceptibility between immunocompetent mice and CBA/H strain nude mice with major immunodeficiency. This was found similarly for both spontaneous and carcinogen-induced tumours (Stutman, 1975). Taken together with inconclusive studies performed by others, scientists failed to either prove or disprove the concept of immunosurveillance. Critics of the hypothesis argued that this was due to a lack of "danger signals" and of “non-self” signals on cancer cells, making them too similar to healthy host cells (Schreiber et al., 2011). It is now understood that nude mice of the used strain are not fully immunocompromised and have a detectable population of αβT lymphocytes. With no means to further investigate the reasons behind these findings, the immunosurveillance hypothesis thus was abandoned in the following years.

Only years later in the 1990s the concept was reassessed, when improved immune-deficient mouse models with pure genetic backgrounds became more established. A new interest in the role of the immune system in cancer control was ignited by the discovery that IFN-γ was promoting the rejection of transplanted tumours through immunological processes, and by experiments showing that mice lacking IFN-γ responsiveness or adaptive immunity altogether were more susceptible to induced and spontaneous cancer formation (Dunn et al., 2002). With others confirming these findings, it became collectively accepted that the adaptive immune system acts as a tumour suppressor, mediated through protection against virus-induced tumours, prevention of the inflammatory environment that facilitates tumorigenesis, and the directed elimination of tumour cells (Schreiber et al., 2011).

Immunoediting

Despite having an active immune system that is technically capable of recognising and eliminating tumour cells, immunocompetent individuals still can develop cancer. Firstly, some monogenic- and epigenetic-driven cancers might display so few neoantigens that they are barely immunogenic from the start. However, studies investigating the immunogenic characteristics of tumours grown in the presence or absence of a working immune system have shown that those formed under the pressure of an active immune response can establish progressively growing tumours when transplanted into another immunocompetent host, while those arising in a system lacking immunity are rejected, implying higher immunogenicity (Shankaran et al., 2001). This formed a first understanding of how the immunologic environment can shape cancer cells towards a non-immunogenic phenotype, thus creating tumours that are better equipped to escape the immunosurveillance. The combination of the selective pressure through immune detection and the inherent genetic instability of tumours can result in changes in genes encoding tumour antigens, components of the major histocompatibility complex (MHC) pathways, or components of the IFN-γ receptor signalling pathway (Dunn et al., 2002; Lengauer et al., 1998). The process is thought to occur at the early stages of cancer formation, when the tumour is not yet clinically detectable, suggesting that the immunogenicity of tumours at the point of diagnosis is often already imprinted by the immune system of the host.

These findings led to a revision of the described role of the immune system in cancer, acting not only via host-protective but also tumour-promoting processes. Schreiber and colleagues postulated a major amendment of the immunosurveillance hypothesis, summarising the sculpting effects of the immune system on tumours under the term cancer immunoediting (Dunn et al., 2002; Schreiber et al., 2011). Generally, the

immunoediting process can be described in three sequential phases that were termed "elimination", "equilibrium", and "escape" (see **Figure 1-4**). However, tumour cells don't always proceed through all three phases, so that sometimes they directly skip into the equilibrium phase or never continue to the escape phase. Additionally, external factors, such as environmental stress, ageing, or even therapeutic effects can influence the flow through immunoediting steps (Schreiber et al., 2011).

The first phase, termed elimination, is an integration of immunosurveillance within the new concept. It describes the process in which adaptive and innate immunity work together to detect and destroy developing tumour cells (see **Figure 1-4**, 1). The exact mechanisms of engagement are not completely understood. Among the suggested initiators are Type I IFNs produced during early tumour development, which act as classical danger signals capable of inducing the innate system and antigen presentation via dendritic cells, ultimately promoting the activation of adaptive immune responses (Matzinger, 1994). Furthermore, apoptotic tumour cells and surrounding damaged tissues release damage-associated molecular patterns (DAMPs) as well as express stress ligands, such as MICA/B (Guerra et al., 2008; Sims et al., 2010). These factors then induce an innate immune response, leading to formation of a pro-inflammatory microenvironment via the release of cytokines, which in turn facilitates engagement of the adaptive immune system. However, for the establishment of an effective immunosurveillance the adaptive immune system has to be additionally stimulated through tumour antigens expressed on cancer cells. Only then the tumour cells will be attacked, and – if completely eradicated – this marks the endpoint of the immunoediting process.

Despite initiation of innate and adaptive immune responses, some tumour cells may survive the elimination phase and enter a dynamic equilibrium. At this stage tumour

outgrowth is prevented by the adaptive immunity, which simultaneously pressures the tumour immunogenicity towards non-immunogenic variants (see **Figure 1-4**, 2). Equilibrium can persist for a long span of time and can act as a second stable endpoint of immunoediting through the life of the host. The remaining tumour cells at this stage are dormant and thus may reside in the host for indefinite time, unless they manage to escape immunosurveillance and eventually resume growth in the form of recurrent primary tumours or metastases (Aguirre-Ghiso, 2007). Analysis of dormant tumours revealed that the adaptive immune system, but not the innate immunity, was responsible for maintaining the equilibrium stage, hence clearly distinguishing this phase from the initial elimination where both arms of immunity play a crucial role (Schreiber et al., 2011).

The activated lymphocytes exert enough pressure to contain the tumour population, but not fully eliminate it, resulting in a Darwinian selection pressure on the genetically unstable and rapidly mutating cancer cells towards increasingly resistant variants. Once a sufficient insensitivity to detection or destruction by the immune system is established, tumour variants can expand in an uncontrolled manner, which marks the beginning of the escape phase of cancer immunoediting where clinically detectable tumours appear (see **Figure 1-4**, 3). Mechanisms through which tumour cells can evade immunity are reviewed in the next chapter.

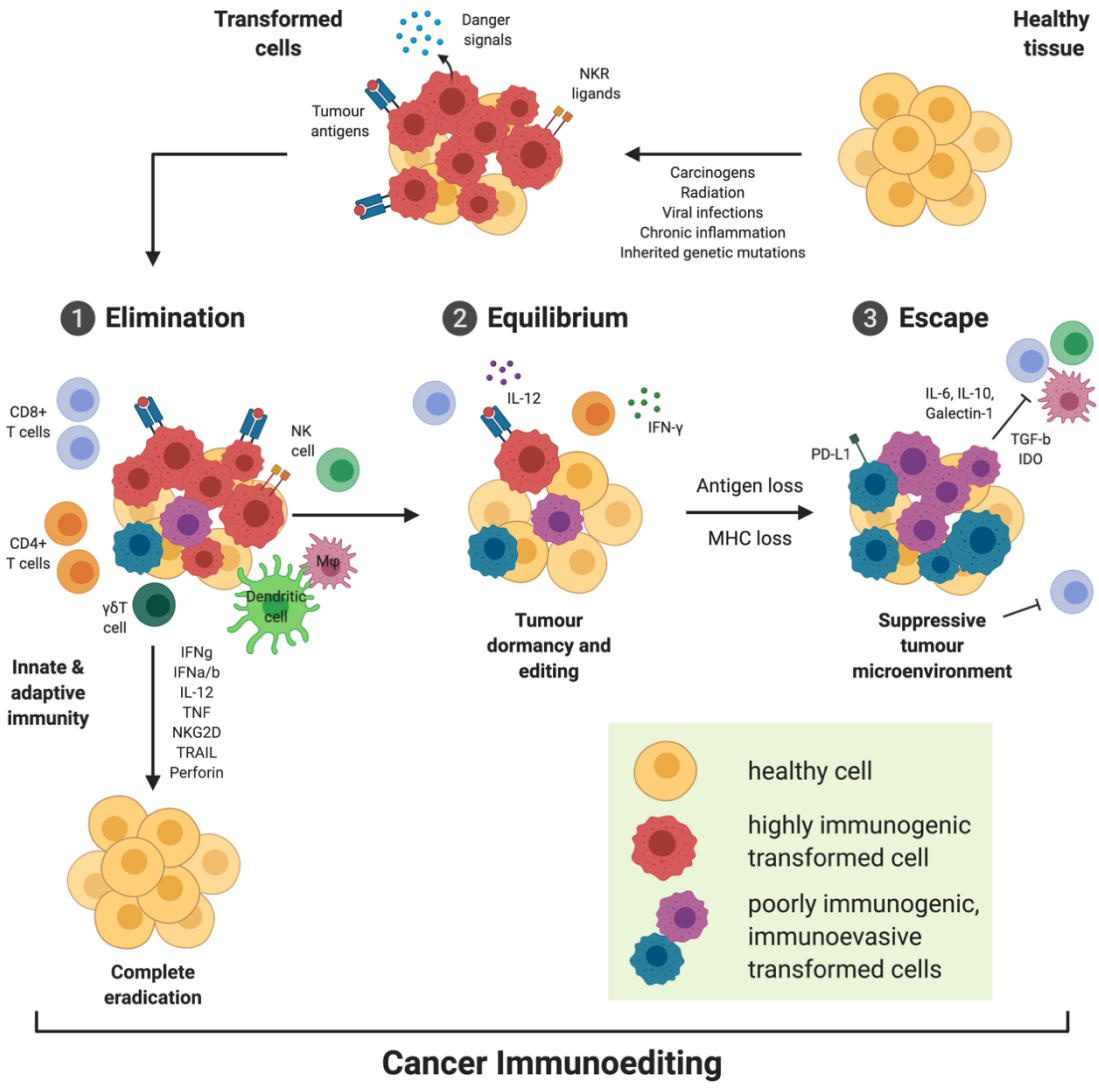

Figure 1-4 Cancer immunoediting as defined by its three phases elimination, equilibrium, and escape. In the elimination phase innate and adaptive immunity combine their effects to destroy developing tumours. If the tumour is completely eradicated this marks the end of the process. Otherwise, the site will continue to the equilibrium phase, in which cancer cell outgrowth is prevented by mechanisms mediated by adaptive immunity, resulting in cell dormancy. This can mark another endpoint. Selective pressure towards editing of tumour immunogenicity however can result in the emergence of tumour cells capable of immune evasion. In the escape phase tumour cells can grow exponentially due to loss of antigen recognition, insensitivity to immune effector mechanisms, or the establishment of an immunosuppressive microenvironment. Only when the last stage is reached, clinically apparent disease will form. Adapted from (Schreiber et al., 2011).

1.3.2. Mechanisms of tumour escape

Immune evasion can be achieved through an alteration of the tumour cells themselves as well as through the establishment of an immunosuppressive environment, in which the adaptive immune system becomes inhibited enough for tumour cells to show net tumour growth. Alterations at the tumour cell level include increases in the resistance to cytotoxic pathways used by the adaptive immunity, for example through induction of anti-apoptotic mechanisms, as well as changes leading to reduced immune recognition. A common and well-studied mechanism to escape surveillance by the immune system is the loss of tumour antigen expression, which can occur via three ways. Firstly, tumour cells lacking antigens associated with strong immune rejection can accumulate amidst the selective pressure in the tumour bed. Furthermore, cancer cells often lose expression of proteins involved in the formation of MHC class I, thus escaping antigen-presentation necessary for T cell activation. Lastly, defects in the antigen processing machinery, which is necessary for the production of the antigenic peptide epitope, can lead to failure to load peptides onto MHC class I molecules and similarly prevent presentation (Khong and Restifo, 2002; Vesely et al., 2011).

Alternatively, tumour cells can escape equilibrium once the mediators of adaptive immunity are suppressed enough in their functions, which can result from the establishment of an immunosuppressive tumour microenvironment (TME). The microenvironment of tumours spans a large array of cellular and non-cellular components, including inflammatory cells of the innate and adaptive immune system, vascular components, fibroblastic cells, and the extracellular matrix (ECM). The immunosuppressive niche can be initiated through the production of an array of immunosuppressive factors by the tumour cells, such as vascular endothelial growth factor (VEGF), TGF-β, and galectin-1 (Vesely et al., 2011). An important enzyme found

in the TME is indoleamine-2,3-dioxygenase (IDO), which catabolises tryptophan and generates kynurenine. Both a local deprivation of the essential amino acid tryptophan and the generation of kynurenine contribute to an inhibition of T cell proliferation (Munn and Mellor, 2013). The cumulative effects of IDO activity and the humoral milieu in the tumour niche pushes recruited immune towards immunosuppressive phenotypes, which adds further to the tumour-protective effects of the TME. The non-transformed cellular elements of the TME are described in more detail in the next chapter.

1.3.3. The tumour microenvironment and specific insights in neuroblastoma

The tumour microenvironment is an integration of various tumour-defined factors, including the individual genetic alterations of the tumour, the recruitment and activation of non-transformed components of the TME, and the cytokine milieu (see **Figure 1-5**). Therefore, it is not unusual to encounter differences in TME compositions across cancer types, patients, and even when comparing individual tumour sites within the same patient (Galon and Bruni, 2019).

In general, the microenvironment of cancer is characterised by its highly inflammatory state, which is a consequence of inflammatory cytokines released by the tumour cells themselves (TH1 cytokines, TGF-β, VEGF) but also by alternatively activated non-transformed cells recruited to the tumour proximity (Quail and Joyce, 2013). Presenting with an altered phenotype and skewed to an immunosuppressive functional profile, cellular components of the TME – including stromal cells, neovascular cells, and immune effectors – actively contribute to carcinogenesis, tumour progression, and metastasis of cancer (Kerkar and Restifo, 2012).

Vasculature

Besides dictating the hypoxic state that has effects on a variety of cellular components of the TME, studies have revealed that the tumour-vasculature can also actively exclude T cells. This is mediated through the expression of apoptosis-inducer FasL on endothelial cells, which is induced by the local factors VEGF, IL-10, and prostaglandin E2 (PGE2). Furthermore, it has been suggested that expression of the ligand selectively only eliminates CD8+ T cells from the TME, while Tregs are protected from apoptosis through the higher expression of the anti-apoptotic factor c-FLIP (Motz et al., 2014). This has been observed in multiple tumour types, such as breast, ovarian, colon, bladder, prostate, and renal cancer.

Cancer-associated fibroblasts

In healthy connective tissues, fibroblasts are responsible for depositing ECM and basement membrane components, modulating immune responses, and mediating homeostasis (Kalluri and Zeisberg, 2006). In the TME however, a population of alternatively activated fibroblasts can be found – cancer-associated fibroblasts (CAFs) accumulate in high numbers at cancer sites and promote tumour formation. This has been supported by findings that epithelial cells, when co-injected with CAFs, can give rise to tumours in mice, which wasn't the case when cells were co-injected with healthy prostatic fibroblasts (Olumi et al., 1999). CAFs are activated by growth factors and cytokines in the tumour proximity, such as TGF-β, and provide a major source of tumour-supporting growth factors, including angiogenic factors such as VEGF (Quail and Joyce, 2013). Furthermore, they regulate the spatial distribution of infiltrating T cells within the tumour, preventing engagement with tumour antigens. This is mediated by CAFs both through increased production of ECM components closer to the tumour and the biosynthesis of

CXCL12, which forms protective coats around tumour cells thus excluding T cell interactions (Joyce and Fearon, 2015).

Regulatory T cells

Tregs play an important role in the regulation of immune responses to ensure homeostasis and peripheral tolerance. Therefore, when activated by the TME, they can exert crucial immunosuppressive functions and heavily contribute to tumour evasiveness. Increased local production of suppressive cytokines by Tregs, such as TGF-β and IL-10, hinders anti-tumour responses from both adaptive (CD4+ and CD8+ T cells) and innate (NK cells) effectors. Moreover, Tregs express high affinity receptors for important cytokines involved in the activation of other immune effectors, such as IL-2, IL-7, IL-12, and IL-15. This leads to an increased consumption of local cytokines and decreased availability for anti-tumour functions of cytotoxic T cells (Kerkar and Restifo, 2012). Lastly, Tregs express inhibitory co-receptors, such as CTLA-4 and PD-1. Due to a higher binding affinity, CTLA-4 on Tregs outcompetes CD28 receptors on effector T cells in binding to ligands of the B7 family (CD80 and CD86), which are found on APCs. This causes both decreased CD28-dependent signalling in T cells, thus leading to anergy, and depletion of B7 ligands on APCs through sequestration (Rotte, 2019). PD-1 on Tregs engages with PD-L1 on tumour cells, which significantly supports Treg induction and proliferation while inhibiting T cell responses (Dong et al., 2016).

Myeloid cells

A heterogeneous group of myeloid cells, including dendritic cells (DCs), tumour-associated macrophages (TAMs) and MDSC, contribute to the inflammatory TME and further inhibit T cell functions. Hypoxic conditions inside the tumour adversely affect

infiltrated myeloid cell phenotypes and functions, and induce PD-L1 expression on cell surfaces (Noman et al., 2014).

DCs in the TME present with impaired antigen-presenting machinery, failing to activate recruited T cells to the same degree as under non-pathologic conditions. This can be attributed to the milieu found in the tumour proximity, with VEGF, M-CSF, GM-CSF, IL-6, IL-10 and gangliosides among reported factors contributing to altered DC differentiation (Kerkar and Restifo, 2012). Additional to defects in the antigen-presenting pathways, tumour-altered DCs also downregulate MHC class I and II molecules and express lower levels of costimulatory molecules needed for T cell priming (Gabrilovich, 2004). Moreover, DCs can also express IDO, which leads to further suppression of T cell effector functions (Munn et al., 2002).

The alternatively activated macrophages in the TME are either tissue-resident or derived from peripheral locations such as the bone marrow and can generally be described as polarised towards an M2-altered profile. While classically-activated M1 macrophages are considered critical effectors during immune responses and are involved in release of pro-inflammatory cytokines, antigen presentation, and elimination of pathogens, the M2-type presents a immunoregulatory version with lower production of proinflammatory cytokines but increased release of immunosuppressive factors, such as IL-10, TGF-β, and VEGF (Sica and Bronte, 2007). Macrophages are recruited to the TME due to the upregulation of macrophage chemoattractants, such as endothelin-2 and VEGF, and the M1-to-M2 transition is suggested to be caused by the local tumour hypoxia (Quail and Joyce, 2013). TAMs lose their ability to mediate target cell lysis and, similar to DCs, are perturbed in their function as APCs, therefore fail to prime T cells (Kerkar and Restifo, 2012).

A third prominent myeloid subpopulation in the TME are MDSC, which represent a heterogeneous population of immature myeloid cells with distinct immunosuppressive potential. It has been shown that accumulation of MDSC in the peripheral blood can be an indicator for the clinical outcome of the therapy of cancer patients (Najjar and Finke, 2013), thus they are considered a key factor in the cancer-induced suppression of the immune system. Since this thesis is focussing on overcoming the effects of MDSC in neuroblastoma, their biology and effects will be discussed more extensively in chapter 1.3.4.

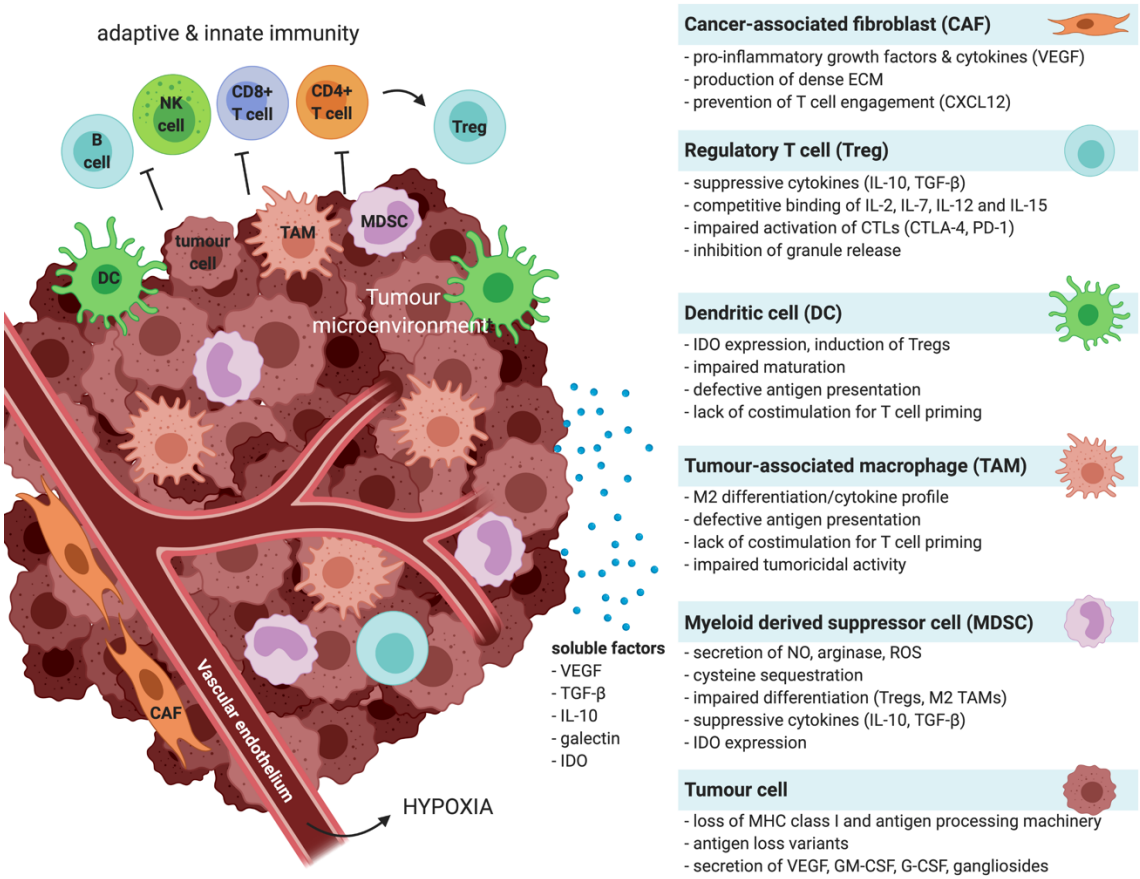

Figure 1-5 Immunosuppressive mechanisms of the tumour microenvironment. Established tumours consist of a wide variety of recruited and alternatively activated immune cells that contribute to the immunoinhibitory niche of the tumour stroma. Suppressor cell types include vascular endothelial cells, CAFs, myeloid cells (TAM, DC, MDSC), and lymphocytes (Tregs). Through the combination cell-mediated mechanisms and soluble effectors the tumoricidal effects from both adaptive and innate immunity are evaded. Adapted from (Kerkar and Restifo, 2012).

The tumour microenvironment of neuroblastoma

Several key cellular players have been identified in the microenvironment of neuroblastoma. The proximity of neuroblastoma lesions is characterised by a high concentration of soluble molecules TGF-β, IL-10, and galectin-1 (Vanichapol et al., 2018). Furthermore, it has been described that hypoxia is linked to more aggressive phenotypes in neuroblastoma patients and can be a marker of disease progression (Applebaum et al., 2016). Together, these factors contribute to a tumour niche capable of accumulating potent immune suppressors. Thus, it has been reported that tumour sites in transgenic TH-MYCN mouse models with spontaneously forming high-risk neuroblastoma undergo a transition from high lymphocyte infiltration within early tumours to an majority of suppressive myeloid populations and lymphocyte inhibition in progressed lesions (Carlson et al., 2013). These findings were confirmed in a immunohistochemical study of human tumour samples, demonstrating a heavy infiltration of CD68+ myeloid cells in neuroblastoma and other paediatric solid cancers (Apps et al., 2013). Analysing tumours from neuroblastoma mouse models and patients have further characterised these myeloid populations to harbour both M2-like TAMs as well as MDSCs (Asgharzadeh et al., 2012; Santilli et al., 2013b, 2013a). Additionally, a 14-gene signature associated with poor prognosis has been derived from expression array analysis of neuroblastoma tumours. The results contained five genes reflecting the TME of neuroblastoma: *CD14*, *CD33*, *IL-10*, *CD16*, and *IL-6R* (Asgharzadeh et al., 2012). This strongly underlines the importance of myeloid cells (*CD14, CD33*, *CD16*); moreover *IL-10* and *IL-6R* are genes that can also be activated as a result of myeloid-associated suppression.

Neuroblastoma cells themselves have been described to evade or suppress immune surveillance in several ways. A lower expression of MHC class I molecules and defects

in the antigen-presenting machinery contribute to escape from the adaptive immune response, while the release of soluble forms of NKG2D ligands, such as MICA and MICB, blocks recognition by innate lymphocytes (Vanichapol et al., 2018). Additional to arginase 1 (Arg1) expressed by myeloid cells in the TME, neuroblastoma cells themselves have been reported to produce arginase 2 (Arg2), cumulatively depleting the tumour environment of the semi-essential amino acid L-arginine (Mussai et al., 2015). The local and systemic depletion leads to a down-regulation of the CD3ζ chain on T cells and an arrest of the proliferation of activated T lymphocytes (Rodriguez et al., 2004). Additionally, the high activity of Arg2 contributes to the cumulative effects of tumour-specific growth factors and cytokines, pushing recruited immune and stromal cells towards immune-inhibitory phenotypes. This has been supported by findings that monocytes can be polarised towards immunosuppressive functions when conditioned with arginine-depleted neuroblastoma medium, indicating a significant influence of arginase activity on the differentiation processes in the TME (Mussai et al., 2015).

1.3.4. Myeloid-derived suppressor cells in cancer

MDSC subpopulations in mice and human

MDSC were first described in tumour-bearing mice, based on expression of the surface markers CD11b and Gr-1. There are two defined subtypes found in mice, Ly6G-positive granulocytic MDSC and Ly6C-positive monocytic MDSC (see **Table 1-1**) (Shipp et al., 2016). The phenotype of MDSC in human however is harder to define, since human MDSC lack the expression of the specific marker Gr-1. Generally, human MDSC can be described as CD33+ CD11b+ HLA-DR low/negative (Najjar and Finke, 2013), however the heterogeneous population consists of various subtypes that can be allocated to at least

three main subsets: monocytic MDSC (M-MDSC), polymorphonuclear MDSC (PMN-MDSC) and the poorly-defined early-stage MDSC (eMDSC) (Mandruzzato et al., 2016) (see **Table 1-1**). Currently, there are no markers unique to human MDSC. Hence, the subpopulations can only be defined by a mixture of myeloid surface proteins that individually cannot distinctively discriminate them from other myeloid cell types. Because of this lack of unique phenotype, a second crucial step for the identification of MDSC is the investigation of their ability to suppress immune cells in functional assays (Bronte et al., 2016).

MDSC in cancer

In healthy individuals immature myeloid cells exist in low numbers in the bone marrow and spleen and are involved in the regulation of immune responses and tissue repair, only expanding upon signals such as infection or inflammation (Draghiciu et al., 2015a). In the course of myelopoiesis these immature cells differentiate into granulocytes, macrophages and dendritic cells. Physiological myelopoiesis is driven by GM-CSF, together with G-CSF and M-CSF, which induce differentiation into granulocytes and macrophages, respectively (Veglia et al., 2018). In cancer the TME changes cytokine homeostasis towards an overproduction of these key factors, leading to defects in myelopoiesis and the accumulation of immature myeloid cells (Serafini et al., 2006a). Tumours and chronic inflammation provide low and constant levels of danger signals involved in the classical activation of myeloid cells, such as Toll-like receptor ligands as well as damage- and pathogen-associated molecular patterns, generating pathologically activated monocytes and neutrophils (Veglia et al., 2018). Together with growth factors and inflammatory mediators, the tumour thereby induces a rapid expansion of immature monocytes in the bone marrow (Gabrilovich and Nagaraj, 2009), followed by a

recruitment to the tumour site by chemoattractants such as CCL2, CXCL12 and CXCL15 (Sawanobori et al., 2008).

In tumour-bearing mice the prevalent subpopulation seems to be PMN-MDSC (Gabrilovich et al., 2012), and also in many types of human cancers, the PMN-MDSC subset represents over 80% of all MDSC (Gabrilovich, 2017). It has been reported that in mice both subpopulations have similar per cell suppressive activity, but that the predominant mechanisms of action differs between the subtypes (Youn et al., 2008). The frequency of each subset appears to be cancer-specific, with more PMN-MDSC found in patients with renal cancer, and more M-MDSC in patients with melanoma, multiple myeloma, prostate cancer, hepatocellular carcinoma, and head and neck cancer (Gabrilovich et al., 2012).

In general, granulocyte-like PMN-MDSC represent the main population in circulation and the peripheral lymphoid organs, whereas monocyte-like M-MDSC can predominantly be found in the tumour proximity. The distinct suppressive potential of M-MDSC leads to a strong immunosuppressive niche in the TME (Kumar et al., 2016). An autocrine feedback loop of IL-6 and the proteins S100A8/A9 sustains the population of MDSC in the tumour environment (Najjar and Finke, 2013). Additionally, M-MDSC can rapidly differentiate into TAMs when close to the tumour (Kumar et al., 2016), further contributing to the variety of suppressive cells.

MDSC subpopulation	Phenotype in human	Phenotype in mouse	Predominant effector functions
Total MDSC	N/A	Gr-1+ CD11b+	nutrient depletion, oxidative stress, lymphocyte trafficking inhibition, Treg induction
PMN-MDSC	CD14- CD11b+ CD15+/CD66+	CD11b+ Ly6C^{low} Ly6G+	ROS production
M-MDSC	CD11b+ CD14+ HLA-DR$^{low/-}$ CD15-	CD11b+^{t} Ly6C^{high} Ly6G-	NO production (iNOS), arginine depletion (Arg1)
eMDSC	Lin- HLA-DR-/CD33+	N/A	N/A

Table 1-1 Myeloid derived suppressor cells subpopulations, their phenotype and primary localisation. Adapted from (Bronte et al., 2016).

Suppressive mechanisms of MDSC

MDSC have a range of redundant mechanisms that form their immunoinhibitory function, which are shared among the known subpopulations, albeit to different extents. As a result, MDSC actively suppress infiltrating effectors while also providing signals to recruited immune cells for a differentiation towards suppressive phenotypes. Generally, all MDSC are able to function via the described mechanisms (Bronte et al., 2016), however it has been observed that subtype and location can influence which mechanism will be the predominant way of suppression (Kumar et al., 2016). The plethora of mechanisms can broadly be grouped into four key effects of suppression.

Firstly, MDSC are capable of depleting essential lymphocyte nutrients, such as L-arginine through Arg1 activity and L-cysteine through its sequestration (Rodriguez et al., 2004; Srivastava et al., 2010). Absence of L-arginine leads to defects in the formation of the ζ-chain of the TCR complex in T cells and subsequently decreased production of cytokines IFN-γ, IL-5, and IL-10 as well as proliferative arrest (Zea et al., 2004). Arg1 furthermore

reinforces T cell dysfunction through cell cycle arrest in the G0-G1 phase through L-arginine starvation (Rodriguez et al., 2007). Secondly, oxidative stress is generated via the release of reactive oxygen species (ROS) and reactive nitrogen species (RNS) through the combined activity of phagocytic oxidase, Arg1 and iNOS (Gabrilovich et al., 2012). Subsequent reactions with these reactive species cause effects such as ζ-chain downregulation, interference with IL-2 signalling and desensitisation of the TCR in T cells. Furthermore, they reduce antigenic peptide binding on MHC molecules on tumour cells and block T cell migration through chemokine nitrification (Gabrilovich, 2017). The third aspect of suppression mediated by MDSC is an interference with lymphocyte trafficking and viability. For example, recirculation to lymph nodes is inhibited via ADAM17 on MDSC which decreases L-selectin expression on T cells (Hanson et al., 2009). Moreover, MDSC can modify CCL2, impairing the chemoattractant for signalling CD8+ T cell migration to the tumour core (Molon et al., 2011). Finally, MDSC also play into the activation and expansion of another predominant population of suppressive immune cells. Not only do MDSC support expansion of antigen specific natural Tregs but they also promote differentiation of naïve CD4+ T cells into induced Tregs. Suggested in this process are cell-to-cell interactions, such as CD40-CD40L (Pan et al., 2010), tryptophan starvation via IDO activity, and production of soluble factors IL-10 and TGF-β by MDSC (Fleming et al., 2018; Huang et al., 2006).

The prevalent subtype found in the peripheral lymphoid organs are PMN-MDSCs. The key suppressive mechanism in this subpopulation is the production of ROS. Because of the short-lived nature of these factors, close cell-to-cell contact is achieved via antigen-specific interaction with T cells (Gabrilovich et al., 2012; Nagaraj et al., 2010a). In close proximity to the tumour, more M-MDSC are found, which produce high amounts of RNS, such as nitric oxide (NO), and immunoregulatory cytokines, both having longer half-

lives. Thus, MDSC in the TME are less dependent on cell-to-cell contact. Through Arg1 activity, they additionally contribute to the local depletion of essential amino acids, forming a potent suppressive environment which makes the tumour a particularly T cell inhibitory location (Dolcetti et al., 2009).

However, the overall consensus is that the prevalence of suppressive mechanisms mediated by MDSC is not only dependent on the predominant subtype, but also on disease stage and tumour site, and could change throughout progression of the disease.

1.3.5. Predictors of response to active immunotherapy

To re-establish an immune system capable of detecting and eliminating immune-evasive tumours, active and passive immunotherapy approaches have been developed. Active immunotherapies, such as the use of checkpoint inhibitors, aim to support the existing host immune response through provision of additional activating stimuli or circumvention of the suppressive effects found in the tumour proximity. Thus, active immunotherapy heavily relies on unleashing a pre-existing adaptive immune response in the host and will fail in the absence of sufficient target antigens for systemic tumour reactivity. In contrast, passive immunotherapy is based on providing the patient with potent, sometimes genetically modified cells or adjuvants to combat cancer, without generating new host adaptive immunity (Galluzzi et al., 2014). Different active and passive immunotherapy concepts are reviewed in more detail in chapter 1.4. Consequently, especially in the light of active immunotherapy, it is crucial to know the immunogenicity of a tumour before administering therapy, to avoid inefficient treatments.

Due to the effects of immunoediting, tumours can present with insufficient or non-existing adaptive immune cell infiltration. Because of this, it has become common practice to classify tumours as "hot" or "cold", based on the presence or absence of intratumor immune cells. First to describe the immune profiles of tumours as hot, altered, and cold were Camus and colleagues in 2009. They reported that the 2-year risk for relapse in colorectal cancer was heavily associated with the availability and quality of tumour-infiltrating immune cells, being 10%, 50%, and 80%, in cold, altered, and hot tumours, respectively (Camus et al., 2009). Recently, Galon and colleagues have amended the altered category into altered-excluded and altered-immunosuppressed (Galon and Bruni, 2019). Furthermore, they have introduced "immune contexture" as a prognostic concept, which in sum refers to nature, density, immune functional orientation, and distribution of immune cells within the tumour, all factors shown to be associated with long-term survival and prediction of response to treatments (Galon et al., 2013).

Typical characteristics of hot tumours are the presence of tumour-infiltrating lymphocytes (TILs), genomic instability, expression of anti-programmed death-ligand 1 (PD-L1) on local immune cells, and a pre-existing antitumour immune response with markers of inflammation. In contrast, cold tumours are non-inflamed, poorly infiltrated, scarcely express PD-L1, and show high proliferation with low mutational burden. Furthermore, they severely lack antigen presentation markers, such as MHC class I (P. S. Hegde et al., 2016). Altered phenotypes include altered-excluded with T cell infiltration stopping at the margin of tumour sites due to physical barriers, and altered-immunosuppressed, where few numbers of infiltrating lymphocytes can be found in the tumour site, but further recruitment is limited by the immunosuppressive TME (Galon and Bruni, 2019). A positive correlation between the presence of TILs and patient

survival has been observed in many types of cancers including breast, melanoma, colorectal, ovarian, and neuroblastoma (Dunn et al., 2002; Palma et al., 1978).

Various escape mechanisms can ultimately affect T cell infiltration into the tumour site. One of them is the lack of tumour antigens, which can be explained by a lower tumour mutation burden (TMB) and decreased inflammation in cold tumours. A higher TMB is associated with higher expression of neoantigens, defined as immunogenic antigens found only in cancer cells and not in healthy tissues. The TMB describes the total number of mutations per coding area of a tumour genome and has been shown to predict responses to active immunotherapy in various cancers (Yarchoan et al., 2017). A second reason for insufficient activity of immune effectors in cold tumours is insufficient T cell priming and activation. Reasons for this include defects in antigen presentation because of reduced recruitment of dendritic cells and other APC to the tumour proximity, and incomplete T cell activation due to a lack of co-stimulatory signals expressed by APC during T cell priming (Bonaventura et al., 2019). Lastly, T cell homing can be reduced either physically through the peritumoral stroma and/or biochemically through decreased production of the cytokines and chemokines that can promote DC trafficking, and the subsequent lack of DC-produced chemokines, such as CXCL16 (Bonaventura et al., 2019).

While in adult cancers both hot and cold tumours are relatively common, childhood solid cancers typically are considered immunologically cold (Downing et al., 2012). A likely reason for this is lower TMB, secondary to oligogenic hit aetiology, leading to less neoantigens and thus less immunogenicity. Childhood solid tumours, such as neuroblastoma, are thus characterised by less TILs, a higher number of suppressor cells in the TME, and lower expression of checkpoint signals such as PD-1/PD-L1 (Pistoia et al., 2013; Voeller et al., 2019). Exceptions of hot tumours can be seen in some childhood

cancers, for example Hodgkin disease, where viral antigens can induce T cell responses, or rare childhood cancers such as high-grade glioma with a hypermutator phenotype, where a high TMB is observed (Anderson, 2017).

Overall, this indicates a need for improved passive immunotherapies to overcome the lack of adaptive immune infiltration and activation in childhood solid tumours. The following section will give an overview about existing approaches and novel concepts.

1.4. Cancer immunotherapy

Immunotherapy is now considered the fourth pillar of cancer treatment and advances in research have turned it into one of the most rapidly growing drug classes (Galon and Bruni, 2019). Moreover, cancer immunotherapy just recently gained particular public interest, when the 2018 Nobel Prize in medicine was awarded to James P. Allison and Tasuku Honjo for their advances in the research of checkpoint inhibitors. Even though the field has grown rapidly in the last three decades particularly, first works harnessing the immune system for therapeutic effects have been documented as early as the late 19th century.

Known as the Father of Immunotherapy, in 1891 William B. Coley injected patient tumours with mixtures of live and inactivated *Streptococcus pyogenes* and *Serratia marcescens*, after noting spontaneous remissions in sarcoma patients following bacterial wound infections. The so-called "Coley's toxins" yielded durable complete remissions in several types of tumours including lymphoma, sarcoma, and testicular carcinoma, with a total of over 1,000 treated patients documented to experience regression or complete cure. However, the risks associated with deliberately infecting cancer patients with pathogens led to an unanimous decision among oncologists to maintain surgery and radiotherapy as standard treatments (Decker and Safdar, 2009). The concept of using bacteria to induce immune reactions was only picked up almost a century later, with a trial investigating the preventative effects of the tuberculosis vaccine Bacille Calmette-Guérin (BCG) on recurring non-muscle invasive bladder cancer in 1976 (Morales et al., 1976). The underlying mechanism of BCG therapy has proven to be mediated by an activation of macrophages in the tumour proximity and is still used as a standard treatment for non-muscle invasive bladder cancer today.

Key events, such as Thomas and Burnet's proposal of cancer immunosurveillance in 1957 (Burnet, 1957) and the identification of IL-2 and its role in supporting T cell mediated tumour regression in 1976 and 1985 (Morgan et al., 1976; Rosenberg et al., 1985), revived the interest in the interplay between the immune system and cancer, and thus the option to exploit these interactions for therapeutic effects. In the 1970s, Milstein and Köhler were the first to generate monoclonal antibodies (mAb) using hybridomas – antibody-secreting cell lines originating from fused lymphocytes and myeloma cell lines (Köhler and Milstein, 1975). The ability of these antibodies to specifically detect tumour markers and subsequently block or induce cellular responses laid the groundwork for various fields of immunotherapy today.

1.4.1. Active and passive immunotherapy approaches

Immunotherapeutic approaches can be classified as either active or passive, depending on whether their effects rely on engaging the host immune system or not.

Passive forms of immunotherapy have intrinsic antineoplastic activity and therefore can act efficiently even when the patient's immune response is suppressed by the TME or when tumours exhibit insufficient effector infiltration. Approaches fitting into the category of passive immunotherapy are adoptive cell transfer – including TCR or CAR-engineered T cells – and tumour-targeting mAb.

In contrast, active immunotherapies exert no intrinsic cytotoxic effects and act through engagement of adaptive or innate immune effectors. Examples for active immune therapies are immunostimulatory cytokines, cancer vaccines, checkpoint inhibitors (CPI), and immunomodulatory mAb.

The following sections will describe selected immunotherapeutic treatments in more detail.

Cancer vaccines

Vaccinations are based on the concept of enhancing immune responses by teaching immune cells to recognise pathogen-associated markers and thus form immunological memory for future encounters of the same pathogen.

Ruth and John Grahams were the first to work on cancer vaccines in 1959. In their study investigating 114 patients with gynaecologic cancers, 22% of patients treated with adjuvanted tumour lysate went into remission or showed stable disease (Graham and Graham, 1959). However, since the underlying mechanism was unknown, work on the Graham vaccine went largely unnoticed. Only decades later with milestones in immunology and oncology, such as the discovery of tumour-associated antigens, the ability of vaccines to prepare the human immune system for the elimination of tumours expressing those antigens subsequently led to increased optimism to battle cancer with immune-based therapies (Mackall et al., 2014).

The first vaccine based on a single cell surface antigen was the hepatitis B (HBV) vaccine, which became available in 1981 (Decker et al., 2017). Both the HBV vaccine as well as the human papillomavirus (HPV) vaccine prevent the formation of cancer through educating the immune system for the identification of cancer-causing viruses. Vaccination as a prevention treatment is seen as the most effective way of lowering cancer incidence through viral carcinogenesis (Dobosz and Dzieciątkowski, 2019).

Cancer vaccines follow the same concept by inducing a tumour-specific antigen-based stimulus for the host's immune system. Vaccines can be generated from autologous or allogenic material, often consisting of small peptides specific for the respective tumour,

such as lysate or RNA (Dobosz and Dzieciątkowski, 2019). Additionally, some cancer vaccines are augmented with adjuvants to enhance endogenous APC migration and presentation of the antigen. Cell-based cancer vaccines additionally provide APCs, such as dendritic cells, to promote antigen presentation at the site of immunisation. Ideally, these treatments can target persisting cancer cells after standard therapies, such as surgery or radiation. First to be approved by the FDA in 2010 for castration-resistant prostate cancer, sipuleucel-T is an autologous cancer vaccine – a personalised vaccine made from the patient's own cancer and immune cells (Dobosz and Dzieciątkowski, 2019; Kantoff et al., 2010). During clinical trials, the dendritic cell-based treatment extended overall survival of patients, however it had no effect on disease progression in clinical settings (Kantoff et al., 2010). Efforts to develop allogeneic vaccines based on laboratory-generated cells have not resulted in any drugs approved by the FDA yet, but promise potentially less expensive off-the-shelf type treatments (de Gruijl et al., 2008; Dobosz and Dzieciątkowski, 2019). Furthermore, various cancer vaccines not based on whole cells have been developed using cancer cell components, such as DNA or proteins, which can be administered directly or via specialised vehicles, such as viruses, plasmids, or nanoparticles (Dobosz and Dzieciątkowski, 2019; Mackall et al., 2014).

In general, animal studies and clinical studies have confirmed that tumour vaccines can efficiently prevent tumour formation when given as a preventative measurement but seem less effective as mediators of regression of already established tumours (Mackall et al., 2014).

Monoclonal antibodies and BiTEs

Antibodies function via several mechanisms which can be exploited for cancer therapy. In immunity, antibodies mainly act through binding antigens on cellular surfaces and thus

marking malignant cells for elimination by the immune system through antibody-dependent cell-mediated cytotoxicity (ADCC) potentially leading to further tumour antigen-presentation. However, they can also mediate antitumour effects as competitive binders, for example through blocking growth factor signalling in tumour cells, or as receptor agonists, when binding death receptors of the TRAIL family (Mackall et al., 2014).

For therapeutic applications, monoclonal antibodies are used. Monoclonal refers to antibodies with specificity for a single antigen ("mono"), which have been produced in large amounts ("clonal") to gain a clinically effective dose (Dobosz and Dzieciątkowski, 2019). After Milstein and Köhler introduced their findings on how to generate mAb from hybridomas, research bloomed and has since led to many variations of therapeutic mAbs. In 1997 rituximab, a CD20-binding antibody, became the first mAb approved by the FDA for the treatment of cancer. CD20 is found on the surface of immature B cells, which can be targeted by rituximab for destruction by NK cells (Rudnicka et al., 2013).

While many mAb, such as rituximab, solely act as mediators to engage host immune responses, conjugated antibodies harbour intrinsic cytotoxic activity. This can be achieved through toxins, drugs, or radioactive agents attached to the mAb, thus enabling localisation of cancer cells as well as targeted destruction (Dobosz and Dzieciątkowski, 2019).

Further modifications of antibodies can be found in the form of bispecific antibodies, which combine a tumour-targeting domain with a domain capable of activating an immune effector cell. An example is blinatumomab, which links an anti-CD19 tumour-binding domain to an anti-CD3 T cell-engaging domain. These so-called bispecific T cell engagers (BiTEs) have been proven to be capable of activating T cells upon binding and

mediate targeted killing of CD19-positive leukemic blasts. First clinical trials in patients with minimal residual B-ALL have shown a 78% complete response after treatment with blinatumomab (Topp et al., 2011).

The most promising antibody-based approach currently tested for the treatment of cancer are checkpoint inhibitors, which will be described in the next section.

Checkpoint inhibitors

The checkpoint molecules CTLA-4 as well as PD-1 and their respective ligands play a crucial role at the tumour proximity, where they mediate immune suppression and subsequently cancer immune evasion. Even through CTLA-4 was first described in 1987 by Brunet and colleagues (Brunet et al., 1987), the function of the immune checkpoint molecule remained unclear for many years. A crucial role in immune regulation was finally proven in 1995 by Jim Allison and colleagues, revealing it to be a promising new target for cancer immunotherapy (Krummel and Allison, 1995; Leach et al., 1996). Only a year later the first CTLA-4 blocking antibody was developed and tested in animal experiments (Leach et al., 1996).

Since then, many antibody variations blocking checkpoint molecules or their ligands have been described (Qin et al., 2019). The first CTLA-4 CPI to gain approval from the FDA was ipilimumab in 2011, which is now approved for advanced melanoma and several other cancer types (Dobosz and Dzieciątkowski, 2019; Hodi et al., 2010). Nivolumab, a PD-1 inhibitor, followed with FDA approval in 2014. Up to date, CPI-based drugs have been approved for more than nine cancer types (Dobosz and Dzieciątkowski, 2019). However, the majority of patients treated with anti-PD-1 or anti-CTLA-4 CPI therapy still develop de novo or adaptive resistance and ongoing studies involve several new immune checkpoint targets, like T cell immunoglobulin and mucin-domain containing-3

(TIM-3), lymphocyte activation gene-3 (LAG-3), T cell immunoglobulin and ITIM domain (TIGIT), and V-domain Ig suppressor of T cell activation (VISTA) (Qin et al., 2019).

Adoptive cell therpapy (ACT)

Adoptive cell therapy describes the isolation of tumour-specific immune cells from the patient, their *ex vivo* modification and/or expansion in the laboratory, and re-injection back into the patient's blood circulation, usually after preparative lymphodepletion (Dobosz and Dzieciątkowski, 2019; Mackall et al., 2014). The concept of ACT is to provide the patient with a cell population specifically enriched for tumour-reactive immune effectors. Most commonly, T lymphocytes are used for ACT. A key factor making these cells specifically suitable for therapeutic transfer is their ability to undergo multi-log expansion in receptive hosts, eradicate large tumour burdens, and their persistence for months to years after injection (Rosenberg et al., 1988; Scholler et al., 2012). To ensure tumour-specific killing upon re-injection, this treatment can either be based on the expansion of tumour-specific TILs from the TME, or the genetic modification of patient T cells with specifically engineered TCRs or chimeric receptors to enhance tumour recognition and elimination (see next section).

A common variation of ACT which doesn't include genetic engineering of cells is the isolation and *ex vivo* expansion of TILs from the tumour bed. Adoptive transfer of TILs together with IL-2 was the first immunotherapy to mediate the regression of large tumours when applied to patients with metastatic malignant melanoma, showing excellent 5-year survival rates for complete responders (93%) (Rosenberg et al., 2011). Furthermore, TILs have also been shown to mediate significant antitumour effects against melanoma brain metastases, indicating the efficiency of systemic immunotherapies even for primary brain

tumours (Hong et al., 2010). However, it has been observed that TILs are logistically difficult to manufacture and cannot be reliably generated from most tumour histologies, demonstrating the need of more robust protocols for therapy (Lim and June, 2017; Mackall et al., 2014).

Genetically engineered T cells

Genetic modifications during ACT can enable the redirection of effector cell specificity towards tumour antigens and improve antitumour effects.

One way to achieve this is the modification of patient T cells with engineered TCRs targeting tumour-associated antigens. In a series of trials with melanoma patients, T cells transduced with an engineered anti-MART-1 TCR were investigated for their tumour toxicity. Importantly, two versions of the TCR with different affinity were tested. While the low-affinity TCR showed little patient toxicity but also low antitumour effects, a high-affinity version caused severe side effects originating from excessive inflammation alongside increased antitumour efficacy (Johnson et al., 2009; Morgan et al., 2006). These findings suggest the existence of a defined affinity window, at which optimal tumour recognition meets minimal host toxicity (Zhong et al., 2013). The avidity of TCRs is determined by various factors, such as the total number of TCRs expressed on the cell surface, the density of the respective antigen on the target cell, and the availability of costimulatory receptors, all of which need to be taken into consideration when designing engineered TCRs for adoptive T cell therapy (Lim and June, 2017).

A more flexible alternative to retarget T cell specificity which has seen notable success in recent years is the use of CARs. Introduction of these synthetic receptor molecules re-directs T cells to detect predominant surface antigens of the targeted malignancy with a sequential intracellular activation of the effector functions. Specific antigen-binding of

the CAR is enabled by an extracellular binding domain consisting of an antibody-derived single chain variable fragment (scFv). This is connected via a transmembrane hinge domain to an intracellular signalling domain, which is responsible for the T cell activation upon binding. The intracellular signalling unit is built from the T cell receptor (TCR) segment CD3ζ (first generation CAR) with or without the addition of one (second generation CAR) or a combination (third generation CAR) of co-stimulatory units, such as CD28 and 4-1BB (Mackall et al., 2014; Scarfò and Maus, 2017) (see **Figure 1-6**).

The first to define the concept of CAR-modified T cells were Kuwana and Eshhar in the late 1980s. They demonstrated that T cells transduced with CARs can bind and recognise targets in an MHC-independent manner, unlike those relying on the endogenous TCR (Gross et al., 1989; Kuwana et al., 1987). Many CARs targeting different cancer antigens have been developed since then, but the most successful group so far have been those targeting CD19 for the therapy of leukaemia. CD19 is a nearly ideal target, as it is highly expressed in B cell malignancies and an associated loss of B cells in CAR T-treated patients can be well tolerated when given replacement antibody therapy (Lim and June, 2017). Earlier versions of CD19-CARs were first generation CAR constructs, thus only using CD3ζ for intracellular activation upon antigen engagement. Only when several groups started incorporating additional costimulatory domains, the expansion and persistence of transduced T cells improved and increased efficacy in patient settings (Mackall et al., 2014; Savoldo et al., 2011). Furthermore, we now know that there are different effects on signal longevity dependent on which type of costimulatory domain is used besides CD3ζ. Studies have shown that CD19-CAR T cells based on the CD28 endodomain show short-lived but potent responses, whereas CAR constructs incorporating the 4-1BB endodomain lead to a notably longer persistence and sustained activation of T cells (Kawalekar et al., 2016). With the improvements, clinical trials using

CAR T cells have reported excellent and durable responses (70-90%) in acute and chronic B cell malignancies (Lim and June, 2017) and now focus on reduction of associated side effects of treatment. The first FDA-approved CAR T cell therapy was tisagenlecleucel (Kymriah) in 2017 for the treatment of B-cell acute lymphoblastic leukaemia, followed by approvals for diffuse large B-cell lymphoma, and certain other types of lymphoma in 2018 (Dobosz and Dzieciątkowski, 2019).

Encouraged by the success of CAR T cells in leukaemia, many investigators are working on the translation of CAR-based therapy in solid cancer. Despite available tumour-expressed antigens and a demonstratable functionality in vitro, CAR T studies in solid cancers have shown mixed responses and indicate a need for improvement (Anderson, 2017).

Based on the success of anti-GD2 monoclonal antibody therapy, which is now integrated into standard protocols, GD2 has become the predominant target for CAR-based approaches in neuroblastoma. Several early phase studies have reported promise in clinical trials (Louis et al., 2011; Straathof et al., 2018), however CAR T cell efficacy has not been as reliable as with haematologic cancers. The major obstacles in neuroblastoma described are suboptimal T cell persistence and potency, a lack of tumour specific antigens, and the suppressive TME (Richards et al., 2018).

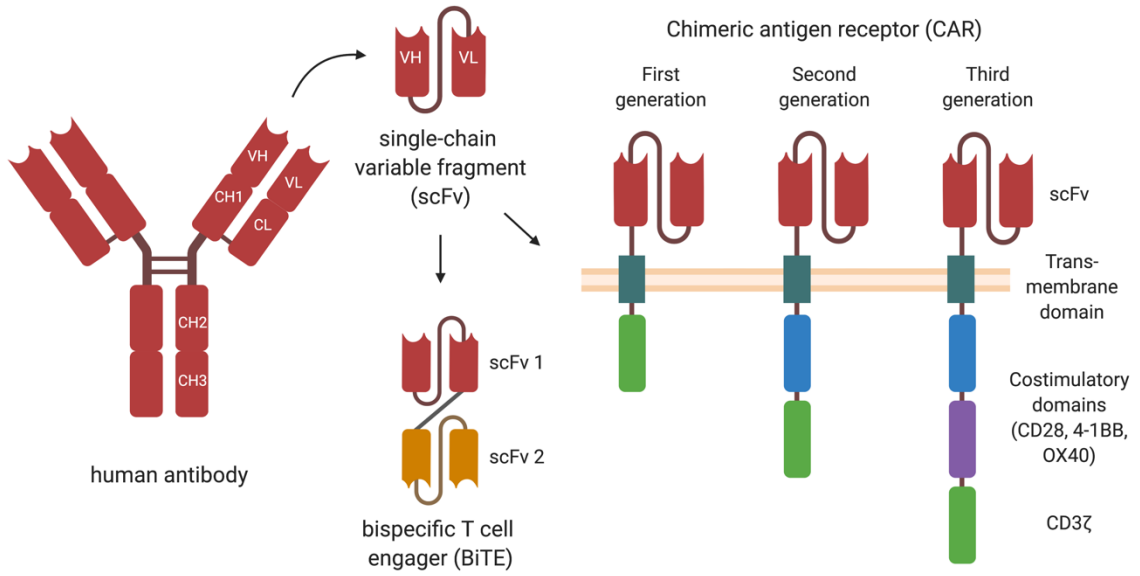

Figure 1-6 Immunotherapies with antigen-specificity. Both CARs and BiTEs obtain antigen specificity through binding of scFvs from antibodies. Besides the extracellular antigen-binding domain, CARs contain a transmembrane domain, as well as a CD3z intracellular activating domain. Second generation CARs additionally have one intracellular costimulatory domain and third generation CARs have a combination of two additional costimulatory domains.

1.4.2. Challenges in T cell therapy of solid cancers

Albeit CAR T therapy has proven itself to have great efficacy in leukaemia, the immunogenic potency of these cells can be accompanied by severe side effects for the patient. Both antibody-dependent and -independent toxicities have been observed (Mackall et al., 2014). Antibody-dependent side effects can occur either as ON-target-OFF-tumour cross-reactions, when CAR T cells attack antigen-expressing healthy tissue, or as OFF-target cross-reactions, when the modified cells unexpectedly interact with stereochemically related antigens expressed outside the tumour. Potentially, this can lead to complications such as nerve pain (GD2 CAR T), B-cell depletion (CD19 CAR T), or even death (HER2 CAR T) (Lim and June, 2017; Mackall et al., 2014), underlining the importance of selecting suitable targets that are not or minimally expressed on non-tumour tissues. Independently of the target, CAR T cells can lead to a major toxicity

called cytokine-release syndrome. Here, the artificial overactivation of the immune cells is associated with a high production of inflammatory cytokines, which through various effects can mediate multisystem failure and death (Lee et al., 2014). First observed following treatment with monoclonal antibodies, cytokine release syndrome has also been described in adoptive cell therapies, specifically when using second- and third-generation CARs (Lee et al., 2014).

Furthermore, sustained efficiency of immunotherapies can be limited by adaption of the tumour cells themselves. The targeted cells can escape immunotherapy-mediated mechanisms by loss of surface molecules necessary for T cell activation. This way, TCR-dependent detection can be avoided through downregulation of MHC molecules on tumour cells, a commonly observed phenomenon (Leone et al., 2013). Moreover, even MHC-independent CAR T cell functions are escaped through acquired resistance – a loss of tumour antigen in single tumour cells and the subsequent emergence of larger escape mutation variants. This was for example shown in B-ALL, where a significant number of patients developed CD19-negative B-ALL following CD19-directed antibody or CAR T therapy (Mackall et al., 2014; Yu et al., 2017).

Besides the risks described for immunotherapy in general, unique challenges arise in the T cell-based treatment of solid cancers. Firstly, while interactions between therapeutic cells and targets happen organically in blood cancers, trafficking can be a significant factor in the efficiency of solid tumour treatments. This can be both due to physical barriers, such as more fibrotic material in the tumour bed, as well as the specific cytokine milieu of the TME with a lack of T cell attracting factors (Lim and June, 2017). Secondly, due to the close proximity of pathologic and non-pathologic tissue in solid tumours, an accurate discrimination between targets and bystanders is essential. CAR T cells provide

the potential to target any marker of choice, however the challenge lies in identifying suitable antigens to avoid cross-reactions. Available choices are limited, as the target needs to be expressed on the tumour surface, homogeneously among all tumour cell populations, and in a significantly higher density than on healthy tissues (Klebanoff et al., 2016; Lim and June, 2017). Moreover, engineered T cells need to expand and persist to achieve an adequate and sustained effector-to-target ratio needed for the complete eradication of a solid tumour. It has been shown that effective proliferative responses reflect clinical success in cell-based therapies (Lim and June, 2017). This is also partly why overcoming the suppressive TME of solid tumours is crucial. It has been described for many types of cancer now that the tumour proximity is characterised by a combination of altered immune cells and soluble factors which effectively downregulate T cell proliferation and function (Joyce and Fearon, 2015). Thus, novel approaches to either engineer T cells resistant to the TME or capable of re-educating the microenvironment are needed. Lastly, control over T cell activity amplitude and timing will be essential for a wider application of T cell-based immunotherapies without the observed toxicities (Lim and June, 2017). New synthetic biology approaches promise answers to several of these challenges through customised cell regulatory circuits capable of sensing and responding to changes in complex diseases.

1.4.3. Synthetic biology approaches

Bioinformatic analysis suggests that tumour discrimination could be significantly improved through systems recognising combinations of two or three antigens (Lim and June, 2017). Several synthetic biology approaches implementing this hypothesis have been developed in the recent years and could help overcome OFF-tumour cross-reactions

as well as provide additional factors equipping T cells in the elimination of solid tumours and the surrounding microenvironment.

OR-gate circuits

Dual-antigen targeting CARs can be activated by two different antigen ligands. These bispecific CARs work as OR-gates, meaning they can be activated by either antigen ligand alone (Ebert et al., 2018). This can address tumour heterogeneity but also provide a tool for preventing accumulation of resistance through antigen loss variants, for example when targeting CD19 and CD20, both B cell specific antigens expressed in B cell malignancies (Zah et al., 2016). Variations include dual CAR T cells expressing two types of CARs with independent activating potential in the same T cell (Ruella et al., 2016) or bispecific CAR constructs capable of intracellular activation via binding of either of two ligands, such as Tandem CAR T cells (M. Hegde et al., 2016). Further studies have shown that the antigen coverage can be even further extended when using tri-specific CAR T cells (Bielamowicz et al., 2018).

AND-gate circuits

To overcome the major threat of ON-target-OFF-tumour toxicities, split-receptor CAR T cells can prevent T cell activation upon encountering antigen-expressing non-tumour cells. Similar to dual CAR T cells, split-receptor CAR T cells express two CAR constructs targeting different antigens. However, these CARs are designed to only contain either CD3ζ or a costimulatory domain in their intracellular regions. Thus, signal 1 and signal 2 for T cell activation are only provided when both receptors encounter their ligands (AND-gate) (Ebert et al., 2018). Challenges however include tuning of antigen expression and affinity to avoid significant activation through signalling of each individual CAR (Kloss et al., 2013).

NOT-gate circuits

Another variation of the split-receptor concept are CAR T cells actively discriminating healthy tissue from tumour cells through inhibitory antigens (NOT-gates). These T cells contain two split receptors, similar to AND-gate based CAR T cells, however one being an activating CAR directed against a tumour-associated antigen and the other being an inhibitory CAR (iCAR) directed at an antigen found on healthy bystander cells (Fedorov et al., 2013). The inhibitory function of iCARs is mediated through intracellular domains taken from immune inhibitory receptors, such as CTLA-4 and PD-1. This inhibitory signal is capable to override activation mediated by the activating CAR, so that T cells won't be activated when binding both antigens (bystander cells) but only when encountering solely the activating signal (tumour cells) (Lim and June, 2017).

Synthetic notch receptors (synNotch)

The recently introduced synNotch receptors promise a regulatable and sophisticated version of T cell engineering based on AND-gate target recognition (Morsut et al., 2016; Kole T. Roybal et al., 2016). The synthetic receptors combine an extracellular antigen targeting scFv with an intracellular transcriptional activator domain, joined via the regulatory transmembrane core region of the Notch receptor. Importantly, both the extracellular as well as the intracellular module are exchangeable, depending on the individual purpose. Because of the transmembrane domain, ligand engagement leads to a proteolytic intramembrane cleavage, like seen with wildtype-Notch, releasing an intracellular transcription domain which can relocate to the nucleus and activate target gene expression. This can be applied as an AND-gate, where activation of the synNotch receptor induces the expression of a second T cell activating receptor (CAR or TCR). Subsequently, target cells only are eliminated when both antigens of the two-receptor circuit are present in a timely and sustained manner (Lim and June, 2017). Preclinically

tested circuits include synNotch-dependent expression of CARs and BiTEs as well as the gated secretion of specific payloads, such as proinflammatory cytokines and adjuvants (Kole T. Roybal et al., 2016; Kole T. Roybal et al., 2016).

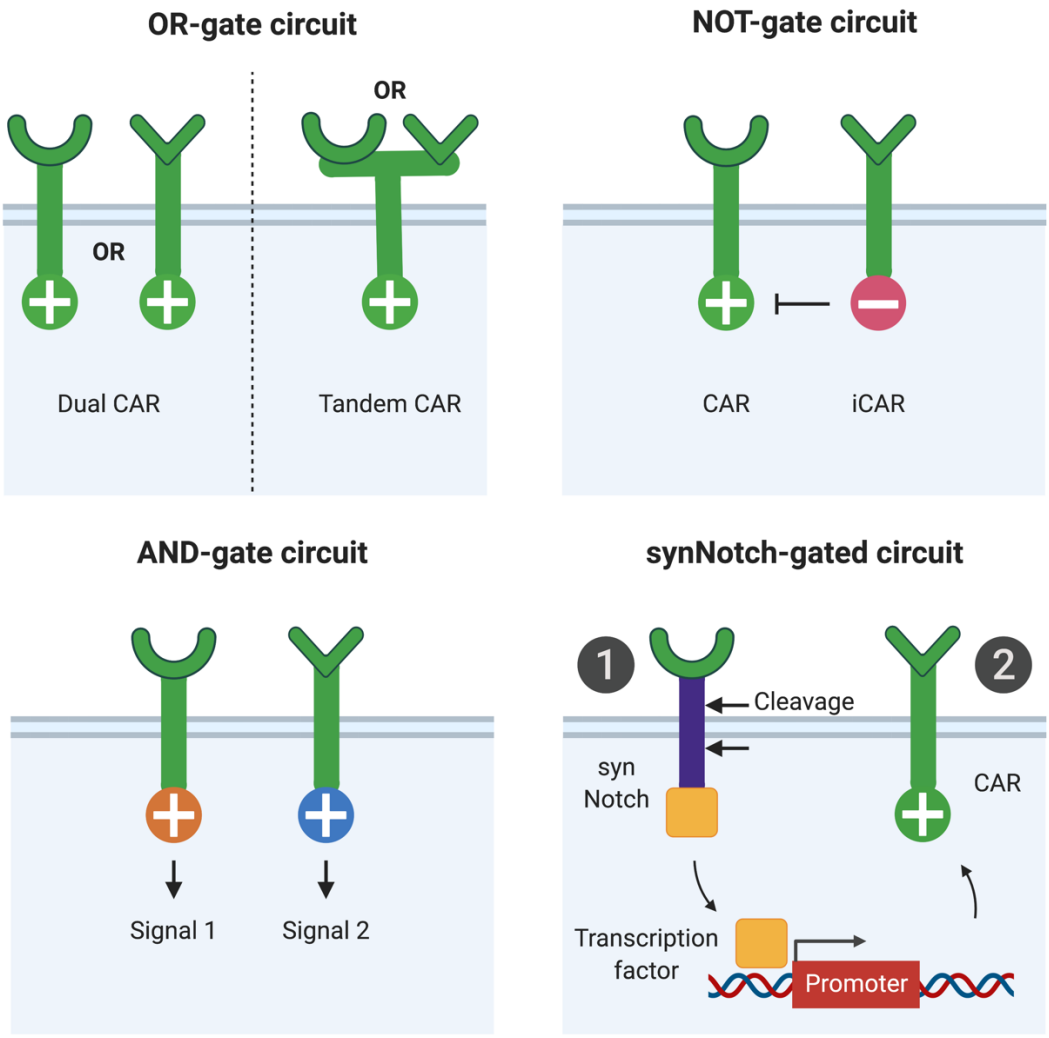

Figure 1-7 Synthetic T cell engineering. ON-target-OFF-tumour toxicities can be prevented through NOT- and AND-gated approaches. OR-gate circuits can be activated by two alternative antigens and can circumvent antigen loss escape mechanisms.

1.5. Research aims and hypothesis

I hypothesise that neuroblastoma-conditioned media can induce suppressive myeloid cells *in vitro* and that the generated cells can be used in co-cultures with T cells to model myeloid-derived suppression in the TME of neuroblastoma. I further hypothesise that the proposed model can be used to investigate novel approaches for combination with adoptive T cell therapies to overcome suppressive myeloid populations.

To research the T cell suppressing effects of individual myeloid populations in neuroblastoma tumours *in vitro*, the TME will have to be deconstructed and simplified first. This will provide the opportunity to correctly dissect effects of interventions targeting the specific interaction between T cells and myeloid populations and can then help identifying approaches to be tested in more complex models which include the other components of the TME.

The following research questions were to be evaluated:

1) How can neuroblastoma-conditioned suppressive myeloid cells be studied *in vitro*?
2) What are the characteristics of *in vitro* neuroblastoma-conditioned monocytes?
3) Can drugs revert myeloid-mediated T cell suppression?
4) Is the proposed model suitable for high throughput drug screens?
5) Can the synNotch system be adapted to target myeloid cells in a neuroblastoma context?
6) How do neuroblastoma-specific synNotch receptors perform in comparison to the published CD19-specific synNotch receptor?

In chapter 3 I optimised a robust *in vitro* assay to condition myeloid cells with neuroblastoma supernatant and test their suppressive potential in co-cultures with CAR-modified and -unmodified T cells (research question 1). The conditioned monocytes further were assessed for their suppressive character through staining for MDSC phenotypes, analysis of suppressive mechanisms, and suppressive effect on T cell proliferation and cytokine release in co-cultures (research question 2). In chapter 4 the optimised assay was used to investigate the drugs Sunitinib and gemcitabine, which have been described to exert MDSC-inhibitory effects, by analysing recovery of T cell proliferation in monocyte/T cell co-cultures (research question 3). Furthermore, the assay was adapted to allow for high throughput drug tests, which was then shown in a proof-of-principle experiment using 80 drugs from the Prestwick chemical library (research question 4). In the final chapter 5, an alternative approach using synNotch receptors to target myeloid cells in the neuroblastoma tumour microenvironment was evaluated. For this, novel synNotch receptors targeting the neuroblastoma antigens GD2 and B7H3 were created and tested in cell lines and primary T cells. Moreover, designing an anti-CD33 CAR under the control of synNotch receptor activation enabled us to switch on expression of the myeloid-targeting receptor in the presence of the synNotch ligand (research question 5). The novel neuroblastoma-specific synNotch receptors were then compared with an prototypic anti-CD19 synNotch receptor for background expression of synNotch-gated responders and upregulation of signal after ligand encounter (research question 6).

In summary, this thesis aimed to develop a robust model for studying suppressive myeloid cells in a neuroblastoma context and to propose examples on how to target these cells in future combination therapies.

2. METHODS

2.1.Microbiological methods

2.1.1. Bacterial culture

E. coli NEB® 10-beta strain was kept at 37 ºC on Luria Bertani (LB) agar plates or as cell suspension in LB medium. Bacteria suspension cultures were shaken at 200 rpm in a conical flask. The selection of ampicillin resistant clones was achieved using LB-Amp with 100 μg/ml ampicillin.

2.1.2. Transformation of bacteria

To amplify plasmid DNA, 50 μl of competent *E. coli* NEB® 10-beta cells were thawed on ice and mixed with up to 1 μg of DNA. Following 30 min of incubation on ice, DNA intake was facilitated by heat shock at 42 ºC for 35 s. Bacterial cells were then cultivated in 250 μl stable outgrowth medium for 45 min at 37 ºC, shaking at 200 rpm. Cells were spread on LB-Amp agar plates and left at 37 ºC overnight to form colonies.

2.1.3. Preparation of plasmid DNA

Mini DNA preparation

To isolate plasmid DNA from bacterial cultures the QIAprep Spin Miniprep Kit (Qiagen) was used. Prior to DNA purification, single bacterial clones were picked with a pipette tip and transferred into 5 ml LB-Amp medium. Bacterial cells were expanded overnight at 37 ºC, shaking at 200 rpm, and spun down the next day to harvest cell pellets (6800 x g, 3 min). DNA was purified according to the protocol provided by Qiagen. Isolated DNA

was reconstituted in 25 µl ddH_2O and concentration was determined using NanoDrop (see 2.2.5.)

Midi DNA preparation

To isolate larger amounts of high-quality plasmid DNA from bacterial cultures the NucleoBond Xtra Midi EF Kit (Macherey-Nagel) was used according to the manufacturer's protocol. Sufficient amounts of bacterial suspension were generated by transferring mini preparation cultures into 150 ml of LB-Amp in a conical flask and expanding cells overnight at 37 ºC, shaking at 200 rpm. Isolated DNA was reconstituted in 200 µl ddH_2O and preparations were kept at -20 ºC for long-term storage.

2.2. Molecular biology methods

2.2.1. Polymerase chain reaction (PCR)

To amplify selected DNA, the Q5 High-Fidelity DNA Polymerase from New England Biolabs (NEB) was used. The annealing temperature of the respective primers was calculated using the T_m calculator tool provided by NEB. Components and cycles used in a standard PCR are listed in **Table 2-1** and **Table 2-2**.

Component	Stock concentration	Volume [µl]	Final concentration
Q5 High-Fidelity 2X Master Mix	2x	12.5	1x
Forward primer	10 µM	1.25	0.5 µM
Reverse primer	10 µM	1.25	0.5 µM
Template DNA	variable	variable	< 1 µg
Nuclease-free water	-	to 25 µl	-

Table 2-1 Composition of a standard PCR master mix.

PCR step	Temperature	Time
Initial denaturation	98 ºC	30 s
Denaturation	98 ºC	10 s
Annealing	Primer Tm +3 ºC	30 s
Synthesis	72 ºC	20-30 s/kb
Terminal synthesis	72 ºC	2 min
End	4 ºC	forever

Table 2-2 Standard PCR cycle.

The size of the resulting PCR products was controlled using agarose gel electrophoresis (see 2.2.3).

2.2.2. Restriction digest of DNA

DNA was incubated with one or a combination of two restriction enzymes in FD buffer at 37 ºC for 30 minutes. **Table 2-3** shows the composition of a 20 µl digest.

Component	Volume [µl]
10X FD buffer	2
FD-Restriction enzyme A	1.25
FD-Restriction enzyme B	1.25
DNA template	< 1 µg
Nuclease-free water	to 20 µl

Table 2-3 Composition of standard enzymatic DNA restriction digest.

2.2.3. Agarose gel electrophoresis

DNA was separated by molecular size using an agarose gel consisting of 0.8-1% agarose dissolved in 1x TAE buffer and diluted SybrSAFE (1:10,000). To run the gel electrophoresis samples were mixed 5 to 1 with Purple loading dye 6x (New England Biolabs) and loaded into the pockets of the agarose gel. The GeneRuler 1kb plus DNA ladder (Thermo Fisher Scientific) was used as a marker for estimating molecular sizes. Gel electrophoresis ran for approximately 1 hour at 120 V and constant current in an

electrophoresis chamber filled with 1x TAE buffer. Detection took place using a Dark Reader transilluminator (Clare Chemical).

2.2.4. DNA gel extraction and purification of DNA fragments

PCR products and restriction digests were cleaned up directly or after cutting out correct bands from agarose gels. Clean DNA products were obtained using the Wizard SV Gel and PCR Clean-Up System (Promega) according to the manufacturer's protocol. Products were eluted using ddH2O.

2.2.5. DNA concentration determination

The concentration of eluted DNA was measured on a NanoDrop ND-100 UV/Vis spectrophotometer via the optical density (OD).

2.2.6. Ligation of DNA fragments

The Quick Ligation Kit (NEB) was used to ligate DNA fragments. The required amounts of insert and vector were calculated using NEB's online tool 'NEBioCalculator'. Insert and vector were typically combined in a 3:1 ratio. To estimate the number of spontaneous re-ligations, an additional 'vector only' control ligation was prepared alongside, which contained all components except the insert. Ligation mix was assembled on ice and left at room temperature for 5 minutes to enable ligation. Mix was put on ice and used in subsequent bacterial transformation. The colony formation of bacteria transformed with

the complete reaction was compared with the 'vector only control to estimate successful ligation.

Table 2-4 shows the components of a ligation mix.

Component	Volume [µl]
Quick Ligase Reaction Buffer (2X)	10
Vector DNA	100 ng
Insert DNA	variable
Quick Ligase	1 µl
Nuclease-free water	to 20 µl

Table 2-4 Composition of standard DNA ligation mix.

2.2.7. DNA sequencing

Sequencing analysis of cloning products was performed by SourceBioscience. Samples were prepared according to the company's specifications and were sent via mail. The results of the sequencing were compared with the expected genotype using SnapGene.

2.2.8. Site-directed mutagenesis of plasmid DNA

Site-specific mutagenesis of double-stranded plasmid DNA was achieved using the Q5 Site-Directed Mutagenesis Kit (NEB) according to the manufacturer's protocol. Primers were designed using NEB's 'NEBaseChanger' online tool.

Table 2-5 and **Table 2-6** show the components and temperature cycles used in PCRs for site-directed mutagenesis.

Component	Stock concentration	Volume [µl]	Final concentration
Q5 High-Fidelity 2X Master Mix	2x	12.5	1x
Forward primer	10 µM	1.25	0.5 µM
Reverse primer	10 µM	1.25	0.5 µM
Template DNA	variable	variable	1-25 µg
Nuclease-free water	-	to 25 µl	-

Table 2-5 Composition of standard DNA mutagenesis PCR master mix.

PCR step	Temperature	Time
Initial denaturation	98 ºC	30 s
Denaturation	98 ºC	10 s
Annealing	Primer Tm +3 ºC	30 s
Synthesis	72 ºC	20-30 s/kb
Terminal synthesis	72 ºC	2 min
End	4 ºC	forever

Table 2-6 Cycles of standard DNA mutagenesis PCR.

PCR products were used directly without additional clean-up steps in a Kinase, Ligase and DpnI (KLD) treatment. **Table 2-7** shows the volumes used for one 10 µl KLD reaction.

Component	Volume [µl]
PCR product	1
2X KLD Reaction Buffer	5
10X KLD Enzyme Mix	1
Nuclease-free water	3

Table 2-7 Composition of standard KLD reaction for DNA mutagenesis.

KLD products were used to transform NEB® 10-beta competent *E. coli* cells and checked for correct mutagenesis via sequencing of bacterial clone DNA.

2.2.9. Plasmids

The plasmids 'pHR-PGK-antiCD19-synNotch-Gal4VP64', 'pHR-PGK-antiCD19-synNotch-TetRVP64', and 'pHR-Gal4UAS-tBFP-PGK-mCherry' were generated by Wendell Lim and made available through Addgene (Addgene plasmids # 79125, # 79126, and # 79130).

2.3. Protein biochemical methods

2.3.1. ELISA

In an ELISA ('Enzyme Linked Immunosorbent Assay') biological components, such as cytokines, can be detected and quantified. In this project BioLegend's ELISA Max Deluxe kit was used according to the manufacturer's protocol for the detection of human Interferon gamma (IFN-γ) in cell co-culture supernatants. Triplets of each sample were measured using a Tecan infinite 200Pro plate reader. A blank control containing only medium was subtracted from the median of the results. To calculate the original concentration of the samples, values were multiplied by the dilution factor and then allocated on a calibration curve, derived from 7 additionally measured standard samples of known concentrations.

2.4. Cell culture methods

2.4.1. Eukaryotic cell culture

All cell work was performed in a sterile environment. Cells were kept in an incubator at 37 ºC, 5% CO_2 and 80% humidity in between experiments. All cell lines and primary cells were kept in complete medium supplemented with 10% fetal calf serum (FCS) and both 1% Penicillin/Streptavidin and 1% L-Glutamine. IMDM medium was additionally supplemented with 5mM HEPES. Medium was changed every three to four days and cells were split appropriately when they reached 80% confluence. For this, adherent cells were washed with phosphate buffered saline (PBS) and then detached with 0.05% Trypsin-EDTA for 3 minutes at 37 ºC. The enzymatic reaction was stopped by adding medium supplemented with FCS. The cell suspension was transferred into a new cell tissue flask and resuspended with an appropriate amount of fresh medium. Suspension cells were directly transferred and diluted in fresh medium for splitting. For primary T cells, 100 IU/ml Proleukin S was added every 3 days.

Cell counting

Cell counting of living cells was performed in a Neubauer counting chamber. Dead cells were excluded via staining of the sample with 0.4% trypan blue solution, which only stains cells with defects of cell membranes. For counting 10 µl of sample was applied to the Neubauer counting chamber, in which cells within 4 superior squares were counted. The cell concentration was then calculated using **Equation 1**

$$\frac{\text{Number of living cells counted in 64 squares}}{4} \times \text{dilution factor} \times 10^4 = \text{cells per ml}$$

Equation 1 Calculation of cell suspension concentration with a Neubauer counting chamber.

Freezing cells

Cell pellets were resuspended in freezing medium consisting of FCS supplemented with 10% DMSO. To ensure a controlled freezing process, Mister Frosty freezing containers containing Isopropanol were used. Cells were transferred into a -80 ºC freezer for at least 48 hours before moving aliquots into a liquid nitrogen tank for long-term storage.

Isolation of primary human peripheral blood mononuclear cells

Approximately 40 ml each of venous blood was collected from consenting healthy donors into Falcon tubes containing 0.5 ml EDTA. Alternatively, leucocyte cones – a by-product of apheresis – were purchased from NHS national blood service and processed in the same way. Blood samples were diluted in an equal amount of PBS and separated along a density gradient, using 20 ml Ficoll solution per 30 ml diluted blood. The blood was carefully layered on top of the Ficoll solution, before it was spun at 1000xg for 20 minutes at room temperature, without break. Following centrifugation, falcons contained heavy erythrocytes on the bottom, followed by the Ficoll solution, followed by a thin layer of peripheral blood mononuclear cells (PBMCs). This layer was transferred into a new Falcon tube with a transfer pipette and washed with PBS, before depleting platelets by resuspending cell pellet in 10 ml ammonium chloride potassium (ACK) lysis buffer and incubating for 15 minutes. After washing, the resulting platelet-depleted lymphocyte suspension was counted. For the expansion of T lymphocytes, PBMCs were re-suspended at 1 x 10^6 cells per ml in complete RPMI and plated on a 24-well plate. T cells were supplemented with 100 IU/ml Proleukin S (interleukin-2) and a 1:1 ratio of CD3/CD28 Dynabeads (ThermoFisher) or 0.5ug/ml anti-CD3 (OKT3) and anti-CD28 (both Miltenyi Biotec). When used at a later timepoint, fresh PBMCs were frozen (see 2.4.1) and needed to be rested in complete media supplemented with 100 IU/ml Proleukin S overnight before expansion with CD3 and CD28 antibody. For the isolation of primary monocytes,

a Pan-monocyte isolation kit (Miltenyi Biotec) was used according to the supplier's protocol. Using negative selection, monocytes were separated from antibody-labelled cells inside a MACS LS column using the magnetic field of a MACS separator. The monocyte-enriched product was collected and counted again, before they were further cultured.

CellTrace Violet staining

To mark cells in co-cultures and to determine proliferation, cells were stained with CellTrace Violet (ThermoFisher). The fluorescent dye gets incorporated into the cytosol of target cells and is evenly split during cell division, leading to a stepwise decline in fluorescent intensity. Cell populations that underwent specific numbers of divisions can then be detected in separated peaks of decreasing intensity using flow cytometry (see **Figure 2-1**). Target cells were incubated with 1 ml of a 1:1000 dilution of the dye for 30 minutes at 37 ºC. The staining was quenched using 5 ml complete medium and a second incubation at 37 ºC for 5 minutes. After washing off the staining mix, the cells could be counted and used in assays.

2.4.2. Generation of viral particles via transient transfection

Gamma-Retrovirus

Gamma-Retroviral supernatant for the transduction with an anti-GD2 CAR was generated by a previously generated producer cell line. This cell line is based on 293T cells, which stably express the envelope protein RD114 and a gag/pol gene, and were transduced with huk666-28-z in SFG, coding for the chimeric antigen receptor (Thomas et al., 2016). Anti-GD2 CAR producer cells were grown until they reached 60-80% confluency and then left with fresh complete RPMI for 24 hours to enrich viral particles. The supernatant

was spun at 500 x g for 5 minutes to exclude transfer of cells of the producer cell line. Retroviral supernatant was always produced freshly for direct use in T cell transduction.

Lentivirus

HEK293T cells were transiently transfected using a three-vector-system according to Soneoka et al. (1995). Thus, the gene of interest was cloned using a lentiviral pHR vector backbone, which contains both the packaging signal ψ and a long terminal repeat (LTR)-sequence. The combination with the two helping vectors VSV-G (contains gene for envelope protein of Vesicular Stomatitis Virus) and psPAX2 (contains a mix of genes for matrix- and capsidproteins and reverse transcriptase) enabled the production of replication-incompetent viral particles.

One day in advance, 2.5 x 10^6 HEK293T cells were seeded into a 10 cm cell culture plate and filled up to 10 ml with complete antibiotic-free IMDM medium. After 24 hours, each plate was transfected using a transfection mix, containing GeneJuice solution and DNA. GeneJuice solution was prepared using 30 µl of GeneJuice stock solution and 470 µl of plain IMDM. The DNA contained a combination of the three vectors: PAX2, VSV-G, and the transgene-containing pHR vector. After incubating the GeneJuice solution for 5 minutes at room temperature, it was combined with the DNA and left for another 15 minutes. After that, 0.5 ml of the mix was added dropwise to each plate of HEK293T cells. The transfection reaction followed over the next 48 hours at 37 °C in the incubator. The virus-containing supernatant was then collected and spun at 500xg for 10 minutes to exclude transfer of transfected cells. Viral supernatant was either used fresh or was concentrated by centrifugation and frozen at -80 °C for long-term storage. To enrich for viral particles, viral supernatants were incubated with 1x Lenti-X concentrator (Takara Biotech) at 4 ºC for at least 30 minutes and then spun for 45 minutes at 4 °C and 1,500 x g.

Each pellet generated from 10 ml of viral supernatant was then reconstituted in 500 µl IMDM, increasing viral concentration by 20 times. To determine viral titre, supernatants were tested in titrations ranging from 0.5 µl to 50 µl on HEK293T cells. Viral titre was then calculated with **Equation 2** from samples where transduction efficiency was between 5 and 20%.

$$\text{viral titre per ml} = \frac{\text{proportion cells expressing transgene} \times \text{number of plated cells}}{\text{virus volume added [ml]}}$$

$$\text{MOI} = \frac{\text{viral titre} \times \text{virus volume added}}{\text{number of plated cells}}$$

Equation 2 Calculation of viral titre and multiplicity of infection (MOI).

For T cell transduction lentivirus was used at a MOI (multiplicity of infection) of 50, whereas for cell lines a MOI 1 was sufficient.

2.4.3. Stable transduction

For stable transduction, 0.3 x 10^6 Jurkat cells or T lymphocytes were seeded into each well of pre-treated 24-well plates. For this, non-tissue culture treated plates were pre-incubated with retronectin overnight at 4 ºC to improve viral transduction. T cells had to be stimulated prior according to chapter 2.4.1, and were supplemented with Proleukin S to a final concentration of 100 IU/ml. When using gamma-retrovirus, cells had to be transduced during exponential growth phase, which was approximately 48 to 72 hours after antibody stimulation for T cells. This was crucial when using gamma-retrovirus, as the virus only integrates into proliferating cells, whereas lentivirus is less dependent on proliferative state and could be used at any time after stimulation. 1.5 ml viral supernatant

was layered on top of the T cells and transduction was promoted using spin inoculation for 40 minutes at 1,000 x g at room temperature. Cells were kept in the incubator for 48 hours (gamma-retrovirus) or 96 hours (lentivirus) respectively, before the virus was washed off and replaced by complete medium. Transduction efficiency was confirmed via flow cytometry staining after at least 24 hours of rest.

2.4.4. Polarisation of monocytes

Conditioned monocytes were generated *in vitro* using a polarising assay protocol adapted from the protocol described by Francis Mussai and colleagues (Mussai et al., 2015). For this, monocytes were cultured in ultra-low adherence 24-well plates for 48 to 72 hours at a density of 1.5 x 10^6 cells per well. The culture medium was a conditioning medium, containing 75% of Lan-1 supernatant and 25% complete RPMI. The Lan-1 supernatant was produced in bulk and frozen down, taken from Lan-1 cells that were cultured for 48 hours starting with a density of 4-6 x 10^6 cells per T-75 flask. Both fresh and re-thawed supernatants were spun down at 500 x g for 3 minutes before use to exclude the transfer of Lan-1 cells. Polarised monocytes were harvested using a transfer pipette, scraping the surface of the plate to ensure that all cells were in suspension. After counting, cells then were used for phenotype staining or functional assays.

2.4.5. Proliferation assay

To investigate effects on T cell proliferation, expanded CAR-transduced or non-transduced T cells were secondarily stimulated with irradiated cells bearing the CAR targets or with CD3/CD28 dynabeads, respectively, and co-cultured with or without polarised monocytes. As a negative control, unstimulated T cells were cultured in complete medium. To distinguish T cells from MDSC, lymphocytes were stained with

CellTrace Violet. T cells, MDSC and irradiated targets, if applicable, were cultured in a 1:1:1 ratio, using 2 x 10^5 cells of each per well in tissue culture treated 48-well plates. Cells were cultured in complete RPMI without the addition of IL-2. For drug ratio studies, to be investigated drugs were added in appropriate concentrations either to the completed culture or in a pre-treatment culture to the monocytes. T cell numbers were assessed after 7 days of co-culture using CountBright Absolute Counting Beads on the flow cytometer. Dead cells were excluded using 7-AAD live/dead staining and an anti-CD34 antibody was used to discriminate CAR-transduced T cells from the untransduced fraction. Cell numbers were analysed as a fold-expansion compared to the non-stimulated control, as well as loss of CellTrace Violet intensity.

2.4.6. Flow cytometry

Flow cytometry uses fluorophore-coupled antibodies for the detection of antigens expressed on cell surfaces. In the flow cytometer, cells pass through a laser light, inducing a scattering of light, and fluorescent emission by fluorophores coupled to surface-bound antibodies. Optical detection systems capture the scattered light as well as the fluorescent signal, receiving information about fluorescent intensity, cell granularity (side scatter, SSC) and cell size (forward scatter, FSC). For the analysis of surface antigens, cells were stained with the respective fluorescently labelled antibodies. To do so, a minimum of 2 x 10^5 cells was washed with PBS and stained with a cocktail of the antibodies of interest (at a concentration according to the manufacturers' recommendation) for 1 hour at 4 ºC. Unbound antibodies were washed off with PBS and cells were re-suspended in 100-200 µl of PBS. Cells with high expression of Fc-binding receptors, such as monocytes, were blocked for non-specific binding using a human Fc-block (Miltenyi Biotec). For

intracellular staining, cytokine secretion was blocked using Monensin overnight. To stain for retained cytosolic cytokines, the intracellular staining kit from BD was used. Live/Dead stains and counting beads were added shortly before analysis on the flow cytometer without washing off. Flow cytometry was performed on LSRII or CytoFlex flow cytometers with compensation controls to avoid fluorescent spill over. All analysis was performed excluding cell debris and duplets using forward- and sideward-scatter dot plots, as shown in **Figure 2-1**.

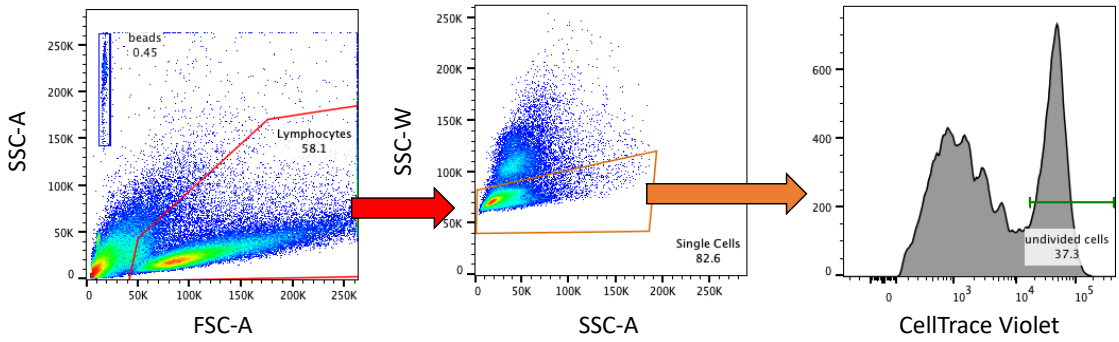

Figure 2-1 Representative dot plots of cell cultures showing gating strategy to exclude dead cells (left) and duplets (middle) using forward scatter (FSC) and sideward scatter (SSC) as well as cell histogram reflecting proliferation through CellTrace Violet (right).

2.4.7. Assays to determine suppression mechanisms

Cellular Reactive Oxygen Species Detection Assay Kit

To assess reactive oxygen species (ROS), cells were stained with 2',7' –dichlorofluorescin diacetate (DCFDA), a fluorogenic dye, which is deacetylated by cellular esterases and then oxidised by ROS into 2', 7' –dichlorofluorescein (DCF), a highly fluorescent compound. Therefore, the DCF-emitted fluorescence intensity can then be used as an indicator for the amount of ROS in the marked cells. Polarised monocytes were stained with 25 µM DCFDA for 30 minutes at 37 ºC and unstained cells

were used to exclude for autofluorescence of cells or components. As a positive control, stained cells were incubated for 4 hours with 25 μM Tert-Butyl Hydrogen Peroxide (TBHP) solution to induce ROS formation. DCF fluorescence could be assessed in the FL2 channel on the flow cytometer.

Arginase activity assay

The arginase activity assay kit by Sigma-Aldrich measures arginase activity in cell lysates or supernatants. Sample lysates are incubated with a buffer containing L-arginine and subsequently analysed for urea content, which is a by-product of arginase-based metabolism of the amino acid. A colour development reagent provided by the kit reacts with the generated urea, which results in a coloured product proportional to the arginase activity present. By generating a standard curve, the specific arginase activity can be determined as units/L. Lysates were generated using a lysis buffer containing 10 mM Tris-HCl (pH 7.4), 1 μM pepstatin A, 1 μM leupeptin and 0.4% (w/v) Triton X-100. Cells were plated on clear 96-well plates and left in a substrate buffer containing arginine and Mn solution to enable arginase activity for 2 hours at 37 ºC. To stop the reaction and visualise arginase activity, Urea reagent solution was added and left for 60 minutes at room temperature, until absorbance was measured with a plate reader. To calculate the correct activity, blank samples as well as water controls were measured alongside.

2.4.8. Synthetic Notch receptor activation

SynNotch receptor activation was investigated through co-culture with ligand-expressing cells or via antibody-binding of the myc-tag. Co-cultures consisted of a 1:1 ratio of synNotch-carrying cells and a target cell line, with 2.5 x 10^5 cells plated per well in a 48-well plate. Co-cultures were spun for 10 minutes at 500 x g and incubated for 24 hours

before analysing expression of synNotch-gated gene expression via flow cytometry. For myc-based activation, Nunc MaxiSorp flat-bottom 96 well plates were incubated overnight with 10 μg/ml purified anti-myc antibody (Biolegend, clone 9E10) in PBS. On the next day, the plates were washed twice with PBS and synNotch-carrying cells were plated at a density of 1 x 10^5 per well. After spinning at 500 x g for 10 minutes, the cells were incubated overnight and analysed for responder induction via flow cytometry.

2.5.Statistical analysis

Statistical analyses were performed using GraphPad Prism Version 7. Error bars, where displayed, indicate the standard deviation of data from replicate experiments unless stated otherwise. Significance of difference between samples within figures was confirmed using ANOVA for multiple comparisons, or t-tests for comparison of two groups or conditions, with $p = <0.05$ indicating significance.

3. RESULTS I – Neuroblastoma-conditioned suppressive monocytes as a model for T cell suppression in the tumour microenvironment

3.1. Introduction

As one of the altered cell types of the TME, MDSC are a heterogeneous population formed of immature myeloid cells, which are characterised by a potent immune suppressive activity (Kumar et al., 2016). Studies spanning various cancer types have revealed that MDSC accumulation positively correlates with more aggressive disease, advanced stage, resistance to treatments, and overall poor prognosis (Anderson, 2017). Also in neuroblastoma MDSC have been shown to significantly contribute to tumour growth, with patients showing major infiltration of myeloid cells producing arginase and iNOS (Apps et al., 2013; Mussai et al., 2015; Santilli et al., 2013b). The aim of this project is to understand and evaluate approaches to overcome the immunosuppressive microenvironment of neuroblastoma as a model of solid tumours with active MDSC pathways. Being a key suppressor of the neuroblastoma (Nb) TME, MDSC have been selected as a target for adoptive T cell combination therapies.

Several drugs and small molecules have been described to influence MDSC function and viability, promising a recovery of adoptive T cell function if used as an addition to cell-based therapies of solid tumours, such as neuroblastoma (Anderson, 2017). For a robust assessment of efficiency of selected adjuvants, a reproducible *in vitro* model for MDSC-mediated T cell suppression in the Nb microenvironment had to be established. Mussai *et al.* have shown that arginine-depleted neuroblastoma medium can condition monocytes towards a suppressive phenotype capable of suppressing T cell proliferation in co-cultures (Mussai et al., 2015). We therefore adapted these findings to establish a protocol for the generation of neuroblastoma-conditioned monocytes (NbM) (**Figure 3-1**). For this,

monocytes were isolated from healthy donor blood using FICOLL gradient followed by negative selection of CD14+ and/or CD16+ monocytes with a pan monocyte isolation kit. The monocyte population was then conditioned in a polarisation assay with a specific conditioning medium containing 25% complete cell culture medium and 75% neuroblastoma cell line (Lan-1) supernatant. After a minimum of 48 hours the polarised monocytes were harvested and used in T cell co-cultures to investigate suppressive potential. Co-cultures were both performed with unmodified T cells and with GD2 CAR T cells as a possible combination treatment in neuroblastoma.

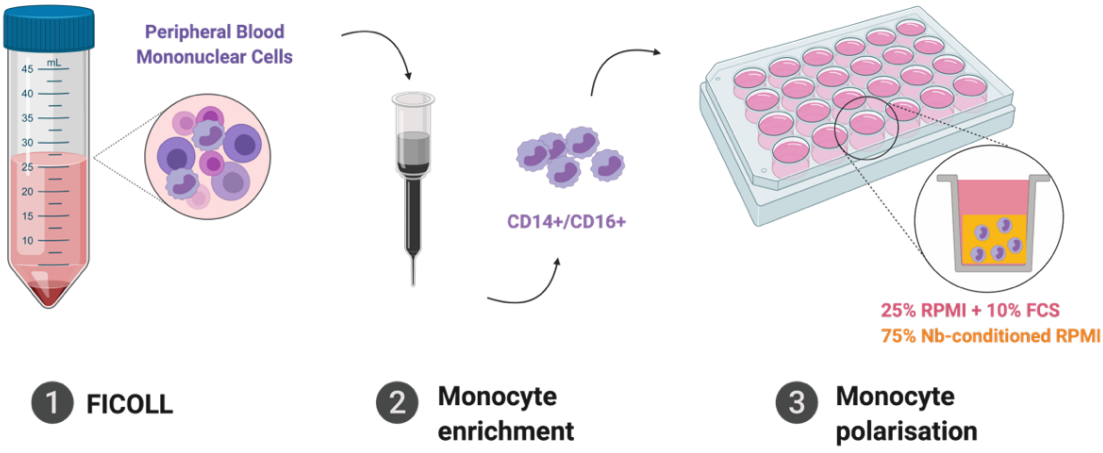

Figure 3-1 Schematic for workflow of monocyte polarisation using neuroblastoma-conditioned medium. Peripheral blood mononuclear cells are isolated from healthy donor blood using FICOLL. In a second step, non-monocyte populations are labelled with MACS beads and removed by passage through a magnetic column. The resulting cell solution is highly enriched for monocytic CD14+/CD16+ cells. These are transferred onto a low-adherence 24-well plate for a polarisation culture in conditioning medium containing 75% supernatant from neuroblastoma cell line Lan-1. Neuroblastoma-conditioned monocytes were harvested after 48 hours for subsequent suppression assays.

In conclusion, this first chapter aims to provide guidelines for an optimised *in vitro* model to study neuroblastoma-conditioned monocytes and to assess the conditioned monocytes for their suppressive and MDSC-like characteristics.

.

3.2. Assay optimisation

3.2.1. Optimisation of T cell proliferation

Proliferation readout

A key measure for the characterisation of suppressive myeloid cells is their ability to suppress T cell proliferation. Hence, a robust T cell proliferation assay had to be established first. Only when providing high enough T cell expansion rates, myeloid-mediated suppression and effects of intervention can be interpreted correctly. For this, T cells were activated with either CD3/CD28 dynabeads (untransduced T cells) or GD2-positive targets (GD2 CAR T cells). Proliferation was assessed by flow cytometry using either counting beads or CellTrace violet loss as a readout.

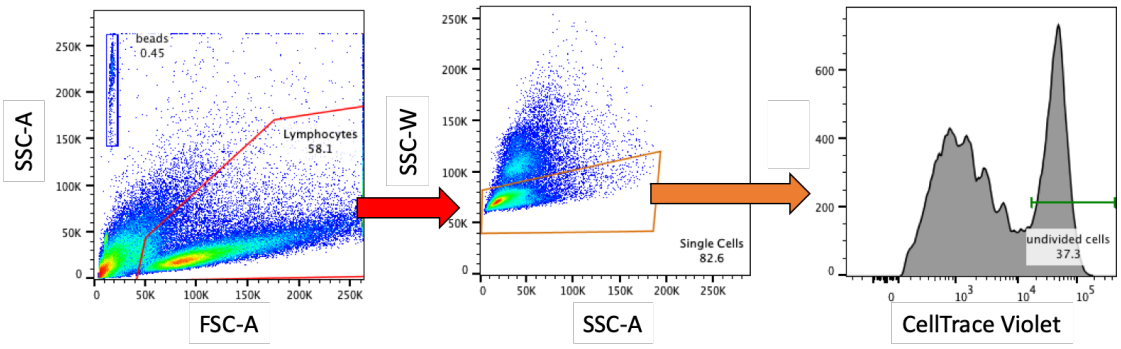

Figure 3-2 Gating strategy for flow cytometry. Representative dot plot of T cell culture showing gating strategy to exclude dead cells (left) and duplets (middle) using forward scatter (FSC) and sideward scatter (SSC). Proliferation can be assessed by either calculating relative numbers of counting beads (gate left plot) and T cells (singlets in middle plot) or by percentage of divided and undivided cells based on CellTrace Violet staining (right plot).

To assess cell numbers or percentage of proliferating cells, the gating strategy displayed in **Figure 3-2** was used. Cell numbers in the 'beads' and in the 'single cells' gate were assessed and total T cell numbers in the sample were calculated using the following formula.

$$Absolute\ T\ cell\ number = \frac{cells\ in\ gate \times total\ beads\ added}{beads\ in\ gate}$$

$$Relative\ proliferation = \frac{Absolute\ T\ cell\ number\ condition\ of\ interest}{Absolute\ T\ cell\ number\ unstimulated\ control}$$

Equation 3 Calculation of T cell proliferation.

CellTrace Violet is a fluorescent dye, which is incorporated into the cytosol of target cells and can be used as an indicator for cell proliferation. With each cell cycle, the dye becomes more diluted, resulting in loss of signal intensity. Therefore, cells with CellTrace signals lower than the 'undivided cells' gate will have proliferated at least once, with each peak representing one completed cell cycle. Due to a lack of availability of software to analyse cell trace results, CellTrace-based figures in this thesis will show percentage of cells in the undivided gate as a marker for T cell proliferation. It has to be pointed out that this marker therefore is not linearly proportionate to total proliferation and may not be as sensitive to small changes in proliferation intensity.

Figure 3-3 shows proliferation readouts of bead-activated unmodified T cells over the course of seven days post-stimulation. **Figure 3-3a** displays T cell numbers calculated by counting beads relative to numbers in an unstimulated control. Relative cell numbers increased significantly compared to the control between day 3 and day 7, with an average 5.6-fold T cell expansion by day 7. In **Figure 3-3b** the same T cells are analysed for loss of CellTrace Violet, with data presented as percentage of cells that are proliferating as defined by downward shift in cell trace violet staining. By day 7 an average of 22.3% of T cells retained the dye fluorescence intensity, meaning that over three quarters have divided at least once. A negative control consisting of unstimulated T cells retained the

original intensity in over 95% of cells, suggesting that the CellTrace loss is not an effect of dye instability.

Based on these findings, all following proliferation assays were read out 7 days post-stimulation. Results are portrayed looking at fold expansion based on calculation with counting beads, as it more accurately depicts proliferation in a quantitative manner.

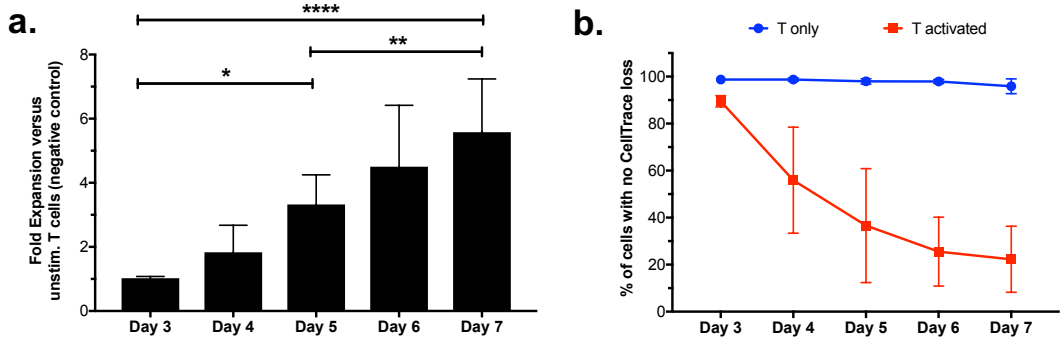

Figure 3-3 T cell proliferation over a course of seven days after stimulation with CD3/CD28 Dynabeads, portrayed by fold expansion or percentage CellTrace Violet loss. Data shown is pooled data from three independent experiments using seven healthy donors. a. Relative T cell numbers increased compared to an unstimulated control, shown by the calculated fold expansion. Fold expansion is shown as mean + SD. b. Proportion of T cells with no CellTrace Violet loss, representing an undivided population, decreases in stimulated T cells (red) but not in the unstimulated control (blue). Percentage is shown as mean + SD. (p=* ≤0.05; ** ≤0.01; ***≤0.001; **** ≤0.0001; one-way ANOVA)

Target selection of GD2 CAR T cells

To study GD2 CAR T cell proliferation after target engagement, several GD2-positive cell lines were tested. **Figure 3-4** shows the expression of GD2 on the surface of all tested cell lines. Lan-1 and TC-71 are cancer cell lines which express GD2 inherently (neuroblastoma and Ewing's sarcoma, respectively), whereas SupT1 GD2 is a cell line originating from T-cell lymphoblastic lymphoma, where GD2 expression has been artificially introduced. SupT1 NT do not express GD2 and serve as a control for CAR-independent T cell activation.

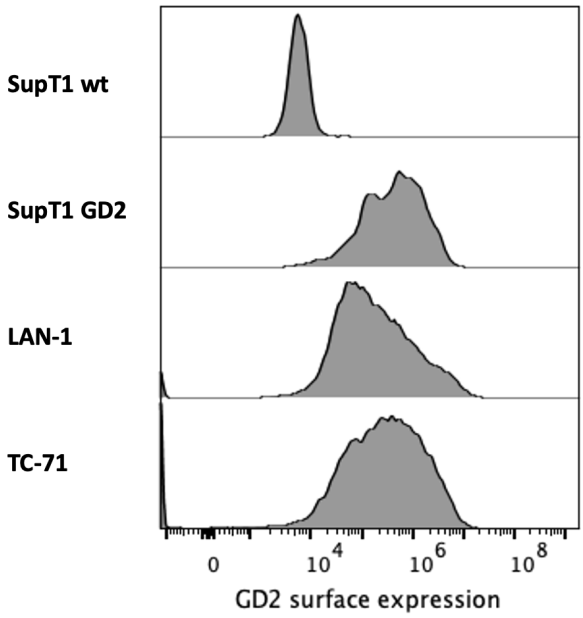

Figure 3-4 Surface GD2 expression on target cell lines.

Figure 3-5 pictures the effects of five different target-to-effector ratios for each cell line in GD2 CAR T cell proliferation assays, calculated with counting beads. SupT1 NT did not induce significant T cell expansion, suggesting no or only negligible effects of the co-culture on T cell activation. Highest unspecific expansion of 1.3-fold was seen at a ratio of 1:3. Interestingly, co-cultures with Lan-1 – despite highly expressing GD2 – did show similar results to the negative control, with a maximum 1.3-fold at 1:3. Both SupT1 GD2 and TC-71 increased T cell proliferation compared to the negative control. TC-71 cells stimulated T cell growths up to 2-fold with higher number of effectors (1:10) and induced an expansion of 1.6-fold when used 1:1. The GD2-equipped SupT1 GD2 cell line displayed a robust expansion of T cells when administered in ratios of 1:1 or lower of an average 1.7 to 1.9-fold. However, no results differed significantly from the unstimulated control, likely due to wide differences in responses between donors.

When focussing only on the 1:1 ratio of CAR T cells and the respective targets, both TC-71 and SupT1 GD2 stimulated a higher average expansion than Lan-1, albeit non-significant when compared to the negative control (**Figure 3-5**b).

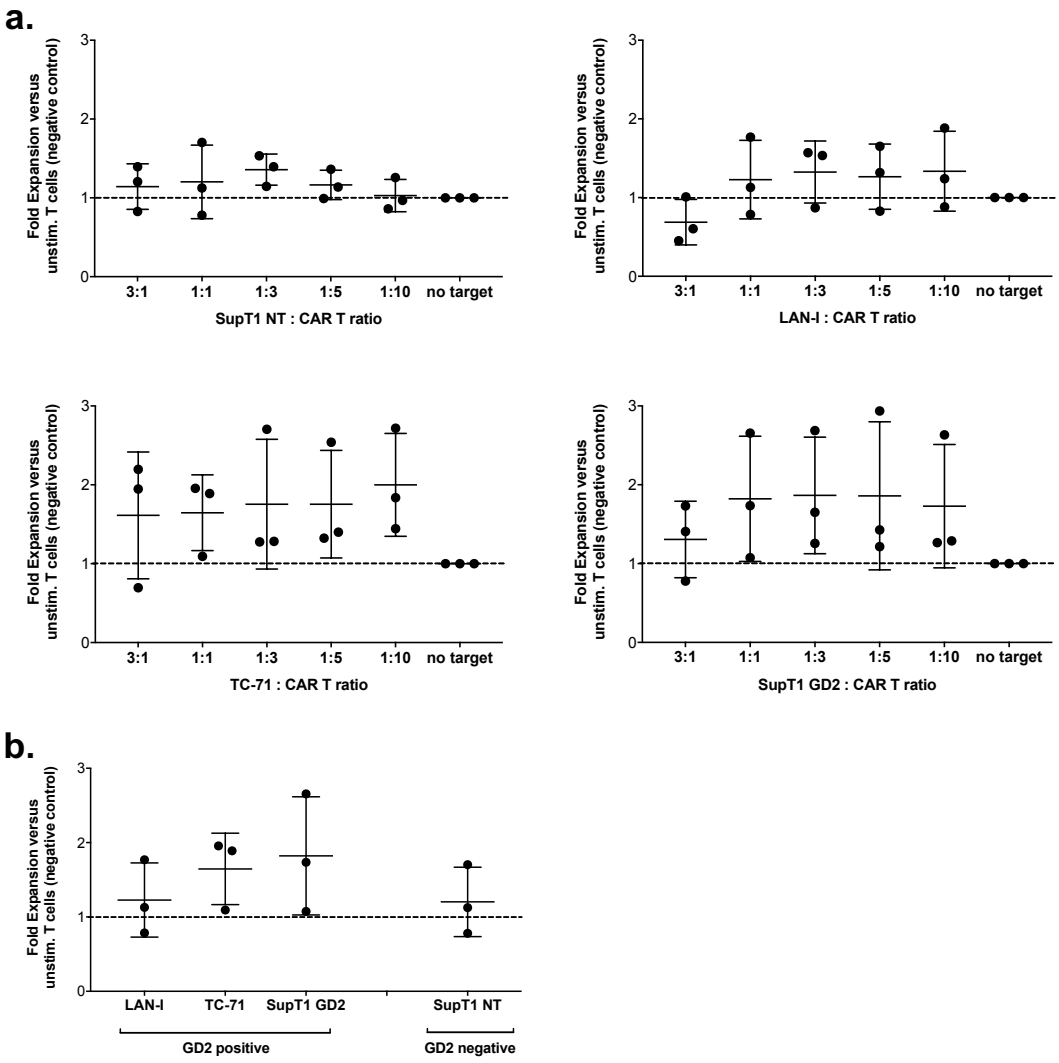

Figure 3-5 Evaluation of suitable targets for GD2 CAR T cell proliferation assay. Fold expansion is shown as mean + SD for the CAR-positive population only. Each point on the graphs represents one donor, each assessed in duplicates. a) Comparison of CAR T cell proliferation in co-cultures with SupT1 NT, SupT1 GD2, Lan-1 and TC-71 cells. Target-to-CAR T cell ratio is shown on the x-axis and proliferation is displayed as a ratio to the unstimulated control on the y-axis. b) Overview of CAR T cell expansions seen with all targets at a 1:1 ratio, sorted by GD2-positive (left) and the GD2-negative control (right). All changes were non-significant when tested in a one-way ANOVA.

Assay scale

Large data spreads seen in the target optimisation experiments in **Figure 3-5** suggested that changing experimental scale might lead to greater reproducibility. For this, experiments performed in 96-well plates were compared to experiments set up in a 48-well plate format. **Figure 3-6** shows a comparison of CAR T cell proliferation stimulated by Lan-1 and SupT1 GD2 cells in 96-well plates versus 48-well plates. All cell numbers were appropriately up-scaled using 1 x 10^5 cells of each CAR T cells and targets in 96-well plates and 2.5 x 10^5 cells in 48-well plates. Reflecting previous experiments, proliferation intensity was heterogeneous between donors, resulting in spread data. Results indicate better fold-expansion when using a larger plate format, with significantly increased expansion compared to the negative control of an average 3-fold using SupT1 GD2 cells. Lan-1 cells did not stimulate T cell proliferation in the majority of experiments, confirming previous findings.

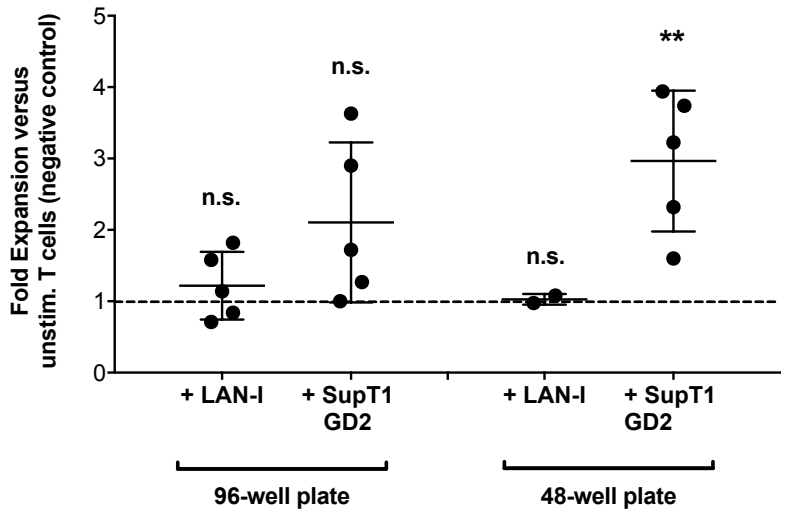

Figure 3-6 Comparison of GD2 CAR T cell proliferation in different plate formats. Fold expansion is shown as mean + SD for the CAR-positive population only. Each point on the graphs represents the mean of two duplicates from one independent donor. Graph shows GD2 CAR T cell proliferation seen in 96-well plates (left) and 48-well plates (right) when co-cultured with the GD2-positive cell lines Lan-1 and SupT1GD2 in a 1:1 effector-to-target ratio. Statistical test: one-way ANOVA (p=* ≤0.05; ** ≤0.01; ***≤0.001; **** ≤0.0001).

Although both TC-71 and SupT1 GD2 induced similar expansion responses, we decided to move forward with SupT1 GD2 as a target, which can be easily compared with the isogenic SupT1 wt as an antigen-negative control. In conclusion to the results displayed in chapter 3.2, the optimised assay was defined by using 2.5 x 10^5 cells of each GD2 CAR T cells, SupT1 GD2 and polarised monocytes in 48-well plates.

3.2.2. Optimisation of monocyte polarisation

Having established a reliable proliferation assay, next ideal conditions for generating suppressive monocytes in vitro had to be assessed.

Dynamics of monocyte conditioning

Figure 3-7a demonstrates the effects of long-term polarisation on the suppressive effect of monocytes. For this, healthy monocytes were left in neuroblastoma-conditioned media for 2-10 days and then co-cultured with activated CAR T cells for 7 days. Relative T cell proliferation was suppressed when monocytes were conditioned for 4 days or less before co-culture. The average proliferation was decreased to 75% after two days and 55% after four, yet results are spread due to donor-to-donor differences. When polarised for 5 days or longer, monocytes more often failed to suppress T cell proliferation in experiments, with T cell proliferation being equal to or higher than proliferation seen in the positive control. We suggest that there is a window of 2-4 days for monocyte condition before they should be used in proliferation assays to see a suppressive effect.

Figure 3-7b displays the effects of monocytes (polarised for 2 days) on the proliferation of bead-stimulated T cells at different timepoints after co-culture set-up, as shown in **Figure 3-3**. Suppressive effects of conditioned monocytes only become noticeable with

appropriate T cell proliferation, with no observed suppression until day 5 after co-culture set-up. Only at day 6 and day 7, was T cell proliferation supressed significantly in cultures with NbM when compared to the positive control. In conclusion, monocytes should be conditioned for 2-4 days and then co-cultured with stimulated T cells for 7 days to robustly assess suppressive effects.

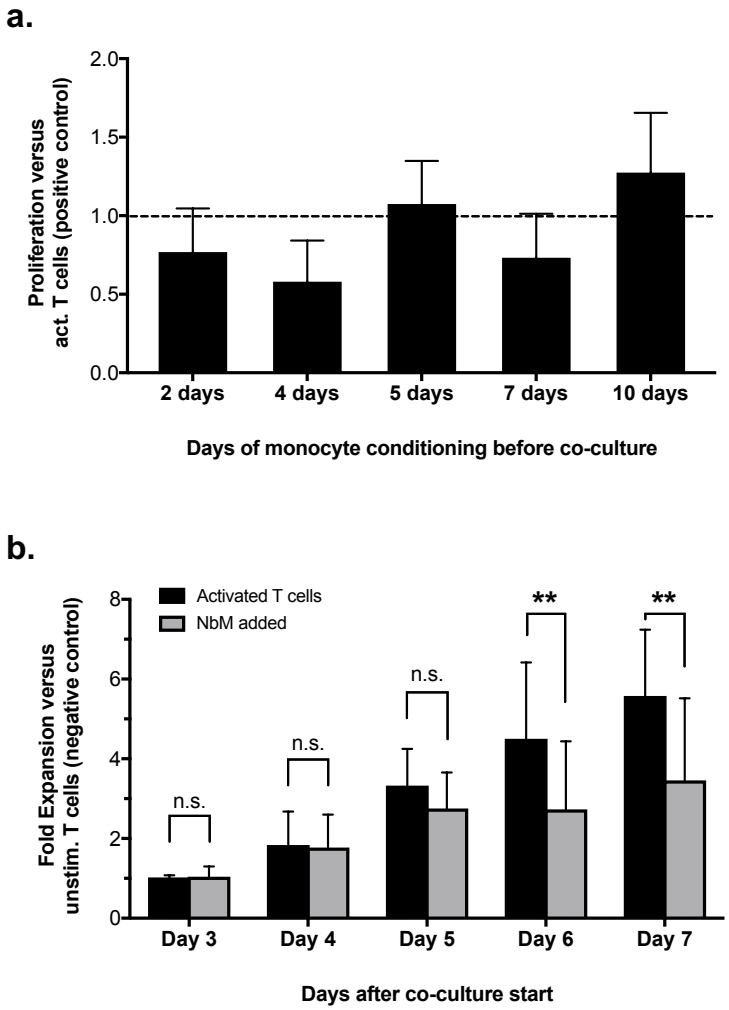

Figure 3-7 Optimising the suppressive potential of neuroblastoma-conditioned monocytes. a. CAR T cell suppression mediated by monocytes conditioned in polarisation medium for 2-10 days. Polarised monocytes were combined with anti-GD2 CAR T cells and SupT1 GD2 target cells and co-cultures were analysed for T cell proliferation after 7 days. Bar graphs show mean + SD of proliferation in cultures with NbM compared to a positive control of stimulated CAR T cells. Dotted line indicates positive control. Data shown is pooled data from two independent experiments using four healthy donors. b. Effects of NbM-mediated T cell suppression measured at different timepoints after co-culture set-up. Mean +SD of fold expansion is shown for both conditions compared to a negative control of unstimulated T cells. Data is pooled from three independent experiments using seven healthy donors. Statistical test: two-way ANOVA (p=* ≤0.05; ** ≤0.01; ***≤0.001; **** ≤0.0001).

Quality of conditioning medium

Furthermore, a stable quality of neuroblastoma-conditioned media had to be established. Therefore, effects of neuroblastoma cell density during media generation and effects of freezing on the quality of T cell suppression were investigated. Lan-1 cells were plated in densities ranging from 1 million to 5 million per flask and left in complete medium for 48 hours before conditioned supernatant was harvested. Fresh as well as frozen and re-thawed supernatants were used for a standard 48-hour polarisation of monocytes, which were then co-cultured with primary T cells for one week to assess for inhibitory potential.

Figure 3-8 displays the suppression mediated with the range of supernatants. Average suppression of proliferation was between 40% and 60% compared to the no monocyte control. No significant differences were seen between the supernatants from increasing Lan-1 densities nor between frozen or fresh samples. However, to avoid variations in future experiments, the protocol to generate conditioning medium was set plating 3 x 10^6 Lan-1 per flask for 48 hours and then freeze aliquots.

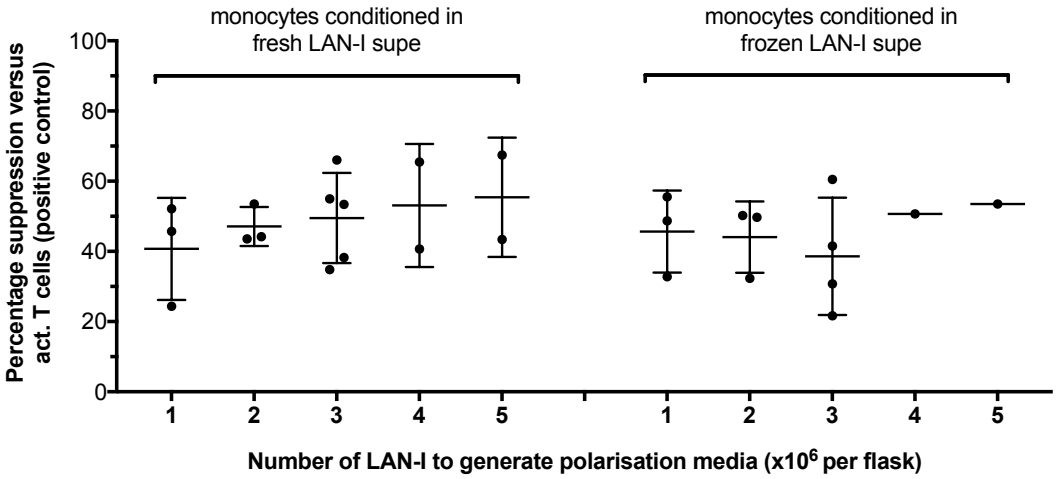

Figure 3-8 Quality of Lan-1-conditioned medium for monocyte polarisation. Graph displays percentage suppression of T cell proliferation after one week of co-culture with NbM generated from different polarisation media. The x-axis displays the number of Lan-1 cells which were used to condition the medium for polarising the monocytes. On the left, conditioned supernatant was used directly for the polarisation assay, on the right it was frozen and re-thawed beforehand. Each dot represents the mean of two duplicates for one independent donor.

3.3. Characterisation of neuroblastoma-conditioned monocytes

3.3.1. Phenotyping

Using flow cytometry, generated NbM were analysed for their expression of typical markers of the three defined human MDSC subpopulations. A 5-colour panel was designed to reliably assess all three human subpopulations (**Table 3-1**).

Antigen	**Antibody clone**	**Fluorochrome**
CD33	P67.6	PE
CD11b	M1/70	PE-CF594
CD14	MΦP9	BV421
CD15	HI98	FITC
HLA-DR	G46-6	APC

Table 3-1 Flow cytometry panel for assessment of human MDSC subpopulations.

To dissect the effects of the polarisation culture, monocytes from the same healthy donor were stained for flow cytometry both directly after isolation from PBMCs (fresh monocytes) as well as after 48 hours culture in either Nb-conditioned medium (NbM) or normal cell culture medium (media control).

Figure 3-9 shows the gating strategy used for all monocyte samples. Live cells and singlets were selected using FSC and SSC. Additionally, for all subpopulations cells were first gated for myeloid cells using markers CD33 and CD11b. Subpopulations were then identified using a combination of markers CD14, CD15, and HLA-DR.

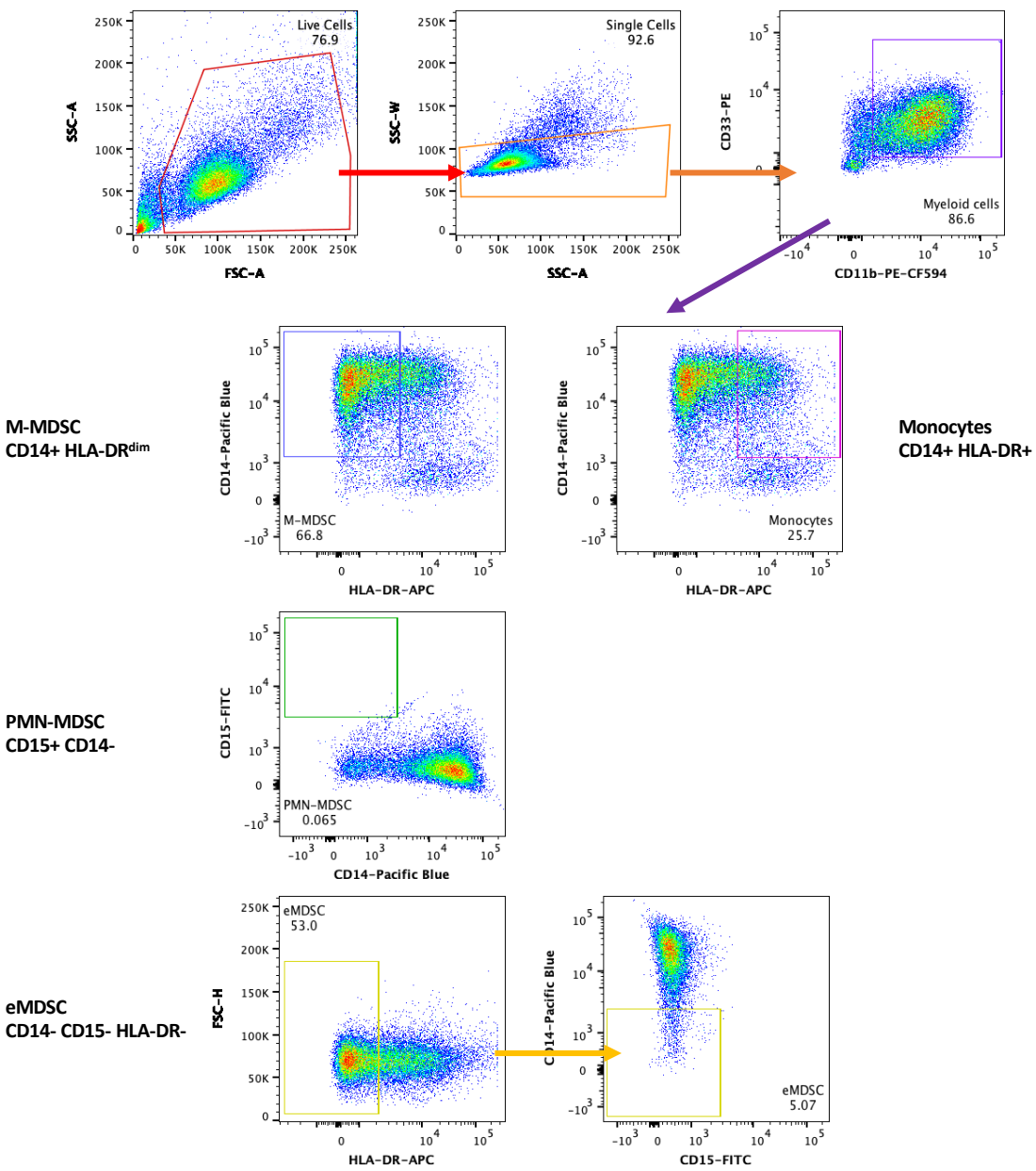

Figure 3-9 Gating strategy for phenotype analysis of polarised monocytes. Flow cytometry data from one representative healthy donor. Correct gating was achieved using FMO control staining. For all analysis, dead cells and duplets were excluded via FSC and SSC first. All subpopulations were gated on CD33+ CD11b+ myeloid cells. Assessed phenotypes reflect healthy monocytes (CD14+ HLA-DR+) and the common MDSC subpopulations M-MDSC (CD14+ HLA-Drdim), PMN-MDSC (CD15+ CD14-), and eMDSC (HLA-DR- CD15- CD14-).

Figure 3-10 compares the expression of surface markers of healthy monocytes (CD14+ HLA-DR+) as well as of MDSC subsets M-MDSC (CD14+ HLA-DR^{dim}), PMN-MDSC (CD15+ CD14-) and eMDSC (HLA-DR- CD14- CD15-) before and after polarisation with Nb-conditioned medium or a media control.

The side-by-side comparison displayed in **Figure 3-10a** suggests an increase in the proportion of cells expressing markers of MDSC subpopulation phenotypes in cultured monocytes, when compared with the freshly isolated control. Simultaneously, healthy monocytes were found less in cultured monocytes, decreasing from 71.4% in fresh isolated monocytes to 38.8% and 35.7% when kept in neuroblastoma supernatant or media, respectively. Both M-MDSC and eMDSC phenotypes were increased in cultured monocytes. While less than 10% of total cells had an M-MDSC-like phenotype in fresh monocyte samples, this population increased to 32.4% in NbM and 22.2% in the media control. Also eMDSC-like cells increased from less than 1% to 5.4% and 9.6% in NbM and media control, respectively. Monocytes with a PMN-MDSC-typical phenotype could not be detected in either fresh monocytes, NbM, or media control.

Interestingly, the phenotype analysis revealed that MDSC-like phenotypes could be significantly increased both via Nb polarisation culture as well as when monocytes were cultured on cell culture plates for 48 hours (**Figure 3-10b**). However, the resulting distributions of subpopulations suggest differences between the two conditions. While monocyte culture in complete medium resulted in a larger increase of immature myeloid cells (eMDSC), Nb conditioning led to a higher average percentage of the M-MDSC-like cell population. However, phenotyping alone cannot validate the MDSC-like character of these cells, mainly because of the lack of unique human MDSC markers. The suppressive character of the generated NbM can only be thoroughly assessed through suppression of T cell proliferation in co-culture assays, which will be discussed in the next section.

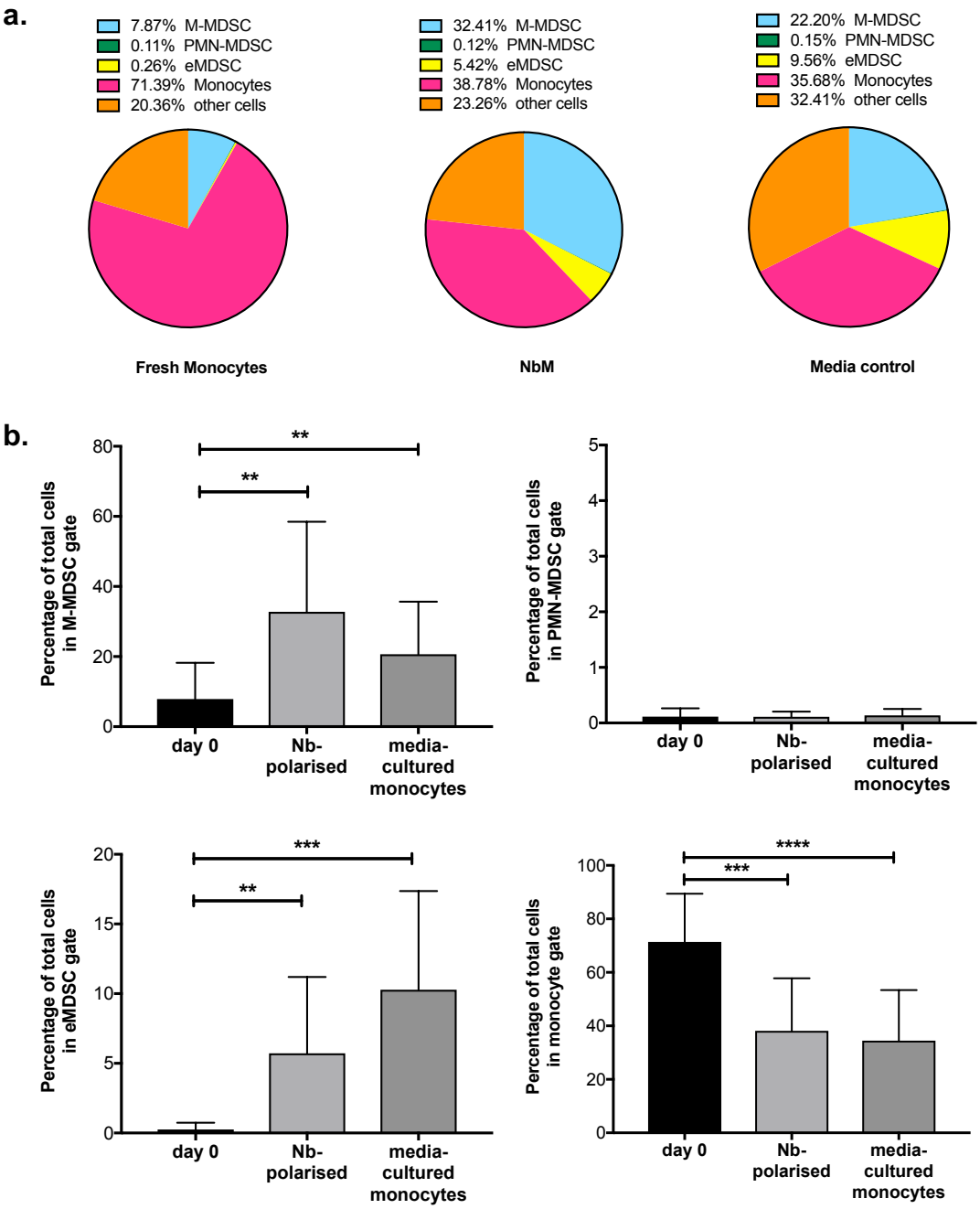

Figure 3-10 Effect of polarisation culture on monocyte phenotype. Data shown are pooled results from 16 healthy donors. a. Pie charts displaying average percentage of total cells in each gate of healthy monocytes and the three common MDSC subpopulations. NbM after 2 days of polarisation culture (middle) were compared with fresh monocytes (left) and monocytes kept in a media control for 2 days (right). b. Bar graphs showing mean + SD percentage of total cells within each condition with the individual MDSC phenotypes and with healthy monocyte phenotype. Statistical test: one-way ANOVA (p=* ≤0.05; ** ≤0.01; ***≤0.001; **** ≤0.0001).

3.3.2. Suppression of T cell proliferation

A consensus in the field recognises that characterisation of cells as myeloid derived suppressors requires demonstration of their ability to suppress T cell proliferation. A total of 27 donors' T cells had been tested in co-cultures with NbM derived from the prior described monocyte polarisation assay. In **Figure 3-11** these experiments are summarised, sorted for CAR-transduced versus non-modified T cells (a) and T cells co-cultured with autologous versus allogeneic NbM (b).

Both CAR T cells as well as non-modified T cells were expanded to an average of 3-fold using stimulation with SupT1-GD2 and CD3/CD28 dynabeads, respectively. The average amplification of both types of T cells could be significantly reduced using generated NbM. When comparing the use of autologous versus allogeneic monocytes, only allogeneic cells suppressed T cells significantly. However, there were only 5 autologous suppression assays, and it is possible significance would have been observed had larger numbers of replicates been performed as was the case for allogeneic suppression (n=22). An overview of all 27 performed proliferation assays is displayed in **Figure 3-11c**, confirming the highly significant T cell suppression mediated by the polarised NbM. The average proliferation decreased from 3.1-fold to 1.8-fold, enabling the investigation of drug effects on the monocyte-mediated mechanisms. The graph also shows several non-responders, reflecting differences between donors. To investigate a possible correlation between quality of T cell proliferation and the subsequent effects of NbM, **Figure 3-11d** shows a dissection of all experiments by fold proliferation of T cells without suppressors versus relative suppression of proliferation with NbM. The data suggests that there were experiments showing strong suppression as well as failure of suppression both in donors with strong (4-5) and weak (1-2) T cell proliferation. Therefore, we proceeded with no further selection of data based on T cell proliferation without NbM.

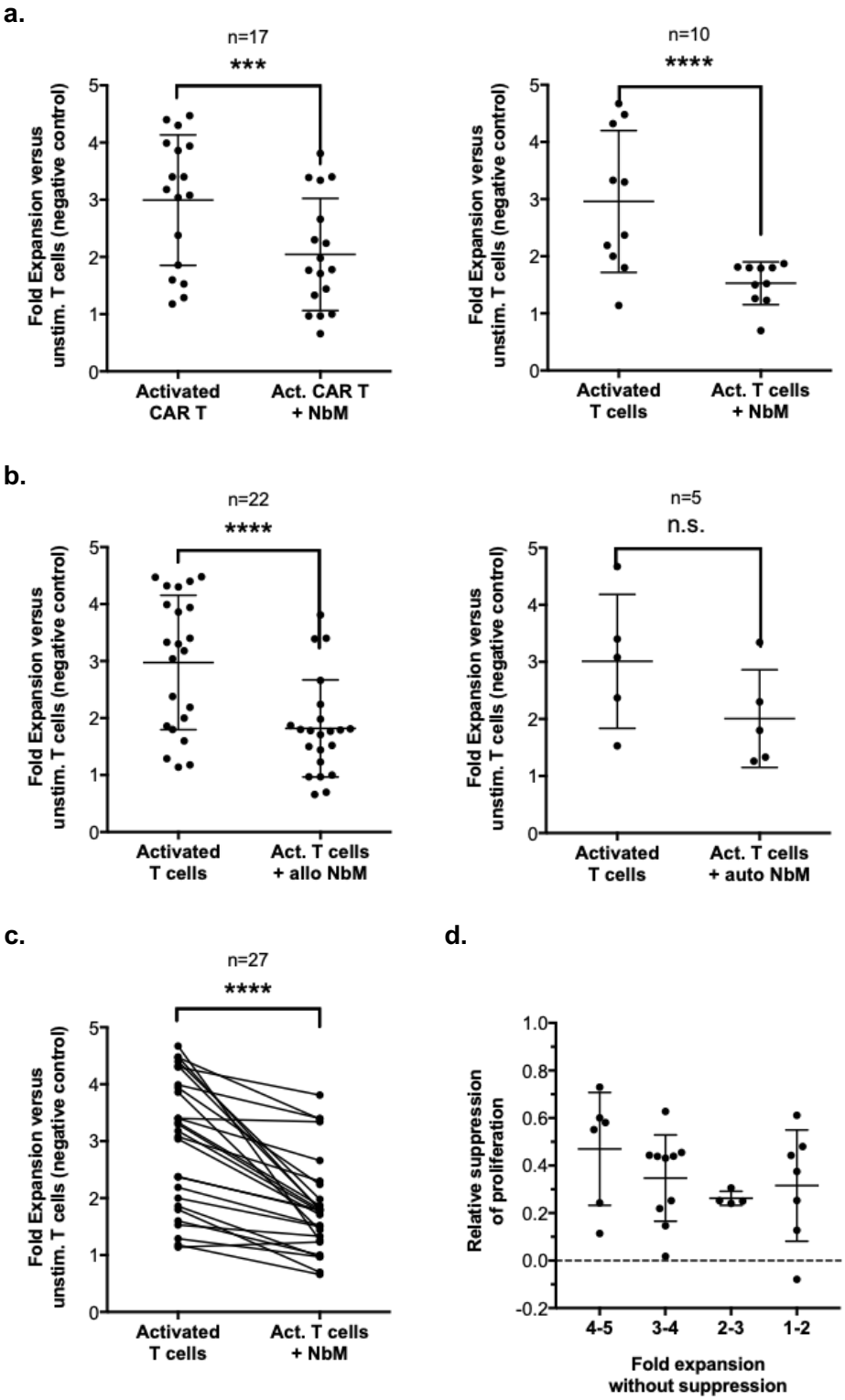

Figure 3-11 Suppressive effect of neuroblastoma-conditioned monocytes on T cell proliferation. Pooled data from 27 donors sorted by (a) CAR-modified T cells versus unmodified T cells, (b) autologous versus allogeneic monocytes, (c) portrayed as a summary of all individual donors, and (d) as a correlation between T cell proliferation without NbM and Relative suppression with NbM. T cell proliferation after 7 days is displayed as a fold ratio compared to the expansion seen in the negative control (unstimulated T cells). Statistical test: Two-way ANOVA (a,b) and donor paired t-test (c) (p=* ≤0.05; ** ≤0.01; ***≤0.001; **** ≤0.0001).

Additional to NbM, the two previously mentioned monocyte controls (fresh monocytes, media-cultured control) were tested for suppressive effects in T cell proliferation cultures. While fresh monocytes only suppressed T cell proliferation in co-cultures with low significance, those kept in cell culture medium for 48 hours suppressed T cell proliferation to a similar extent as NbM. Both types of cultured monocytes suppressed T cell proliferation significantly when compared to stimulated T cells alone (**Figure 3-12**). Differences could only be seen in the previously described phenotype analysis, which indicated a predominant M-MDSC-like phenotype in Nb-conditioned monocytes and a larger proportion of immature eMDSC-like phenotypes in the media control.

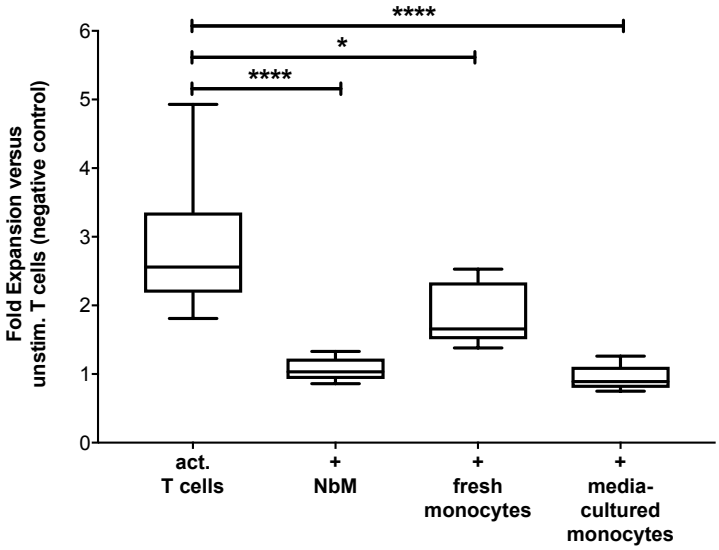

Figure 3-12 Suppressive effects of monocyte controls on T cell proliferation. T cell proliferation after 7 days is displayed as a fold ratio compared to the expansion seen in the negative control (unstimulated T cells). Box plots show average and 5-95 percentile from 6 healthy donors. Statistical test: one-way ANOVA (p=* ≤0.05; ** ≤0.01; ***≤0.001; **** ≤0.0001).

3.3.3. Suppression of T cell cytokine release

Since the release of pro-inflammatory cytokines is a crucial part of T cell activation, effects of NbM on T cell IFN-γ release into co-culture supernatants were analysed via ELISA. Cytokine release was significantly increased in the positive control when T cells were stimulated with CD3/CD28 Dynabeads (**Figure 3-13a**). This activation was significantly suppressed in co-cultures with added NbM, indicating that the conditioned monocytes robustly suppress both T cell proliferation and cytokine release. **Figure 3-13**b also shows a comparison of NbM-mediated cytokine suppression with the previously mentioned monocyte controls. Albeit all conditions significantly decreased the average IFN-γ concentrations in the co-culture supernatant, donor-to-donor variations were more common among both fresh monocytes and the media control reflected in wide data spreads.

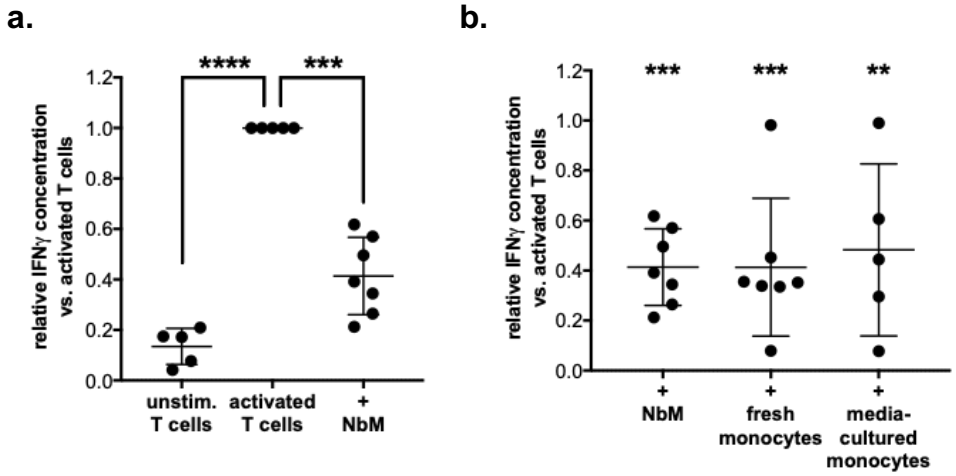

Figure 3-13 Suppression of T cell IFN-γ release mediated by NbM and monocyte controls. Pooled data from 7 healthy donors. a. Relative IFN-γ concentration in co-culture supernatants compared to a positive control of bead-activated T cells. b. Relative IFN-γ concentration in experiments containing activated T cells and either NbM, fresh monocytes or a monocyte media control. Stars indicate significance of difference from positive control (activated T cells alone). Statistical test: one-way ANOVA (p=* ≤0.05; ** ≤0.01; ***≤0.001; **** ≤0.0001).

3.3.4. Mechanisms of monocyte-mediated suppression

MDSC can mediate immunosuppressive effects through various mechanisms, which couldn't all be tested due to time limitations. For this thesis the generated NbM were tested for arginase activity and production of reactive oxygen species (ROS), both mechanisms which have been reported to be involved in MDSC-mediated T cell suppression.

NbM arginase activity

After generating cell lysates, the arginase activity assay kit by Sigma-Aldrich was used to investigate arginase activity in the generated NbM. Since it has been shown that neuroblastoma cells display a high arginase activity (Mussai et al., 2015), lysates of the neuroblastoma cell line Lan-1 were used as a positive control. Additionally, media conditioned monocytes were tested for arginase activity. The readouts indicated an average arginase activity in Lan-1 lysates of 124.5 mU/10^6 (**Figure 3-14a**), higher than the previously described 24 mU/10^6 in neuroblastoma cells (Mussai et al., 2015). The lysates of NbM however, displayed an average of 5.5 mU/10^6 suggesting much lower arginase activity in the conditioned monocytes. Similarly, only low arginase activity could be measured in the media conditioned monocyte control.

NbM ROS production

Production of reactive oxygen species was assessed in the flow cytometry based DCFDA assay. For this, the monocytes were stained with DCFDA, a fluorogenic dye, which is oxidised into a highly fluorescent compound (DCF) when reactive oxygen species are available. Therefore, the DCF-emitted fluorescence intensity can be used as an indicator for ROS activity in the stained cells (**Figure 3-14c**). As a positive control, cells were stimulated with the ROS inducing TBHP, whereas a negative control contained cells

which were not stained with DCFDA to correct for auto-fluorescent signals. Results showed that the mean DCF intensity of stained NbM after 4 hours incubation was 54% as bright as the DCF MFI measured when stimulated with TBHP (**Figure 3-14b**). Also the media control indicated a production of ROS, with a MFI of 42% compared to the positive control. NbM showed significant DCF signal when compared to the unstained control, whereas ROS production by the media control prove to be not significant. This suggests that ROS activity could be one of the suppressive mechanisms through which the polarised monocytes suppress T cell activation and proliferation. Similarly, media culturing of monocytes also results in detectable oxidation activity.

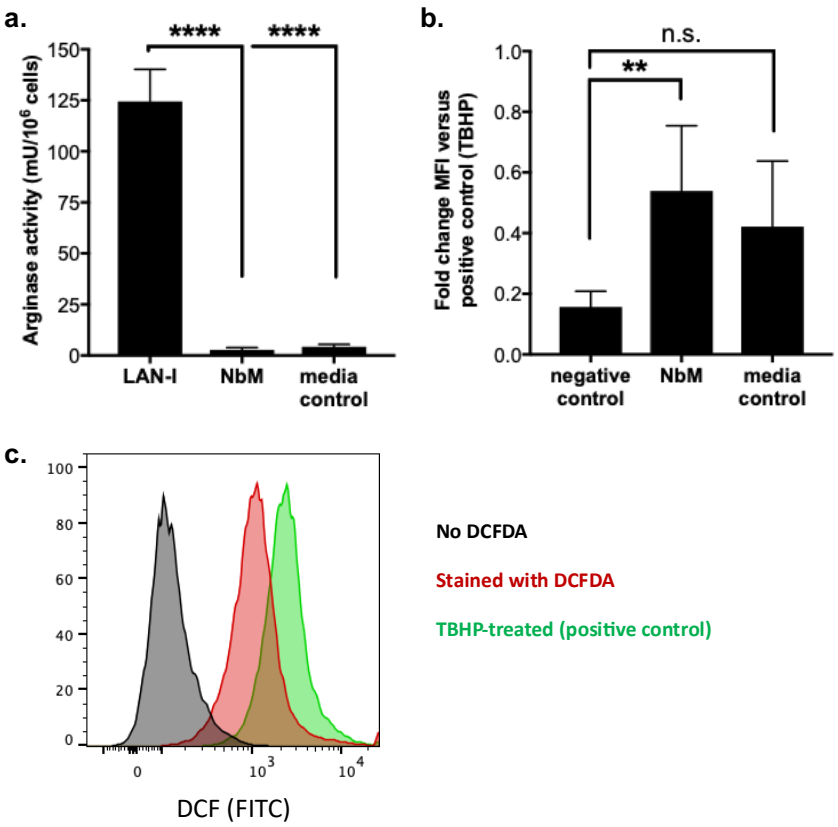

Figure 3-14 Functional characterisation of neuroblastoma-conditioned monocytes. a. Arginase activity measured in NbM lysates (middle) and the media control (right) versus lysates of the neuroblastoma cell line Lan-1 (left). The vertical axis describes arginase activity in mU/106 cells. One unit of Arginase is the amount of enzyme that will convert 1.0 µmole of L-arginine to ornithine and urea per minute at pH 9.5 and 37 ºC. Diagram shows average of pooled results from 3 donors performed in duplicates. Statistical test: one-way ANOVA. b. ROS production of NbM measured in a DCFDA-based assay. Bar on the left shows an unstained control to exclude auto-fluorescence of cells. Bar on the right shows the positive control stimulated with TBHP. Incubation time during stimulation was 4 hours. Diagram shows average of pooled results from 5 donors. Statistical test: one-way ANOVA. c. DCFDA assay flow cytometry data from one representative healthy donor. The histogram displays the DCF intensity which is proportional to the availability of ROS in each sample. (p=* ≤0.05; ** ≤0.01; ***≤0.001; **** ≤0.0001).

3.4. Discussion

The aim of this first chapter was to optimise and establish a feasible model for the investigation of MDSC-inhibitory drugs in neuroblastoma T cell therapy. Based on the literature (Mussai et al., 2015), we suggested that healthy monocytes can be differentiated towards a suppressor phenotype when conditioned in neuroblastoma cell supernatant. To validate their suppressive character, these polarised cells had to be analysed for phenotype as well as function in co-cultures with T cells. To ensure a robust baseline T cell proliferation for subsequent investigation of suppression, a flow cytometry-based proliferation assay was optimised.

Experiments conducted in unmodified T cells showed average 5.6-fold expansion 7 days after stimulation with CD3/CD28 dynabeads. Furthermore, cells stained with the proliferation marker CellTrace Violet lost fluorescent intensity in 77.7% of total cells, whereas an unstimulated control retained the marker over 7 days (**Figure 3-3**). This suggests that bead-mediated activation of unstimulated T cells is a feasible method to establish robust T cell expansion rates for subsequent use in co-cultures. We decided to rely on counting beads to calculate proliferation for all subsequent experiments as it has a more quantitative character than detection of CellTrace Violet and will enable us to adequately observe differences in co-cultures with suppressive monocytes.

As this study aims to overcome suppressive effects of the TME in adoptive therapies using CAR-modified T cells, assay conditions also had to be optimised for CAR T cell proliferation. In this context, proliferation of neuroblastoma-specific anti-GD2 CAR-modified T cells was observed comparing GD2-positive target cell lines. Flow cytometry analysis confirmed that the three investigated targets Lan-1, TC-71, and SupT1 GD2 were all expressing the antigen on their surface, whereas SupT1 wt cells did not and were

therefore used as a negative control (**Figure 3-4**). When co-cultured with target-specific CAR T cells (**Figure 3-5**), neither the negative control, nor the neuroblastoma cell line Lan-1 stimulated T cell proliferation above 1.3-fold. Since the CAR showed capacity to induce proliferation with other GD2-positive targets, this suggests a neuroblastoma-specific suppression of proliferation. Indeed, Mussai and colleagues have demonstrated that both murine and human neuroblastoma cells can suppress T cell proliferation, and that this likely is an effect of increased arginase 2 activity in these tumours (Mussai et al., 2015). At a 1:1 ratio, the GD2-positive targets SupT1 GD2 and TC-71 induced an average 1.7- or 1.6-fold expansion, respectively, when compared to an unstimulated control. However, no statistical significance was observed, which was likely a result of large data spreads between donors.

In an attempt to improve proliferation rates seen with stimulated CAR T cells, an increased assay scale (48-well plate versus 96-well plate) was investigated. In the upscaled assay, previous results were confirmed. Again, Lan-1 cells did not stimulate CAR T cell expansion, however SupT1-GD2-mediated proliferation was improved compared to the smaller format, significantly increasing T cell proliferation by 3-fold (**Figure 3-6**). This suggests that in a 96-well plate assay the smaller well surface might have limited CAR T cell proliferation, possibly because of a lack of space for cell growth or because of insufficient binding of targets.

Having established the T cell proliferation assay using either bead-stimulated T cells or SupT1-GD2-stimulated anti-GD2 CAR T cells in a 48-well plate, next generation of suppressive monocytes was optimised. First, the effects of duration of monocyte conditioning were investigated in terms of suppressive potential of the conditioned monocytes. When comparing monocytes conditioned for 2-7 days, suppression in CAR

T cell co-cultures was observed in those conditioned for 2, 4, and 7 days, but not 5 or 10 days (**Figure 3-7**). We hypothesise that the suppressive character of NbM is more reliable when conditioned for no longer than 4 days before used in T cell proliferation assays. Secondly, the dynamics of T cell suppression were investigated using NbM conditioned for 2 days in co-cultures with bead-stimulated unmodified T cells. Analysis of T cell numbers over the 7 days after co-culture start indicated that NbM-mediated suppression was most noticeable after 6 days or longer. No difference was seen when conditioning medium was used fresh or frozen, or when changing density of neuroblastoma cells for the generation of the conditioning medium (**Figure 3-8**). In conclusion, we suggest to condition monocytes for 2 days for the generation of NbM and analyse the effects on T cell proliferation in co-cultures after 7 days.

In the last section of this chapter, NbM were assessed for their MDSC-like characteristics. When analysed for MDSC-typical markers, NbM mostly reflected the phenotype of the M-MDSC subpopulation (**Figure 3-10**). The population increased to 32.4% of myeloid cells in the neuroblastoma-conditioned group, but also increased in a control grown in regular cell culture medium. Moreover, a population with an eMDSC-like phenotype increased in both NbM and media control. The increase in this immature subpopulation might indicate a lack of differentiation signalling, similar to the defective myelopoiesis seen in cancer patients. Both NbM and the media control were found to induce MDSC-like phenotypes, confirming reports of an effect of *in vitro* culture alone on monocyte phenotype (Veglia et al., 2018). However, the differences in subpopulations (more M-MDSC in NbM, more eMDSC in media control) indicate that there are differences in phenotype and possibly function between the two types of conditioned monocytes. These differences likely result from neuroblastoma-generated stimuli in the conditioned medium. No PMN-MDSC-like cells were seen in any of the tested conditions. Since the

protocol used for monocyte isolation included FICOLL and a negative selection for CD14+ CD16+ cells, granulocytic CD15+ cells were lost, explaining the complete lack of CD15+ cells in the unconditioned control. This did not change with the polarisation of monocytes, suggesting no transition of isolated cell types towards the PMN-MDSC phenotype during this process. Casacuberta-Serra and colleagues have described the generation of both PMN- and M-MDSC from purified CD34+ haematopoietic progenitors using stem cell factor, thrombopoietin, FLT3 ligand, GM-CSF and IL-6. However, when applying a similar cocktail on peripheral blood monocytes, they only saw an enrichment of M-MDSC, not PMN-MDSC (Casacuberta-Serra et al., 2017). Taken together with the findings reported in this thesis, this suggests that PMN-MDSC cannot be generated from monocytes *in vitro*. Indeed, suppressive myeloid populations, including MDSC, TAM and DC, typically originate from bone marrow-derived monocytes and neutrophils. Chronic activation by extended and weak signalling in cancer and other diseases through factors like GM-CSF, G-CSF, and M-CSF stimulates an altered myelopoiesis of local progenitors and ultimately leads to the accumulation of a heterogeneous group of suppressive myeloid cells (Veglia et al., 2018). A lack of neutrophils or common progenitors may prevent accumulation of PMN-MDSC in our assay, however we decided that this model of monocyte de-differentiation was sufficient in the context of developing an in vitro screening tool amenable to evaluation in larger numbers of biological replicates.

To be considered MDSC, more important than matching phenotypes is the ability of suppressive monocytes to inhibit T cell growth. Comparison of 27 proliferation assays using CAR T cells and unmodified T cells showed robust suppression mediated by NbM (from 3.1-fold to 1.8-fold expansion; **Figure 3-11**). When dissecting experiments for autologous versus allogeneic T cells and monocytes, statistical significance was only seen

with allogeneic cells. However, there were four times as many experiments performed with allogeneic cells (22 versus 5 donors), suggesting that the inhibition seen with autologous NbM might have proven significant if there had been more biological replicates. No correlation between T cell proliferation and subsequent extent of suppression could be found. Similar suppression as with NbM was seen when co-culturing media control monocytes with T cells, suggesting that both conditions are able to generate suppressive phenotypes, as discussed previously (**Figure 3-12**).

As a second indication of T cell suppression, IFN-γ levels in co-culture supernatants were analysed by ELISA. Experiments showed that CD3/CD28 dynabeads also stimulated cytokine release in T cells, which was significantly suppressed when adding NbM (**Figure 3-13**). This strong inhibition of IFN-γ release was only observed with the neuroblastoma-conditioned cells, but not in the media control, indicating a specific suppression of T cell activation and signalling in the presence of NbM.

To narrow down mechanisms leading to the observed T cell suppression, two known pathways of MDSC-mediated suppression were investigated for NbM and media control. Analysis of arginase showed no significant activity in the suppressive monocytes, but significant activity was seen in Lan-1 cells, which served as a positive control (**Figure 3-14**). This again confirms the findings of Mussai and colleagues, which reported that neuroblastoma cells can suppress immunity through arginase 2-dependent depletion of L-arginine (Mussai et al., 2015). Furthermore, using a DCFDA assay, ROS activity was assessed. Indications for intermediate ROS activity were found both in NbM and the media control.

A more comprehensive evaluation of suppressive mechanisms by NbM was beyond the scope of this thesis but the combined results of this chapter are consistent with

characteristics common with M-MDSC, as described in the literature. Although media-cultured monocytes and NbM both have phenotypic and functional characteristics of MDSC, there are reproducible phenotypic differences. This increases our confidence that NbM represent a population that is likely to have features in common with MDSC in the neuroblastoma microenvironment. It would be of interest to define the key features in terms of functions by looking at other mechanisms of suppression, such as TGF-β production, NO generation and IDO activity. However, since the focus of the thesis is on MDSC inhibition, on the basis of these findings we felt we had established a tractable model of monocyte-mediated suppression in neuroblastoma that could be used to identify possible mechanisms to counteract these effects.

In conclusion, in this chapter we established a robust T cell proliferation assay and a neuroblastoma-based model for the assessment of suppressive monocyte effects on T cell functions. This can form the basis for subsequent applications to investigate drug- or cell-based solutions to overcome monocyte-mediated suppressive effects in the TME of neuroblastoma.

4. RESULTS II – Drug retargeting to overcome monocyte-mediated suppression

4.1. Introduction

Combination therapy provides the opportunity to combine two or more therapeutics to achieve improved efficacy and function at lower doses. The resulting effects might be of additive nature but in some circumstances can be synergistic, providing greater efficacy than obtained by simple addition of two agents in combination. Recent clinical studies have demonstrated improvements to the anticancer effects of CAR T cell when administered in combination with other treatments, such as chemotherapy, radiotherapy, or CPI (Xu et al., 2018). Furthermore, it has been reported that certain chemotherapeutic agents can selectively inhibit immunosuppressive cells of the TME, thus enhancing T cell function and proliferation in the tumour proximity (Xu et al., 2018). This is especially important in the context of MDSC: Since the myeloid suppressors have no unique surface antigens that can be co-targeted with adoptive T cell therapy, combination therapies with chemotherapeutics or other drugs could provide a promising alternative. Several molecules have been described to possess MDSC-regulatory or -depleting functions, some of them already FDA-approved.

One possibility is to prevent the formation of MDSC and the depletion of existing populations. Sunitinib malate is an orally administered broad tyrosine kinase (TK) inhibitor, that is FDA-approved for advanced renal cell carcinoma and affects c-kit and VEGFR in MDSC, both receptors that are involved in the formation of the suppressive phenotype (Draghiciu et al., 2015a). A similar depletion of MDSC levels has been observed when administering the nucleoside analogue gemcitabine hydrochloride,

commonly used as a chemotherapeutic. It induces apoptosis and necrosis in MDSC, lowering MDSC levels found in the spleen of tumour bearing mice (Suzuki et al., 2005).

A second approach to target MDSC-mediated suppression is to promote their differentiation into mature non-suppressive myeloid cells. A candidate that has been shown to induce MDSC differentiation into mature dendritic cells *in vitro* and *in vivo* is all-trans retinoic acid (ATRA), a vitamin A metabolite. ATRA specifically upregulates protein levels of glutathione synthase in MDSC, leading to an accumulation of glutathione. This neutralises the high levels of ROS, one of the primary mechanisms of T cell suppression as well as the main contributor to inhibition of differentiation in MDSC (Nefedova et al., 2007). Other substances in discussion for promoting MDSC differentiation are Vitamin D3 and Curcumin (Draghiciu et al., 2015a).

A final strategy to counteract MDSC is by interfering with their suppressive mechanisms. The characteristic nutrient depletion in the TME can be prevented by inhibiting responsible enzymes in MDSC, Arg1 and iNOS. These enzymes can be targeted via different ways. Phosphodiesterase-5 (PDE-5) inhibitors, for example, inhibit cGMP degradation which as a result downregulates expression of Arg1 and iNOS. In turn, this inhibits MDSC, induces antitumour immune responses and delays tumour progression (Serafini et al., 2006b). Another essential mechanism of suppression by MDSC is the accumulation of reactive oxygen species. By activating the transcription factor NFR2, bardoxolone methyl (CDDO-Me) induces the expression of antioxidant genes, thereby neutralising the effects of ROS and RNS. *In vivo*, CDDO-Me abrogated MDSC-mediated suppression and decreased tumour growth, indicating the important role of this mechanism (Nagaraj et al., 2010b).

The repurposing of drugs such as these, which have been approved by the FDA in the context of other malignancies, has several benefits during the development of new therapies. A major potential advantage compared with developing new drugs, is the known safety profile of approved drugs. Additionally, both cost and time to the clinic can be significantly reduced, allowing for quick adjustments of therapies that are already at the clinical trials stage. Compound libraries, such as the Prestwick chemical library, enable the investigation of a large variation of FDA-approved drugs in high-throughput screens.

The aim of the following chapter was to investigate the established Nb-based myeloid suppressor model for its suitability in drug repurposing screens. For this, selected drugs (Sunitinib malate, gemcitabine) were investigated for their ability to re-establish T cell proliferation and function in NbM co-cultures. Furthermore, the system was adjusted to fit high-throughput screens using a chemical library, which was then demonstrated in a pilot screen using part of the Prestwick chemical library.

4.2. Individual drug screens

To investigate the suitability of the established neuroblastoma-based suppressive monocyte model for drug screenings, the first experiments were set up testing effects of individual MDSC-inhibitory drugs rather than multi-component screens. As summarised in chapter 3.2, proliferation in co-cultures was read out in a 48-well plate format with equal numbers of stimulated T cells and NbM. To assess effects, co-cultures were left for 7 days with or without a range of concentrations of the drug of interest, and then investigated for relative T cell proliferation compared to a negative (unstimulated T cells) and positive (stimulated T cells) control. Additionally, a DMSO-only vehicle control (VC) was included, to allow for effects of the DMSO used for drug dilution.

4.2.1. Sunitinib malate

The TK inhibitor Sunitinib malate has been described to deplete MDSC populations via interference with c-kit and VEGFR (Draghiciu et al., 2015a). Studies indicated that Sunitinib reduced the expansion of M-MDSC while depleting PMN-MDSC via induction of apoptosis (Ko et al., 2010). When administered to advanced RCC patients, Sunitinib significantly increased the amount of activated T cells, decreased MDSC levels and decreased the expression of inhibitory cytokines found in the TME – IL-10, TGF-β, FoxP3 and IL-4. Furthermore, the checkpoint proteins CTLA4 and PD-1 on T cells as well as PDL-1 on MDSC were downregulated (Ozao-Choy et al., 2009). Altogether, these findings suggest strong evidence for Sunitinib to deliver a suitable support against the TME in combination therapies with CAR T cells.

Recovery of T cell proliferation in NbM co-cultures

To investigate the effects of Sunitinib on NbM-mediated mechanisms, an effective concentration range suitable for the use in T cell proliferation cultures had to be determined first.

Firstly, direct effects of Sunitinib on T cell proliferation and viability had to be investigated. Therefore, GD2 CAR T cells were co-cultured with target cells and increasing concentrations of Sunitinib ranging from 0.01 μM to 500 μM. When assessing T cell numbers after 7 days, Sunitinib exhibited no significant effects up to a concentration of 2.5 μM (see **Figure 4-1**a). When using higher concentrations (5-500 μM), Sunitinib had an inhibitory effect on T cell proliferation.

To see effects on MDSC-mediated suppression, the same co-culture was set up with the addition of NbM. As previously described, the suppressive cells inhibited T cell proliferation significantly down to 49% of proliferation seen in activated T cells alone (see **Figure 4-1**b). Adding increasing concentrations of Sunitinib, T cell expansion could partly be recovered, with a maximum rescue of 76% of average CAR T cell proliferation using 0.1 μM of the inhibitor. However, findings weren't statistically significant and fluctuated between donors. Above concentrations of 2.5 μM, T cell counts were similar to or lower than the negative control. This suggests a cytotoxic effect of high concentrations of Sunitinib, coherent with the observations from MDSC-free experiments.

Despite insignificant results, the concentration range between 0.01 μM and 1 μM was further investigated in subsequent experiments focussing on alternative readouts for T cell suppression.

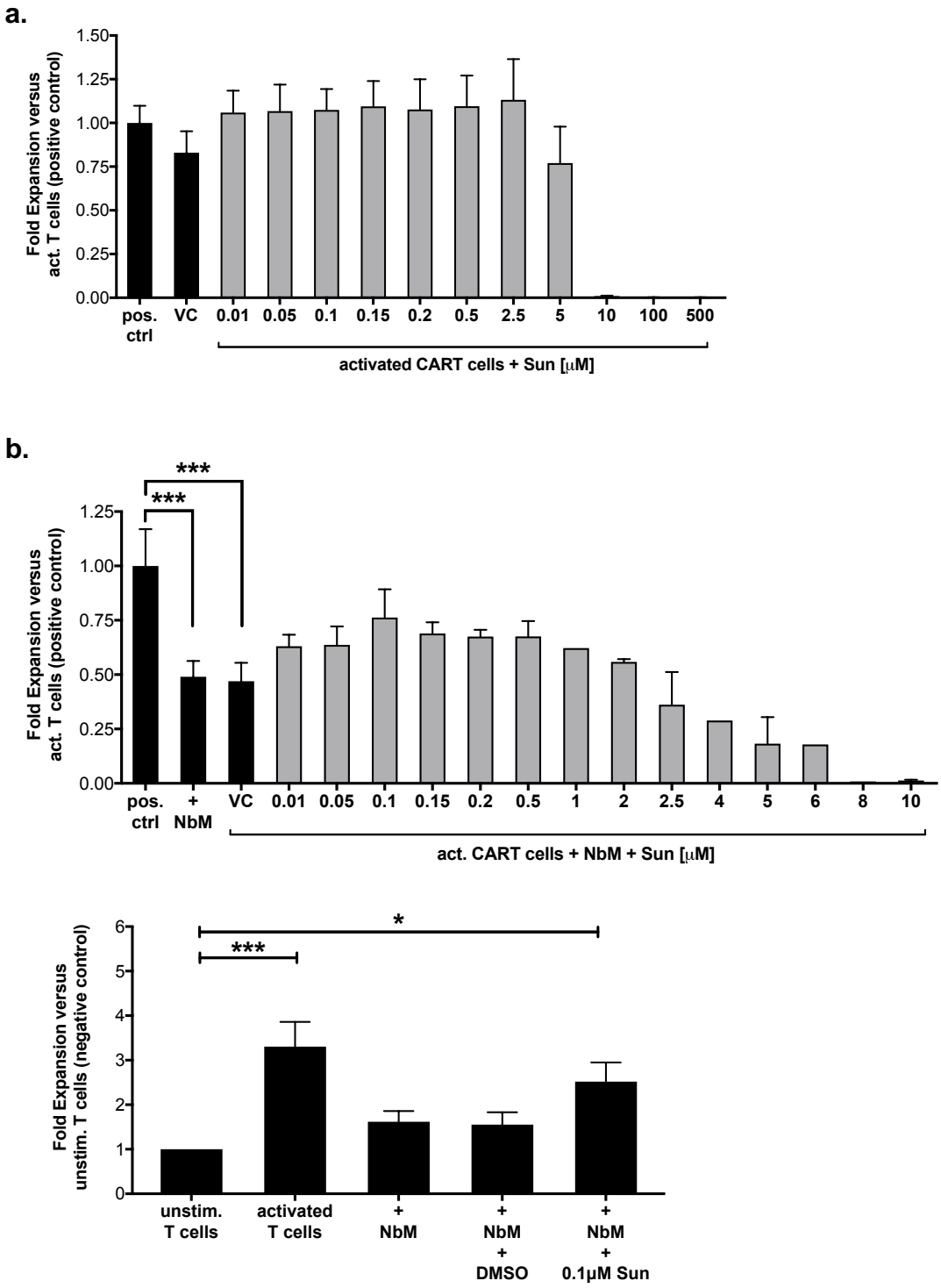

Figure 4-1 Effects of Sunitinib malate on NbM-mediated T cell suppression measured by T cell proliferation. a. Sunitinib drug tolerance in T cell cultures measured as fold expansion compared to a positive control without Sunitinib. Concentrations ranging from 0.01μM to 500μM were tested. VC= vehicle control (DMSO). b. Sun-mediated influence on T cell proliferation in co-cultures with NbM. T cell proliferation after 7 days is displayed as a fold expansion compared to a positive control (activated T cells, top) and compared to the negative control (unstimulated T cells, bottom). Concentrations ranging from 0.01μM to 10μM were tested. All bar graphs display mean + SEM from 6 donors performed in duplicates. Statistical test: one-way ANOVA (p=* ≤0.05; ** ≤0.01; ***≤0.001; **** ≤0.0001).

Recovery of T cell cytokine release in NbM co-cultures

Since the release of pro-inflammatory cytokines is a crucial part of T cell activation, effects of MDSC and Sunitinib on cytokine levels was investigated using intracellular flow cytometry. To further exclude direct effects on T cells, NbM were pre-treated with Sunitinib for 48 hours, before adding T cells to the co-culture.

Levels of IL-2, TNFα and IFN-γ in unstimulated and PMA/Ionomycin-stimulated cells are shown in **Figure 4-2**. A significant increase in the production of all three cytokines could be seen when comparing stimulated with unstimulated T cells. Cytokine levels significantly decreased when adding NbM to stimulated T cells. Detection of MFI of cytokine-binding fluorescent antibodies indicated average signals of 27%, 39%, and 42% compared to the positive control looking at IL-2, TNFα, and IFN-γ, respectively. Pre-treating the NbM with increasing concentrations of Sunitinib partly recovered all three cytokine signals in a dose-dependent manner. IL-2 release was recovered to a signal 70% as bright as the positive control with 1μM of Sunitinib. The detected TNFα signal in samples pre-treated with 1mM Sunitinib even recovered back to 90% MFI compared to the positive control, which prove to be highly significant. With the strongest donor-to-donor variations, IFN-γ recovery was not as statistically significant as the effects seen on the other two cytokines but still indicated a relative MFI of 79% on average.

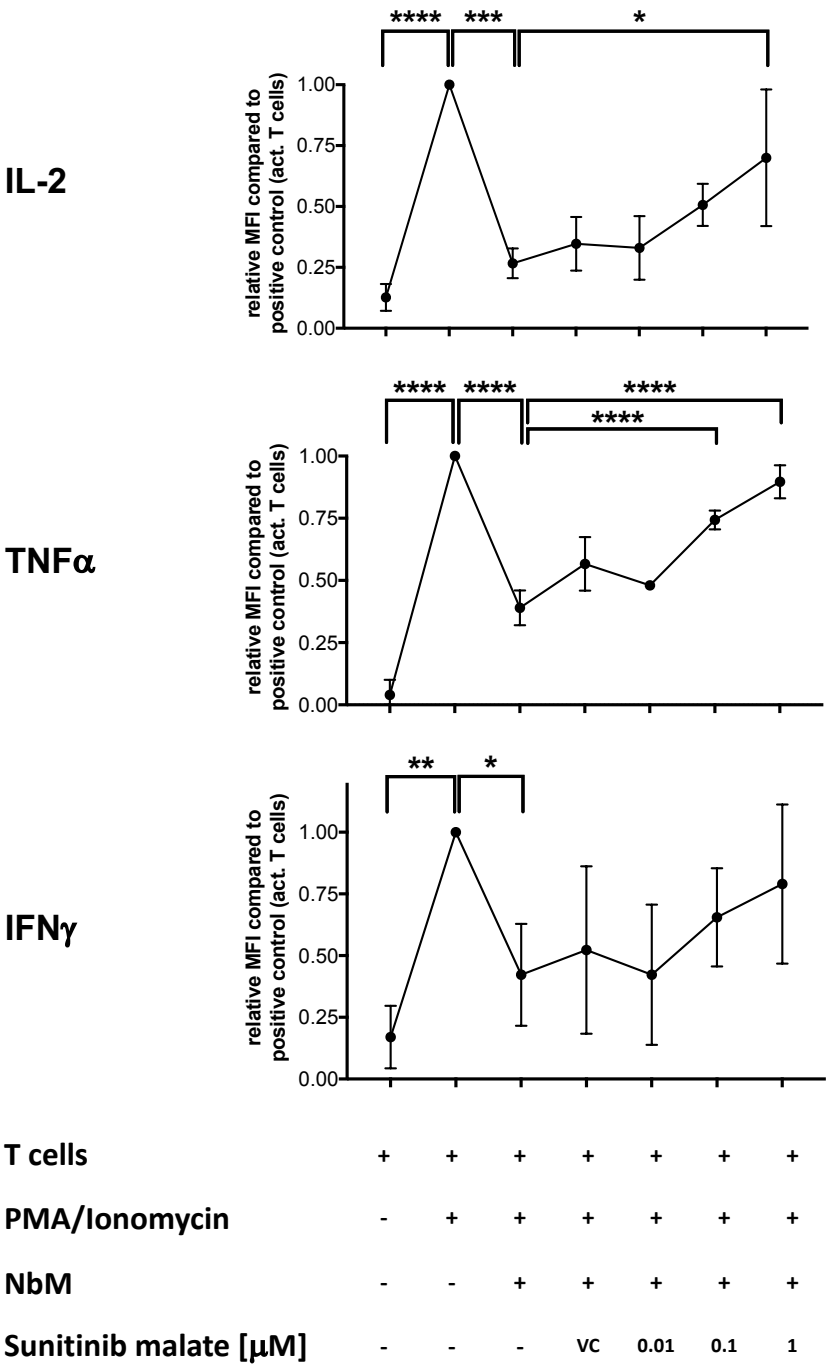

Figure 4-2 Effects of Sunitinib malate on NbM-mediated T cell suppression measured by T cell cytokine release. Sunitinib-mediated influence on T cell cytokine production in a pre-treatment model. NbM were pretreated with 0.01µM, 0.1µM, or 1µM Sun for 48h before adding the T cells. Levels of IL-2 (top), TNFα (middle), and IFN-γ (bottom) were investigated in a flow cytometry-based intracellular staining. Data points show relative MFI compared to positive control (activated T cells) of results generated from 3 healthy donors. Statistical test: one-way ANOVA (p=* ≤0.05; ** ≤0.01; ***≤0.001; **** ≤0.0001).

4.2.2. Gemcitabine

Similar depletions of MDSC levels as seen with Sunitinib have been reported for the chemotherapeutic gemcitabine hydrochloride. It has been suggested that Gemcitabine induces apoptosis and necrosis in MDSC.

The approach to test Gemcitabine effects on T cell proliferation was similar to the experiments testing Sunitinib effects (**Figure 4-3**a). Firstly, direct effects on T cell proliferation without the influence of suppressive monocytes were tested for concentrations 0.01 nM to 250 nM. T cell proliferation was not negatively affected up to a concentration of 0.5 nM. Starting from 2 nM, Gemcitabine had a cytotoxic effect on T cells, indicating a possible effective range without side effects between 0.01 nM and 0.5 nM. Pharmacokinetic studies in paediatrics have shown an average plasma concentration of 24.4 μM one hour after 10mg/m2/min gemcitabine (Steinherz et al., 2002), thus the much lower concentration investigated here should be attainable when reducing doses.

Subsequent experiments were to test the effect of Gemcitabine on NbM-mediated suppression of T cell proliferation (**Figure 4-3**b). Similar to previous co-cultures, T cell proliferation could be significantly induced with bead-stimulation and equally significantly suppressed to an average 49% with the addition of NbM. However, no Gemcitabine concentration of the tested range (0.01 nM to 250 nM) resulted in recovery of T cell expansion. As shown in **Figure 4-3**a, concentrations above 5 nM also led to decreased proliferation due to T cell toxicity (**Figure 4-3**b).

Since there was no improvement of T cell proliferation seen with any of the tested concentrations of Gemcitabine, no further investigations of its effects were performed.

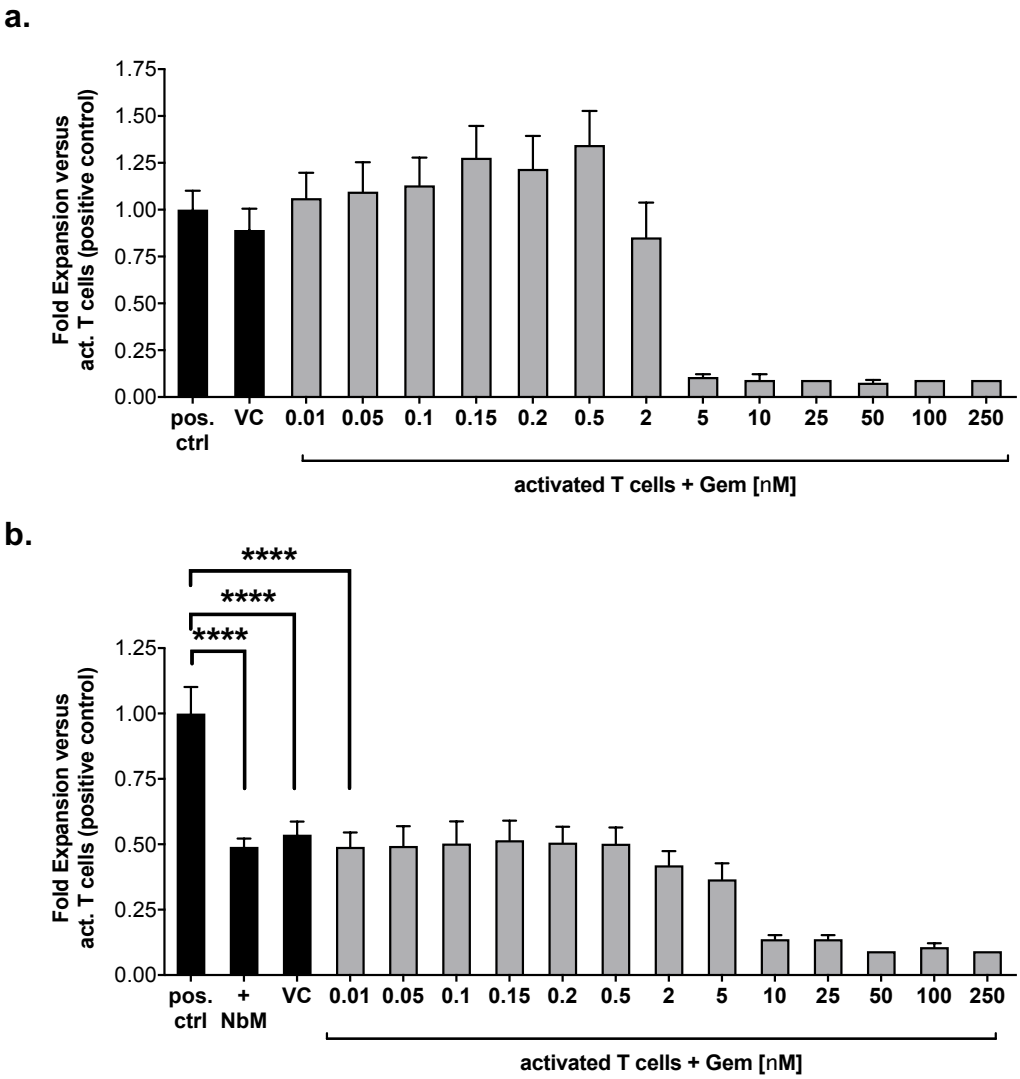

Figure 4-3 Effects of gemcitabine on NbM-mediated T cell suppression measured by T cell proliferation. a. Gemcitabine drug tolerance in T cell cultures measured as fold expansion compared to a positive control without Sunitinib. Concentrations ranging from 0.01 nM to 250 nM were tested. VC= vehicle control (DMSO). b. Gemcitabine-mediated influence on T cell proliferation in co-cultures with NbM. T cell proliferation after 7 days is displayed as a fold expansion compared to a positive control (activated T cells). Concentrations ranging from 0.01 nM to 250 nM were tested. All bar graphs display mean + SEM from 4 donors performed in duplicates. Statistical test: one-way ANOVA (p=* ≤0.05; ** ≤0.01; ***≤0.001; **** ≤0.0001).

4.3. Prestwick library screen

The Prestwick chemical library contains 1280 off-patent small molecules, of which 95% have been FDA-approved. Thus, the library can provide a platform to widely screen for drugs which could be retargeted for the use in combination therapies for solid tumours.

4.3.1. Preliminary screens

Due to the large number of different chemicals covered by the library, the established model had to be adjusted to fit criteria for a high throughput screening. An ideal screening platform needs to be reproducible and provides the option for biological replicates and high throughput plate-based assessment. As described in previous sections, we have achieved standardisation of reagents used for monocyte polarisation (chapter 3.2.2) and optimised co-culture conditions for analysis in 48-well plates (chapter 3.2.1). For screening the many compounds of the Prestwick library, the co-culture size was reduced back to 96-well plate format. Furthermore, to streamline readout we decided to assess T cell inhibition through IFN-γ release rather than cell proliferation. Cytokine release can be robustly investigated using classical methods, such as ELISA, but also novel high-throughput readouts, such as cytokine bead array (CBA) and alphaLISA. As before, resulting cytokine concentrations were compared to standard controls, including wells of unstimulated T cells, stimulated T cells, and stimulated T cells with NbM without drug. Based on this screen, wells with significant recovery of IFN-γ production despite the presence of NbM will be selected and analysed in further readouts looking at other measures, such as effect on T cell proliferation and cytotoxicity.

Previous experiments with NbM had demonstrated that donor-to-donor variations sometimes led to failure in the generation of suppressive myeloid cells and absence of T cell suppression. To avoid exhausting the limited resources of the Prestwick library, we decided that a validation of NbM suppressive potential had to be performed for each donor before setting up the library screen. Only with successful suppressive character of the monocytes, recovering effects mediated by the library components can be measured. Given that monocytes could not be frozen without significant cytotoxicity, each donor's polarised monocytes had to be tested for suppressive character immediately before used in a library screen. Therefore, a first experiment was to investigate whether suppression exerted by NbM polarised for one day could be predictive for suppression seen with NbM from the same donor after two days of polarisation. If so, shortly polarised monocytes could be assessed for suppressive potential in parallel to the ongoing polarisation of monocytes used in the library screen.

The flow chart in **Figure 4-4** shows the approach to validate monocyte suppression before drug screen set-up. Monocytes were isolated from blood of healthy donors and cultured in Nb conditioning medium as described in chapter 3.1. Polarisation of the cells was conducted on two separate plates. After 24 hours, NbM from one plate were harvested and co-cultured with stimulated T cells. The co-culture supernatants were collected after a further 24 hours and then immediately analysed for IFN-γ via CBA. The short protocol of the CBA allows for assessment of cytokine concentration and subsequent set-up of other assays on the same day. If NbM-mediated suppression was observed, monocytes from the second plate (now polarised for 48 hours) were harvested and used in a T cell co-culture testing the effects of Sun or GM-CSF. Sun and GM-CSF are two arbitrarily selected substances to mimic conditions of the assay when adding a drug library. If the first co-culture failed to show sufficient NbM-mediated suppression, monocytes were

discarded, and the protocol was restarted with a different blood donor. Supernatants of the second co-culture were harvested after 24 hours and either used directly for ELISA-based analysis of IFN-γ concentration, or frozen for analysis at a later timepoint.

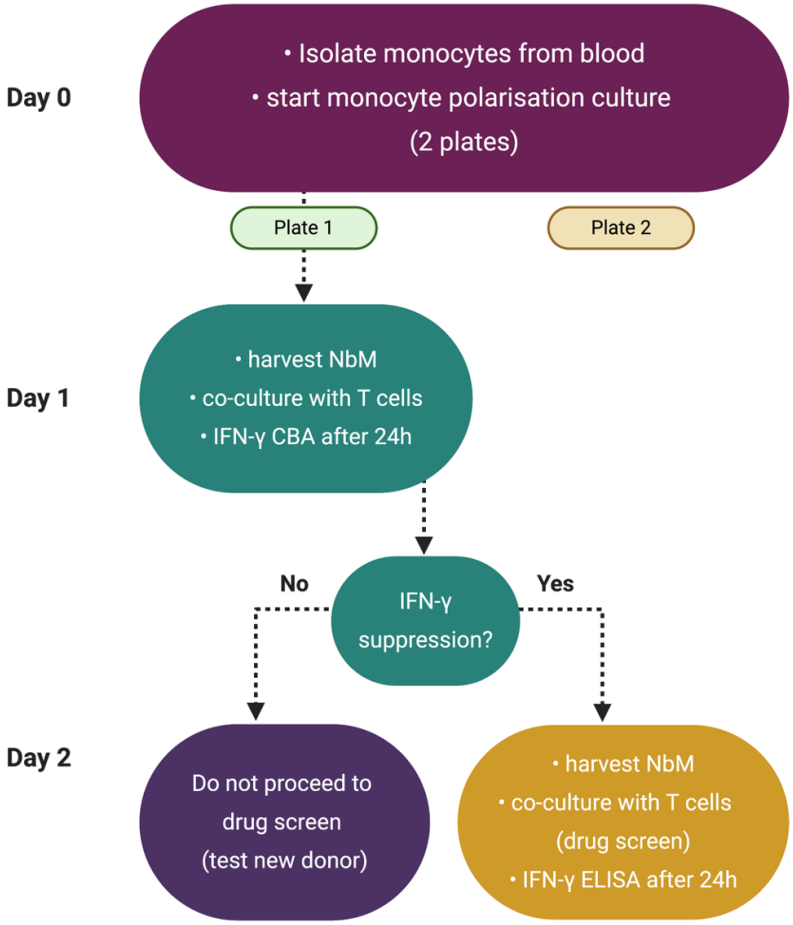

Figure 4-4 NbM validation for library screen. Flow chart showing steps to test suppressive potential of NbM for each donor before their use in chemical library screening assays. Only those showing T cell suppressive effects after 24h will be taken forward for co-cultures involving drugs to be tested.

Figure 4-5 portrays the results from two donors using the described protocol. Monocytes were polarised and tested both in a preliminary suppression assay after 24 hours via CBA (a) and in a drug screen after 48 hours via ELISA (b). IFN-γ suppression was robustly mediated by NbM from both donors and comparable between the two used methods. Using bead stimulation, T cell cytokine release was increased significantly, which could be reversed in a significant manner to an average of 11% (CBA) and 15% (ELISA) in wells containing NbM when compared to the positive control.

Furthermore, when testing Sunitinib in this assay, a similar recovery of cytokine release was observed as seen in chapter 4.2.1. Whereas NbM-mediated suppression decreased IFN-γ concentrations down to an average of 15% of those seen in the positive control, addition of 0.5 µM of Sun weakened the suppression to 42%. GM-CSF, a cytokine shown to induce MDSC subsets *in vitro* (Lechner et al., 2011), was used as a negative control and did not instigate changes in IFN-γ concentration.

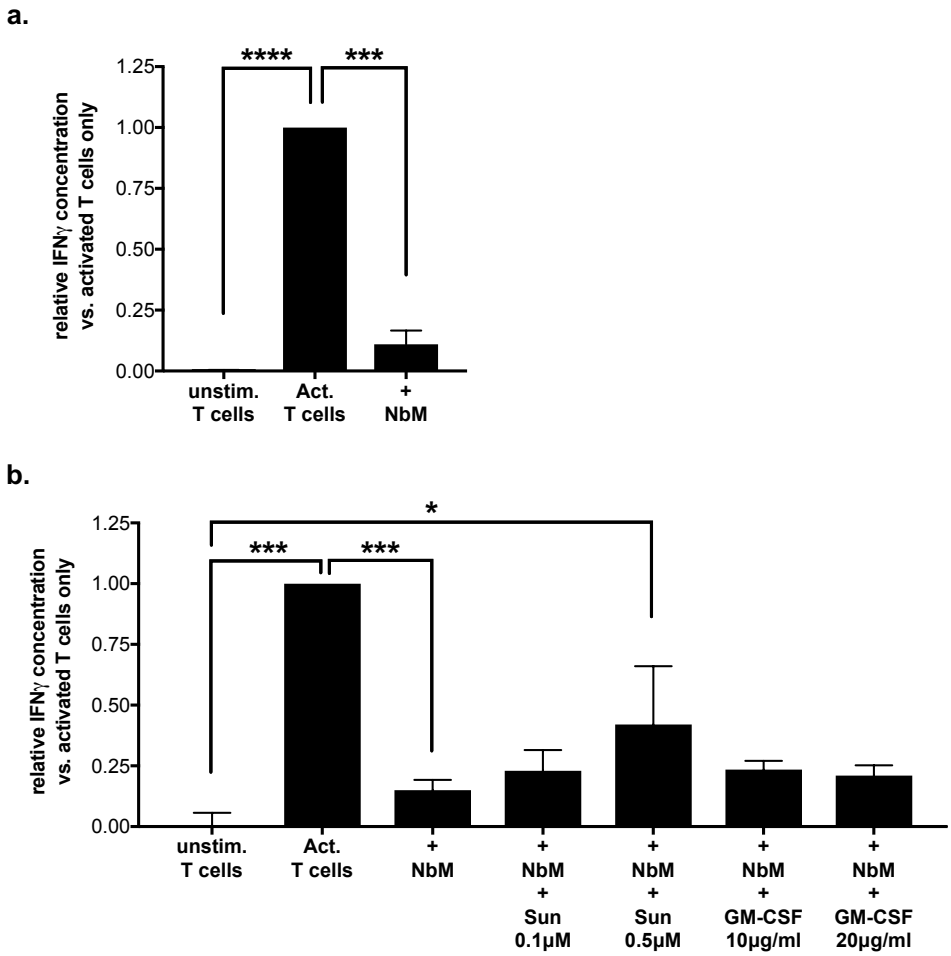

Figure 4-5 Pilot experiment to prepare for Prestwick library screen. All graphs show data from two healthy donors, performed in duplicates. a. Bar diagram showing mean + SD of relative IFN-γ concentration compared to a positive control (bead-stimulated T cells) measured by CBA. NbM used were polarised in Nb-conditioned medium for 24h. b. Bar diagram showing mean + SD of relative IFN-γ concentration compared to a positive control (bead-stimulated T cells) measured by ELISA. NbM used were polarised in Nb-conditioned medium for 48h. Statistical test: one-way ANOVA (p=* ≤0.05; ** ≤0.01; ***≤0.001; **** ≤0.0001).

4.3.2. Example library screen

With the streamlined protocol in place, an exemplary library screen testing 80 of the 1280 available drugs of the Prestwick chemical library was performed.

As described in the previous section, conditioned monocytes from healthy donors were validated for suppressive potential before used in the library screen co-cultures. **Figure 4-6** shows the results of an IFN-γ ELISA using co-culture supernatants from six independent donors and illustrates the importance of pre-screening NbM suppressive effects. Of the six tested donors, only NbM generated from three were suppressing T cell proliferation significantly, while the others only showed limited suppressive activity.

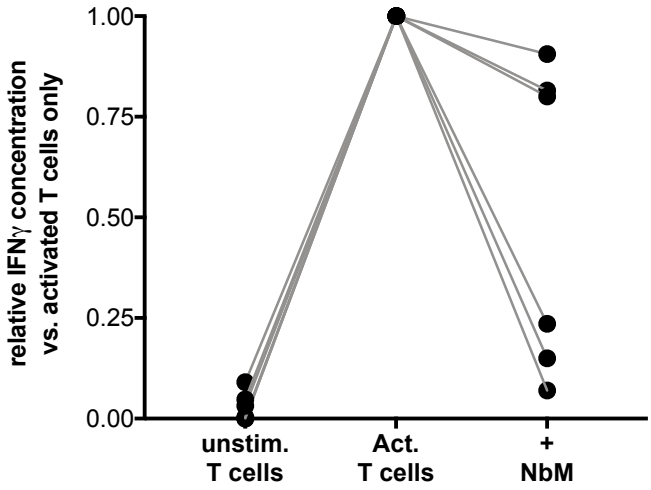

Figure 4-6 Validation of NbM suppressive potential before library screen. Relative IFN-γ concentration in co-culture supernatants compared to a positive control (bead-stimulated T cells), assessed by ELISA. Each point on the graph represents the mean of triplicates from one independent donor. NbM used were polarised in Nb-conditioned medium for 24h.

To ensure for an adequate therapeutic window, one of the highly suppressive donors was selected for the subsequent library screen. Additional to the standard controls (unstimulated T cells, bead-stimulated T cells, stimulated T cells + NbM), the co-culture contained one well for each of the 80 drugs of the Prestwick library. The respective chemicals were then added to a final concentration of 10 μM.

Figure 4-7 shows the results from an IFN-γ ELISA performed on the supernatants taken from the library co-culture after 24 hours. The dotted lines indicate the IFN-γ concentrations seen in the positive control (stimulated T cells, blue), the negative control (stimulated T cells + NbM, red) and a cut-off value indicating 50% of the positive control as a reference (black). Of the 80 tested substances, 10 resulted in an IFN-γ concentration lower than the negative control, 64 were similar to the negative control and below the 50% cut-off, and 6 lead to a recovery of IFN-γ to over 50% of the positive control.

The library drug which recovered cytokine release the most was number G10 which is the toll-like receptor 7 (TLR7) agonist Imiquimod. With Imiquimod, 79% of the IFN-γ production in the positive control was observed.

Furthermore, a recovery above 50% was seen with Montelukast (G7), Rufloxacin (H5), Rivastigmine (H8), Sildenafil (H9), and Acetylsalicylic acid (H10), although to a less extent.

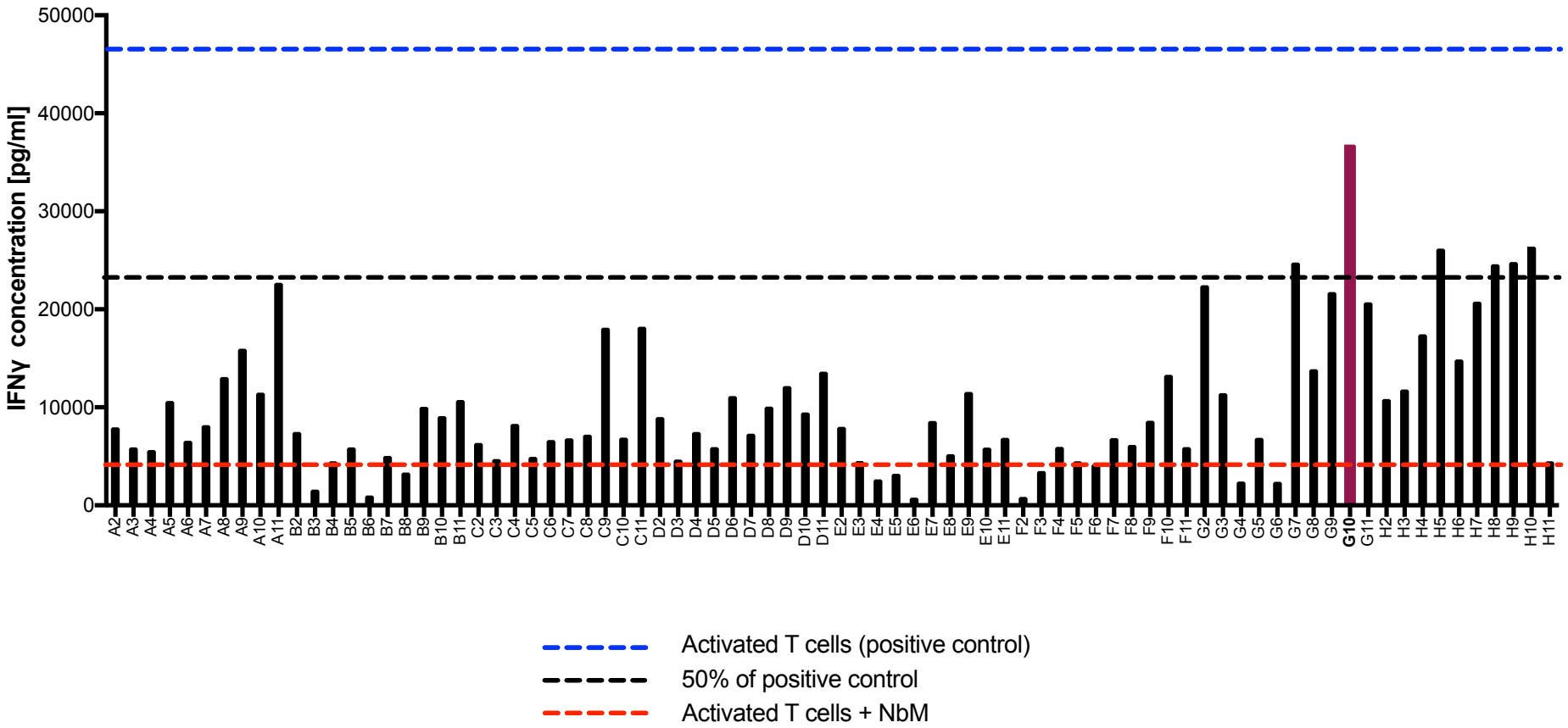

Figure 4-7 Exemplary library screen. Bar diagram shows IFN-γ concentration measured by ELISA from a 24-hour co-culture using one donor performed in singlets. NbM used were polarised in Nb-conditioned medium for 48h. Dashed lines indicate concentrations measured in positive control (stimulated T cells, blue), negative control (stimulated T cells + NbM, red) 50% of the positive control (black). The x-axis lists all drugs tested from the Prestwick chemical library, plate 15, at 10 µM (see supplementary for full list).

4.4. Discussion

In this chapter we demonstrated the suitability of our neuroblastoma-based model to screen for MDSC-inhibitory drugs for the purpose of drug retargeting in cancer immunotherapy. The optimised plate-based proliferation assay was used to investigate the effects of selected substances with MDSC-toxicity found in the literature. Furthermore, the assay was adjusted to suit a high-throughput drug library screen using recovery of T cell cytokine release, rather than proliferation, as a readout. In an exemplary library screen, we illustrated the successful application of the adjusted assay.

In a first series of experiments the effects of the TK inhibitor Sunitinib malate were tested in NbM/CAR T cell co-cultures. In preliminary assays without NbM, the drug did not show any effects on CAR T cell proliferation up until a concentration of 2.5 μM (**Figure 4-1**). At higher concentrations, the drug had a toxic effect on T cells, resulting in decreased proliferation rates. When testing the non-toxic range on CAR T cell co-cultures with NbM, the low proliferation seen with suppressive monocytes (49% of positive control) was partly recovered. The highest proliferation in co-cultures with NbM was seen when using 0.1 μM of Sunitinib, resulting in a proliferation that was an average of 76% of the proliferation seen in unsuppressed T cells. As before, donor-to-donor differences lead to large error bars and thus prevented statistical significance of the results.

To further validate the effects of Sunitinib on NbM/T cell co-cultures, T cell cytokine release was analysed using intracellular cytokine staining. Through treatment with PMA and Ionomycin, T cells were stimulated to produce significant levels of IL-2, TNFα, and IFN-γ (**Figure 4-2**). In co-cultures with NbM this cytokine production was significantly suppressed down to 27%, 39%, and 42%, respectively. A recovery of all three cytokine

signals was seen when pre-treating NbM with Sunitinib ranging from 0.1 μM to 1 μM. With 1 μM Sunitinib IL-2, TNF-α, and IFN-γ levels increased to 70%, 90%, and 79%, respectively. Interestingly, in this pre-treatment model 1 μM of Sunitinib resulted in a better recovery of T cell function than the previously best working 0.1 μM. This difference might be caused by direct interactions with T cell proliferation when the drug is added to the co-cultures rather than as a monocyte pre-treatment. Therefore, higher concentrations could have passed a threshold causing T cell inhibition, which masks beneficial effects they may have on NbM-mediated suppression. To maximise efficacy, future applications could involve pre-treatment of patients with Sunitinib followed by CAR T cell injection at a later time, when Sunitinib concentrations have declined. Altogether, this shows how crucial the determination of optimal concentration is for successful application in combination therapies.

Overall, the experiments investigating Sunitinib indicated a counteracting effect to NbM-mediated T cell suppression, recovering both T cell proliferation and cytokine release, two crucial measurements of T cell effector function. This suggests an involvement of the Sunitinib-targeted protein kinase receptors KIT and VEGFR in the suppressive functions or cell viability of the developed NbM model. If this results also in changes in T cell cytotoxic potential under the effects of NbM remains to be investigated in future experiments.

The second drug tested with the established model was the chemotherapeutic gemcitabine hydrochloride. Similar to the experiments with Sunitinib, a suitable concentration range was determined in T cell proliferation cultures. No direct effects on T cell proliferation were seen with concentrations up to 0.5 nM (**Figure 4-3**). Higher amounts of Gemcitabine mediated cytotoxic effects on T cells and were therefore unsuitable. In experiments with

NbM, Gemcitabine did not reverse the monocyte-mediated suppressive effects as demonstrated by low T cell proliferation with all tested Gemcitabine concentrations. With no indication of a beneficial effect of Gemcitabine, the drug was not further investigated in subsequent assays.

As both Sunitinib and Gemcitabine have been reported to inhibit MDSC functions, they were selected for a validation of the established co-culture assay to detect reversal of monocyte-mediated suppression. Neither chemical could significantly recover T cell proliferation in the tested concentration range, which could be explained by suboptimal doses and time of application or because the generated NbM might lack certain pathways and characteristics found in human MDSC. Due to time limitations, no further individual drugs were tested in proliferation assays.

In a second approach to screen for MDSC-inhibitory drugs, the plate-based assay was adjusted to suit a high-throughput library screen. To accommodate for the Prestwick library, which encompasses 1280 small molecules on 16 96-well plates, the proposed neuroblastoma-based model was modified to fit the 96-well plate layout. Additionally, to allow for a feasible assessment of T cell suppression, IFN-γ cytokine release was chosen as a readout rather than proliferation.

A preliminary screen using this revised assay aimed to investigate the feasibility to screen for NbM suppressive potential before use in library screen assays, to avoid wasting materials. We demonstrated that IFN-γ suppression using NbM conditioned for only 24h correctly predicted effects seen in assays using the same donors conditioned for 48h, with relative IFN-γ levels of 11% and 15%, respectively (**Figure 4-5**). As previously observed, Sunitinib recovered IFN-γ release (42%), however not to the same extent as seen in prior co-cultures involving pre-treatment of NbM. As discussed before, this decreased

efficiency likely is a result of direct effects of Sunitinib on T cell functions and could possibly be avoided when pre-treating the monocytes instead of adding the drug to co-cultures.

To demonstrate the suitability of the adjusted suppression assay for a high-throughput screen, 80 drugs of the Prestwick chemical library were investigated for IFN-γ recovery at a working concentration of 10 μM. Of the tested chemicals, 12.5% further decreased IFN-γ concentration, indicating a toxic effect on T cells at the tested concentration. An example is chemical G04, which is the previously tested Gemcitabine. In the experiments with Gemcitabine, we had concluded that concentrations above 0.5 nM led to T cell toxicity, which explains the very low IFN-γ concentration measured when added 10μM Gemcitabine in the library screen. A further 80% of the tested drugs did not recover IFN-γ concentrations above the cut-off value at 50% of the concentration seen in the positive control. For example, C6 is the COX-2 inhibitor Celecoxib, which has been described to prevent local and systemic MDSC expansion in tumour-bearing mice (Veltman et al., 2010). However, the reported effects in this model were mainly seen through decreased ROS production by PMN-MDSC. The lack of recovery of T cell function in our assay with Celecoxib might be caused by a suboptimal concentration of the drug but could also be explained by a reduced involvement of ROS for suppression, as our NbM seem to be phenotypically closer to M-MDSC. Finally, six drugs have recovered IFN-γ release above the 50% threshold. Out of those six drugs, five (Montelukast, Rufloxacin, Rivastigmine, Sildenafil, Acetylsalicylic acid) barely crossed the threshold with all showing about 55% recovery of cytokine concentration and might require testing of further drug concentrations to evaluate efficacy. However, one chemical restored cytokine release to 79% of the positive control: the TLR7 agonist Imiquimod. The immunomodulatory

compound is known to induce antitumour effects through stimulation of the innate immune system but has also been shown to activate T and B lymphocytes when delivered systemically (Adlard et al., 2014). In tumour-bearing mice topical treatment of Imiquimod in combination with therapeutic HPV DNA vaccination also has been reported to lead to a decrease in the number of MDSC in the TME (Chuang et al., 2010). A mechanism by how Imiquimod might affect MDSC function is not described in the literature, suggesting that the increased IFN-γ concentration in our library experiment might be caused by a boost of T cell activation, rather than an inhibition of suppression mediated by NbM.

In conclusion, based on the results of the exemplary library screen, Imiquimod would be the top candidate from the 80 tested compounds. We advise that in future experiments testing the remaining 1200 small molecules, all compounds leading to IFN-γ recovery above a set threshold should be selected to be further investigated in subsequent experiments. As all screens were performed at 10 μM, further screens may have to be performed for the individual drugs to test for pharmacologically attainable concentrations. The selection will be narrowed down further through investigating pre-treatment variations and alternative readouts, such as effects on NbM-inhibition of T cell proliferation and cytotoxicity. Only then the ideal concentration and therapeutic window can be efficiently determined and tested in combination with CAR T cell therapy.

5. RESULTS III – Synthetic notch receptors as an alternative to overcome monocyte-mediated T cell suppression

5.1. Introduction

The highly customisable synNotch receptors created by Lim and colleagues are a typical example for novel synthetic biology approaches in cell-based therapies. Inspired by the wild-type (WT) Notch receptor, synNotch enables the cellular engineer to exactly decide which extracellular cue should be combined with which intracellular response (Morsut et al., 2016). WT Notch has a unique mechanism to directly transduce signals upon target engagement (**Figure 5-1**): When encountering its ligand (Delta family proteins), an intracellular protease cleavage site becomes available for cleavage by a disintegrin and metalloproteinases/tumour necrosis factor-α converting enzyme (ADAM/TACE) (Kopan and Ilagan, 2009; Morsut et al., 2016). This enables the release of a intracellular domain which can translocate to the nucleus and function as a transcriptional regulator for target genes mostly involved in cell-cell signalling during development (Artavanis-Tsakonas et al., 1999). The design of synNotch receptors takes advantage of the modularity of WT Notch receptors and enables replacement of the extracellular and intracellular domains with customised circuits. Extracellularly synNotch receptors can be designed to recognise specific antigens via the use of antibody-based domains (e.g. scFvs), while intracellularly transcription factors (e.g. Gal4-VP64) can be used to induce specific promotor-paired target genes (Morsut et al., 2016). Thus, only the minimal transmembrane domain of the WT Notch receptor is unchanged, maintaining the controlled proteolysis upon receptor activation. For customised outputs, modified cells need to express both the synNotch receptor as well as an appropriate responding element, containing the respective transcription factor-binding site and transgene of interest. The modification therefore involves transduction with two vectors.

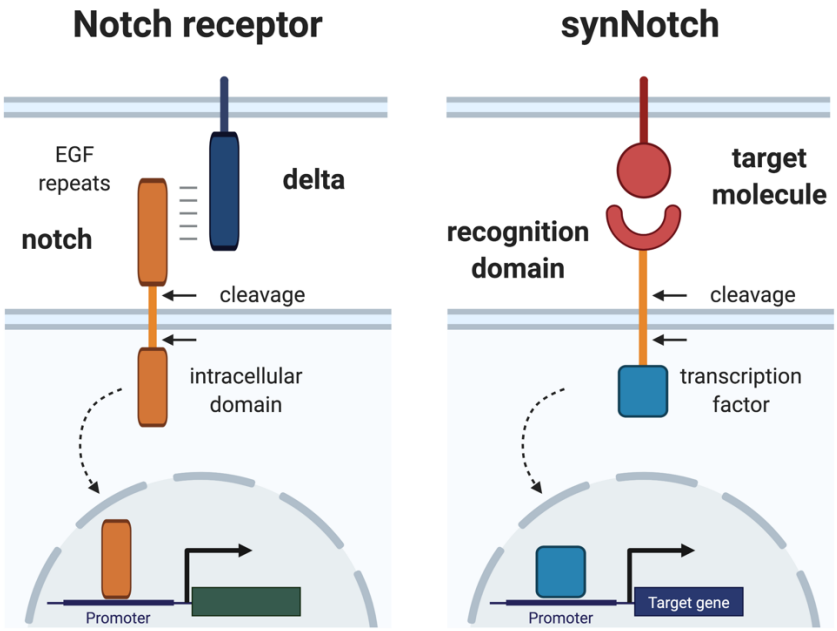

Figure 5-1 Ligand-receptor interactions of wild-type notch and synthetic notch receptors. Left: when encountering its ligand delta, the wild-type Notch receptor undergoes proteolytic cleavage within the transmembrane domain, leading to release of the intracellular domain. The cleaved domain then translocates to the nucleus where it mediates expression of target genes. Right: the synthetic notch receptor works by the same principle as the wild-type receptor but replaces the extracellular domain with an antibody-based recognition domain and the intracellular domain with a transcription factor suitable for the expression of introduced transgenes.

Lim and colleagues have demonstrated that the synNotch system can have various applications in T cell engineering. Besides a local and timed release of customised payloads (such as the release of cytokines or antibodies) or an induction of T cell differentiation, synNotch receptors can also induce an antigen-dependent expression of CARs for tumour recognition (Kole T. Roybal et al., 2016; Kole T. Roybal et al., 2016). This enables a sequential AND-gated CAR T response limited to targets harbouring both of the two antigens (**Figure 5-2**). The short ON- and OFF-kinetics of synNotch-gated CAR expression prevent off-target effects in tissues carrying only one of the two antigens, so that mice with single- and double-positive tumours in their respective flanks will only encounter elimination of the double-positive masses when injected with synNotch-modified T cells intravenously (Kole T. Roybal et al., 2016).

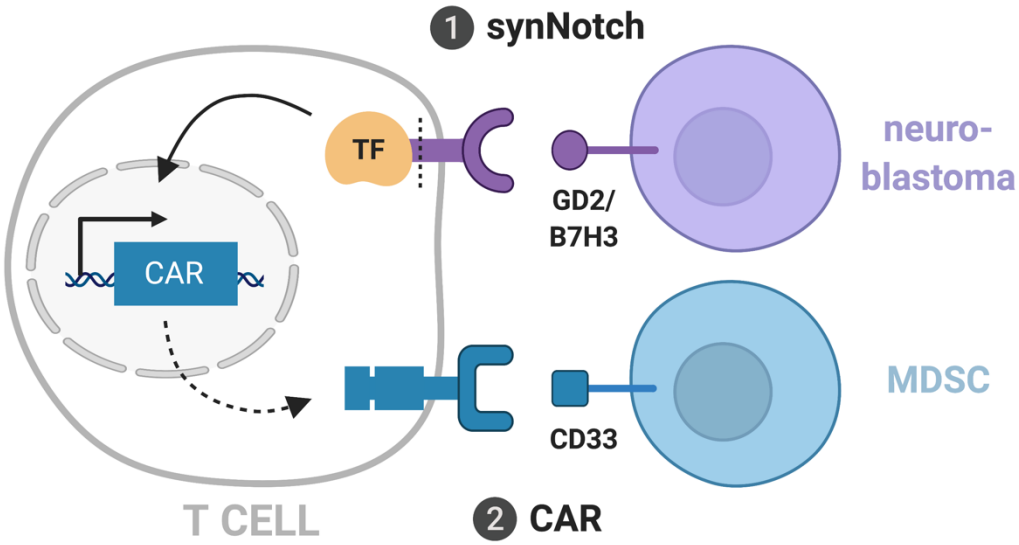

Figure 5-2 AND-gated circuit for precise tumour recognition using synNotch-gated CAR T cells. (1) When the synNotch receptor binds the targeted tumour-associated antigen, the intracellular transcription factor domain is released and induces CAR expression in the nucleus. (2) Now expressed on the cell surface, the CAR can bind its target antigen, resulting in elimination of the expressing cell. Only when both signals are available effector functions of the T cell will be activated.

The aim of the final chapter of this thesis is to translate this novel design for the cell-based treatment of solid cancers using CAR-mediated targeting of suppressive myeloid cells in the TME alongside CAR-mediated elimination of tumour cells. We hypothesise that the synNotch system can allow for elimination of altered myeloid cells in the tumour proximity, while sparing healthy myeloid populations in other locations within the same patient. Furthermore, we propose that this will avoid early T cell exhaustion resulting from tonic CAR signalling when expressed constitutively. As a neuroblastoma-based model had been established in the previous chapters, synNotch receptors were to be designed targeting neuroblastoma-associated antigens, which then induce expression CAR constructs targeting myeloid markers. For this, the commercially available constructs (anti-CD19 synNotch, fluorescent responder) had to be edited so that the synNotch receptor would detect neuroblastoma markers (anti-GD2 synNotch, anti-B7H3 synNotch) which then led to the expression of a CAR capable of detecting and eliminating

myeloid cells (anti-CD33 CAR) (**Figure 5-3**). The constructs were tested first in a suitable cell line (Jurkat) and then in T cells for subsequent applications in immunotherapy.

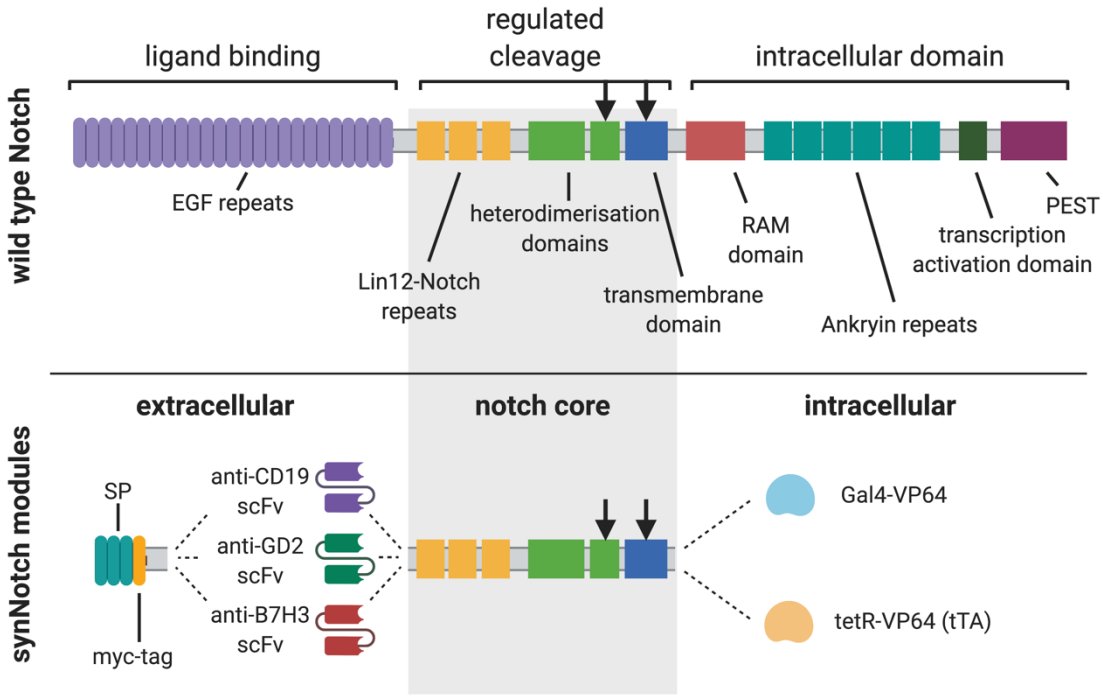

Figure 5-3 Structure of wild type Notch and synthetic Notch receptors. Top: Modules of the wild-type Notch receptor including extracellular ligand binding domain, transmembrane domain for regulated cleavage, and intracellular transcription activation domain. Bottom: synNotch receptor variations covered in this thesis (SP=signal peptide).

5.2. Validation of anti-CD19 synNotch-gated circuits

5.2.1. Comparison of synNotch systems (Gal4 vs tTA)

Firstly, two commercially acquired CD19-targeting synNotch receptors variants were compared. Both vectors code for identical synNotch receptors, only differing in their intracellular domain. The tested signal-transducing TF domains are Gal4-VP64 and tetR-VP64 (tTA), which both are cleaved from the receptor upon target engagement and translocate to the nucleus, where they can induce target gene transcription. For this, transduced cells always have to be modified with both the synNotch receptor construct and a paired responder vector, which comprises a transcription factor responsive element controlling the expression of an inducible marker (BFP and GFP, respectively) (**Figure 5-4**). Transduced cells were controlled for tonic signalling, meaning synNotch receptor signalling without encounter of targets, and for increase in fluorescent marker expression when co-cultured with CD19-positive and -negative targets.

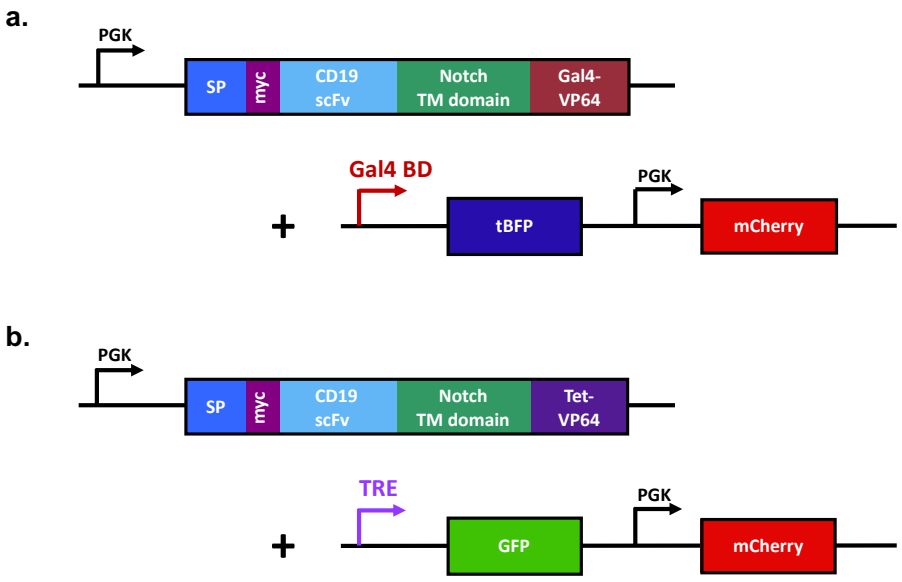

Figure 5-4 Vector construct combinations needed for the two variants of synNotch circuits. a. The anti-CD19 synNotch receptor with intracellular Gal4-VP64 domain is paired with a responding element expressing a Gal4 binding domain (BD) controlling expression of BFP. b. The anti-CD19 synNotch receptor with intracellular tet-VP64 (tTA) domain is paired with a responding element expressing a Tet responsive element (TRE) controlling expression of GFP.

Target cell lines

To avoid false-positive results from target-expressing cells in the transduced population, Jurkat cells were stained for CD19 surface expression. No CD19 was found on the Jurkat cell line as well as on SupT1 wt cells, which thus were taken as a negative target control. The Raji cell line originates from B lymphocytes of a Burkitt's lymphoma patient and therefore expresses the B cell marker CD19 on cell surfaces. Hence, this cell line was used as a target for anti-CD19 synNotch-transduced effectors.

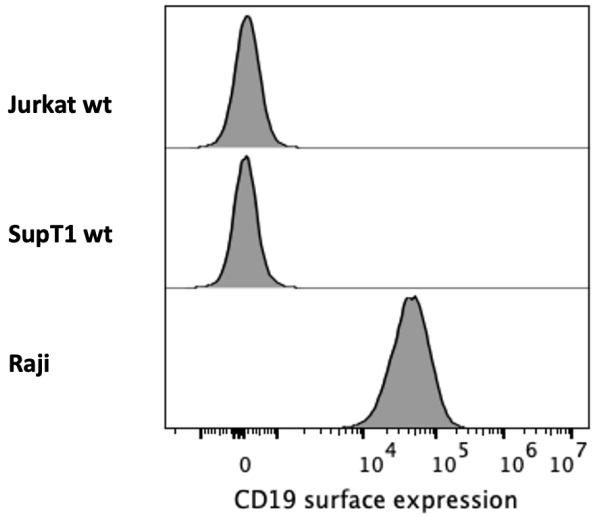

Figure 5-5 Surface expression of CD19 on targets. The three cell lines Jurkat, SupT1 and Raji were assessed for surface expression of CD19 using flow cytometry.

SynNotch receptor tonic signalling

Tonic signalling describes basal signalling through engineered cell receptors in the absence of ligand. This has been previously observed in CARs, where certain antigen-binding domains, such as the GD2 scFv 14.18, are associated with increased background signalling and T cell exhaustion prior to target encounter. It has been suggested that this is likely a result of receptor clustering leading to false signal transduction (Long et al., 2015).

Jurkat wt cells were co-transduced with the plasmids coding for the two synNotch receptor variants and their respective responding elements. The double-transduced population was identified by flow cytometry using the incorporated markers c-myc (synNotch receptor) and mCherry (responding element). After transduction the double transduced population was 43.2% and 63.6% of total cells with the tTA- and the Gal4-based constructs, respectively (**Figure 5-6**). To prevent variations caused by differences in transduction efficiency, the transduced cells were flow-sorted for c-myc- and mCherry-expressing cells to achieve a pure double-positive population containing both the synNotch receptor and the responding element.

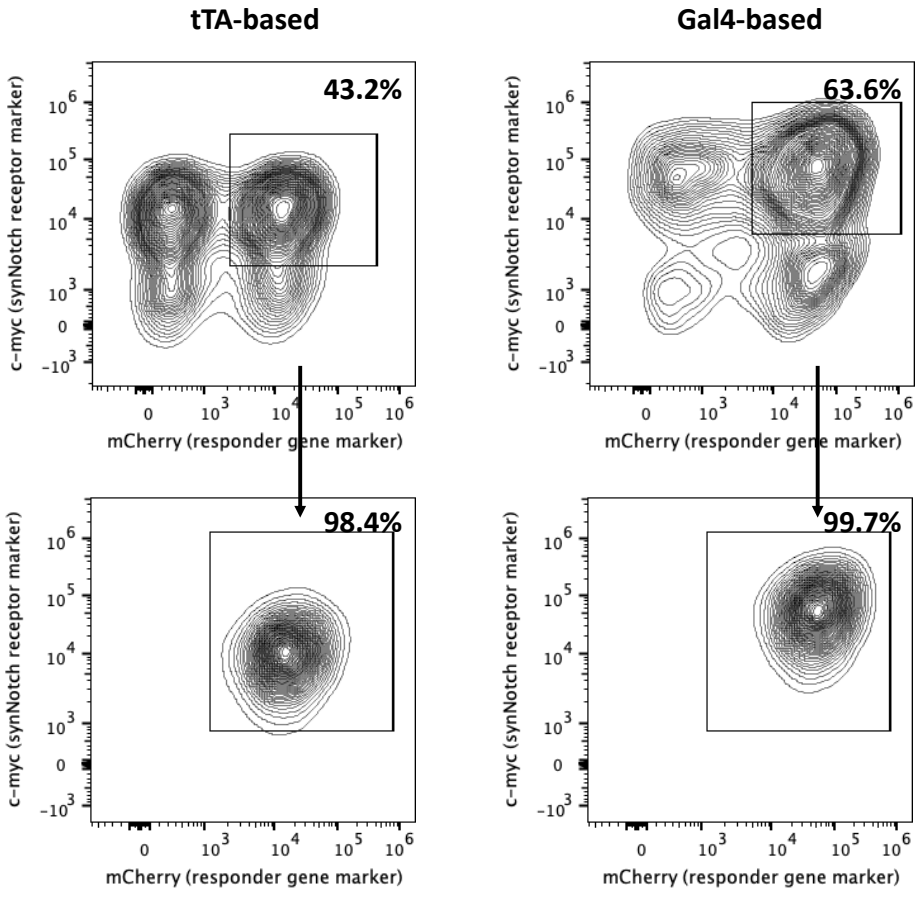

Figure 5-6 Jurkat cells after double-transduction with anti-CD19 synNotch and fluorescent responder elements. Transduction efficiency was detected with flow cytometry analysis of the included markers c-myc (synNotch receptor) and mCherry (responder element). Contour plots on the top display cell populations for both circuits before and bottom plots after flow-based cell sort.

To investigate background expression of the responder element in the absence of synNotch binding, transduced Jurkat cells were compared to an untransduced control (**Figure 5-7**). When comparing the tTA- and Gal4-based systems, tonic expression of the responding fluorescent marker was only seen in cells transduced with the synNotch receptor using tTA-mediated induction (86.2%; ΔMFI=37,619). Those modified with a synNotch receptor using a Gal4-based intracellular domain showed no significant difference in BFP expression in the absence of target when compared to an untransduced control (0.27%; ΔMFI=546).

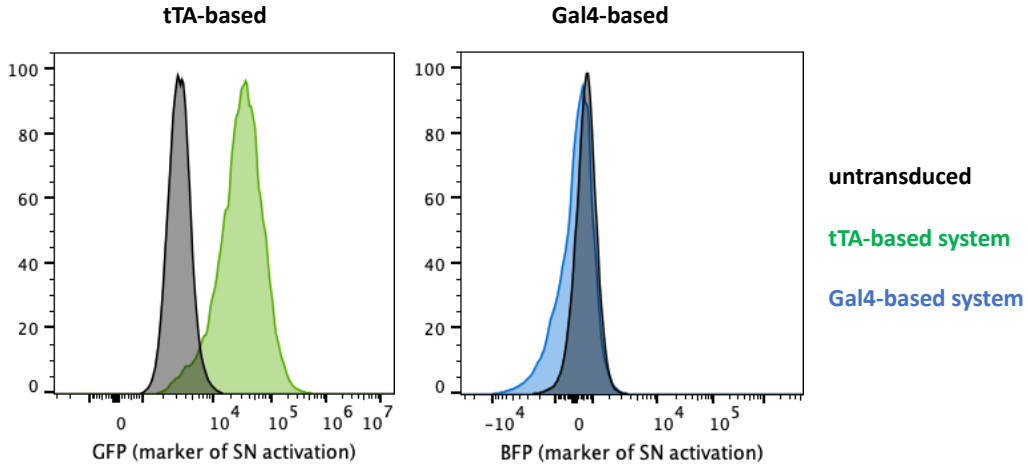

Figure 5-7 Tonic signalling of synNotch-gated expression of fluorescent markers. Both unmodified and synNotch-transduced Jurkats were analysed for their expression of the introduced inducible fluorescent markers using flow cytometry. Histogram on the left shows GFP expression in Jurkats transduced with a synNotch circuit using tTA (green), right histogram displays BFP expression in Jurkats modified with the Gal4-based circuit (blue). Black histograms represent the untransduced control.

CD19-gated responder gene expression

Next, the synNotch-modified cells were co-cultured for 24 hours with targets that were either positive or negative for CD19 expression. Based on the design of the constructs, the fluorescent markers should only be detected when CD19-positive targets are available, thus activating the anti-CD19 synNotch receptor leading to expression of the responding element. Expression of the fluorescent markers GFP and BFP increased in

both the tTA and the Gal4 system, respectively, when co-cultured with CD19+ targets (**Figure 5-8**a). The increase in cells expressing the fluorescent marker compared to a control co-culture with CD19-negative targets was higher in the Gal4-based synNotch system (73.2% versus 0.8%) than in the tTA-based system (93.6% versus 85.2%), mainly because of the basal signal seen in tTA-mediated GFP expression. In general, signal intensity was much higher in the cells with the GFP marker (MFI control: 37,183; MFI activated: 325,566), whereas the system using BFP showed negligible signal intensity with the negative control target and a clear shift after encounter of CD19 antigen (MFI control: 247; MFI activated: 67,920) (**Figure 5-8**b). However, an advantage to tet-based systems is their possibility to "switch off" signal transduction through tetracycline and its derivatives ("Tet-Off"). When the antibiotic is added, it binds tTA and therefore prevents expression of the inducible target genes (Gossen et al., 1995). Indeed, when adding doxycycline, a tetracycline derivative, to the co-cultures GFP expression was reduced to the baseline, thus enabling “switching off” the synNotch-gated expression (**Figure 5-8**c).

Even though the switchability of tTA-based signalling is a valuable feature, the tonic signalling in the absence of target suggests that this variation of the synNotch vector would result in unfavourable off-target effects when used for cancer therapy. We therefore decided to use Gal4-VP64 as an intracellular domain of all synNotch receptors in the following experiments.

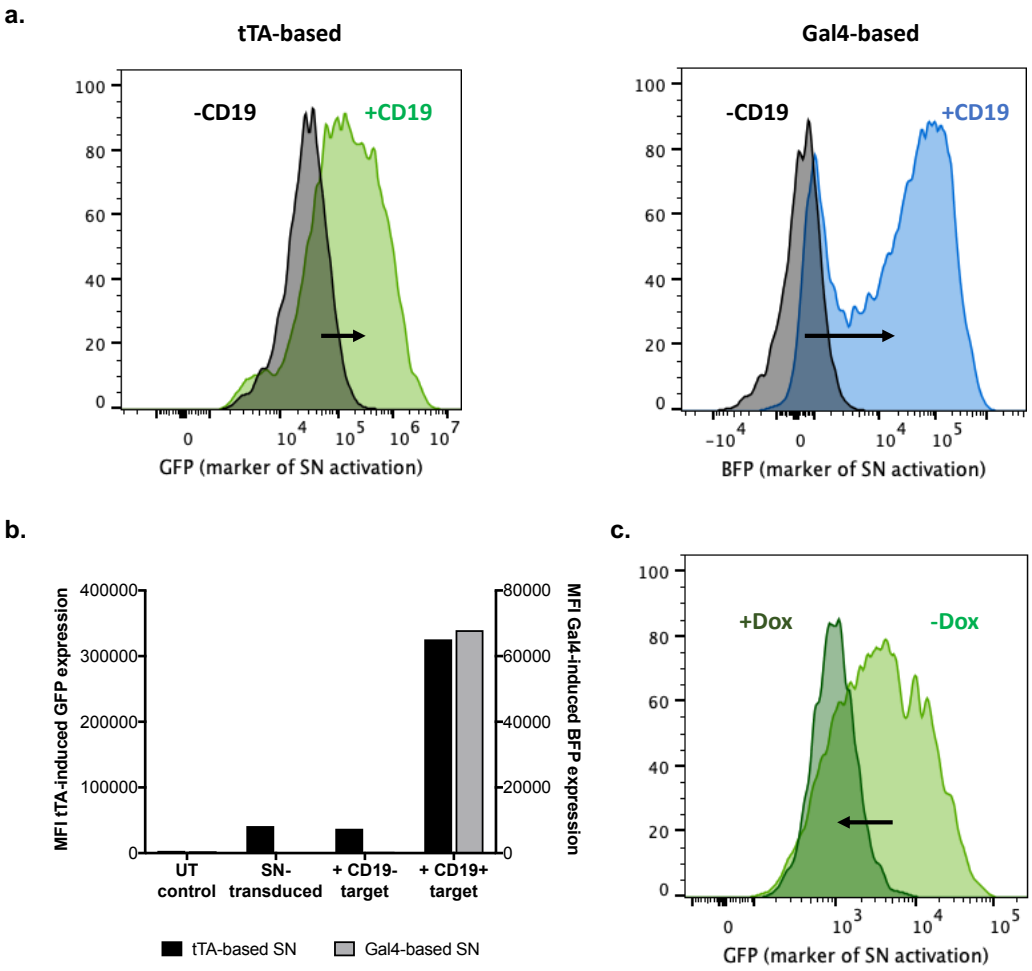

Figure 5-8 CD19-gated expression of fluorescent markers in tTA- and Gal4-based circuits. Responder gene expression was assessed in transduced Jurkat cells co-cultured with CD19-positive targets or a CD19-negative control using flow cytometry. a. Histograms showing fluorescent marker signals in transduced Jurkats co-cultured with the negative control (black) or a target carrying the synNotch ligand CD19 (tTA: green; Gal4: blue). b. Bar diagram showing mean fluorescent intensity (MFI) of fluorescent responders in the tTA-based (black) and the Gal4-based (grey) circuits. c. Doxycycline-dependent suppression of synNotch-gated GFP expression in Jurkats through activation of the Tet-OFF mechanism.

5.2.2. Optimisation of co-culture conditions

To ensure for optimal signal induction, we investigated different co-culture conditions using the anti-CD19 synNotch with inducible BFP in Jurkat cells. Both incubation time beyond 24 hours and changes in effector-to-target ratio were assessed.

Increased incubation period

Figure 5-9 shows BFP readout of anti-CD19 synNotch-transduced Jurkat cells cultured either alone (unstim.), with a CD19-negative target (SupT1) or a CD19-positive target (Raji). Induced BFP expression was assessed 24, 48, and 72 hours after co-culture set-up (**Figure 5-9**a). Expression of the fluorescent marker was found in 61% of transduced Jurkat cells after 24 hours, which did not change when measured at two more timepoints within the following 2 days. This indicates that the anti-CD19 synNotch receptor reaches maximum signal transduction within the first 24 hours of target engagement and suggests no need for an extension of incubation time.

Effector-to-target ratio

Besides incubation time, the ratio between effector and target can also affect receptor saturation and subsequent signal induction. Therefore, we tested co-cultures with increased numbers of synNotch-modified Jurkats (3:1) as well as with increased numbers of target cells (1:3). Both conditions led to a similar activation of BFP expression when Jurkat cells were co-cultured with the CD19-positive cell line Raji (**Figure 5-9**b), indicating an optimised receptor engagement at the previously used 1:1 effector-to-target ratio.

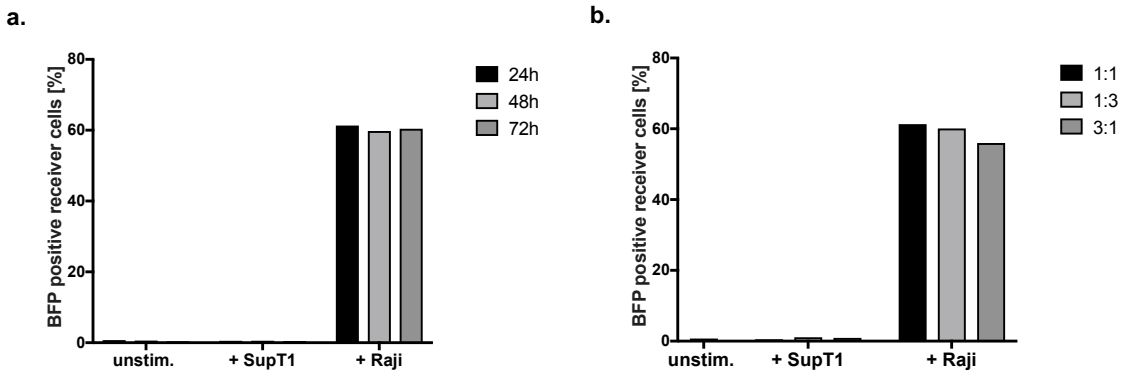

Figure 5-9 Optimisation of synNotch activation.BFP responder gene expression was assessed in anti-CD19 synNotch transduced Jurkat cells co-cultured with CD19-positive targets or a CD19-negative control using flow cytometry a. Bar diagram showing percentage of fluorescent responder expressing cells within the transduced Jurkat population after 24h, 48h, and 72h of co-culture. b. Bar diagram showing percentage of fluorescent responder expressing cells within the transduced Jurkat population at an effector-to-target ratio of 1:1, 1:3, and 3:1.

5.2.3. Anti-CD19 synNotch-gated BFP expression in T cells

After validating the function of the anti-CD19 synNotch receptor in Jurkat cells, the receptor was tested for BFP induction in primary T lymphocytes from a healthy donor. The T cells were co-transduced with lentiviruses containing the plasmids for the anti-CD19 synNotch receptor and the BFP responder gene, respectively, which achieved a double-positive population of 13.4%. However, when analysing the transduced T cells, a high basal expression of BFP in over half of the synNotch receptor-carrying cells was observed (**Figure 5-10a**). This was seen without the addition of target cells carrying the synNotch-matched antigen, suggesting either tonic signalling of the receptor or a CD19-expressing population within the expanded T lymphocytes. Staining of the samples with anti-CD19 antibody revealed a distinct CD19-positive population, which was found to be between 5-10% for all tested blood donors (**Figure 5-10b**). We suspect that this population is caused by a contamination with persisting B cells from the blood products used for T cell expansion. Due to this high background expression of the inducible

responder gene, no clear increase in signal was detectable in the T cells when co-cultured with the CD19-positive cell line Raji (**Figure 5-10**c).

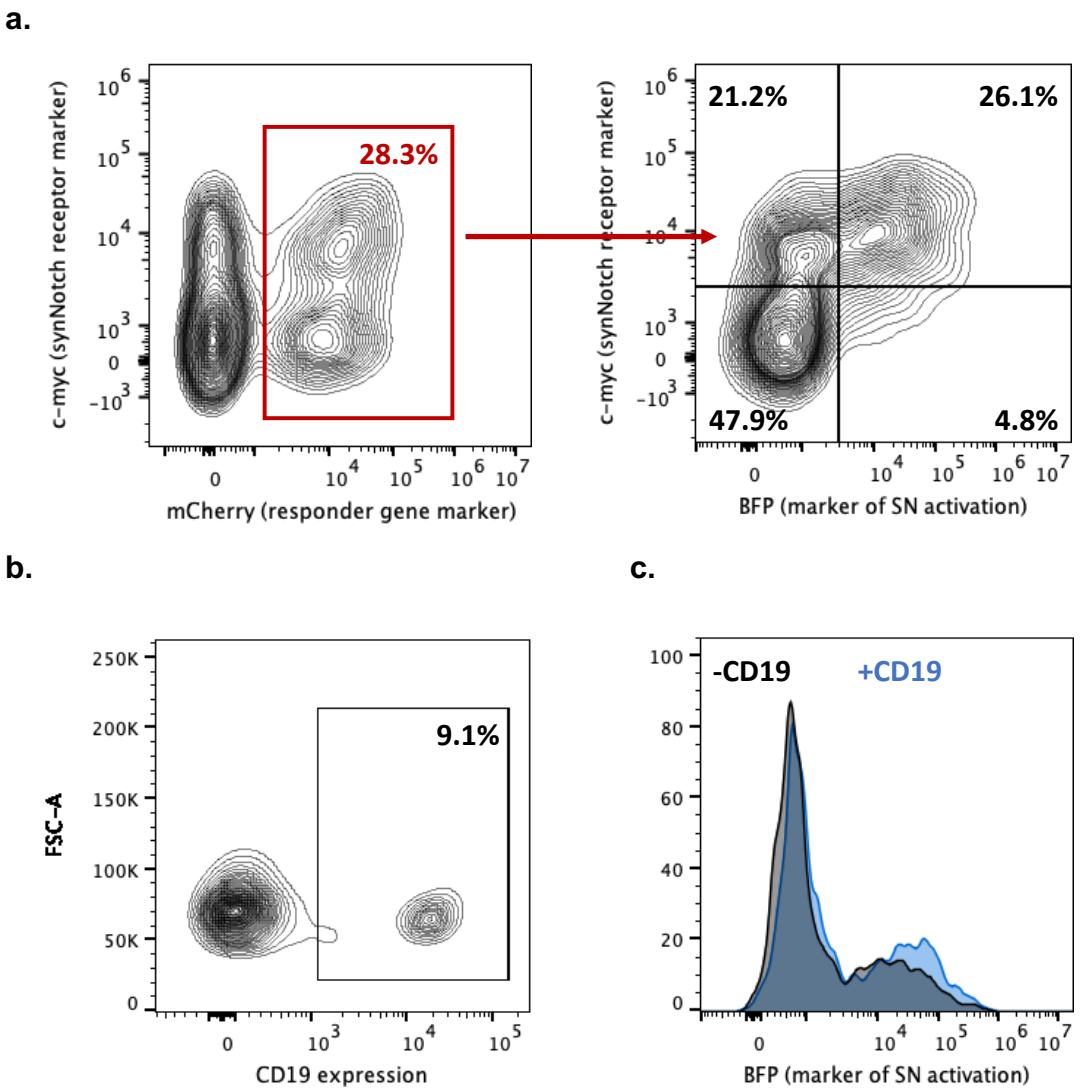

Figure 5-10 Tonic expression of the responder gene in anti-CD19 synNotch-modified T cells. Primary T cells were co-transduced with the Gal4-based anti-CD19 synNotch receptor and the BFP responder element. Transduction efficiency was detected with flow cytometry analysis of the included markers c-myc (synNotch receptor) and mCherry (responder element). a. Contour plots showing mCherry-positive population after transduction (left) and c-myc and BFP expression within the mCherry positive population (right). b. Representative contour plot showing CD19-positive population within the expanded T cell population of one healthy donor. c. Histogram showing synNotch-gated expression of BFP expression in T cells co-cultured with CD19-positive Jurkat cells (blue) compared to co-culture with the negative control SupT1 (black).

Hoping to reduce this basal induction of the fluorescent responder, transduced T cells from another donor were flow-sorted to exclude the CD19-positive population, while enriching for the mCherry-positive population (marker for the synNotch responder gene). A caveat of this is that the FACS-sort does also include cells that only carry the responder element but not the synNotch receptor (c-myc-negative), which have no means to upregulate BFP expression, even when co-cultured with CD19-positive targets. However, to avoid artificial activation of the receptor via cross linking of antibodies against the myc-tag, this "untouched" flow sort was favoured over a specific selection of the double positive population. **Figure 5-11**a shows the flow-sorted T lymphocytes, of which 22.4% were carrying both the anti-CD19 synNotch receptor and the BFP responder gene and therefore were able to form the complete synNotch circuit. When analysed 5 days after the flow sort, these T cells did not induce any basal BFP expression when compared to an untransduced control (**Figure 5-11**b). This enabled a clear shift in synNotch-gated BFP expression when the T cells were then co-cultured with CD19-positive Raji cells, but not when co-cultured with the CD19-negative control (SupT1) (**Figure 5-11**c). In summary, exclusion of CD19-positive populations within the expanded T cells reduced background signalling and enabled a clean switch-on of CD19-synNotch-induced signalling in presence of antigen-carrying target cells (**Figure 5-11**d).

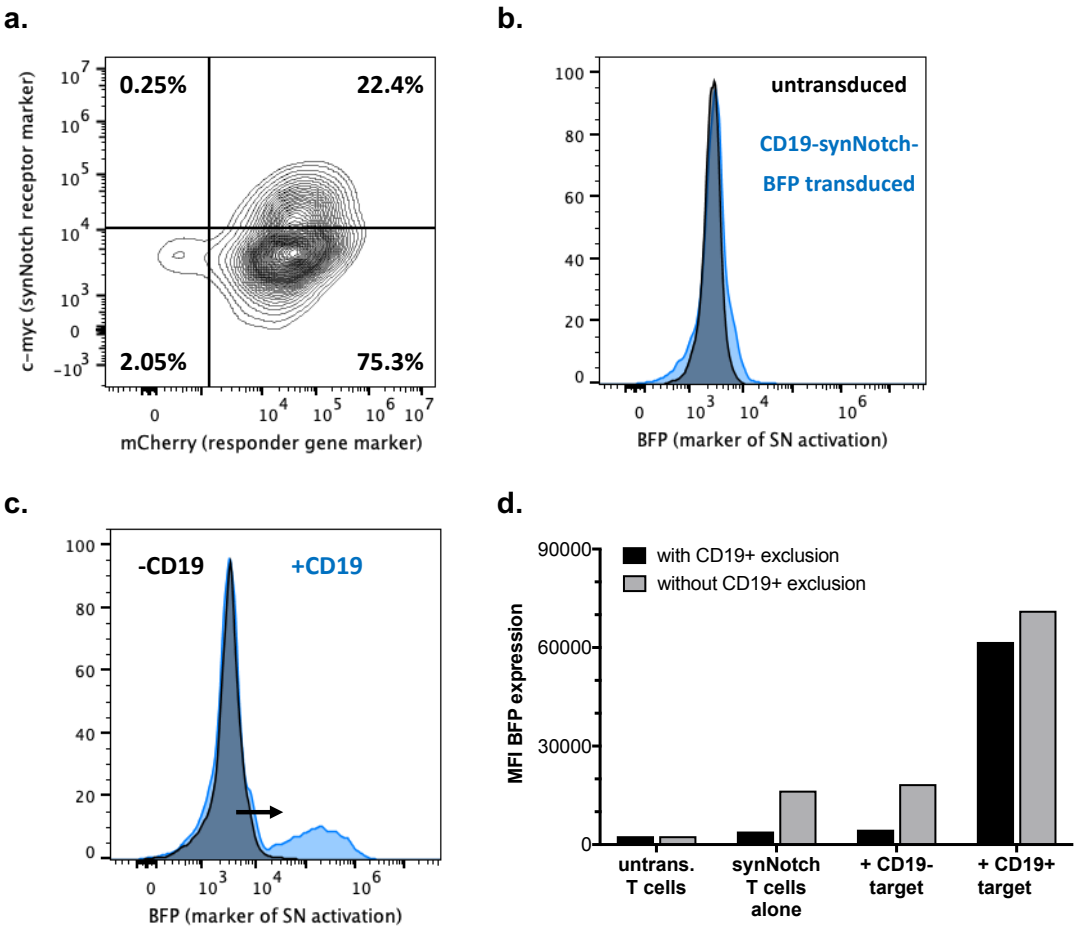

Figure 5-11 Anti-CD19 synNotch-gated expression of BFP in flow-sorted T cells after CD19 exclusion. Primary T cells were co-transduced with the Gal4-based anti-CD19 synNotch receptor and the BFP responder element. Transduction efficiency was detected with flow cytometry analysis of the included markers c-myc (synNotch receptor) and mCherry (responder element). a. Contour plot showing mCherry- and c-myc-expression in T lymphocyte population after flow-sorting for mCherry-positive/CD19-negative cells. b. Histogram showing basal expression of BFP in untransduced (black) and sorted synNotch-transduced T cells (blue). c. Histogram showing anti-CD19 synNotch-gated expression of BFP in sorted modified T cells co-cultured with CD19-positive Jurkat cells (blue) compared to co-culture with the negative control SupT1 (black). d. Mean fluorescent intensity (MFI) of BFP expression in T cells flow-sorted to include CD19-positive population (grey) or sorted to exclude CD19-positive cells (black).

In summary, in this section we efficiently demonstrated an optimised synNotch-gated system to form the basis of all further effort to adjust the AND-gated strategy for a localised targeting of monocytes in the neuroblastoma TME.

5.3. A novel synNotch-gated inducible CD33 CAR

5.3.1. Cloning strategy for a CD33 CAR responding element

To efficiently target monocytes in a synNotch-gated context, the responder gene had to be redesigned to contain an inducible CAR. As a target we chose CD33, which is highly expressed on cells of the myeloid lineage, including MDSC.

The transgenes coding for the variations of synNotch and the Gal4-dependent responder were all incorporated into separate lentiviral vectors using the pHR vector as a backbone. This self-inactivating HIV-1 vector has a 400-nucleotide deletion in the 3′ long terminal repeat (LTR), abolishing LTR promoter activity (Zufferey et al., 1998). It is a second-generation lentiviral vector and also contains a phosphoglycerate kinase 1 (PGK) promoter and ampicillin resistance (**Figure 5-12**). In addition to a PGK promoter driving mCherry marker gene, the responder plasmid includes a more 5' transgene region under control of the Gal4 binding sequence UAS (Upstream Activation Sequence) (**Figure 5-13**). Both plasmids were modified using restriction and insertion cloning.

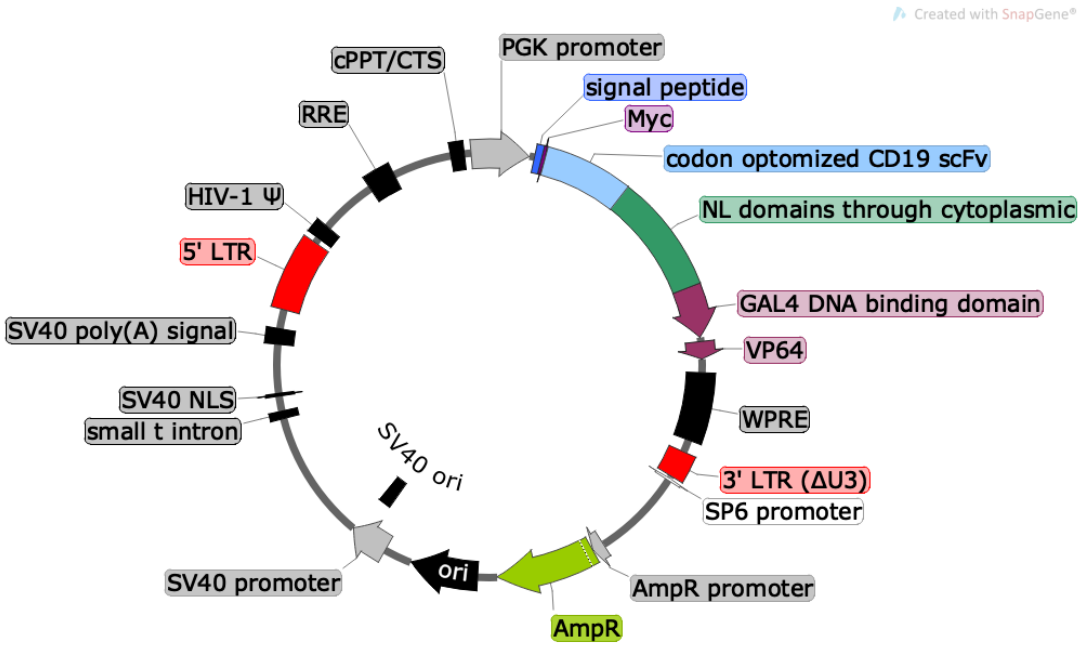

Figure 5-12 Plasmid map of pHR-PGK -MYC-CD19-synNotch-Gal4VP64.

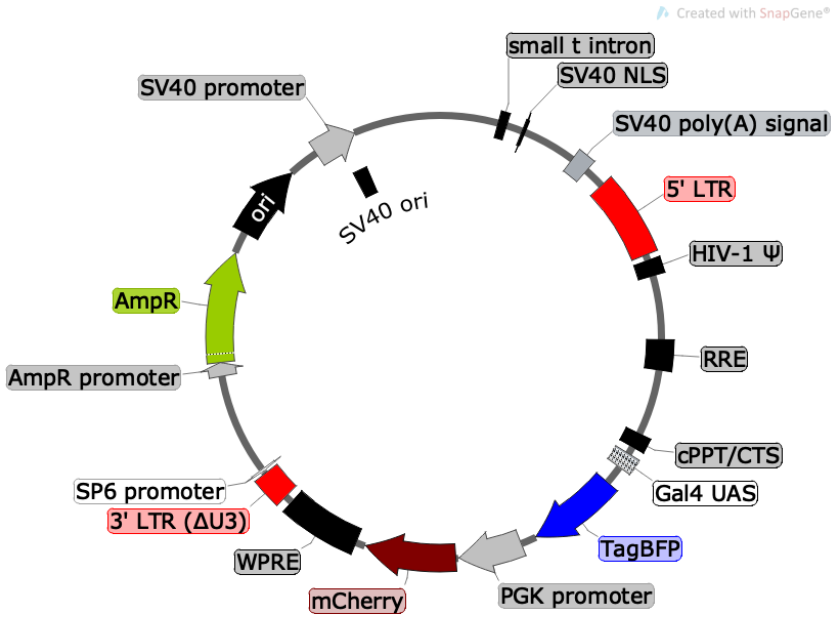

Figure 5-13 Plasmid map of pHR-Gal4UAS-tBFP-PGK-mCherry.

To introduce synNotch-gated CAR expression, the BFP marker in the responder plasmid was replaced with a second generation anti-CD33 CAR using CD28 and CD3ζ for intracellular signal transduction (**Figure 5-14**). This construct encodes for an scFv

flanked by the restriction sites SnaBI and BamHI to facilitate an easy exchange of scFv in future experiments.

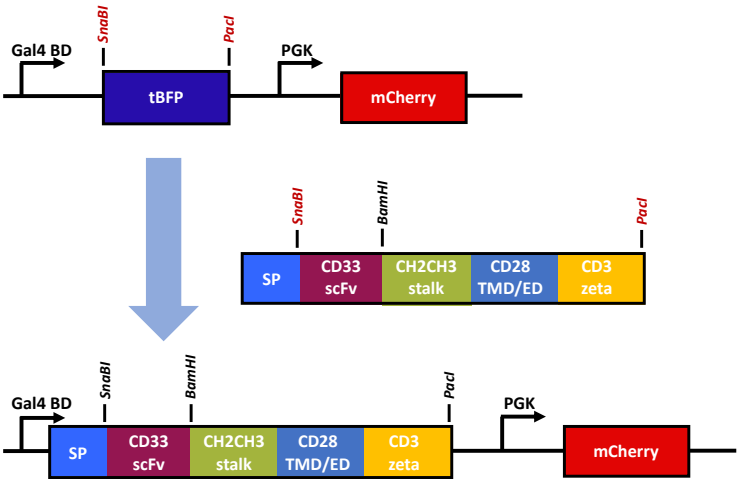

Figure 5-14 Cloning strategy for responder element-encoding plasmid.

The CAR responder element had to be validated for its functionality and was therefore tested in combination with the anti-CD19 synNotch receptor construct which had already been tested in previous experiments. Only when proven functional, can it be combined in a novel neuroblastoma- and monocyte-targeting context.

5.3.2. Validation of the anti-CD33 CAR responding element

The Gal4-induced anti-CD33 CAR responder was tested in combination with the established anti-CD19 synNotch receptor to test inducible expression of anti-CD33 CARs after CD19 binding via synNotch. Co-transduction with both constructs resulted in a double positive population of 20.8% of synNotch/CD33-CAR responder-expressing Jurkats (**Figure 5-15**a). No further selection was conducted. Since the single positive mCherry population was not very substantial, in subsequent co-culture experiments the population of interest was observed gating for mCherry-positive Jurkat cells.

Similar to experiments using a BFP-expressing responding element, transduction of Jurkats with the system using the anti-CD19 synNotch receptor did not result in expression of the anti-CD33 CAR responder in the absence of target (0.84%; **Figure 5-15**b). When co-cultured with CD19-positive target cells (Raji), flow analysis revealed a significant upwards shift of detected anti-CD33 CAR on transduced Jurkat cells (52.6%; ΔMFI 47,596), indicating synNotch-gated gene expression (**Figure 5-15**c,d). This was not observed when the effectors were co-cultured with a CD19-negative control (SupT1 wt).

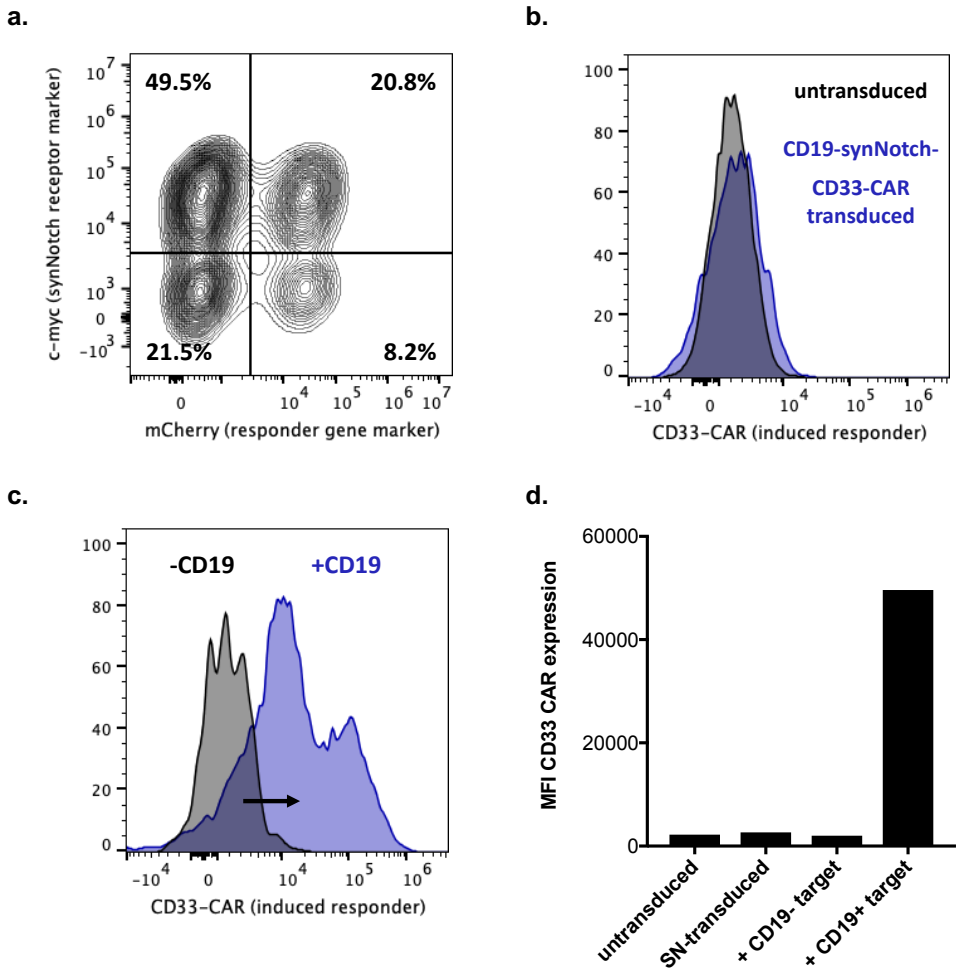

Figure 5-15 CD19-gated anti-CD33 CAR expression in Jurkats. a. Contour plot displaying c-myc and mCherry expression on double-transduced cells. b. Tonic expression of synNotch-dependent CAR in transduced Jurkats (purple) compared to a non-transduced control (black). c. Histogram showing CAR expression in synNotch modified Jurkats co-cultured with CD19-positive (purple) and -negative (black) targets, analysed via flow cytometry. d. Mean fluorescent intensity (MFI) of CAR expression in Jurkats modified with the anti-CD19 synNotch/anti-CD33 CAR circuit. SN= synNotch

5.3.3. Dynamics of synNotch-gated CAR expression

Analysing for surface anti-CD33 CAR expression, dynamics of synNotch-gated target gene expression were investigated. To simplify the work flow, synNotch-modified cells were alternatively stimulated using anti-myc antibody, which was previously described by Wendell Lim's group (Kole T. Roybal et al., 2016). They have found that the synNotch receptor could also be activated via its myc-tag, when treated with plate-bound antibody, allowing for rapid stimulus removal. Therefore, transduced Jurkats were observed during 24 hours after stimulus addition as well as 24 hours after stimulus removal to identify the dynamics of synNotch-induced CAR expression (**Figure 5-16**).

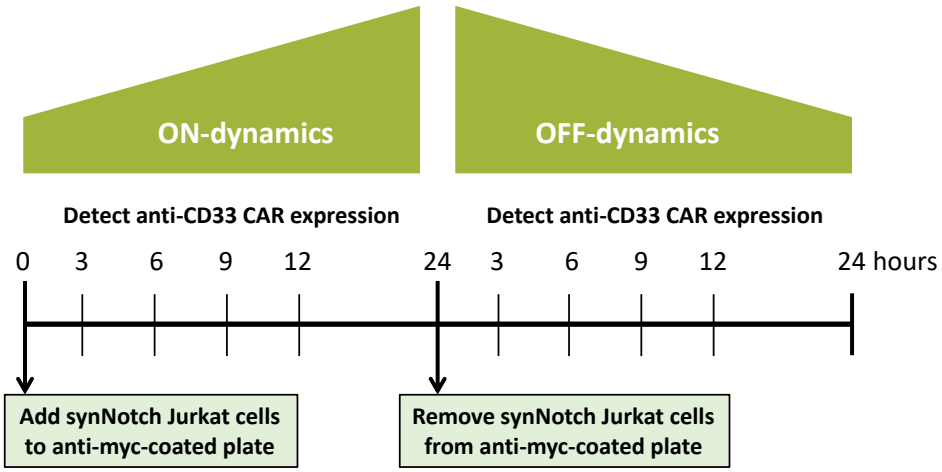

Figure 5-16 Schematic for assessment of dynamics of myc-gated expression of an anti-CD33 CAR in Jurkat cells.

To ensure the availability of cells containing both constructs necessary for synNotch-gated CAR expression, initial experiments were performed in Jurkat rather than primary T cells. Jurkats were co-transduced with concentrated lentivirus. This achieved successful double transduction of 75.6% of cells, which could be used in subsequent experiments (**Figure 5-17**).

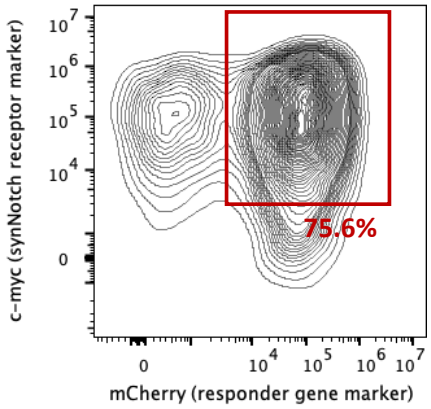

Figure 5-17 Transduction efficiency with anti-CD19 synNotch and anti-CD33 CAR responder in Jurkat cells using concentrated lentivirus.

SynNotch-modified Jurkat cells reached steady-state CAR expression within 24 hours in response to anti-myc stimulation, with a $t_{1/2}$ of 5 hours (**Figure 5-18**a). Looking at the decay dynamics of the receptor-mediated response, CAR expression after removal of the stimulus decreased significantly in the following 24 hours, with the half-life of CAR expression being 8 hours (**Figure 5-18**b).

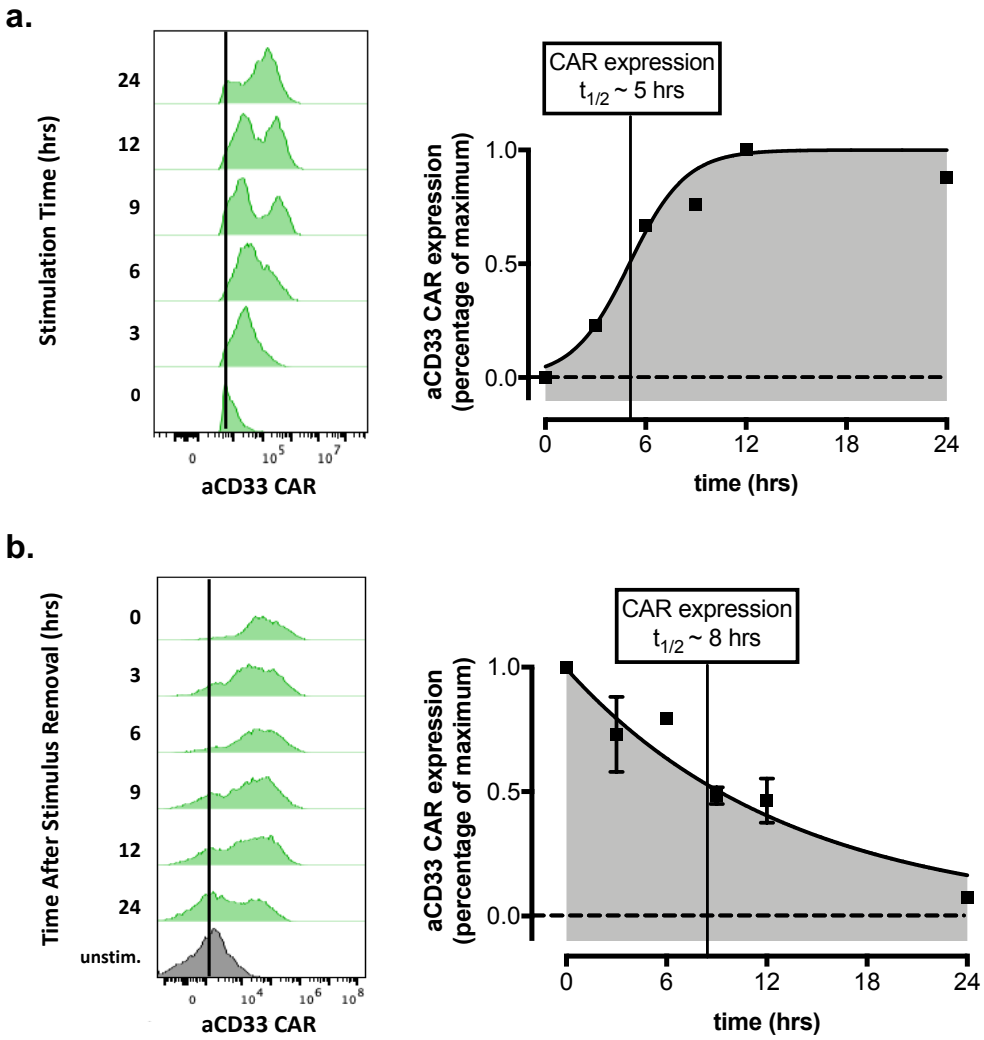

Figure 5-18 ON- and OFF-dynamics of CD19-gated anti-CD33 CAR expression in Jurkat cells. a. Left: Histograms showing upregulation of anti-CD33 CAR expression over 24 hours of myc-mediated stimulation of synNotch-modified Jurkat cells, assessed via flow cytometry. Right: Relative CAR expression in the time course of 24 hours after stimulation. b. Left: Histograms showing downregulation of anti-CD33 CAR expression over 24 hours after removal from myc-coated plates. Right: Relative CAR expression in the time course of 24 hours after stimulus removal.

5.3.4. Anti-CD19 synNotch-gated CD33 CAR expression in T cells

T cells transduced both with an anti-CD19 synNotch receptor and the anti-CD33 CAR responder gene were flow-sorted as described in chapter 5.2.3 to exclude CD19-positive cells and enrich for the mCherry-transduced population. **Figure 5-19**a shows the flow-sorted cells, of which 23.1% expressed the complete synNotch circuit. When analysed for basal CD33 CAR expression on the cell surface, there was minimal background signal (8.1%; MFI 2,918; **Figure 5-19**b,d), which resulted in a clear shift towards increased CAR expression when co-cultured with CD19-positive targets (30.5%; MFI 96,464; **Figure 5-19**c,d).

In conclusion, this data shows that we have successfully created a synNotch-inducible anti-CD33 CAR circuit which can be applied for localised targeting of myeloid cells.

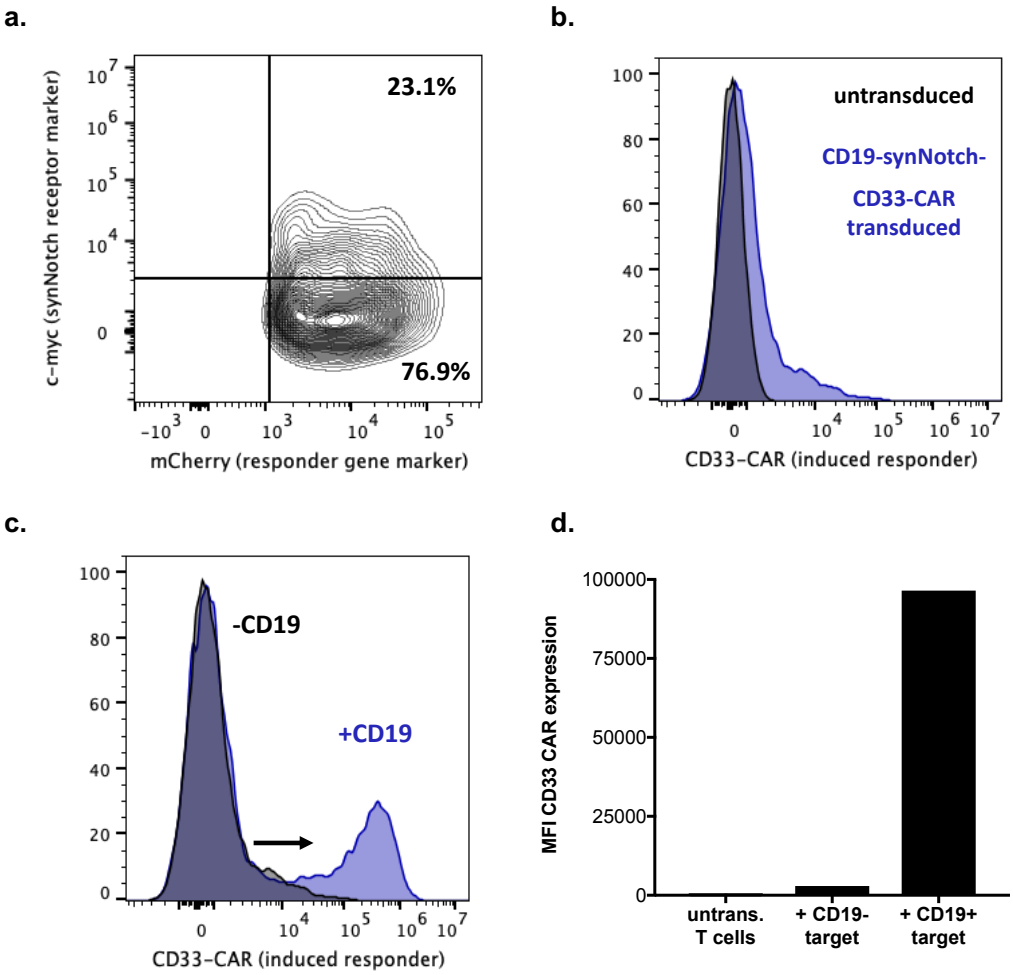

Figure 5-19 Anti-CD19 synNotch-gated expression of anti-CD33 CAR in T cells. Primary T cells were co-transduced with the Gal4-based anti-CD19 synNotch receptor and the anti-CD33 CAR responder element. Transduction efficiency was detected with flow cytometry analysis of the included markers c-myc (synNotch receptor) and mCherry (responder element). a. Contour plot showing mCherry- and c-myc-expression in T lymphocyte population after flow-sorting for mCherry-positive/CD19-negative cells. b. Histogram showing basal expression of anti-CD33 CAR in untransduced (black) and sorted synNotch-transduced T cells (purple). c. Histogram showing anti-CD19 synNotch-gated expression of anti-CD33 CAR in sorted modified T cells co-cultured with CD19-positive Jurkat cells (purple) compared to co-culture with the negative control SupT1 (black). d. Mean fluorescent intensity (MFI) of anti-CD33 CAR expression in flow-sorted T cells.

5.4.Novel synNotch receptors targeting neuroblastoma antigens

5.4.1. Cloning strategy

Four alternative synNotch receptors were designed to target the neuroblastoma antigens GD2 and B7H3 respectively. The scFvs targeting GD2 originated from the 14.18 (Zeng et al., 2005) or the huk666 (humanized KM8138) monoclonal antibody (Thomas et al., 2016), respectively. B7H3-binding synNotch receptors carried either an scFv derived from MGA271 (Loo et al., 2012) or a novel anti-B7H3 scFv developed by our team called TE9 (see **Figure 5-20**).

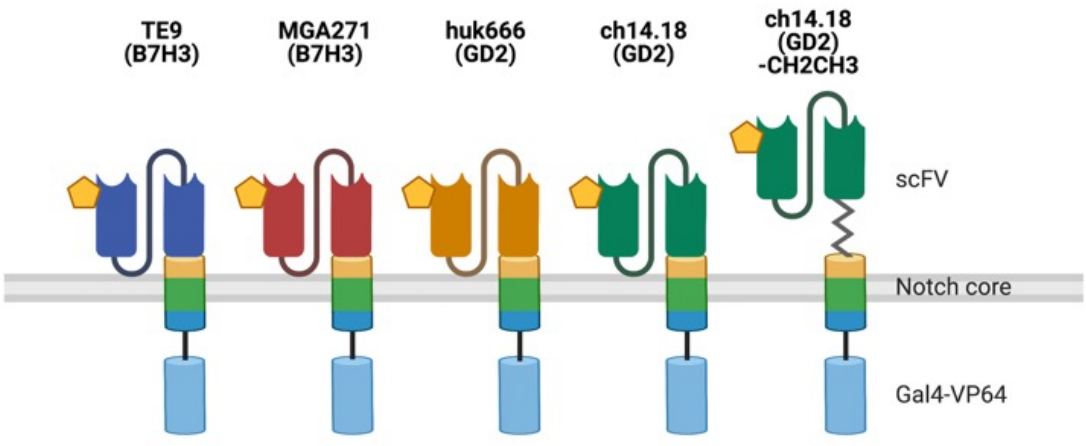

Figure 5-20 Generated synNotch receptors targeting neuroblastoma antigens. All receptors contain the synNotch building blocks of the transmembrane Notch core and the intracellular signal-transducing Gal4-VP64. The difference lies in the extracellular scFv and the CH2CH3 stalk.

For the MGA271-synNotch receptor, the CD19 scFv was replaced by the MGA271 scFv as well as an added AsiSI restriction site on the 3' end of the scFv (**Figure 5-21**a). In this step, six extra bases were added in between myc and scFv (CTCGAG → Leu, Glu) and nine bases between scFv and Notch transmembrane domain (GCGATCGCA → Ala, Ile, Ala) (indicated in grey). This enabled subsequent cloning to replace the extracellular domain for generation of the 14.18-, huk666- and TE9-synNotch vectors (**Figure 5-21**b). Lastly, an IgG1-derived hinge-CH2CH3 spacer was added in between the 14.18 scFv and

the notch transmembrane domains to investigate the effect of increasing space between scFv and the transmembrane region in a 14.18-synNotch receptor (**Figure 5-21**c).

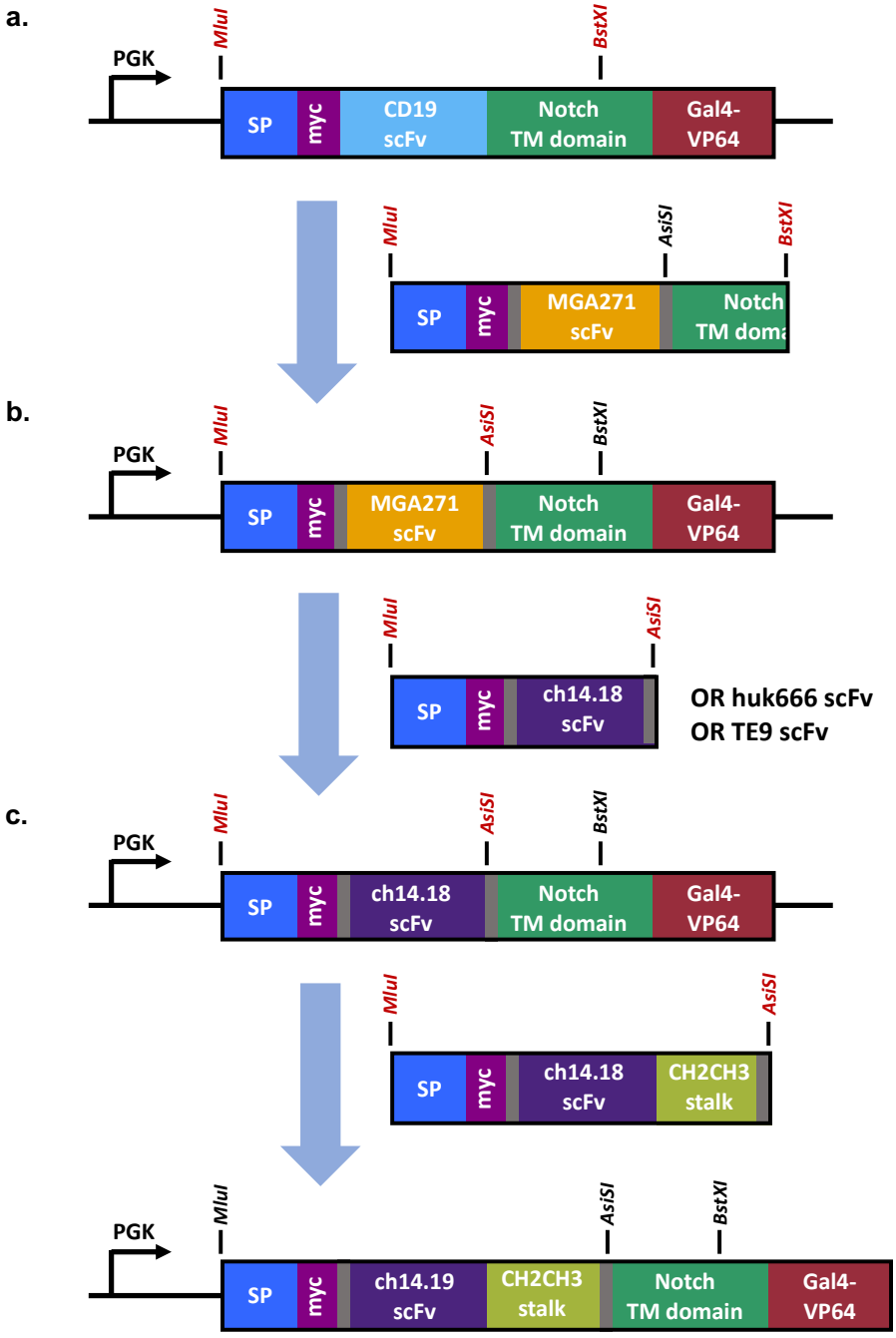

Figure 5-21 Cloning strategy for synNotch receptor-encoding plasmids.

The created synNotch receptors had to be validated for their functionality through inducible expression of the already tested Gal4-dependent BFP responder gene.

5.4.2. Validation of neuroblastoma-specific synNotch receptors

All neuroblastoma-targeting synNotch receptors were tested in combination with the Gal4-induced BFP responder to test for basic functionality through cleavage of intracellular Gal4-VP64 upon ligand binding leading to induction of BFP expression.

Target cell lines

Targets were stained for GD2 and B7H3 surface expression using flow cytometry. Again, no expression of either antigen could be found on the transduced Jurkat cell line, making it a suitable effector. Similarly, no GD2 and B7H3 could be detected on the surface of SupT1 wt which were used as a negative control target. To induce synNotch-gated transgene expression, the neuroblastoma cell lines Lan-1 and Kelly were used, which both expressed GD2 as well as B7H3. Another target carrying GD2 was the isogenic cell line SupT1 GD2, which only differed from the wild-type by expression of the antigen.

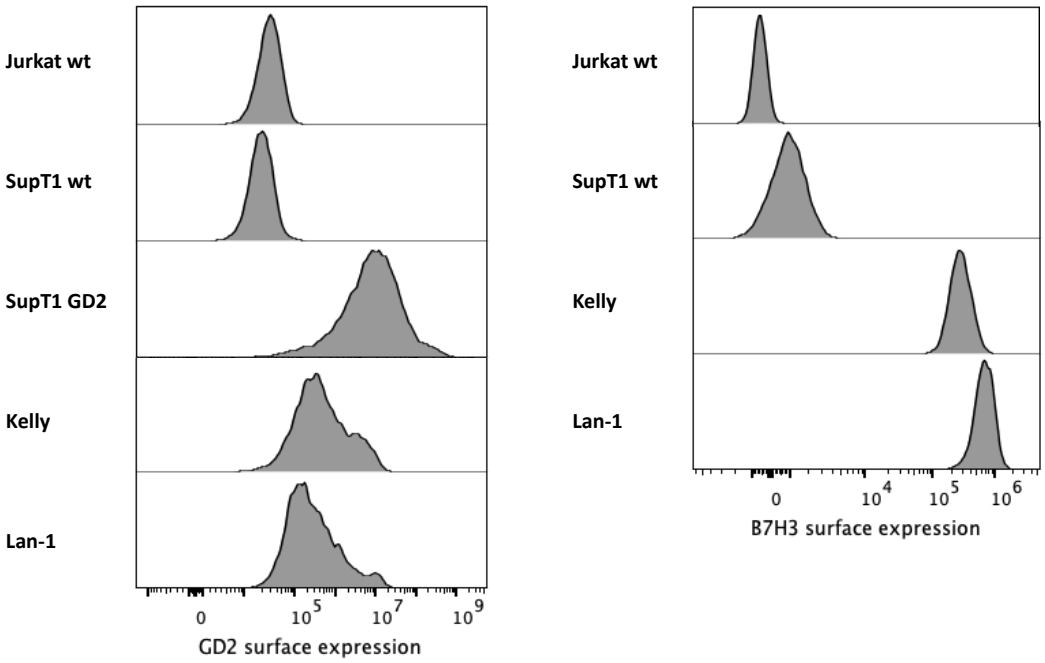

Figure 5-22 Surface expression of GD2 (left) and B7H3 (right) on targets. The cell lines Jurkat, SupT1 wt, SupT1 GD2, Kelly and Lan-1 were assessed for surface expression of the synNotch-targeted antigens using flow cytometry.

A novel anti-GD2 synNotch using the 14.18 scFv

Stepwise transduction of Jurkat cells with both lentiviral constructs achieved generation of a double positive population of 89.2% (**Figure 5-23**a). Therefore, cells could be used in co-cultures with no need for pre-sort.

Despite only changing the extracellular scFv, the anti-GD2 synNotch receptor displayed significantly more tonic BFP expression (30.8%; **Figure 5-23**b) than the anti-CD19 synNotch, which had no detectable baseline expression without target stimulation in Jurkat cells (0.27%; **Figure 5-7**). This basal transgene expression was increased when co-cultured with GD2-positive targets for 24 hours. In co-cultures both a 'classical' anti-GD2 synNotch and a modified version with an added CH2CH3 stalk were compared (**Figure 5-23**c,d). Results indicated that there was no notable improvement in BFP leakiness and signal induction when the synNotch receptor was modified with a stalk region (59.2%; ΔMFI 40,302) when compared to no stalk (67.4%; ΔMFI 64,149).

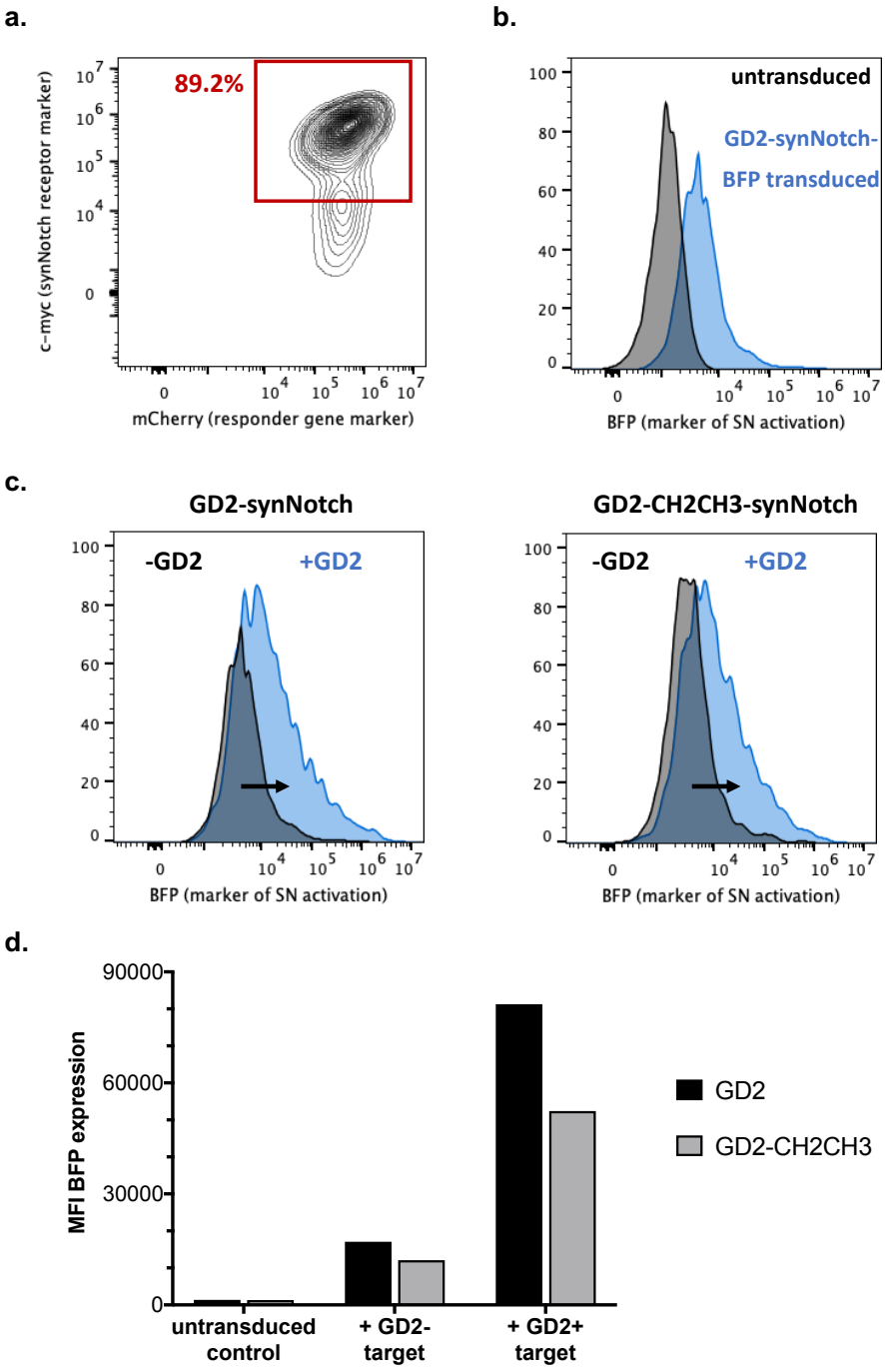

Figure 5-23 anti-GD2(14.18) synNotch-gated BFP expression in Jurkats. a. Contour plot displaying c-myc and mCherry expression on double-transduced cells. b. Tonic expression of synNotch-dependent BFP in transduced Jurkats (blue) compared to a non-transduced control (black). c. Jurkats transduced with either a classical anti-GD2 synNotch or a modified synNotch with a stalk region (CH2CH3) were co-cultured with GD2-positive (blue) and negative (black) targets. Histograms showing fluorescent intensity assessed via flow cytometry. d. Mean fluorescent intensity (MFI) of BFP expression in Jurkats modified with the anti-GD2 synNotch (black) and anti-GD2-CH2CH3 synNotch (grey) circuit.

Alternative neuroblastoma-specific synNotch receptors

Having realised that the anti-GD2 synNotch receptor using the 14.18 scFv results in a measurable background expression in the absence of synNotch targets, several other neuroblastoma-targeting synNotch receptors (GD2: huk666; B7H3: MGA271, TE9) were tested in Jurkat cells and compared to anti-CD19 synNotch-modified Jurkat cells (**Figure 5-24**). All receptors were tested without addition of a stalk region to enable a direct comparison with the published anti-CD19 receptor version.

To investigate induced expression of the BFP responder gene marker, double-transduced Jurkat cells with the Nb-specific synNotch receptors were either co-cultured with Lan-1 cells, which are positive for both GD2 and B7H3, or alternatively activated using anti-myc antibody (as described in chapter 5.3.3). For a positive control, Jurkat cells with the anti-CD19 synNotch receptor were also either co-cultured with the CD19-positive target cell line Raji or myc-stimulated.

As previously described, flow analysis of target co-cultures revealed that the anti-CD19 synNotch led to an induced expression of BFP in presence of the CD19-positive target, while not expressing the fluorescent marker when cultured alone or with CD19-negative cells (61.3%; ΔMFI 70,312). However, neither of the Nb-specific synNotch receptors could mirror the clean switch-on of induced BFP seen with the CD19-targeting receptor. While the receptors carrying scFvs from huk666 (4.6%; ΔMFI 2,170) and MGA271 (10.4%; ΔMFI 3,136) seemed to not induce expression strong enough to clearly distinguish from the background, those carrying the TE9 (24.7%; ΔMFI 7,198) or 14.18 (27.4%; ΔMFI 12,875) scFv regions showed more distinct upregulation of the BFP marker upon target encounter, albeit to less extent than the positive control. Furthermore,

all of the novel receptors displayed a small amount of tonic expression of the responder gene without target engagement (**Figure 5-24**a).

Surprisingly, when stimulated via crosslinking of the myc-tag, all Nb-specific synNotch receptors displayed a more significant shift towards increased BFP signalling. Again, the receptors cloned from huk666 (35.5%; ΔMFI 39,172) and MGA271 (37.0%; ΔMFI 47,941) induced lower levels of BFP in the Jurkat cells than those from 14.18 (61.5%; ΔMFI 149,737) and TE9 (52.3%; ΔMFI 112,465). Interestingly, myc-induced induction of BFP could not be achieved to the same extent when using the anti-CD19 synNotch receptor, despite showing the ability to switch on CAR expression with the same protocol (as shown in 5.3.3).

Figure 5-24b shows as an example, how when using the B7H3-specific TE9 synNotch receptor in Jurkats (top), there is no indication of a BFP-bright population when co-cultured with the B7H3-positive cell line Lan-1 (left), but when activated alternatively via the myc-tag (right). The anti-CD19 synNotch receptor on the other hand (bottom), can induce a strong expression of the fluorescent responder gene marker via engagement of the antigen-binding region (left) but showed only weak induction when activated via the myc-tag (right).

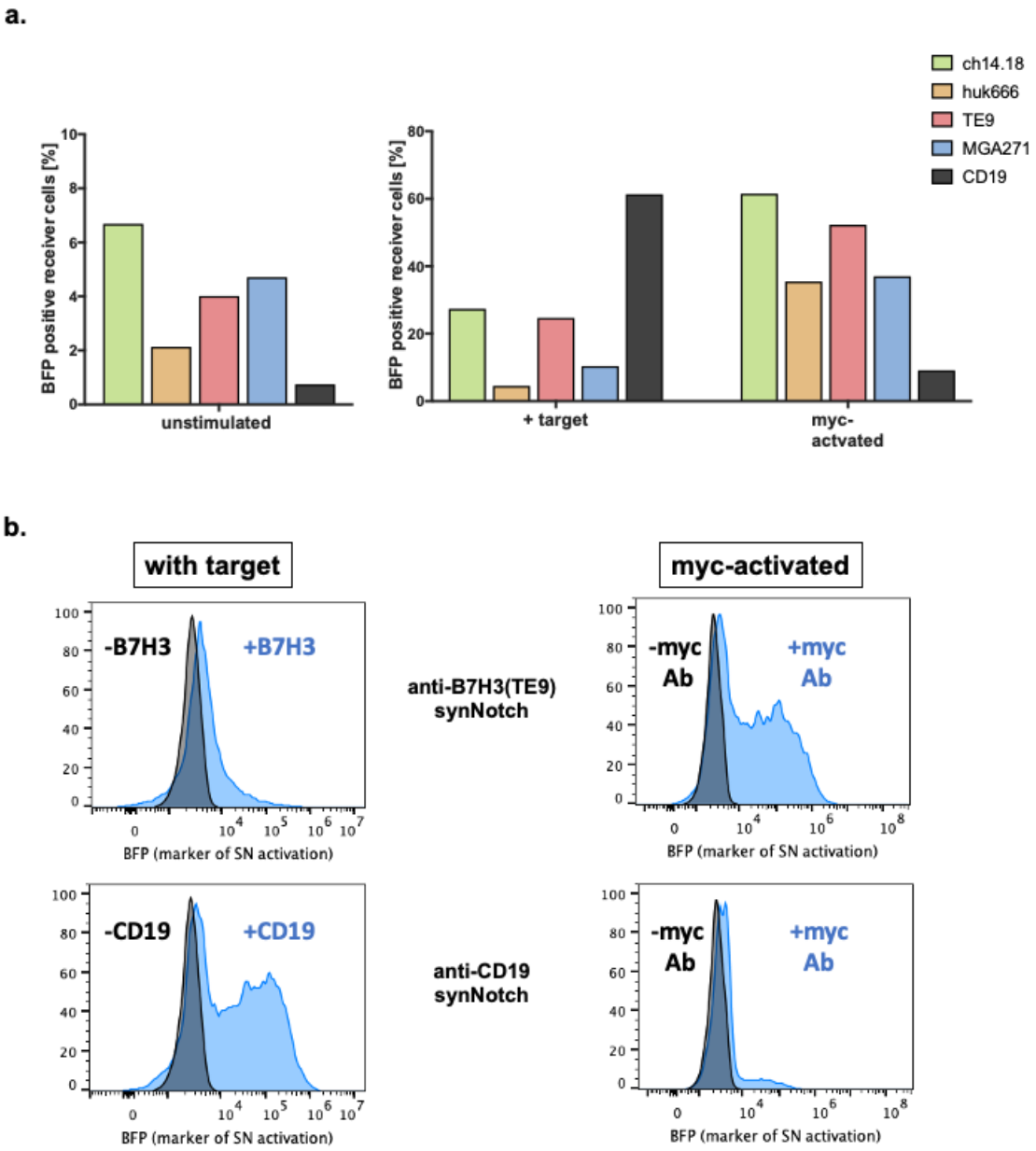

Figure 5-24 Comparison of BFP expression in Jurkat cells modified with neuroblastoma-specific synNotch receptor circuits compared to those modified with an anti-CD19 synNotch receptor.a. Bar diagrams showing percentage of BFP expression within each synNotch-receptor transduced Jurkat cell population. Cells were either kept alone (unstimulated, left), co-cultured with a target expressing the synNotch receptor ligand (target) or alternatively activated via immobilised anti-myc antibody (myc-activated) (right). b. Representative histograms showing BFP expression within the transduced population for anti-B7H3(TE9) synNotch-transduced Jurkat cells (top) or anti-CD19 synNotch-transduced Jurkat cells (bottom) either activated via target co-culture (left) or via crosslinking of the myc-tag (right). Black overlaid histogram shows BFP expression in the respective cell line when cultured alone (i.e., background expression).

5.4.3. Optimisation of co-culture conditions

In an attempt to improve BFP induction in co-cultures with the neuroblastoma-specific synNotch circuits, both increased incubation time as well as different effector-to-target ratios were investigated. For this, Jurkats modified with BFP-inducing synNotch circuits gated by the scFvs 14.18 (anti-GD2) and TE9 (anti-B7H3) were co-cultured with the ligand-positive targets Kelly and Lan-1 and compared to unstimulated Jurkat cells and the ligand-negative target SupT1.

Incubation period

An increase in incubation time beyond 24 hours did not improve expression of BFP in cells modified with either of the synNotch receptors (**Figure 5-25**a). Interestingly, BFP expression seemed to decrease slightly with both receptors when cells were left in co-cultures for 48 to 72 hours, when compared to expression measured at 24 hours. Highest expression of BFP was seen with Lan-1 cells as a target, measured after 24 hours, inducing 27.4% of BFP-positive Jurkat cells with 14.18 (ΔMFI 12,875) and 24.7% with TE9 (ΔMFI 7,198).

Effector-to-target ratio

Effector-to-target ratios of 1:1, 1:3, and 3:1 were compared after 24 hours of co-culture for both synNotch receptor variations (**Figure 5-25**b). Neither an increase nor a decrease in available targets seemed to improve BFP induction in the co-cultured Jurkat cells. Best expression was seen at a 1:1 ratio with Lan-1 cells in the 14.18-carrying receptor (27.4%; ΔMFI 12,875) and at a 1:3 ratio with Lan-1 cells in the TE9 variation (27.7%; ΔMFI 8,022).

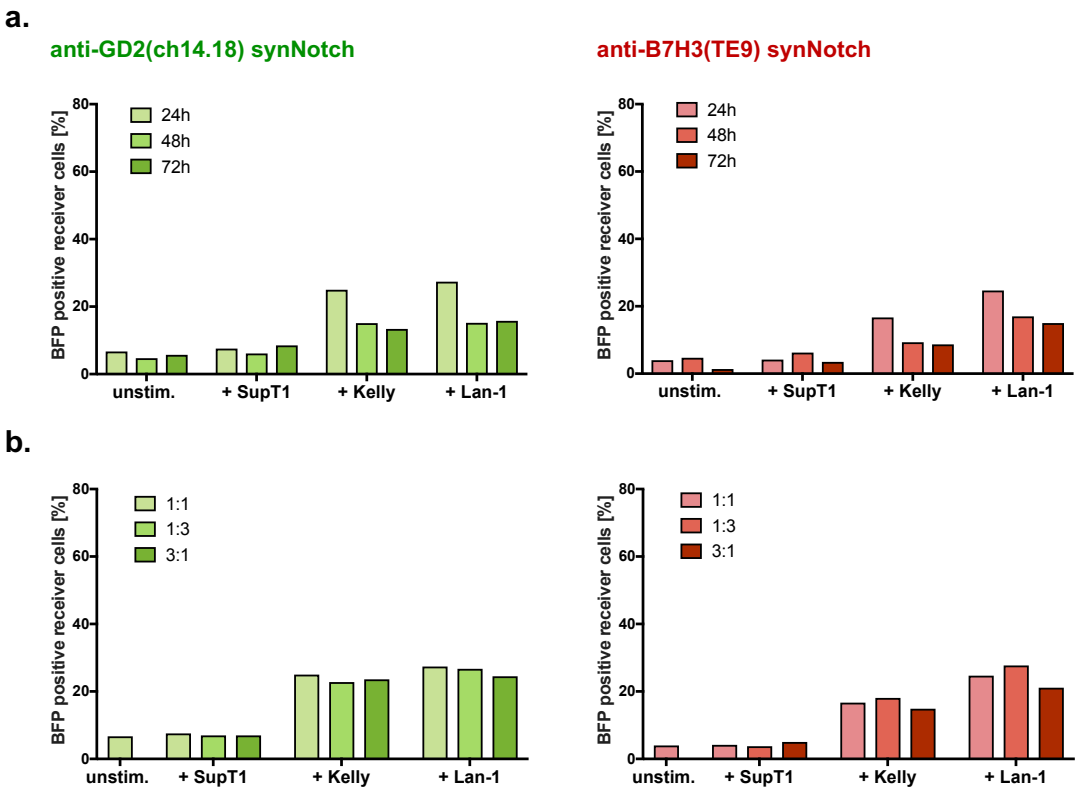

Figure 5-25 Optimisation of co-culture conditions for neuroblastoma-specific synNotch Jurkat cells. BFP responder gene expression was assessed in anti-GD2 (14.18, green) and anti-B7H3 (TE9, red) synNotch transduced Jurkat cells co-cultured with the ligand-positive targets Lan-1 and Kelly or a negative control using flow cytometry a. Bar diagrams showing percentage of fluorescent responder expressing cells within the transduced Jurkat population after 24h, 48h, and 72h of co-culture. b. Bar diagrams showing percentage of fluorescent responder expressing cells within the transduced Jurkat population at an effector-to-target ratio of 1:1, 1:3, and 3:1.

5.4.4. GD2-gated anti-CD33 CAR expression

A final attempt of GD2-synNotch-gated anti-CD33 CAR expression was conducted in Jurkat cells using the 14.18 scFv. Stepwise transduction with the two constructs achieved a strong double positive population of 89.5% (**Figure 5-26**a).

As previously observed with the BFP reporter, the anti-GD2 synNotch receptor resulted in tonic expression of the responder gene in 13.1% of transduced cells (**Figure 5-26**b). When co-cultured with GD2-positive target cells (SupT1 GD2), this CAR expression

increased (43.7%; ΔMFI 22,744) compared to when co-cultured with a negative control (SupT1 wt) (**Figure 5-26**c,d).

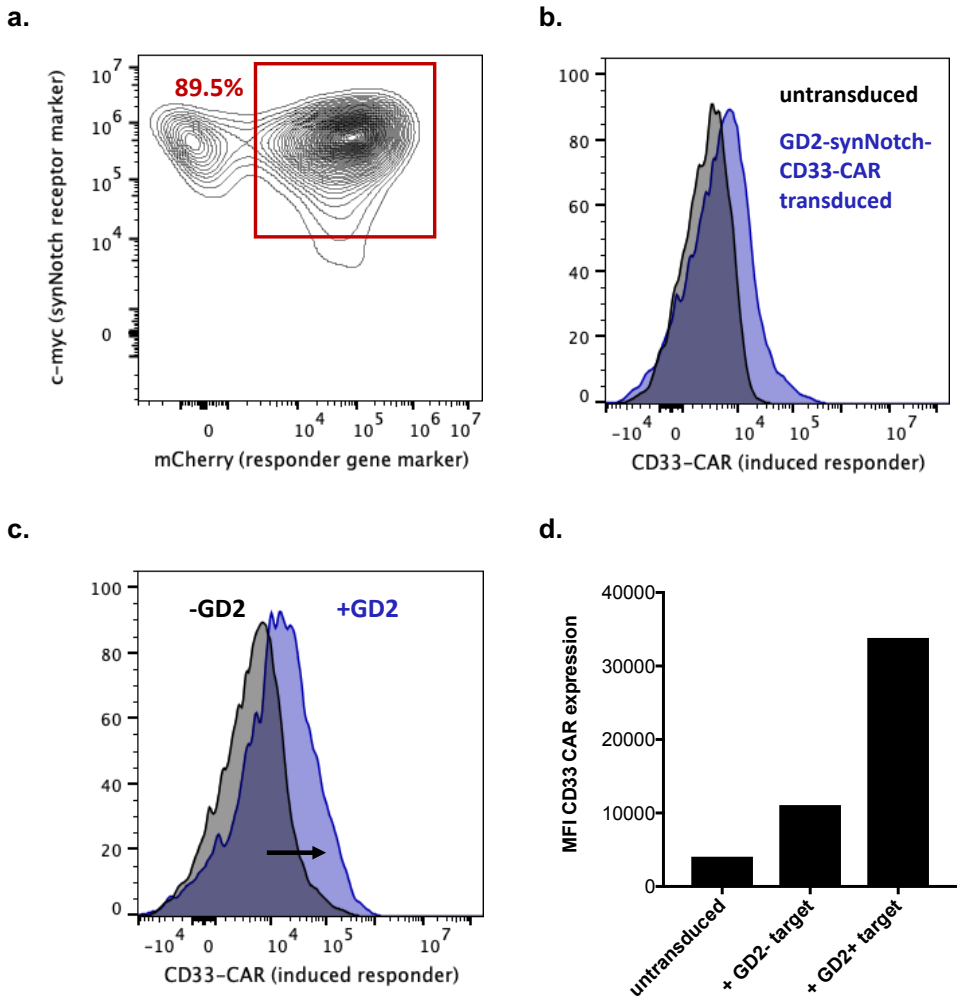

Figure 5-26 GD2-gated anti-CD33 CAR expression in Jurkats. a. Contour plot displaying c-myc and mCherry expression on double-transduced cells. b. Tonic expression of synNotch-dependent CAR in transduced Jurkats (purple) compared to a non-transduced control (black). c. Histogram showing CAR expression in synNotch modified Jurkats co-cultured with CD19-positive (purple) and -negative (black) targets, analysed via flow cytometry. d. Mean fluorescent intensity (MFI) of CAR expression in Jurkats modified with the anti-GD2 synNotch/anti-CD33 CAR circuit.

In conclusion, all neuroblastoma-specific synNotch receptor variations exhibited tonic expression of the responder gene with additional induction in the presence of the synNotch receptor ligand. Albeit displaying basic functionality, we do not think that the tested receptors are suitable for the application aimed for in this thesis at this point.

5.5. Discussion

In the final chapter of this thesis, alternative approaches were explored to design T cells capable of overcoming suppressive myeloid effects in the TME of neuroblastoma. Synthetic Notch receptors provide a range of applications, among them a localised and timed expression of CARs, which can be used for an AND-gated elimination of targets. We hypothesised that a circuit with a neuroblastoma-specific synNotch receptor gating for the expression of a monocyte-directed CAR could enable tumour-localised elimination of suppressive monocytes by engineered T cells, while sparing healthy monocytes in the periphery. In combination with a second population of T cells modified to express a neuroblastoma-directed CAR, this system could provide a new combinatorial therapy design targeting both the tumour cells and the TME.

To establish synNotch circuits for this purpose, two available variations of anti-CD19 synNotch receptors were compared first. The difference between the two receptors can be found in the intracellular transcription factor domain, using either Gal4-VP64 or tet-VP64 (tTA), which were paired with matching responder elements gating the expression of fluorescent reporters. Side-by-side comparison of the two synNotch receptors in Jurkat cells revealed tonic responder expression in cells transduced with the tTA circuit but not in those modified with the Gal4-based system. This baseline expression of the responder marker was unchanged when cells were co-cultured with CD19-negative targets but was increased for both circuit variations when the transduced Jurkats were co-cultured with cells expressing the synNotch target. The tet-based circuit additionally could be switched off when adding doxycycline to the co-culture.

Based on the results seen in the direct comparison of the two receptor variations we concluded that the Gal4-based circuit is more suitable for the aims of this project. The

background expression of GFP in cells transduced with the tTA-based synNotch system (ΔMFI=37,619) indicates a tonic expression of the responder element without antigen binding of the receptor, which was not observed in cells transduced with the Gal4 variant. This high basal expression suggests translation of the transgene in absence of transcription factor binding. Despite the benefits of having a switchable system with tTA, we therefore preferred the use of a Gal4-VP64 intracellular domain and decided to move forward to design all synNotch receptors and responders with Gal4-based circuits. A further optimisation step, investigating longer incubation time and effector-to-target ratios with either an increased Jurkat or target population, did not indicate an improvement in BFP induction mediated by the anti-CD19 synNotch receptor. We therefore concluded that co-cultures left for 24 hours at a 1:1 effector-to-target ratio would be the standard for all subsequent validations of synNotch circuits.

Testing the anti-CD19-Gal4-VP64 synNotch receptor in T cells, flow analysis revealed a basal responder expression in half of the transduced population. This high expression of the reporter gene masked further upregulation of expression in the presence of the receptor ligand. Based on the negligible background expression of the fluorescent responder in Jurkat cells, we suspected these results originated from actual binding of the synNotch receptor. Indeed, phenotype analysis of the expanded T cells revealed a CD19-positive population in all tested donors, ranging from 5-10%. We therefore repeated the co-culture with a preceding flow sort to exclude CD19-positive cells within the transduced T cell population. The sorted cells did not express BFP in the absence of target and upregulated expression when co-cultured with the ligand-carrying cell line Raji, reflecting the prior results found using the same synNotch circuit in the Jurkat cell line.

For the local elimination of myeloid cells, we designed a responder element encoding for synNotch-gated expression of a monocyte-specific CAR (second generation anti-CD33 CAR, see **Figure 5-14**), thus replacing the fluorescent marker BFP. To validate the construct for its functionality, we combined the new CAR responder element with the anti-CD19 synNotch receptor in initial test runs in Jurkat cells, as the functionality of this receptor had already been tested and published (Morsut et al., 2016). In Jurkats co-transduced with the CD19-CD33 CAR circuit no CAR expression was detected, both when cultured alone or with the target-negative control (SupT1 wt). Only when co-cultured with the CD19-positive cell line Raji, CAR expression on the synNotch-transduced cell's surface was significantly upregulated. This reflects results seen when the same synNotch receptor was used with a BFP-expressing responder element, suggesting a similar functionality of the newly designed construct.

Analysis of the dynamics of up- and downregulation of CAR expression after alternative activation of the synNotch receptor via its myc-tag showed steady-state expression of the responder after 24 hours, with a half-time of about 5 hours after stimulation start, and a downregulation of CAR expression within 24 hours of stimulus removal, with a half-time of circa 8 hours. This mirrors results reported by Roybal and colleagues, which reported a $t_{1/2}$ of 6 hours for upregulation and 8 hours for downregulation, respectively, when investigating CD19-gated expression of an anti-mesothelin CAR (Kole T. Roybal et al., 2016).

Likewise, in T cells CAR expression could be induced in the presence of CD19-positive targets. As described previously, existing CD19-positive populations within the expanded T cells had to be excluded before co-cultures with targets to correctly dissect synNotch

activation. This concluded validation of the novel construct, which was proven functional and suitable for fast on-and off-switching of CAR expression in the TME.

Moving on, we designed four neuroblastoma-specific synNotch receptors, targeting either GD2 (14.18, huk666) or B7H3 (TE9, MGA271) (see **Figure 5-21**). Furthermore, a variation of the anti-GD2 (14.18) synNotch with a CH2CH3 stalk was tested to examine if receptor activation could be further optimised. Again, to look at the engineered constructs individually, the novel synNotch receptors were paired with the well-established fluorescent responder plasmid carrying an inducible BFP gene. Double-transduced Jurkats were co-cultured either with a negative control cell line that did not express the ligands (SupT1 wt) or with the neuroblastoma cell lines Lan-1 and Kelly, which simultaneously express both tumour markers.

In cells modified with the GD2-targeting system, BFP expression was increased when co-cultured with antigen-positive targets, indicating the availability of a functional synNotch-gated circuit. This was observed both in the classical version of the receptor as well as in the variation with a stalk region. However, a basal expression of the responder element was also recorded in about 30% of transduced cells cultured alone or together with a GD2-negative target. Since no tonic signalling was observed when combining the same responder element with the anti-CD19 synNotch receptor, this suggests a nonspecific signal transduction mediated by the GD2-targeting construct. Based on flow cytometry analysis of both cell lines, any presence of GD2 antigen in the transduced Jurkat cell line as well as in the negative target control SupT1 could be excluded (**Figure 5-22**). We therefore propose that the basal signalling could be affected by the framework regions of the scFv of the 14.18-derived antibody that had been cloned into the novel synNotch receptor. It has been reported that through framework region-dependent tonic

clustering, the same antibody can result in tonic signalling when used for CAR designs, leading to over-activation and early exhaustion in transduced T cells (Long et al., 2015). With this in mind we moved on to investigate other Nb-specific scFv regions in the synNotch receptor context.

To review all synNotch receptor variations, Jurkats were transduced with the BFP responder gene in combination with all four novel Nb-specific synNotch receptors and compared in their ability to induce BFP expression either through ligand binding in target co-cultures or through alternative activation using anti-c-myc antibody, as described in section 5.3.3. As a positive control, Jurkats with the anti-CD19 synNotch circuit were treated alongside. As before, the CD19-specific receptor showed no basal induction of BFP when cells were cultured alone, but upregulated expression significantly when co-cultured with a CD19-positive target (61.3%). Jurkat cells modified with the Nb-specific circuits on the other hand, did not upregulate expression of the responder marker to the same extent as the positive control. While there was only negligible upregulation in the receptors carrying the scFvs huk666 and MGA271, the synNotch circuits with scFv 14.18 and TE9 could induce moderate expression of the responder gene (27.4% and 24.7%, respectively). Surprisingly, when alternatively activating the same cells via the myc-tag, situated on the N-terminus of the synNotch receptor, all Nb-specific synNotch circuits showed much higher expression of BFP (35.5% to 61.5%). This indicates that the receptors are functional, but that there are problems with ligand binding when encountering target cells. Albeit outside of the scope of this thesis, ligand binding of the receptors could be further explored in the future by using soluble antigen (B7H3) or antibodies for the scFvs (14.18 anti idiotype). A reason for the lack of signalling could be problems in the formation of a functional immune synapse (IS), which is known to also be a crucial factor for predicting the efficacy of CARs (Liu et al., 2020). Moreover, during

cloning two and three amino acids have been introduced in between myc-tag/scFv and scFv/Notch transmembrane, respectively. This could possibly interfere with the 3D structures of the translated protein (see **Figure 5-21**), although it is unlikely that changes outside the scFv would affect ligand binding. Whether binding could have been improved by redesign of the receptor or deletion of the introduced bases unfortunately exceeded the scope of this PhD project and will be focus of future investigations. Interestingly, the observed effects were reversed for the anti-CD19 synNotch receptor. While a high induction of BFP was observed when co-cultured with CD19-positive target cells, receptor activation via its myc-tag was very low. This was incoherent with the findings of chapter 5.3.3 where we used the same protocol and successfully induced expression of an anti-CD33 CAR by myc-activation of the same anti-CD19 synNotch receptor. Without further investigation we cannot make conclusions to explain this mechanism.

Moving on, we examined changes in co-culture conditions using the two better performing Nb-specific synNotch receptors (14.18, TE9) in hope of improving synNotch-induced signals. However, neither increase in incubation time, nor changes in effector-to-target ratio changed BFP induction significantly. This suggests that the low responder induction is not caused by a limitation of antigen availability or insufficient time to upregulate expression and hints at problems in the process of crosslinking with antigen provided on the target cells. As all these experiments have been conducted with synNotch receptors without linkers or spacers, further optimisation to improve crosslinking with the respective antigens will be of particular interest in the future.

Co-transduction of the anti-GD2 synNotch receptor and the anti-CD33 CAR responder in Jurkats enabled synNotch-gated expression of the CAR in co-cultures with GD2-positive targets. However, as described before in combination with the BFP responder

element, the anti-GD2 synNotch receptor also displayed basal expression of the responder in the absence of the ligand, suggesting tonic signal transduction.

Overall, all Nb-specific synNotch circuits turned out to express a baseline of tonic responder expression, which could be somewhat increased when provided with the synNotch ligand. Concerning the background expression in the absence of target, Long and colleagues observed similar tonic signalling to varying degrees with other scFv based CARs (including 14.18), with the exception being the CD19 CAR (Long et al., 2015). This potentially explains the results we found using the scFv in synNotch receptors. Moreover, when activated, the expression of the Nb-specific synNotch responder seemed to be less effective compared to the published anti-CD19 synNotch receptor. We suggest that similar to CARs, synNotch receptors depend on forming a functional IS with the target cells. A natural IS is formed during the interaction of TCRs and MHC-peptide complexes, and defined by three concentric rings of clustered molecules, including the central, peripheral, and distal supramolecular activation cluster (SMAC) (Watanabe et al., 2018). Involved in correct synapse formation are therefore not only the receptor complex, but also interactions of co-receptors and proteins involved in cell adhesion, such as integrins. While the IS formed by CARs is more disorganised, it is crucial to the quick and effective killing of target cells. Several studies have demonstrated the impact of CAR design on the quality of IS formation. For example, it has been reported that third generation CARs constructed with both CD28 and 4-1BB co-stimulatory domains exhibited higher quality IS than those with just either one of the domains (Xiong et al., 2018). Being a similar antibody-based construct, synNotch receptor design might equally influence IS formation, which may have to be considered when translating the system to different targets.

In conclusion, in this chapter we have successfully established the synNotch system and have provided the basis for future endeavours to provide an AND-gated elimination of myeloid cells in the TME through inducible expression of an anti-CD33 CAR.

6. CONCLUSIONS AND FUTURE WORK

The TME of solid tumours, such as neuroblastoma, presents a major hurdle in the translation of CAR T therapy. The cumulative suppressive effects of cancer cells and recruited alternatively activated immune effectors like MDSC significantly reduce T cell proliferation and function. Within this thesis we have established a neuroblastoma-based model to study interactions of T cells and myeloid cells in a tumour-conditioned environment. Furthermore, the proposed model was applied as a platform to screen for therapeutic interventions against myeloid-derived suppression.

Using an adapted protocol for the polarisation of healthy monocytes with Nb-conditioned supernatant, we have shown to generate NbM capable of reproducible suppression of T cell proliferation. Through extensive optimisation of proliferation readout, culture conditions and incubation span we have established in a robust protocol for monocyte-mediated T cell suppression in a 48-well plate format. Comparison of the NbM-mediated suppression revealed that the conditioned cells were most effective when used at a maximum of 4 days after polarisation. The resulting decrease of T cell proliferation was reproducible among unmodified and CAR-modified T cells, with no clear allogeneic effects between donors. Moreover, T cell suppression could also be measured by means of decreased levels of IFN-γ.

NbM were further characterised for phenotype and suppressive mechanisms. Using a flow cytometry panel composed of five MDSC markers, we observed an increase of M-MDSC-like populations after Nb-conditioning as well as a slight increase in immature populations (eMDSC), but not PMN-MDSC. Next, two MDSC-specific suppressive mechanisms were investigated to identify the cause of NbM-mediated suppression. Our findings indicate that NbM do not display arginase activity but could reproduce published

findings that the Nb cell line Lan-1 does. A DCFDA-based assay suggested the presence of ROS within NbM, although this has been described to be a mechanism predominantly seen within PMN-MDSC. Unfortunately, a lack of a comprehensive negative control, i.e., cells completely free of ROS, makes this assay difficult to interpret. The negative control presented in the results, which is unstained monocytes, only allows for exclusion of autofluorescence of cells without DCFDA, however cannot give information about unspecific binding of the dye, which could lead to false-positive results.

Further characterisation of NbM may reveal more about their commonalities with the known human MDSC subpopulations, but unfortunately exceeded the limitations of this thesis. Future experiments to investigate suppressive pathways could look at generation of NO, which is predominantly executed by M-MDSC, or release of regulatory cytokines such as IL-10 or TGF-β. Additionally, it may be of interest to identify whether NbM-mediated T cell suppression is dependent on cell-to-cell contact, which could be explored via co-culture in a transwell setting. Nevertheless, the robust suppression in the established assay provided a platform for subsequent experiments looking at approaches to overcome the NbM-mediated effects.

A first approach to overcome myeloid derived suppression examined in this thesis is through drug retargeting for combination treatments. We hope that if applied together with a suitable MDSC-inhibitory drug, CAR T cells may overcome local suppression in solid cancers and more efficiently eliminate tumour cells. We therefore used the Nb-based model established in this thesis to screen for T cell proliferation recovery potential of drugs, described in the literature to inhibit MDSC function. First we tested increasing concentrations of Sunitinib malate, which has been described to dose-dependently deplete MDSC populations in mice, causing an increase in CD8+ T cells numbers and activation

(Draghiciu et al., 2015b). Within the non-toxic range, Sunitinib partially recovered T cell proliferation in the presence of NbM to 76% of proliferation seen in the positive control. Further readouts looking at T cell cytokine release revealed NbM-mediated suppression of IL-2, TNFα and IFN-γ. Again, intermediate recovery of all three cytokines could be achieved when pre-treating NbM with 1μM Sunitinib. However, within the tested range no full recovery of T cell proliferation of cytokine release could be accomplished. A second drug we chose to investigate in this format is gemcitabine hydrochloride. Despite reports of cytotoxic effects on MDSC, we have not seen any recovery of T cell proliferation in co-cultures testing this drug. Interestingly, blood analysis of patients with pancreatic cancer has shown that treatment with gemcitabine significantly reduces PMN-MDSC, while not affecting M-MDSC (Eriksson et al., 2016). This subtype-specific effect could explain the lack of efficacy in our model, which has been shown to show more phenotypic similarity with M-MDSC.

There are several other drugs which could be investigated in this setting in future endeavours. However, for this a clearer picture about the suppressive mechanisms mediated by of our Nb-based model would be essential. Of interest could be for example reagents that have been reported to drive myeloid differentiation, therefore transforming the immature MDSC populations towards mature non-suppressive myeloid cells. Drugs described to have this effect are, among others, ATRA, Vitamin D3 and Curcumin. Furthermore, another strategy could be to choose reagents that directly interfere with the suppressive mechanisms seen with MDSC. Depending on the predominant way of action, described agents include PDE-5 inhibitors such as Sildenafil, inductors of antioxidant genes such as CDDO-Me, or the COX-2 inhibitors Acetylsalicylic acid and Celecoxib (Anderson, 2017; Draghiciu et al., 2015a). Interestingly, both Sildenafil and Acetylsalicylic acid have induced a partial recovery of T cell functions in the performed

Prestwick library screen, further confirming our confidence in the developed model for investigating myeloid suppression and drug interventions.

An alternative approach to cover a large variation of MDSC-inhibitory drugs as well as not previously investigated compounds is to use a chemical library. To optimise our suppression assay for high-throughput drug screens, we have translated it into a 96-well-based assay with cytokine readout, which delivers results within 72 hours. To ensure quality of NbM-mediated suppression, we included a preliminary assessment of T cell suppression 24 hours before library screen set-up and have shown that this robustly predicts suppressive potential of each donor.

In a pilot screen using $1/16^{th}$ of the Prestwick chemical library (contains 1280 small molecules), we have demonstrated the sensibility of our assay for cytokine recovery potential of the tested drugs. Within the arbitrary threshold of more than 50% (compared to the positive control without NbM), we could identify six compounds that showed signs of IFN-γ recovery despite the presence of NbM. One of them, Imiquimod, showed significant recovery to 79%. However, there are a few limitations to these findings. For instance, due to the large number of tested small molecules, we decided to only investigate them at one concentration (10μM), which reflects a typical physiological dose for most drugs. Especially with the dosage-dependent effects seen in prior drug tests in mind, this means that some of the tested chemicals may have an effect at a lower or higher concentration, which we will miss in the library screen. Likewise, hits falling above the 50% threshold may show even better recovery when tested at additional concentrations. In addition, we have shown that our generated NbM do not fully reflect all suppressive mechanisms mediated by MDSC. Analysis of arginase activity, for example, has shown no expression of this enzyme in our NbM, despite being a key function described for

some MDSC subtypes in the literature. Therefore, some potential MDSC-inhibitory drugs may fall through the grid in our library screen despite possibly being able to contribute to efficacy *in vivo*.

However, we hope that by means of this novel screening platform it will be feasible to identify several hits that significantly recover T cell cytokine release in our model. The chosen compounds can then be taken forward for subsequent experiments looking at effects of a wider concentration range, evaluating alternate Nb cell lines to induce NbM cells, as well as for functional readouts beyond cytokine recovery, such as effects on T cell proliferation and cytotoxicity. Ultimately, *in vivo* mouse experiments will be needed to provide essential preclinical proof of concept, comparing treatment of tumour bearing mice with either CAR T cells only or CAR T cells combined with the drug of interest. This could then justify future clinical trials to investigate benefits of the proposed drug retargeting in human subjects. An important caveat will be that – to fully understand the effects of the combination treatment – we will need to ensure the formation of a functional TME when carrying out *in vivo* experiments. There are several options to be considered for this, among them using either mice carrying a human immune system (humanised mice), the establishment of organoid tumours that are composed of both tumour and suppressive myeloid cells, or translation of the therapy in a murine system, which would require murine endodomain-optimised CAR design.

A second strategy to overcome myeloid-derived suppression explored in this thesis is through T cell engineering. Using Wendell Lim's synthetic Notch receptors, we hypothesised that we could combine Nb-specific CAR T cells with a local and timed expression of myeloid-specific CARs, leading to local depletion of myeloid populations and improved tumour killing. Testing of previously published anti-CD19 synNotch

receptors with either a tTA- or Gal4-based intracellular domain in the Jurkat cells line showed that the transcription factor Gal4 showed less tonic signalling and clean induction of the responder in presence of the ligand. When excluding B cell contaminations, the same effect could be seen using this synNotch circuit in primary T cells, showing that the basic system works in our hands.

We then moved on to engineer a synNotch circuit suitable for the desired application in Nb immunotherapy. The suggested system includes a Nb-directed (anti-GD2 or anti-B7H3) synNotch receptor gating for the expression of a myeloid-directed CAR (anti-CD33). We successfully demonstrated CAR expression under the control of the anti-CD19 synNotch in Jurkat cells and in T cells. Moreover, dynamics of CAR expression before and after target encounter indicated a quick on- and off-switch mechanism mediated by the synNotch receptor, which we hypothesise will guarantee that only local CD33-positive targets will be eliminated, while myeloid populations in the periphery will be spared.

Engineering of Nb-specific synNotch receptors proved to be less efficient. We successfully produced constructs coding for synNotch receptors against GD2 (14.18, huk666) and B7H3 (TE9, MGA271), however all were characterised by tonic expression when combined with the fluorescent responder and induced only low levels of the reporter in the presence of ligand-positive targets. Interestingly, Jurkat cells carrying either of the four synNotch variations could be alternatively activated via the myc-tag, indicating the observed changes were not caused by dysfunction of synNotch signalling, but likely by insufficient binding of the scFv ligands. Further optimisation attempts could not improve the weak signalling in target co-cultures and the same results were seen when the anti-GD2 synNotch receptor was combined with the previously successful anti-CD33 CAR

responder. We therefore conclude that replacing the scFv domain of anti-CD19 synNotch receptors requires specific optimisation depending on the antigen-binding sequence used. This insight will help with further engineering plans for synNotch receptors and indicates a need for scFv-specific receptor design. Before novel receptors can be applied for local myeloid targeting, clean on- and off-dynamics of signalling as well as target-specific responder expression have to be ensured. We propose that tonic activation of the receptors could be a result of receptor clustering, as seen with CAR receptors carrying anti-GD2 scFvs before (Long et al., 2015). This effect has been contributed to framework regions of the 14.18 scFv but can be detected to varying degrees in several other scFv-based CARs, with the exception of the anti-CD19 CAR. Long *et al.* reported that CARs specific for CD22 show lower level of activation when using the HA22 scFv, but higher level of activation when using the m971 scFv as well as ErbB2 (4D5 scFv)-specific CARs. This relative activation correlated with an increase in expression of exhaustion markers and exhaustion-associated transcription factors (Long et al., 2015).

Seeing that the receptors can signal when cross-linked via their myc-tag, antigen binding of the created synNotch receptors seems to cause the limited signalling in co-cultures and will have to be improved. We suggest that receptor cross-linking could be enhanced by introduction of spacers allowing the scFv to bind antigen with more flexibility, which will be tested in future endeavours. Alternatively, other scFvs will have to be tested for improved responder induction. Various other publications have shown the successful application of the synNotch strategy for targeting of Axl (Cho et al., 2018), GPC3 (Tseng et al., 2020), ROR1(Srivastava et al., 2019) and even B7H3 (scFv BRCA69D) and GD2 (scFv 14.18/E101K) (Moghimi et al., 2021; Srivastava et al., 2019), none of them having added a spacer in between scFv and transmembrane domain. Interestingly, Moghimi *et al.* have reported similar baseline expression of their synNotch-gated responders at

around 20%, and only weak signalling upon target encounter when using the 14.18 scFv, both without linker and when adding an IgG hinge or IgG CH2CH3. However, when using their high affinity anti-GD2 scFv E101K with no spacer, signal induction was significantly higher than with 14.18 and led to significant expression of a fluorescent responder or an anti-B7H3 CAR in T cells (Moghimi et al., 2021). These results suggest that the platform is suitable for the translation to other targets in general but may require precise adjustments by adding linkers or using high affinity scFvs.

Unfortunately, further optimisation of the proposed system went beyond the scope available for this thesis. Once a suitable Nb-specific synNotch receptor has been established, we will be able to test it in combination with the myeloid-specific inducible CAR in T cells. Co-cultures of synNotch-modified T cells with either or both Nb cells and NbM should then show selected killing of myeloid cells only in the presence of Nb. Readouts will have to include effects on numbers and viability of myeloid cells as well as effect on T cells, such as cytokine release, degranulation and expression of activation markers. If *in vitro* experiments show successful Nb-induced cytotoxicity, *in vivo* experiments could look at the effects of combinational approaches with CAR T cells.

There are several possibilities for how to combine the two strategies. For instance, synNotch-modified T cells with an inducible anti-CD33 CAR could be given alongside Nb-specific CAR T cells, resulting in a therapy consisting of two different T cell populations. To avoid eliminating the ligand for the synNotch receptor, priming with the synNotch T cells before giving the CAR T cells could be considered. Secondly, we could engineer both a myeloid-specific CAR as well as a Nb-specific CAR under the control of a synNotch receptor. We suggest this could be achieved either in form of a mixed T cell population carrying either synNotch circuit, or within the same T cell population, in form

of a 2A-cleavable induced responder coding for both CARs sequentially. However, the resulting large construct may make the latter suggestion difficult to transduce. Another possibility to put both effects under the control of a synNotch receptor could be to design an inducible Tandem CAR targeting both CD33 and a Nb marker, such as B7H3 or GD2. Independently of how this is achieved, the synNotch-controlled CAR expression could provide several benefits over traditional CAR T therapy. Besides the advantage of localised elimination of target-positive cells, the AND-gated strategy ensures the modified T cells to stay more naïve due to no preliminary CAR signalling, and spares ligand-carrying targets in the periphery, which reduces on-target/off-tumour effects.

Overall, this thesis has provided a novel model to study myeloid-derived suppression in the neuroblastoma microenvironment and showed examples of how it can be used to investigate approaches to overcome this T cell suppression *in vitro*.

7. SUPPLEMENTARY

Table S1 List of drugs tested in library screen.

A2	Buspirone hydrochloride	**E2**	Clofibrate
A3	Anastrozole	**E3**	Cyclophosphamide
A4	Doxycycline hydrochloride	**E4**	Aripiprazole
A5	Sulbactam	**E5**	Ethinylestradiol
A6	Fleroxacin	**E6**	Fluocinolone acetonide
A7	Clavulanate potassium salt	**E7**	Sparfloxacin
A8	Valproic acid	**E8**	Desloratadine
A9	Mepivacaine hydrochloride	**E9**	Clarithromycin
A10	Rifaximin	**E10**	Tripelennamine hydrochloride
A11	Estradiol Valerate	**E11**	Tulobuterol
B2	Acetylcysteine	**F2**	Topotecan
B3	Melengestrol acetate	**F3**	Atorvastatin
B4	Bromhexine hydrochloride	**F4**	Azithromycin
B5	Anethole-trithione	**F5**	Ibudilast
B6	Amcinonide	**F6**	Losartan
B7	Caffeine	**F7**	Benztropine mesylate
B8	Carvedilol	**F8**	Vecuronium bromide
B9	Methenamine	**F9**	Telmisartan
B10	Phentermine hydrochloride	**F10**	Nalmefene hydrochloride
B11	Diclazuril	**F11**	Bifonazole
C2	Famciclovir	**G2**	Gatifloxacin
C3	Dopamine hydrochloride	**G3**	Bosentan
C4	Cefdinir	**G4**	Gemcitabine
C5	Carprofen	**G5**	Olmesartan
C6	Celecoxib	**G6**	Racepinephrine HCl
C7	Candesartan	**G7**	Montelukast
C8	Fludarabine	**G8**	Docetaxel
C9	Cladribine	**G9**	Cilnidipine
C10	Vardenafil	**G10**	Imiquimod
C11	Fluconazole	**G11**	Fosinopril
D2	5-fluorouracil	**H2**	Imatinib
D3	Mesna	**H3**	Moxifloxacin
D4	Mitotane	**H4**	Formoterol fumarate
D5	Ambrisentan	**H5**	Rufloxacin
D6	Triclosan	**H6**	Pravastatin
D7	Enoxacin	**H7**	Rosiglitazone Hydrochloride
D8	Olopatadine hydrochloride	**H8**	Rivastigmine
D9	Granisetron	**H9**	Sildenafil
D10	Anthralin	**H10**	Acetylsalicylic acid
D11	Lamotrigine	**H11**	Hexachlorophene

8. BIBLIOGRAPHY

Adlard, A.L., Dovedi, S.J., Telfer, B.A., Koga-Yamakawa, E., Pollard, C., Honeychurch, J., Illidge, T.M., Murata, M., Robinson, D.T., Jewsbury, P.J., Wilkinson, R.W., Stratford, I.J., 2014. A novel systemically administered toll-like receptor 7 agonist potentiates the effect of ionizing radiation in murine solid tumor models. International Journal of Cancer 135, 820–829. https://doi.org/10.1002/ijc.28711

Aguirre-Ghiso, J.A., 2007. Models, mechanisms and clinical evidence for cancer dormancy. Nat. Rev. Cancer 7, 834–846. https://doi.org/10.1038/nrc2256

Anderson, J., 2017. Unleashing the immune response against childhood solid cancers. Pediatric Blood & Cancer 64, e26548. https://doi.org/10.1002/pbc.26548

Applebaum, M.A., Jha, A.R., Kao, C., Hernandez, K.M., DeWane, G., Salwen, H.R., Chlenski, A., Dobratic, M., Mariani, C.J., Godley, L.A., Prabhakar, N., White, K., Stranger, B.E., Cohn, S.L., 2016. Integrative genomics reveals hypoxia inducible genes that are associated with a poor prognosis in neuroblastoma patients. Oncotarget 7, 76816–76826. https://doi.org/10.18632/oncotarget.12713

Apps, J.R., Hasan, F., Campus, O., Behjati, S., Jacques, T.S., Sebire, N.J., Anderson, J., 2013. The immune environment of paediatric solid malignancies: evidence from an immunohistochemical study of clinical cases. Fetal and Pediatric Pathology 32, 298–307. https://doi.org/10.3109/15513815.2012.754527

Artavanis-Tsakonas, S., Rand, M.D., Lake, R.J., 1999. Notch Signaling: Cell Fate Control and Signal Integration in Development. Science 284, 770–776. https://doi.org/10.1126/science.284.5415.770

Asgharzadeh, S., Salo, J.A., Ji, L., Oberthuer, A., Fischer, M., Berthold, F., Hadjidaniel, M., Liu, C.W.-Y., Metelitsa, L.S., Pique-Regi, R., Wakamatsu, P., Villablanca, J.G., Kreissman, S.G., Matthay, K.K., Shimada, H., London, W.B., Sposto, R., Seeger, R.C., 2012. Clinical significance of tumor-associated inflammatory cells in metastatic neuroblastoma. J. Clin. Oncol. 30, 3525–3532. https://doi.org/10.1200/JCO.2011.40.9169

Attiyeh, E.F., London, W.B., Mossé, Y.P., Wang, Q., Winter, C., Khazi, D., McGrady, P.W., Seeger, R.C., Look, A.T., Shimada, H., Brodeur, G.M., Cohn, S.L., Matthay, K.K., Maris, J.M., 2005. Chromosome 1p and 11q Deletions and Outcome in Neuroblastoma. New England Journal of Medicine 353, 2243–2253. https://doi.org/10.1056/NEJMoa052399

Barber, E.K., Dasgupta, J.D., Schlossman, S.F., Trevillyan, J.M., Rudd, C.E., 1989. The CD4 and CD8 antigens are coupled to a protein-tyrosine kinase (p56lck) that phosphorylates the CD3 complex. Proc Natl Acad Sci U S A 86, 3277–3281.

Beach, D., Gonen, R., Bogin, Y., Reischl, I.G., Yablonski, D., 2007. Dual Role of SLP-76 in Mediating T Cell Receptor-induced Activation of Phospholipase C-γ1. J. Biol. Chem. 282, 2937–2946. https://doi.org/10.1074/jbc.M606697200

Berke, G., 1995. The CTL's kiss of death. Cell 81, 9–12. https://doi.org/10.1016/0092-8674(95)90365-8

Bielamowicz, K., Fousek, K., Byrd, T.T., Samaha, H., Mukherjee, M., Aware, N., Wu, M.-F., Orange, J.S., Sumazin, P., Man, T.-K., Joseph, S.K., Hegde, M., Ahmed, N., 2018. Trivalent CAR T cells overcome interpatient antigenic variability in glioblastoma. Neuro-oncology 20, 506–518. https://doi.org/10.1093/neuonc/nox182

Bonaventura, P., Shekarian, T., Alcazer, V., Valladeau-Guilemond, J., Valsesia-Wittmann, S., Amigorena, S., Caux, C., Depil, S., 2019. Cold Tumors: A Therapeutic Challenge for Immunotherapy. Front Immunol 10. https://doi.org/10.3389/fimmu.2019.00168

Brodeur, G.M., Pritchard, J., Berthold, F., Carlsen, N.L., Castel, V., Castelberry, R.P., De Bernardi, B., Evans, A.E., Favrot, M., Hedborg, F., 1993. Revisions of the international criteria for neuroblastoma diagnosis, staging, and response to treatment. JCO 11, 1466–1477. https://doi.org/10.1200/JCO.1993.11.8.1466

Brodeur, G.M., Seeger, R.C., Schwab, M., Varmus, H.E., Bishop, J.M., 1984. Amplification of N-myc in untreated human neuroblastomas correlates with advanced disease stage. Science 224, 1121–1124. https://doi.org/10.1126/science.6719137

Bronte, V., Brandau, S., Chen, S.-H., Colombo, M.P., Frey, A.B., Greten, T.F., Mandruzzato, S., Murray, P.J., Ochoa, A., Ostrand-Rosenberg, S., Rodriguez, P.C., Sica, A., Umansky, V., Vonderheide, R.H., Gabrilovich, D.I., 2016. Recommendations for myeloid-derived suppressor cell nomenclature and characterization standards. Nat Commun 7. https://doi.org/10.1038/ncomms12150

Brunet, J.-F., Denizot, F., Luciani, M.-F., Roux-Dosseto, M., Suzan, M., Mattei, M.-G., Golstein, P., 1987. A new member of the immunoglobulin superfamily—CTLA-4. Nature 328, 267–270. https://doi.org/10.1038/328267a0

Burnet, F.M., 1970. The Concept of Immunological Surveillance. Immunological Aspects of Neoplasia 13, 1–27. https://doi.org/10.1159/000386035

Burnet, M., 1957. Cancer—A Biological Approach. Br Med J 1, 841–847.

Camus, M., Tosolini, M., Mlecnik, B., Pagès, F., Kirilovsky, A., Berger, A., Costes, A., Bindea, G., Charoentong, P., Bruneval, P., Trajanoski, Z., Fridman, W.-H., Galon, J., 2009. Coordination of intratumoral immune reaction and human colorectal cancer recurrence. Cancer Res. 69, 2685–2693. https://doi.org/10.1158/0008-5472.CAN-08-2654

Carlson, L.-M., Rasmuson, A., Idborg, H., Segerström, L., Jakobsson, P.-J., Sveinbjörnsson, B., Kogner, P., 2013. Low-dose aspirin delays an inflammatory tumor progression in vivo in a transgenic mouse model of neuroblastoma. Carcinogenesis 34, 1081–1088. https://doi.org/10.1093/carcin/bgt009

Carpenter, E.L., Mossé, Y.P., 2012. Targeting ALK in neuroblastoma—preclinical and clinical advancements. Nat Rev Clin Oncol 9, 391–399. https://doi.org/10.1038/nrclinonc.2012.72

Casacuberta-Serra, S., Parés, M., Golbano, A., Coves, E., Espejo, C., Barquinero, J., 2017. Myeloid-derived suppressor cells can be efficiently generated from human hematopoietic progenitors and peripheral blood monocytes. Immunol Cell Biol 95, 538–548. https://doi.org/10.1038/icb.2017.4

Chan, A.C., Iwashima, M., Turck, C.W., Weiss, A., 1992. ZAP-70: A 70 kd protein-tyrosine kinase that associates with the TCR ζ chain. Cell 71, 649–662. https://doi.org/10.1016/0092-8674(92)90598-7

Chen, L., 2004. Co-inhibitory molecules of the B7–CD28 family in the control of T-cell immunity. Nat Rev Immunol 4, 336–347. https://doi.org/10.1038/nri1349

Chen, L., Flies, D.B., 2013. Molecular mechanisms of T cell co-stimulation and co-inhibition. Nat Rev Immunol 13, 227–242. https://doi.org/10.1038/nri3405

Cho, J.H., Okuma, A., Al-Rubaye, D., Intisar, E., Junghans, R.P., Wong, W.W., 2018. Engineering Axl specific CAR and SynNotch receptor for cancer therapy. Scientific Reports 8, 3846. https://doi.org/10.1038/s41598-018-22252-6

Chuang, C.-M., Monie, A., Hung, C.-F., Wu, T.-C., 2010. Treatment with Imiquimod enhances antitumor immunity induced by therapeutic HPV DNA vaccination. Journal of Biomedical Science 17, 32. https://doi.org/10.1186/1423-0127-17-32

Cohn, S.L., Pearson, A.D.J., London, W.B., Monclair, T., Ambros, P.F., Brodeur, G.M., Faldum, A., Hero, B., Iehara, T., Machin, D., Mosseri, V., Simon, T., Garaventa, A., Castel, V., Matthay, K.K., 2009. The International Neuroblastoma Risk Group (INRG) Classification System: An INRG Task Force Report. J Clin Oncol 27, 289–297. https://doi.org/10.1200/JCO.2008.16.6785

Curtsinger, J.M., Mescher, M.F., 2010. Inflammatory Cytokines as a Third Signal for T Cell Activation. Curr Opin Immunol 22, 333–340. https://doi.org/10.1016/j.coi.2010.02.013

de Gruijl, T.D., van den Eertwegh, A.J.M., Pinedo, H.M., Scheper, R.J., 2008. Whole-cell cancer vaccination: from autologous to allogeneic tumor- and dendritic cell-based vaccines. Cancer Immunol. Immunother. 57, 1569–1577. https://doi.org/10.1007/s00262-008-0536-z

Decker, W.K., da Silva, R.F., Sanabria, M.H., Angelo, L.S., Guimarães, F., Burt, B.M., Kheradmand, F., Paust, S., 2017. Cancer Immunotherapy: Historical Perspective of a Clinical Revolution and Emerging Preclinical Animal Models. Front. Immunol. 8. https://doi.org/10.3389/fimmu.2017.00829

Decker, W.K., Safdar, A., 2009. Bioimmunoadjuvants for the treatment of neoplastic and infectious disease: Coley's legacy revisited. Cytokine Growth Factor Rev. 20, 271–281. https://doi.org/10.1016/j.cytogfr.2009.07.004

Dobosz, P., Dzieciątkowski, T., 2019. The Intriguing History of Cancer Immunotherapy. Front Immunol 10. https://doi.org/10.3389/fimmu.2019.02965

Dolcetti, L., Peranzoni, E., Ugel, S., Marigo, I., Gomez, A.F., Mesa, C., Geilich, M., Winkels, G., Traggiai, E., Casati, A., Grassi, F., Bronte, V., 2009. Hierarchy of immunosuppressive strength among myeloid-derived suppressor cell subsets is determined by GM-CSF. European Journal of Immunology 40, 22–35. https://doi.org/10.1002/eji.200939903

Dong, Y., Sun, Q., Zhang, X., 2016. PD-1 and its ligands are important immune checkpoints in cancer. Oncotarget 8, 2171–2186. https://doi.org/10.18632/oncotarget.13895

Downing, J.R., Wilson, R.K., Zhang, J., Mardis, E.R., Pui, C.-H., Ding, L., Ley, T.J., Evans, W.E., 2012. The Pediatric Cancer Genome Project. Nat. Genet. 44, 619–622. https://doi.org/10.1038/ng.2287

Draghiciu, O., Lubbers, J., Nijman, H.W., Daemen, T., 2015a. Myeloid derived suppressor cells—An overview of combat strategies to increase immunotherapy efficacy. Oncoimmunology 4. https://doi.org/10.4161/21624011.2014.954829

Draghiciu, O., Nijman, H.W., Hoogeboom, B.N., Meijerhof, T., Daemen, T., 2015b. Sunitinib depletes myeloid-derived suppressor cells and synergizes with a cancer vaccine to enhance antigen-specific immune responses and tumor eradication. Oncoimmunology 4. https://doi.org/10.4161/2162402X.2014.989764

Dunn, G.P., Bruce, A.T., Ikeda, H., Old, L.J., Schreiber, R.D., 2002. Cancer immunoediting: from immunosurveillance to tumor escape. Nat Immunol 3, 991–998. https://doi.org/10.1038/ni1102-991

Ebert, L.M., Yu, W., Gargett, T., Brown, M.P., 2018. Logic-gated approaches to extend the utility of chimeric antigen receptor T-cell technology. Biochem Soc Trans 46, 391–401. https://doi.org/10.1042/BST20170178

Ehrlich, P., 1908. Ueber den jetzigen Stand der Karzinomforschung.

Eriksson, E., Wenthe, J., Irenaeus, S., Loskog, A., Ullenhag, G., 2016. Gemcitabine reduces MDSCs, tregs and TGF-β-1 while restoring the teff/treg ratio in patients with pancreatic cancer. J Transl Med 14, 282. https://doi.org/10.1186/s12967-016-1037-z

Fedorov, V.D., Themeli, M., Sadelain, M., 2013. PD-1– and CTLA-4–Based Inhibitory Chimeric Antigen Receptors (iCARs) Divert Off-Target Immunotherapy Responses. Sci Transl Med 5, 215ra172. https://doi.org/10.1126/scitranslmed.3006597

Fleming, V., Hu, X., Weber, R., Nagibin, V., Groth, C., Altevogt, P., Utikal, J., Umansky, V., 2018. Targeting Myeloid-Derived Suppressor Cells to Bypass Tumor-Induced Immunosuppression. Front. Immunol. 9. https://doi.org/10.3389/fimmu.2018.00398

Fong, C.T., Dracopoli, N.C., White, P.S., Merrill, P.T., Griffith, R.C., Housman, D.E., Brodeur, G.M., 1989. Loss of heterozygosity for the short arm of chromosome 1 in human neuroblastomas: correlation with N-myc amplification. Proc Natl Acad Sci U S A 86, 3753–3757.

Gabrilovich, D., 2004. Mechanisms and functional significance of tumour-induced dendritic-cell defects. Nature Reviews Immunology 4, 941–952. https://doi.org/10.1038/nri1498

Gabrilovich, D.I., 2017. Myeloid-Derived Suppressor Cells. Cancer Immunol Res 5, 3–8. https://doi.org/10.1158/2326-6066.CIR-16-0297

Gabrilovich, D.I., Nagaraj, S., 2009. Myeloid-derived-suppressor cells as regulators of the immune system. Nat Rev Immunol 9, 162–174. https://doi.org/10.1038/nri2506

Gabrilovich, D.I., Ostrand-Rosenberg, S., Bronte, V., 2012. Coordinated regulation of myeloid cells by tumours. Nat Rev Immunol 12, 253–268. https://doi.org/10.1038/nri3175

Galluzzi, L., Vacchelli, E., Pedro, J.-M.B.-S., Buqué, A., Senovilla, L., Baracco, E.E., Bloy, N., Castoldi, F., Abastado, J.-P., Agostinis, P., Apte, R.N., Aranda, F., Ayyoub, M., Beckhove, P., Blay, J.-Y., Bracci, L., Caignard, A., Castelli, C., Cavallo, F., Celis, E., Cerundolo, V., Clayton, A., Colombo, M.P., Coussens, L., Dhodapkar, M.V., Eggermont, A.M., Fearon, D.T., Fridman, W.H., Fučíková, J., Gabrilovich, D.I., Galon, J., Garg, A., Ghiringhelli, F., Giaccone, G., Gilboa, E., Gnjatic, S., Hoos, A., Hosmalin, A., Jäger, D., Kalinski, P., Kärre, K., Kepp, O., Kiessling, R., Kirkwood, J.M., Klein, E., Knuth, A., Lewis, C.E., Liblau, R., Lotze, M.T., Lugli, E., Mach, J.-P., Mattei, F., Mavilio, D., Melero, I., Melief, C.J., Mittendorf, E.A., Moretta, L., Odunsi, A., Okada, H., Palucka, A.K., Peter, M.E., Pienta, K.J., Porgador, A., Prendergast, G.C., Rabinovich, G.A., Restifo, N.P., Rizvi, N., Sautès-Fridman, C., Schreiber, H., Seliger, B., Shiku, H., Silva-Santos, B., Smyth, M.J., Speiser, D.E., Spisek, R., Srivastava, P.K., Talmadge, J.E., Tartour, E., Van Der Burg, S.H., Van Den Eynde, B.J., Vile, R., Wagner, H., Weber, J.S., Whiteside, T.L., Wolchok, J.D., Zitvogel, L., Zou, W., Kroemer, G., 2014. Classification of current anticancer immunotherapies. Oncotarget 5, 12472–12508.

Galon, J., Angell, H.K., Bedognetti, D., Marincola, F.M., 2013. The Continuum of Cancer Immunosurveillance: Prognostic, Predictive, and Mechanistic Signatures. Immunity 39, 11–26. https://doi.org/10.1016/j.immuni.2013.07.008

Galon, J., Bruni, D., 2019. Approaches to treat immune hot, altered and cold tumours with combination immunotherapies. Nat Rev Drug Discov 18, 197–218. https://doi.org/10.1038/s41573-018-0007-y

Germain, R.N., 2002. T-cell development and the CD4–CD8 lineage decision. Nat Rev Immunol 2, 309–322. https://doi.org/10.1038/nri798

Gilbert, F., Feder, M., Balaban, G., Brangman, D., Lurie, D.K., Podolsky, R., Rinaldt, V., Vinikoor, N., Weisband, J., 1984. Human Neuroblastomas and Abnormalities of Chromosomes 1 and 17. Cancer Res 44, 5444–5449.

Gossen, M., Freundlieb, S., Bender, G., Müller, G., Hillen, W., Bujard, H., 1995. Transcriptional activation by tetracyclines in mammalian cells. Science 268, 1766–1769. https://doi.org/10.1126/science.7792603

Graham, J.B., Graham, R.M., 1959. The effect of vaccine on cancer patients. Surg Gynecol Obstet 109, 131–138.

Gross, G., Waks, T., Eshhar, Z., 1989. Expression of immunoglobulin-T-cell receptor chimeric molecules as functional receptors with antibody-type specificity. Proc Natl Acad Sci U S A 86, 10024–10028.

Guerra, N., Tan, Y.X., Joncker, N.T., Choy, A., Gallardo, F., Xiong, N., Knoblaugh, S., Cado, D., Greenberg, N.M., Greenberg, N.R., Raulet, D.H., 2008. NKG2D-deficient mice are defective in tumor surveillance in models of spontaneous malignancy. Immunity 28, 571–580. https://doi.org/10.1016/j.immuni.2008.02.016

Hanson, E.M., Clements, V.K., Sinha, P., Ilkovitch, D., Ostrand-Rosenberg, S., 2009. Myeloid-derived suppressor cells down-regulate L-selectin expression on CD4+ and CD8+ T cells. J Immunol 183, 937–944. https://doi.org/10.4049/jimmunol.0804253

Hasan, M.K., Nafady, A., Takatori, A., Kishida, S., Ohira, M., Suenaga, Y., Hossain, S., Akter, J., Ogura, A., Nakamura, Y., Kadomatsu, K., Nakagawara, A., 2013. ALK is a MYCN target gene and regulates cell migration and invasion in neuroblastoma. Sci Rep 3, 1–11. https://doi.org/10.1038/srep03450

Hegde, M., Mukherjee, M., Grada, Z., Pignata, A., Landi, D., Navai, S.A., Wakefield, A., Fousek, K., Bielamowicz, K., Chow, K.K.H., Brawley, V.S., Byrd, T.T., Krebs, S., Gottschalk, S., Wels, W.S., Baker, M.L., Dotti, G., Mamonkin, M., Brenner, M.K., Orange, J.S., Ahmed, N., 2016. Tandem CAR T cells targeting HER2 and IL13Rα2 mitigate tumor antigen escape. J Clin Invest 126, 3036–3052. https://doi.org/10.1172/JCI83416

Hegde, P.S., Karanikas, V., Evers, S., 2016. The Where, the When, and the How of Immune Monitoring for Cancer Immunotherapies in the Era of Checkpoint Inhibition. Clin Cancer Res 22, 1865–1874. https://doi.org/10.1158/1078-0432.CCR-15-1507

Henderson, T.O., Bhatia, S., Pinto, N., London, W.B., McGrady, P., Crotty, C., Sun, C.-L., Cohn, S.L., 2011. Racial and Ethnic Disparities in Risk and Survival in Children With Neuroblastoma: A Children's Oncology Group Study. J Clin Oncol 29, 76–82. https://doi.org/10.1200/JCO.2010.29.6103

Hodi, F.S., O'Day, S.J., McDermott, D.F., Weber, R.W., Sosman, J.A., Haanen, J.B., Gonzalez, R., Robert, C., Schadendorf, D., Hassel, J.C., Akerley, W., van den Eertwegh, A.J.M., Lutzky, J., Lorigan, P., Vaubel, J.M., Linette, G.P., Hogg, D., Ottensmeier, C.H., Lebbé, C., Peschel, C., Quirt, I., Clark, J.I., Wolchok, J.D., Weber, J.S., Tian, J., Yellin, M.J., Nichol, G.M., Hoos, A., Urba, W.J., 2010. Improved survival with ipilimumab in patients with metastatic melanoma. N. Engl. J. Med. 363, 711–723. https://doi.org/10.1056/NEJMoa1003466

Hogan, P.G., Chen, L., Nardone, J., Rao, A., 2003. Transcriptional regulation by calcium, calcineurin, and NFAT. Genes Dev. 17, 2205–2232. https://doi.org/10.1101/gad.1102703

Hong, J.J., Rosenberg, S.A., Dudley, M.E., Yang, J.C., White, D.E., Butman, J.A., Sherry, R.M., 2010. Successful treatment of melanoma brain metastases with adoptive cell therapy. Clin. Cancer Res. 16, 4892–4898. https://doi.org/10.1158/1078-0432.CCR-10-1507

Huang, B., Pan, P.-Y., Li, Q., Sato, A.I., Levy, D.E., Bromberg, J., Divino, C.M., Chen, S.-H., 2006. Gr-1+CD115+ immature myeloid suppressor cells mediate the development of tumor-induced T regulatory cells and T-cell anergy in tumor-bearing host. Cancer Res 66, 1123–1131. https://doi.org/10.1158/0008-5472.CAN-05-1299

Jenkins, M.R., Griffiths, G.M., 2010. The synapse and cytolytic machinery of cytotoxic T cells. Curr Opin Immunol 22, 308–313. https://doi.org/10.1016/j.coi.2010.02.008

Johnson, L.A., Morgan, R.A., Dudley, M.E., Cassard, L., Yang, J.C., Hughes, M.S., Kammula, U.S., Royal, R.E., Sherry, R.M., Wunderlich, J.R., Lee, C.-C.R., Restifo, N.P., Schwarz, S.L., Cogdill, A.P., Bishop, R.J., Kim, H., Brewer, C.C., Rudy, S.F., VanWaes, C., Davis, J.L., Mathur, A., Ripley, R.T., Nathan, D.A., Laurencot, C.M., Rosenberg, S.A., 2009. Gene therapy with human and mouse T-cell receptors mediates cancer regression and targets normal tissues expressing cognate antigen. Blood 114, 535–546. https://doi.org/10.1182/blood-2009-03-211714

Joyce, J.A., Fearon, D.T., 2015. T cell exclusion, immune privilege, and the tumor microenvironment. Science 348, 74–80. https://doi.org/10.1126/science.aaa6204

Kalluri, R., Zeisberg, M., 2006. Fibroblasts in cancer. Nat Rev Cancer 6, 392–401. https://doi.org/10.1038/nrc1877

Kaneko, Y., Kanda, N., Maseki, N., Sakurai, Masaharu, Tsuchida, Y., Takeda, T., Okabe, I., Sakurai, Minoru, 1987. Different Karyotypic Patterns in Early and Advanced Stage Neuroblastomas. Cancer Res 47, 311–318.

Kantoff, P.W., Higano, C.S., Shore, N.D., Berger, E.R., Small, E.J., Penson, D.F., Redfern, C.H., Ferrari, A.C., Dreicer, R., Sims, R.B., Xu, Y., Frohlich, M.W., Schellhammer, P.F., IMPACT Study Investigators, 2010. Sipuleucel-T immunotherapy for castration-resistant prostate cancer. N. Engl. J. Med. 363, 411–422. https://doi.org/10.1056/NEJMoa1001294

Kawalekar, O.U., O'Connor, R.S., Fraietta, J.A., Guo, L., McGettigan, S.E., Posey, A.D., Patel, P.R., Guedan, S., Scholler, J., Keith, B., Snyder, N.W., Snyder, N., Blair, I.A., Blair, I., Milone, M.C., June, C.H., 2016. Distinct Signaling of Coreceptors Regulates Specific Metabolism Pathways and Impacts Memory Development in CAR T Cells. Immunity 44, 380–390. https://doi.org/10.1016/j.immuni.2016.01.021

Kerkar, S.P., Restifo, N.P., 2012. Cellular Constituents of Immune Escape within the Tumor Microenvironment. Cancer Res 72, 3125–3130. https://doi.org/10.1158/0008-5472.CAN-11-4094

Khong, H.T., Restifo, N.P., 2002. Natural selection of tumor variants in the generation of "tumor escape" phenotypes. Nat Immunol 3, 999–1005. https://doi.org/10.1038/ni1102-999

Klebanoff, C.A., Rosenberg, S.A., Restifo, N.P., 2016. Prospects for gene-engineered T cell immunotherapy for solid cancers. Nat Med 22, 26–36. https://doi.org/10.1038/nm.4015

Kloss, C.C., Condomines, M., Cartellieri, M., Bachmann, M., Sadelain, M., 2013. Combinatorial antigen recognition with balanced signaling promotes selective tumor eradication by engineered T cells. Nat Biotechnol 31, 71–75. https://doi.org/10.1038/nbt.2459

Ko, J.S., Rayman, P., Ireland, J., Swaidani, S., Li, G., Bunting, K.D., Rini, B., Finke, J.H., Cohen, P.A., 2010. Direct and Differential Suppression of Myeloid-derived Suppressor Cell Subsets by Sunitinib is Compartmentally Constrained. Cancer Res 70, 3526–3536. https://doi.org/10.1158/0008-5472.CAN-09-3278

Köhler, G., Milstein, C., 1975. Continuous cultures of fused cells secreting antibody of predefined specificity. Nature 256, 495–497. https://doi.org/10.1038/256495a0

Kopan, R., Ilagan, Ma.X.G., 2009. The Canonical Notch Signaling Pathway: Unfolding the Activation Mechanism. Cell 137, 216–233. https://doi.org/10.1016/j.cell.2009.03.045

Krummel, M.F., Allison, J.P., 1995. CD28 and CTLA-4 have opposing effects on the response of T cells to stimulation. J. Exp. Med. 182, 459–465. https://doi.org/10.1084/jem.182.2.459

Kumar, V., Patel, S., Tcyganov, E., Gabrilovich, D.I., 2016. The nature of myeloid-derived suppressor cells in the tumor microenvironment. Trends Immunol 37, 208–220. https://doi.org/10.1016/j.it.2016.01.004

Kuwana, Y., Asakura, Y., Utsunomiya, N., Nakanishi, M., Arata, Y., Itoh, S., Nagase, F., Kurosawa, Y., 1987. Expression of chimeric receptor composed of immunoglobulin-derived V regions and T-cell receptor-derived C regions. Biochem. Biophys. Res. Commun. 149, 960–968. https://doi.org/10.1016/0006-291x(87)90502-x

La Motte-Mohs, R.N., Herer, E., Zúñiga-Pflücker, J.C., 2005. Induction of T-cell development from human cord blood hematopoietic stem cells by Delta-like 1 in vitro. Blood 105, 1431–1439. https://doi.org/10.1182/blood-2004-04-1293

LaRosa, D.F., Orange, J.S., 2008. 1. Lymphocytes. Journal of Allergy and Clinical Immunology, 2008 Mini-Primer on Allergic and Immunologic Diseases 121, S364–S369. https://doi.org/10.1016/j.jaci.2007.06.016

Leach, D.R., Krummel, M.F., Allison, J.P., 1996. Enhancement of antitumor immunity by CTLA-4 blockade. Science 271, 1734–1736. https://doi.org/10.1126/science.271.5256.1734

Lechner, M.G., Megiel, C., Russell, S.M., Bingham, B., Arger, N., Woo, T., Epstein, A.L., 2011. Functional characterization of human Cd33+ And Cd11b+ myeloid-derived suppressor cell subsets induced from peripheral blood mononuclear cells co-cultured with a diverse set of human tumor cell lines. J Transl Med 9, 90. https://doi.org/10.1186/1479-5876-9-90

Lee, D.W., Gardner, R., Porter, D.L., Louis, C.U., Ahmed, N., Jensen, M., Grupp, S.A., Mackall, C.L., 2014. Current concepts in the diagnosis and management of cytokine release syndrome. Blood 124, 188–195. https://doi.org/10.1182/blood-2014-05-552729

Lengauer, C., Kinzler, K.W., Vogelstein, B., 1998. Genetic instabilities in human cancers. Nature 396, 643–649. https://doi.org/10.1038/25292

Leone, P., Shin, E.-C., Perosa, F., Vacca, A., Dammacco, F., Racanelli, V., 2013. MHC Class I Antigen Processing and Presenting Machinery: Organization, Function, and

Defects in Tumor Cells. J Natl Cancer Inst 105, 1172–1187. https://doi.org/10.1093/jnci/djt184

Lim, W.A., June, C.H., 2017. The Principles of Engineering Immune Cells to Treat Cancer. Cell 168, 724–740. https://doi.org/10.1016/j.cell.2017.01.016

Little, A.J., Matthews, A., Oettinger, M., Roth, D.B., Schatz, D.G., 2015. Chapter 2 - The Mechanism of V(D)J Recombination, in: Alt, F.W., Honjo, T., Radbruch, A., Reth, M. (Eds.), Molecular Biology of B Cells (Second Edition). Academic Press, London, pp. 13–34. https://doi.org/10.1016/B978-0-12-397933-9.00002-3

Liu, D., Badeti, S., Dotti, G., Jiang, J., Wang, H., Dermody, J., Soteropoulos, P., Streck, D., Birge, R.B., Liu, C., 2020. The Role of Immunological Synapse in Predicting the Efficacy of Chimeric Antigen Receptor (CAR) Immunotherapy. Cell Communication and Signaling 18, 134. https://doi.org/10.1186/s12964-020-00617-7

Liu, S.K., Fang, N., Koretzky, G.A., McGlade, C.J., 1999. The hematopoietic-specific adaptor protein gads functions in T-cell signaling via interactions with the SLP-76 and LAT adaptors. Curr. Biol. 9, 67–75. https://doi.org/10.1016/s0960-9822(99)80017-7

London, W.B., Castel, V., Monclair, T., Ambros, P.F., Pearson, A.D.J., Cohn, S.L., Berthold, F., Nakagawara, A., Ladenstein, R.L., Iehara, T., Matthay, K.K., 2011. Clinical and Biologic Features Predictive of Survival After Relapse of Neuroblastoma: A Report From the International Neuroblastoma Risk Group Project. J Clin Oncol 29, 3286–3292. https://doi.org/10.1200/JCO.2010.34.3392

Long, A.H., Haso, W.M., Shern, J.F., Wanhainen, K.M., Murgai, M., Ingaramo, M., Smith, J.P., Walker, A.J., Kohler, M.E., Venkateshwara, V.R., Kaplan, R.N., Patterson, G.H., Fry, T.J., Orentas, R.J., Mackall, C.L., 2015. 4-1BB Costimulation Ameliorates T Cell Exhaustion Induced by Tonic Signaling of Chimeric Antigen Receptors. Nat Med 21, 581–590. https://doi.org/10.1038/nm.3838

Loo, D., Alderson, R.F., Chen, F.Z., Huang, L., Zhang, W., Gorlatov, S., Burke, S., Ciccarone, V., Li, H., Yang, Y., Son, T., Chen, Y., Easton, A.N., Li, J.C., Rillema, J.R., Licea, M., Fieger, C., Liang, T.W., Mather, J.P., Koenig, S., Stewart, S.J., Johnson, S., Bonvini, E., Moore, P.A., 2012. Development of an Fc-Enhanced Anti–B7-H3 Monoclonal Antibody with Potent Antitumor Activity. Clin Cancer Res 18, 3834–3845. https://doi.org/10.1158/1078-0432.CCR-12-0715

Look, A.T., Hayes, F.A., Nitschke, R., McWilliams, N.B., Green, A.A., 1984. Cellular DNA Content as a Predictor of Response to Chemotherapy in Infants with Unresectable Neuroblastoma. New England Journal of Medicine 311, 231–235. https://doi.org/10.1056/NEJM198407263110405

Louis, C.U., Savoldo, B., Dotti, G., Pule, M., Yvon, E., Myers, G.D., Rossig, C., Russell, H.V., Diouf, O., Liu, E., Liu, H., Wu, M.-F., Gee, A.P., Mei, Z., Rooney, C.M., Heslop, H.E., Brenner, M.K., 2011. Antitumor activity and long-term fate of chimeric antigen receptor–positive T cells in patients with neuroblastoma. Blood 118, 6050–6056. https://doi.org/10.1182/blood-2011-05-354449

Mackall, C.L., Merchant, M.S., Fry, T.J., 2014. Immune-based therapies for childhood cancer. Nat Rev Clin Oncol 11, 693–703. https://doi.org/10.1038/nrclinonc.2014.177

Mandruzzato, S., Brandau, S., Britten, C.M., Bronte, V., Damuzzo, V., Gouttefangeas, C., Maurer, D., Ottensmeier, C., van der Burg, S.H., Welters, M.J.P., Walter, S., 2016. Toward harmonized phenotyping of human myeloid-derived suppressor cells by flow cytometry: results from an interim study. Cancer Immunol Immunother 65, 161–169. https://doi.org/10.1007/s00262-015-1782-5

Matthay, K.K., Maris, J.M., Schleiermacher, G., Nakagawara, A., Mackall, C.L., Diller, L., Weiss, W.A., 2016. Neuroblastoma. Nat Rev Dis Primers 2, 1–21. https://doi.org/10.1038/nrdp.2016.78

Matzinger, P., 1994. Tolerance, danger, and the extended family. Annu. Rev. Immunol. 12, 991–1045. https://doi.org/10.1146/annurev.iy.12.040194.005015

Moghimi, B., Muthugounder, S., Jambon, S., Tibbetts, R., Hung, L., Bassiri, H., Hogarty, M.D., Barrett, D.M., Shimada, H., Asgharzadeh, S., 2021. Preclinical assessment of the efficacy and specificity of GD2-B7H3 SynNotch CAR-T in metastatic neuroblastoma. Nature Communications 12, 511. https://doi.org/10.1038/s41467-020-20785-x

Molon, B., Ugel, S., Del Pozzo, F., Soldani, C., Zilio, S., Avella, D., De Palma, A., Mauri, P., Monegal, A., Rescigno, M., Savino, B., Colombo, P., Jonjic, N., Pecanic, S., Lazzarato, L., Fruttero, R., Gasco, A., Bronte, V., Viola, A., 2011. Chemokine nitration prevents intratumoral infiltration of antigen-specific T cells. J Exp Med 208, 1949–1962. https://doi.org/10.1084/jem.20101956

Monclair, T., Brodeur, G.M., Ambros, P.F., Brisse, H.J., Cecchetto, G., Holmes, K., Kaneko, M., London, W.B., Matthay, K.K., Nuchtern, J.G., von Schweinitz, D., Simon, T., Cohn, S.L., Pearson, A.D.J., 2009. The International Neuroblastoma Risk Group (INRG) Staging System: An INRG Task Force Report. J Clin Oncol 27, 298–303. https://doi.org/10.1200/JCO.2008.16.6876

Morales, A., Eidinger, D., Bruce, A.W., 1976. Intracavitary Bacillus Calmette-Guerin in the treatment of superficial bladder tumors. J. Urol. 116, 180–183. https://doi.org/10.1016/s0022-5347(17)58737-6

Morgan, D.A., Ruscetti, F.W., Gallo, R., 1976. Selective in vitro growth of T lymphocytes from normal human bone marrows. Science 193, 1007–1008. https://doi.org/10.1126/science.181845

Morgan, R.A., Dudley, M.E., Wunderlich, J.R., Hughes, M.S., Yang, J.C., Sherry, R.M., Royal, R.E., Topalian, S.L., Kammula, U.S., Restifo, N.P., Zheng, Z., Nahvi, A., de Vries, C.R., Rogers-Freezer, L.J., Mavroukakis, S.A., Rosenberg, S.A., 2006. Cancer regression in patients after transfer of genetically engineered lymphocytes. Science 314, 126–129. https://doi.org/10.1126/science.1129003

Morsut, L., Roybal, K.T., Xiong, X., Gordley, R.M., Coyle, S.M., Thomson, M., Lim, W.A., 2016. Engineering Customized Cell Sensing and Response Behaviors Using Synthetic Notch Receptors. Cell 164, 780–791. https://doi.org/10.1016/j.cell.2016.01.012

Mosmann, T.R., Cherwinski, H., Bond, M.W., Giedlin, M.A., Coffman, R.L., 1986. Two types of murine helper T cell clone. I. Definition according to profiles of lymphokine activities and secreted proteins. The Journal of Immunology 136, 2348–2357.

Mossé, Y.P., Deyell, R.J., Berthold, F., Nagakawara, A., Ambros, P.F., Monclair, T., Cohn, S.L., Pearson, A.D., London, W.B., Matthay, K.K., 2014. Neuroblastoma in older children, adolescents and young adults: A report from the International Neuroblastoma Risk Group project. Pediatric Blood & Cancer 61, 627–635. https://doi.org/10.1002/pbc.24777

Mossé, Y.P., Laudenslager, M., Longo, L., Cole, K.A., Wood, A., Attiyeh, E.F., Laquaglia, M.J., Sennett, R., Lynch, J.E., Perri, P., Laureys, G., Speleman, F., Kim, C., Hou, C., Hakonarson, H., Torkamani, A., Schork, N.J., Brodeur, G.M., Tonini, G.P., Rappaport, E., Devoto, M., Maris, J.M., 2008. Identification of ALK as a major familial neuroblastoma predisposition gene. Nature 455, 930–935. https://doi.org/10.1038/nature07261

Motz, G.T., Santoro, S.P., Wang, L.-P., Garrabrant, T., Lastra, R.R., Hagemann, I.S., Lal, P., Feldman, M.D., Benencia, F., Coukos, G., 2014. Tumor endothelium FasL establishes a selective immune barrier promoting tolerance in tumors. Nat. Med. 20, 607–615. https://doi.org/10.1038/nm.3541

Munn, D.H., Mellor, A.L., 2013. Indoleamine 2,3 dioxygenase and metabolic control of immune responses. Trends Immunol. 34, 137–143. https://doi.org/10.1016/j.it.2012.10.001

Munn, D.H., Sharma, M.D., Lee, J.R., Jhaver, K.G., Johnson, T.S., Keskin, D.B., Marshall, B., Chandler, P., Antonia, S.J., Burgess, R., Slingluff, C.L., Mellor, A.L., 2002. Potential regulatory function of human dendritic cells expressing indoleamine 2,3-dioxygenase. Science 297, 1867–1870. https://doi.org/10.1126/science.1073514

Mussai, F., Egan, S., Hunter, S., Webber, H., Fisher, J., Wheat, R., McConville, C., Sbirkov, Y., Wheeler, K., Bendle, G., Petrie, K., Anderson, J., Chesler, L., De Santo, C., 2015. Neuroblastoma arginase activity creates an immunosuppressive microenvironment that impairs autologous and engineered immunity. Cancer Res 75, 3043–3053. https://doi.org/10.1158/0008-5472.CAN-14-3443

Nagaraj, S., Schrum, A.G., Cho, H.-I., Celis, E., Gabrilovich, D.I., 2010a. Mechanism of T-cell tolerance induced by myeloid-derived suppressor cells. J Immunol 184, 3106–3116. https://doi.org/10.4049/jimmunol.0902661

Nagaraj, S., Youn, J.-I., Weber, H., Iclozan, C., Lu, L., Cotter, M.J., Meyer, C., Becerra, C.R., Fishman, M., Antonia, S., Sporn, M.B., Liby, K.T., Rawal, B., Lee, J.-H., Gabrilovich, D.I., 2010b. Anti-inflammatory triterpenoid blocks immune suppressive function of myeloid-derived suppressor cells and improves immune response in cancer. Clin Cancer Res 16, 1812–1823. https://doi.org/10.1158/1078-0432.CCR-09-3272

Najjar, Y.G., Finke, J.H., 2013. Clinical Perspectives on Targeting of Myeloid Derived Suppressor Cells in the Treatment of Cancer. Front Oncol 3. https://doi.org/10.3389/fonc.2013.00049

Nakagawara, A., Li, Y., Izumi, H., Muramori, K., Inada, H., Nishi, M., 2018. Neuroblastoma. Jpn J Clin Oncol 48, 214–241. https://doi.org/10.1093/jjco/hyx176

Nefedova, Y., Fishman, M., Sherman, S., Wang, X., Beg, A.A., Gabrilovich, D.I., 2007. Mechanism of All-Trans Retinoic Acid Effect on Tumor-Associated Myeloid-Derived Suppressor Cells. Cancer Res 67, 11021–11028. https://doi.org/10.1158/0008-5472.CAN-07-2593

Noman, M.Z., Desantis, G., Janji, B., Hasmim, M., Karray, S., Dessen, P., Bronte, V., Chouaib, S., 2014. PD-L1 is a novel direct target of HIF-1α, and its blockade under hypoxia enhanced MDSC-mediated T cell activation. J. Exp. Med. 211, 781–790. https://doi.org/10.1084/jem.20131916

Olumi, A.F., Grossfeld, G.D., Hayward, S.W., Carroll, P.R., Tlsty, T.D., Cunha, G.R., 1999. Carcinoma-associated fibroblasts direct tumor progression of initiated human prostatic epithelium. Cancer Res. 59, 5002–5011. https://doi.org/10.1186/bcr138

Ozao-Choy, J., Ma, G., Kao, J., Wang, G.X., Meseck, M., Sung, M., Schwartz, M., Divino, C.M., Pan, P.-Y., Chen, S.-H., 2009. The Novel Role of Tyrosine Kinase Inhibitor in the Reversal of Immune Suppression and Modulation of Tumor Microenvironment for Immune-Based Cancer Therapies. Cancer Res 69, 2514–2522. https://doi.org/10.1158/0008-5472.CAN-08-4709

Ozinsky, A., Underhill, D.M., Fontenot, J.D., Hajjar, A.M., Smith, K.D., Wilson, C.B., Schroeder, L., Aderem, A., 2000. The repertoire for pattern recognition of pathogens by the innate immune system is defined by cooperation between Toll-like receptors. Proc Natl Acad Sci U S A 97, 13766–13771.

Palma, L., Di Lorenzo, N., Guidetti, B., 1978. Lymphocytic infiltrates in primary glioblastomas and recidivous gliomas. Incidence, fate, and relevance to prognosis in 228 operated cases. J. Neurosurg. 49, 854–861. https://doi.org/10.3171/jns.1978.49.6.0854

Pan, P.-Y., Ma, G., Weber, K.J., Ozao-Choy, J., Wang, G., Yin, B., Divino, C.M., Chen, S.-H., 2010. Immune stimulatory receptor CD40 is required for T-cell suppression and T regulatory cell activation mediated by myeloid-derived suppressor cells in cancer. Cancer Res 70, 99–108. https://doi.org/10.1158/0008-5472.CAN-09-1882

Park, J.R., Bagatell, R., London, W.B., Maris, J.M., Cohn, S.L., Mattay, K.M., Hogarty, M., 2013. Children's Oncology Group's 2013 blueprint for research: Neuroblastoma. Pediatric Blood & Cancer 60, 985–993. https://doi.org/10.1002/pbc.24433

Pistoia, V., Morandi, F., Bianchi, G., Pezzolo, A., Prigione, I., Raffaghello, L., 2013. Immunosuppressive Microenvironment in Neuroblastoma. Front Oncol 3. https://doi.org/10.3389/fonc.2013.00167

Qin, S., Xu, L., Yi, M., Yu, S., Wu, K., Luo, S., 2019. Novel immune checkpoint targets: moving beyond PD-1 and CTLA-4. Mol Cancer 18. https://doi.org/10.1186/s12943-019-1091-2

Quail, D., Joyce, J., 2013. Microenvironmental regulation of tumor progression and metastasis. Nat Med 19, 1423–1437. https://doi.org/10.1038/nm.3394

Richards, R.M., Sotillo, E., Majzner, R.G., 2018. CAR T Cell Therapy for Neuroblastoma. Front Immunol 9. https://doi.org/10.3389/fimmu.2018.02380

Rodriguez, P.C., Quiceno, D.G., Ochoa, A.C., 2007. L-arginine availability regulates T-lymphocyte cell-cycle progression. Blood 109, 1568–1573. https://doi.org/10.1182/blood-2006-06-031856

Rodriguez, P.C., Quiceno, D.G., Zabaleta, J., Ortiz, B., Zea, A.H., Piazuelo, M.B., Delgado, A., Correa, P., Brayer, J., Sotomayor, E.M., Antonia, S., Ochoa, J.B., Ochoa, A.C., 2004. Arginase I Production in the Tumor Microenvironment by Mature Myeloid Cells Inhibits T-Cell Receptor Expression and Antigen-Specific T-Cell Responses. Cancer Res 64, 5839–5849. https://doi.org/10.1158/0008-5472.CAN-04-0465

Roose, J.P., Mollenauer, M., Gupta, V.A., Stone, J., Weiss, A., 2005. A Diacylglycerol-Protein Kinase C-RasGRP1 Pathway Directs Ras Activation upon Antigen Receptor Stimulation of T Cells. Mol Cell Biol 25, 4426–4441. https://doi.org/10.1128/MCB.25.11.4426-4441.2005

Rosenberg, S.A., Lotze, M.T., Muul, L.M., Leitman, S., Chang, A.E., Ettinghausen, S.E., Matory, Y.L., Skibber, J.M., Shiloni, E., Vetto, J.T., Seipp, C.A., Simpson, C., Reichert, C.M., 1985. Observations on the Systemic Administration of Autologous Lymphokine-Activated Killer Cells and Recombinant Interleukin-2 to Patients with Metastatic Cancer. New England Journal of Medicine 313, 1485–1492. https://doi.org/10.1056/NEJM198512053132327

Rosenberg, S.A., Packard, B.S., Aebersold, P.M., Solomon, D., Topalian, S.L., Toy, S.T., Simon, P., Lotze, M.T., Yang, J.C., Seipp, C.A., 1988. Use of tumor-infiltrating lymphocytes and interleukin-2 in the immunotherapy of patients with metastatic melanoma. A preliminary report. N. Engl. J. Med. 319, 1676–1680. https://doi.org/10.1056/NEJM198812223192527

Rosenberg, S.A., Yang, J.C., Sherry, R.M., Kammula, U.S., Hughes, M.S., Phan, G.Q., Citrin, D.E., Restifo, N.P., Robbins, P.F., Wunderlich, J.R., Morton, K.E., Laurencot, C.M., Steinberg, S.M., White, D.E., Dudley, M.E., 2011. Durable complete responses in heavily pretreated patients with metastatic melanoma using T-cell transfer immunotherapy. Clin. Cancer Res. 17, 4550–4557. https://doi.org/10.1158/1078-0432.CCR-11-0116

Rotte, A., 2019. Combination of CTLA-4 and PD-1 blockers for treatment of cancer. Journal of Experimental & Clinical Cancer Research 38, 255. https://doi.org/10.1186/s13046-019-1259-z

Roybal, Kole T., Rupp, L.J., Morsut, L., Walker, W.J., McNally, K.A., Park, J.S., Lim, W.A., 2016. Precision Tumor Recognition by T Cells With Combinatorial Antigen-Sensing Circuits. Cell 164, 770–779. https://doi.org/10.1016/j.cell.2016.01.011

Roybal, Kole T., Williams, J.Z., Morsut, L., Rupp, L.J., Kolinko, I., Choe, J.H., Walker, W.J., McNally, K.A., Lim, W.A., 2016. Engineering T cells with Customized Therapeutic Response Programs Using Synthetic Notch Receptors. Cell 167, 419-432.e16. https://doi.org/10.1016/j.cell.2016.09.011

Rudnicka, D., Oszmiana, A., Finch, D.K., Strickland, I., Schofield, D.J., Lowe, D.C., Sleeman, M.A., Davis, D.M., 2013. Rituximab causes a polarization of B cells that augments its therapeutic function in NK-cell-mediated antibody-dependent cellular cytotoxicity. Blood 121, 4694–4702. https://doi.org/10.1182/blood-2013-02-482570

Ruella, M., Barrett, D.M., Kenderian, S.S., Shestova, O., Hofmann, T.J., Perazzelli, J., Klichinsky, M., Aikawa, V., Nazimuddin, F., Kozlowski, M., Scholler, J., Lacey, S.F., Melenhorst, J.J., Morrissette, J.J.D., Christian, D.A., Hunter, C.A., Kalos, M., Porter, D.L., June, C.H., Grupp, S.A., Gill, S., 2016. Dual CD19 and CD123 targeting prevents antigen-loss relapses after CD19-directed immunotherapies. J Clin Invest 126, 3814–3826. https://doi.org/10.1172/JCI87366

Santilli, G., Anderson, J., Thrasher, A.J., Sala, A., 2013a. Catechins and antitumor immunity. Oncoimmunology 2. https://doi.org/10.4161/onci.24443

Santilli, G., Piotrowska, I., Cantilena, S., Chayka, O., D'Alicarnasso, M., Morgenstern, D.A., Himoudi, N., Pearson, K., Anderson, J., Thrasher, A.J., Sala, A., 2013b. Polyphenol E Enhances the Antitumor Immune Response in Neuroblastoma by Inactivating Myeloid Suppressor Cells. Clin Cancer Res 19, 1116–1125. https://doi.org/10.1158/1078-0432.CCR-12-2528

Savoldo, B., Ramos, C.A., Liu, E., Mims, M.P., Keating, M.J., Carrum, G., Kamble, R.T., Bollard, C.M., Gee, A.P., Mei, Z., Liu, H., Grilley, B., Rooney, C.M., Heslop, H.E., Brenner, M.K., Dotti, G., 2011. CD28 costimulation improves expansion and persistence of chimeric antigen receptor-modified T cells in lymphoma patients. J. Clin. Invest. 121, 1822–1826. https://doi.org/10.1172/JCI46110

Sawanobori, Y., Ueha, S., Kurachi, M., Shimaoka, T., Talmadge, J.E., Abe, J., Shono, Y., Kitabatake, M., Kakimi, K., Mukaida, N., Matsushima, K., 2008. Chemokine-mediated rapid turnover of myeloid-derived suppressor cells in tumor-bearing mice. Blood 111, 5457–5466. https://doi.org/10.1182/blood-2008-01-136895

Scarfò, I., Maus, M.V., 2017. Current approaches to increase CAR T cell potency in solid tumors: targeting the tumor microenvironment. J Immunother Cancer 5, 28. https://doi.org/10.1186/s40425-017-0230-9

Schmidt, A., Oberle, N., Krammer, P.H., 2012. Molecular mechanisms of treg-mediated T cell suppression. Front Immunol 3, 51. https://doi.org/10.3389/fimmu.2012.00051

Scholler, J., Brady, T.L., Binder-Scholl, G., Hwang, W.-T., Plesa, G., Hege, K.M., Vogel, A.N., Kalos, M., Riley, J.L., Deeks, S.G., Mitsuyasu, R.T., Bernstein, W.B., Aronson, N.E., Levine, B.L., Bushman, F.D., June, C.H., 2012. Decade-Long Safety and Function of Retroviral-Modified Chimeric Antigen Receptor T Cells. Science Translational Medicine 4, 132ra53-132ra53. https://doi.org/10.1126/scitranslmed.3003761

Schreiber, R.D., Old, L.J., Smyth, M.J., 2011. Cancer Immunoediting: Integrating Immunity's Roles in Cancer Suppression and Promotion. Science 331, 1565–1570. https://doi.org/10.1126/science.1203486

Schwartzberg, P.L., Finkelstein, L.D., Readinger, J.A., 2005. TEC-family kinases: regulators of T-helper-cell differentiation. Nat Rev Immunol 5, 284–295. https://doi.org/10.1038/nri1591

Serafini, P., Borrello, I., Bronte, V., 2006a. Myeloid suppressor cells in cancer: Recruitment, phenotype, properties, and mechanisms of immune suppression. Seminars in Cancer Biology, The Inflammation-Cancer Linkage: A Double-Edged Sword? 16, 53–65. https://doi.org/10.1016/j.semcancer.2005.07.005

Serafini, P., Meckel, K., Kelso, M., Noonan, K., Califano, J., Koch, W., Dolcetti, L., Bronte, V., Borrello, I., 2006b. Phosphodiesterase-5 inhibition augments endogenous antitumor immunity by reducing myeloid-derived suppressor cell function. J Exp Med 203, 2691–2702. https://doi.org/10.1084/jem.20061104

Shankaran, V., Ikeda, H., Bruce, A.T., White, J.M., Swanson, P.E., Old, L.J., Schreiber, R.D., 2001. IFN-γ and lymphocytes prevent primary tumour development and shape tumour immunogenicity. Nature 410, 1107–1111. https://doi.org/10.1038/35074122

Shipp, C., Speigl, L., Janssen, N., Martens, A., Pawelec, G., 2016. A clinical and biological perspective of human myeloid-derived suppressor cells in cancer. Cell. Mol. Life Sci. 73, 4043–4061. https://doi.org/10.1007/s00018-016-2278-y

Shojaei-Brosseau, T., Chompret, A., Abel, A., Vathaire, F. de, Raquin, M.-A., Brugières, L., Feunteun, J., Hartmann, O., Bonaïti-Pellié, C., 2004. Genetic epidemiology of neuroblastoma: A study of 426 cases at the Institut Gustave-Roussy in France. Pediatric Blood & Cancer 42, 99–105. https://doi.org/10.1002/pbc.10381

Sica, A., Bronte, V., 2007. Altered macrophage differentiation and immune dysfunction in tumor development. J Clin Invest 117, 1155–1166. https://doi.org/10.1172/JCI31422

Sims, G.P., Rowe, D.C., Rietdijk, S.T., Herbst, R., Coyle, A.J., 2010. HMGB1 and RAGE in inflammation and cancer. Annu. Rev. Immunol. 28, 367–388. https://doi.org/10.1146/annurev.immunol.021908.132603

Smith-Garvin, J.E., Koretzky, G.A., Jordan, M.S., 2009. T Cell Activation. Annu Rev Immunol 27, 591–619. https://doi.org/10.1146/annurev.immunol.021908.132706

Srivastava, M.K., Sinha, P., Clements, V.K., Rodriguez, P., Ostrand-Rosenberg, S., 2010. Myeloid-derived suppressor cells inhibit T-cell activation by depleting cystine and cysteine. Cancer Res 70, 68–77. https://doi.org/10.1158/0008-5472.CAN-09-2587

Srivastava, S., Salter, A.I., Liggitt, D., Yechan-Gunja, S., Sarvothama, M., Cooper, K., Smythe, K.S., Dudakov, J.A., Pierce, R.H., Rader, C., Riddell, S.R., 2019. Logic-Gated ROR1 Chimeric Antigen Receptor Expression Rescues T Cell-Mediated Toxicity to Normal Tissues and Enables Selective Tumor Targeting. Cancer Cell 35, 489-503.e8. https://doi.org/10.1016/j.ccell.2019.02.003

Steinherz, P.G., Seibel, N.L., Ames, M.M., Avramis, V.I., Krailo, M.D., Liu-Mares, W., Reid, J.M., Safgren, S.L., Reaman, G.H., 2002. Phase I Study of Gemcitabine (Difluorodeoxycytidine) in Children with Relapsed or Refractory Leukemia (CCG-0955): A Report from the Children's Cancer Group. Leukemia & Lymphoma 43, 1945–1950. https://doi.org/10.1080/1042819021000015880

Straathof, K., Flutter, B., Wallace, R., Thomas, S., Cheung, G., Collura, A., Gileadi, T., Barton, J., Wright, G., Inglott, S., Edwards, D., Barton, C., Dyer, K., Westwood, N., Loka, T., Depani, S., Howe, K., Barone, G., Pule, M., Anderson, J., 2018. Abstract CT145: A Cancer Research UK phase I trial of anti-GD2 chimeric antigen receptor (CAR) transduced T-cells (1RG-CART) in patients with relapsed or refractory neuroblastoma. Cancer Res 78, CT145–CT145. https://doi.org/10.1158/1538-7445.AM2018-CT145

Strother, D.R., London, W.B., Schmidt, M.L., Brodeur, G.M., Shimada, H., Thorner, P., Collins, M.H., Tagge, E., Adkins, S., Reynolds, C.P., Murray, K., Lavey, R.S., Matthay, K.K., Castleberry, R., Maris, J.M., Cohn, S.L., 2012. Outcome After Surgery Alone or With Restricted Use of Chemotherapy for Patients With Low-Risk Neuroblastoma: Results of Children's Oncology Group Study P9641. J Clin Oncol 30, 1842–1848. https://doi.org/10.1200/JCO.2011.37.9990

Stutman, O., 1975. Immunodepression and malignancy. Adv. Cancer Res. 22, 261–422. https://doi.org/10.1016/s0065-230x(08)60179-7

Suzuki, E., Kapoor, V., Jassar, A.S., Kaiser, L.R., Albelda, S.M., 2005. Gemcitabine Selectively Eliminates Splenic Gr-1+/CD11b+ Myeloid Suppressor Cells in Tumor-Bearing Animals and Enhances Antitumor Immune Activity. Clin Cancer Res 11, 6713–6721. https://doi.org/10.1158/1078-0432.CCR-05-0883

Thomas, L., Lawrence, H., 1959. Cellular and humoral aspects of the hypersensitive states. New York: Hoeber-Harper 529–532.

Thomas, S., Straathof, K., Himoudi, N., Anderson, J., Pule, M., 2016. An Optimized GD2-Targeting Retroviral Cassette for More Potent and Safer Cellular Therapy of Neuroblastoma and Other Cancers. PLOS ONE 11, e0152196. https://doi.org/10.1371/journal.pone.0152196

Topp, M.S., Kufer, P., Gökbuget, N., Goebeler, M., Klinger, M., Neumann, S., Horst, H.-A., Raff, T., Viardot, A., Schmid, M., Stelljes, M., Schaich, M., Degenhard, E., Köhne-Volland, R., Brüggemann, M., Ottmann, O., Pfeifer, H., Burmeister, T., Nagorsen, D., Schmidt, M., Lutterbuese, R., Reinhardt, C., Baeuerle, P.A., Kneba, M., Einsele, H., Riethmüller, G., Hoelzer, D., Zugmaier, G., Bargou, R.C., 2011. Targeted therapy with the T-cell-engaging antibody blinatumomab of chemotherapy-refractory minimal residual disease in B-lineage acute lymphoblastic leukemia patients results in high response rate and prolonged leukemia-free survival. J. Clin. Oncol. 29, 2493–2498. https://doi.org/10.1200/JCO.2010.32.7270

Tseng, H., Xiong, W., Badeti, S., Yang, Y., Ma, M., Liu, T., Ramos, C.A., Dotti, G., Fritzky, L., Jiang, J., Yi, Q., Guarrera, J., Zong, W.-X., Liu, C., Liu, D., 2020. Efficacy of anti-CD147 chimeric antigen receptors targeting hepatocellular carcinoma. Nature Communications 11, 4810. https://doi.org/10.1038/s41467-020-18444-2

Vanichapol, T., Chutipongtanate, S., Anurathapan, U., Hongeng, S., 2018. Immune Escape Mechanisms and Future Prospects for Immunotherapy in Neuroblastoma. Biomed Res Int 2018. https://doi.org/10.1155/2018/1812535

Veglia, F., Perego, M., Gabrilovich, D., 2018. Myeloid-derived suppressor cells coming of age. Nature Immunology 19, 108–119. https://doi.org/10.1038/s41590-017-0022-x

Veltman, J.D., Lambers, M.E.H., van Nimwegen, M., Hendriks, R.W., Hoogsteden, H.C., Aerts, J.G.J.V., Hegmans, J.P.J.J., 2010. COX-2 inhibition improves immunotherapy and is associated with decreased numbers of myeloid-derived suppressor cells in mesothelioma. Celecoxib influences MDSC function. BMC Cancer 10, 464. https://doi.org/10.1186/1471-2407-10-464

Vesely, M.D., Kershaw, M.H., Schreiber, R.D., Smyth, M.J., 2011. Natural innate and adaptive immunity to cancer. Annu. Rev. Immunol. 29, 235–271. https://doi.org/10.1146/annurev-immunol-031210-101324

Voeller, J., Erbe, A.K., Slowinski, J., Rasmussen, K., Carlson, P.M., Hoefges, A., VandenHeuvel, S., Stuckwisch, A., Wang, X., Gillies, S.D., Patel, R.B., Farrel, A., Rokita, J.L., Maris, J., Hank, J.A., Morris, Z.S., Rakhmilevich, A.L., Sondel, P.M., 2019. Combined innate and adaptive immunotherapy overcomes resistance of immunologically cold syngeneic murine neuroblastoma to checkpoint inhibition. J Immunother Cancer 7. https://doi.org/10.1186/s40425-019-0823-6

von Boehmer, H., Fehling, H.J., 1997. Structure and function of the pre-t cell receptor. Annu. Rev. Immunol. 15, 433–452. https://doi.org/10.1146/annurev.immunol.15.1.433

von Boehmer, H., Teh, H.S., Kisielow, P., 1989. The thymus selects the useful, neglects the useless and destroys the harmful. Immunology Today 10, 57–61. https://doi.org/10.1016/0167-5699(89)90307-1

Wan, Y.Y., Flavell, R.A., 2009. How Diverse—CD4 Effector T Cells and their Functions. J Mol Cell Biol 1, 20–36. https://doi.org/10.1093/jmcb/mjp001

Watanabe, K., Kuramitsu, S., Posey, A.D.J., June, C.H., 2018. Expanding the Therapeutic Window for CAR T Cell Therapy in Solid Tumors: The Knowns and Unknowns of CAR T Cell Biology. Front. Immunol. 9. https://doi.org/10.3389/fimmu.2018.02486

Wherry, E.J., Kurachi, M., 2015. Molecular and cellular insights into T cell exhaustion. Nat Rev Immunol 15, 486–499. https://doi.org/10.1038/nri3862

Whittle, S.B., Smith, V., Doherty, E., Zhao, S., McCarty, S., Zage, P.E., 2017. Overview and recent advances in the treatment of neuroblastoma. Expert Review of Anticancer Therapy 17, 369–386. https://doi.org/10.1080/14737140.2017.1285230

Xiong, W., Chen, Y., Kang, X., Chen, Z., Zheng, P., Hsu, Y.-H., Jang, J.H., Qin, L., Liu, H., Dotti, G., Liu, D., 2018. Immunological Synapse Predicts Effectiveness of Chimeric Antigen Receptor Cells. Molecular Therapy 26, 963–975. https://doi.org/10.1016/j.ymthe.2018.01.020

Xu, J., Wang, Y., Shi, J., Liu, J., Li, Q., Chen, L., 2018. Combination therapy: A feasibility strategy for CAR-T cell therapy in the treatment of solid tumors. Oncol Lett 16, 2063–2070. https://doi.org/10.3892/ol.2018.8946

Yarchoan, M., Johnson, B.A., Lutz, E.R., Laheru, D.A., Jaffee, E.M., 2017. Targeting neoantigens to augment antitumour immunity. Nat Rev Cancer 17, 209–222. https://doi.org/10.1038/nrc.2016.154

Yatim, K.M., Lakkis, F.G., 2015. A Brief Journey through the Immune System. CJASN 10, 1274–1281. https://doi.org/10.2215/CJN.10031014

Youn, J.-I., Nagaraj, S., Collazo, M., Gabrilovich, D.I., 2008. Subsets of Myeloid-Derived Suppressor Cells in Tumor Bearing Mice. J Immunol 181, 5791–5802.

Yu, H., Sotillo, E., Harrington, C., Wertheim, G., Paessler, M., Maude, S.L., Rheingold, S.R., Grupp, S.A., Thomas-Tikhonenko, A., Pillai, V., 2017. Repeated loss of target surface antigen after immunotherapy in primary mediastinal large B cell lymphoma. Am. J. Hematol. 92, E11–E13. https://doi.org/10.1002/ajh.24594

Zah, E., Lin, M.-Y., Silva-Benedict, A., Jensen, M.C., Chen, Y.Y., 2016. T Cells Expressing CD19/CD20 Bispecific Chimeric Antigen Receptors Prevent Antigen Escape by Malignant B Cells. Cancer Immunol Res 4, 498–508. https://doi.org/10.1158/2326-6066.CIR-15-0231

Zea, A.H., Rodriguez, P.C., Culotta, K.S., Hernandez, C.P., DeSalvo, J., Ochoa, J.B., Park, H.-J., Zabaleta, J., Ochoa, A.C., 2004. L-Arginine modulates CD3zeta expression and T cell function in activated human T lymphocytes. Cell Immunol 232, 21–31. https://doi.org/10.1016/j.cellimm.2005.01.004

Zeng, Y., Fest, S., Kunert, R., Katinger, H., Pistoia, V., Michon, J., Lewis, G., Ladenstein, R., Lode, H.N., 2005. Anti-neuroblastoma effect of ch14.18 antibody produced in CHO cells is mediated by NK-cells in mice. Molecular Immunology 42, 1311–1319. https://doi.org/10.1016/j.molimm.2004.12.018

Zhang, D.H., Cohn, L., Ray, P., Bottomly, K., Ray, A., 1997. Transcription factor GATA-3 is differentially expressed in murine Th1 and Th2 cells and controls Th2-specific expression of the interleukin-5 gene. J. Biol. Chem. 272, 21597–21603. https://doi.org/10.1074/jbc.272.34.21597

Zhong, S., Malecek, K., Johnson, L.A., Yu, Z., Vega-Saenz de Miera, E., Darvishian, F., McGary, K., Huang, K., Boyer, J., Corse, E., Shao, Y., Rosenberg, S.A., Restifo, N.P., Osman, I., Krogsgaard, M., 2013. T-cell receptor affinity and avidity defines antitumor response and autoimmunity in T-cell immunotherapy. Proc. Natl. Acad. Sci. U.S.A. 110, 6973–6978. https://doi.org/10.1073/pnas.1221609110

Zufferey, R., Dull, T., Mandel, R.J., Bukovsky, A., Quiroz, D., Naldini, L., Trono, D., 1998. Self-Inactivating Lentivirus Vector for Safe and Efficient In Vivo Gene Delivery. J Virol 72, 9873–9880.